

(ทุนองค์ความรู้ใหม่ที่เป็นพื้นฐานต่อการพัฒนา)

สัญญาเลขที่ BRG6080016



รายงานวิจัยฉบับสมบูรณ์

การศึกษาคุณลักษณะของฟิล์มผสมโซเดียมเคซีเนต-เคลย์สำหรับการนำส่ง
ฟลูโคนาโซลเฉพาะที่ในแคนดิดิเอซิสช่องปาก
Characterization of sodium caseinate-clay composite films for
local fluconazole delivery in oral candidiasis

โดย

ศาสตราจารย์ ดร. ธเนศ พงศ์จรรยากุล
คณะเภสัชศาสตร์ มหาวิทยาลัยขอนแก่น

พฤษภาคม 2562

(ทุนองค์ความรู้ใหม่ที่เป็นพื้นฐานต่อการพัฒนา)

สัญญาเลขที่ BRG6080016

รายงานวิจัยฉบับสมบูรณ์

การศึกษาคุณลักษณะของฟิล์มผสมโซเดียมเคซีเนต-เคลย์สำหรับการนำส่ง
ฟลูโคนาโซลเฉพาะที่ในแคนดิดิเอซิสช่องปาก
Characterization of sodium caseinate-clay composite films for
local fluconazole delivery in oral candidiasis

ผู้วิจัย

ศาสตราจารย์ ดร. ธเนศ พงศ์จรรยากุล
คณะเภสัชศาสตร์ มหาวิทยาลัยขอนแก่น

สนับสนุนโดยสำนักงานกองทุนสนับสนุนการวิจัยและมหาวิทยาลัยขอนแก่น

(ความเห็นในรายงานนี้เป็นของผู้วิจัย สกว. และ มข. ไม่จำเป็นต้องเห็นด้วยเสมอไป)

Introduction to the research problem and its significance

Material development for use in foods and pharmaceuticals has been raised in order to find a suitable material for some purposes. For pharmaceuticals, macromolecules, such as polymers, have been widely applied for developing drug formulations and drug delivery systems. A use of polymer blends by varying ratios of two polymers offers a different property when comparing with the use of single polymer (Siepmann et al., 2008). Alternatively, a polymer can be blended with a clay to achieve an appreciated property. Importantly, molecular interactions of the polymer chains with the clay compounds can occur, which can effectively alter the physicochemical properties of the polymers (Pongjanyakul et al., 2005; Khunawattanakul et al. 2010; Rongthong et al., 2013). The polymer-clay composites have been characterized and used as tablet coating films (Pongjanyakul et al., 2005a; Khunawattanakul et al. 2011) and as microparticles for matrix forming agents (Khlibsuwan and Pongjanyakul, 2015).

Caseins, biomacromolecules from milk, are composed of 94% protein and 6% colloidal calcium phosphate (Walstra et al., 2006). Casein proteins have distinct hydrophobic and hydrophilic domains that self-assemble into stable micellar structures in aqueous solutions. Casein micelles are composed of four phosphoproteins held together by hydrophobic interaction and by bridging of calcium phosphate nanoclusters (De Kruif and Grinberg, 2002; Qi, 2007). For this characteristic, caseins are used as emulsifying and foaming agents in food industry. Furthermore, caseins have been pharmaceutically applied as a solubilizing agent for poorly soluble drugs (Millar and Corrigan, 1991; Millar and Corrigan, 1993). Caseins also possess a film forming properties that can be used for tablets film coating (Abu Diak et al., 2007; Elzoghby et al., 2011) and food packaging (Wihodo and Moraru, 2013). However, it is necessary to modify the casein film properties by adding plasticizers (Audic and Chaufer, 2005), cross-linking agent (Audic and Chaufer, 2005; Perada et al., 2010) and water insoluble additives (Fabra et al., 2008; Perada et al., 2011a, b). These modifications result in a change of mechanical properties and water vapor permeability. Moreover, caseins also have a potential use as drug delivery systems, particularly microparticles (Knepp et al., 1993; Magee et al., 1993) and nanoparticles (Elzoghby et al., 2013; Pan et al., 2013). Thus, it is interesting that incorporation of clays may cause a change of the casein films to use as drug delivery systems.

Oral candidiasis caused by *Candida albicans* is the most common opportunistic fungal infection in human immunodeficiency virus-infected patients and other immunocompromised hosts. (Pelletier et al., 2000). The current treatment regimen for this infection is clotrimazole lozenges or torches, which is available in Thailand. However, the use of clotrimazole is discontinued because the relapses of oral candidiasis in the patients usually occur that may be an emergence of resistance to this drug. For this reason, other antifungal agent, such as fluconazole, is alternative drug for use in this disease (Pelletier et al., 2000). Fluconazole used clinically for the treatment of oral candidiasis is commercially

available as oral conventional tablets. However, high dose and long term regimen for treatment of oral candidiasis cause disturbances in GI tract and hepatotoxicity (Dollery, 1999). Thus, to minimize the adverse effects and the risk of drug resistance, local delivery of fluconazole is considered.

In fact, fluconazole is a slightly soluble drug (Dollery, 1999; Clarke, 2004), which several methods, such as solid dispersion (Papageorgiou et al., 2008), complexation (Yurtdaş et al., 2011; Li et al., 2016) and micellization (Bhardwaj et al., 2014), are used to enhance water solubility of this drug. Several researchers have developed and evaluated bioadhesive local delivery of fluconazole in the form of films (Yehia et al., 2009; Patel et al., 2015), gels (Suresh and Manhar, 2014) and tablets (Pathak et al., 2016). Polymers, such as chitosan, carbomer, hydroxypropyl methylcellulose, and sodium alginate were used as a matrix-forming agent. However, the use of sodium caseinate as a film matrix of fluconazole is yet unknown. Therefore, it is possible to investigate the use of casein micelles for solubility enhancement of fluconazole. The fluconazole-casein dispersions can be potentially prepared as a continuous film. Furthermore, an immediate drying of the fluconazole-casein dispersion may cause an amorphous form of fluconazole embedded in the matrix of the films, leading to an enhancement of fluconazole dissolution. The casein films may provide a modified-release of fluconazole in mild acidic-neutral pHs (pH of oral cavity). Thus, they may offer a potential use for a localized oral fluconazole delivery. Additionally, characteristics of the fluconazole-loaded casein films may be modified by incorporating clays.

In this research project, casein in the sodium salt, sodium caseinate, will be prepared as a film, which the characteristics of the sodium caseinate films will be modified by using clays, such as magnesium aluminum silicate and halloysite. Aqueous solubility enhancement of fluconazole using various concentrations of sodium caseinate and plasticizer, such as glycerin, will be studied. The sodium caseinate and sodium caseinate-clay films containing fluconazole will be prepared using a spraying method. Film properties, such as surface and internal structure morphologies, thermal behavior, molecular interaction, crystallinity, mechanical properties, water uptake, mucoadhesive properties and drug release, will be examined. Moreover, the surface of the films will be modified by using chitosan for enhance mucoadhesive properties. Microbial activity of fluconazole released from the films will be evaluated as well. The fluconazole films obtained may potentially use as drug delivery systems for oral candidiasis.

Literature review

Sodium caseinate

Caseins are the major milk proteins that compose of 94% protein and 6% colloidal calcium phosphate. There are four different peptide chains: αS_1 -, αS_2 -, β - and κ -caseins in the ratio of 4:1:4:1, which have a difference in phosphorylation and glycosylation (Walstra et al., 2006). Their molecule weights are in the range of 19 and 25 kDa. The average of isoelectric point (pI) of casein is about 4.6 to 4.8. Caseins in the form of acid have a low aqueous solubility, but sodium caseinate, sodium salt of casein, is freely soluble in water except the pH is close to isoelectric point (Elzoghby et al., 2011). Caseins are amphiphilic protein which provide self-association into micelle structures (Neha et al., 2012).

Caseins are proline residues, open-structured and a few cysteine residues (Elzoghby et al., 2011; Neha et al., 2012). β -casein is the most hydrophobic casein which has a large number of proline residues. αS_1 -casein has a high net negative charge and high phosphate content, but αS_2 -casein contains two cysteine residues and no carbohydrate groups. κ -Casein differs from the other caseins. It has two cysteine residues that form intermolecular disulfide bonds (Walstra et al., 2006). The αS_1 -, αS_2 - and β -caseins are precipitated by calcium ion, whereas κ -casein can be soluble in calcium ion (Qi, 2007). The surface of casein micelle is covered with κ -casein providing hydrophilic property and charged surface layer which stabilizes the micelles through intermicellar electrostatic and steric repulsion (Walstra et al., 2006).

Casein micelle characteristics

Amphiphilic molecules are characterized by having two distinct regions of opposing solution affinities within the same molecule. The amphiphilic molecules exist separately when they are present in low concentration medium. As the concentration is increased, aggregation occurs over a narrow concentration range. These aggregations are called micelles. The concentration at which micelles form is termed the critical micelle concentration (CMC).

Casein micelles are composed of four phosphoproteins held together by hydrophobic interaction and by bridging of calcium phosphate nanoclusters. The CMC of casein is reported to be about 1.0 mg/mL. β -casein self-association is the most popular for investigation when compared with other caseins. The CMC for β -casein is determined and found to be 0.05 mg/mL. While β -casein exhibits a micellization behavior similar to β -Casein and the CMC has been determined to be in the range 0.2-0.5 mg/mL (Horne and Euston, 2005). Casein micelles are presented in roughly spherical particles, mostly 50-500 nm in diameter (average about 120 nm) and a molecular mass from 10^6 - 10^9 Da. The particles comprise approximately 10^4 casein molecules. They have negative charge. In the sub-micelle model, the caseins aggregate by hydrophobic interaction into subunits of 15-20 molecules (De Kruif et al., 2012). Some of the properties of casein micelles are summarized in Table 1.

Table 1 Average characteristic of casein micelles (Horne and Euston, 2005)

Characteristic	Value
Diameter	120 nm (range: 50-500 nm)
Surface area	$8 \times 10^{-10} \text{ cm}^2$
Volume	$2.1 \times 10^{-15} \text{ cm}^3$
Density	1.0632 g/cm^3
Mass	$2.2 \times 10^{-15} \text{ g}$
Water content	63%
Molecular weight	$1.3 \times 10^9 \text{ Da}$
Number of peptide chains	10^4
Critical micelle concentration (CMC)	1.0 mg/mL

The core of a micelle consists of roughly equal amounts of αS_1 -, αS_2 - and β -caseins with very little κ -casein, whereas the micelle surface is primarily covered with κ -casein that provides a hydrophilic and charged surface layer, which stabilizes the micelle through intermicellar electrostatic and steric repulsion (Farrell et al., 2006; De Kruif et al., 2012). Furthermore, casein micelles are stabilized by two main factors that a surface zeta potential is approximately -20 mV at pH 6.7 and steric stabilization occurs from the protruding κ -casein layer hairs (Horne and Euston, 2005).

Several years ago, various models of casein micelle assembly and structure have appeared and have been subjected to regular review and appraisal. The subunit model relies on the known preference of the caseins for self-association. The basic of models is the observation that caseins self-assemble and micellar structures even in the absence of calcium ion, they form rather large aggregates. The colloidal calcium phosphate then glues together the protein sub-micelles. It is for these reasons that casein sub-micelles are imagined, which are glued together by the colloidal calcium phosphate (De Kruif et al., 2012). In this sub-micelle model, the caseins firstly aggregate by hydrophobic interaction into subunits of 15-20 molecules each and hold together by colloidal calcium phosphate linkages with a micelle structure covered by κ -casein. The pattern of interaction is such that it brings about a variation in the κ -casein content of these sub-micelles (Farrell et al., 2006).

The most commonly accepted model in the sub-micelle model category is displayed in Figure 1. This model suggests that casein micelles are built of roughly spherical subunits or sub-micelles. The composition of sub-micelles is variable and the size is in range 12-15 nm in diameter, and each sub-micelle has 20-25 casein molecules. The sub-micelles are kept together by hydrophobic interactions between proteins, and by calcium phosphate linkages. There are two main types of sub-micelles; one mainly amount to αS - and β -casein, hydrophobic regions embed in the center of the sub-micelle, another type amount to αS - and κ -casein, which is more hydrophilic because of the sugar residues on κ -casein. The hydrophobic part of the C-terminal end bulging from the micelle surface to form a hairy layer

that avoid further aggregation of sub-micelles by electrostatic and steric repulsion. Therefore, micelles are stable. However, micelle equilibrium is occurred (Figure 2). Those components in rapid equilibrium quickly exchange and yield one result, whereas those slow to equilibrate emphasize another feature. It has also been suggested that calcium binding to caseinates must precede phosphate binding (Qi, 2007).

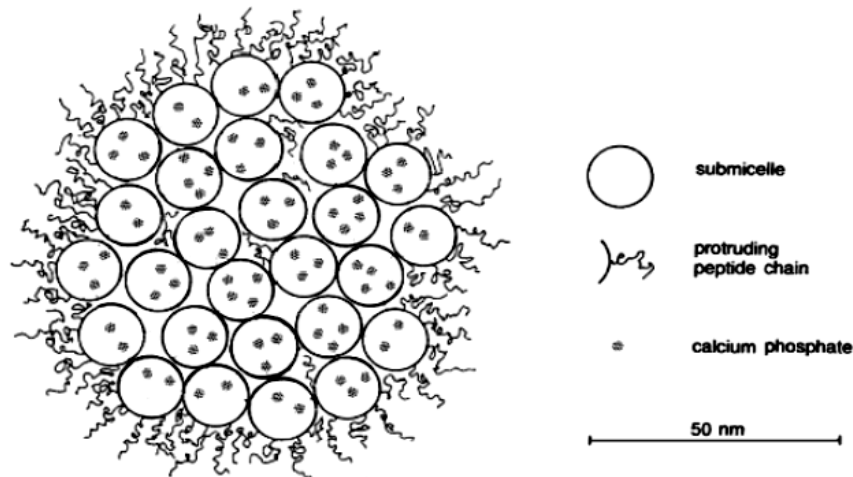


Figure 1. Structure of casein micelle in sub-micelle model (De Kruif et al., 2012).

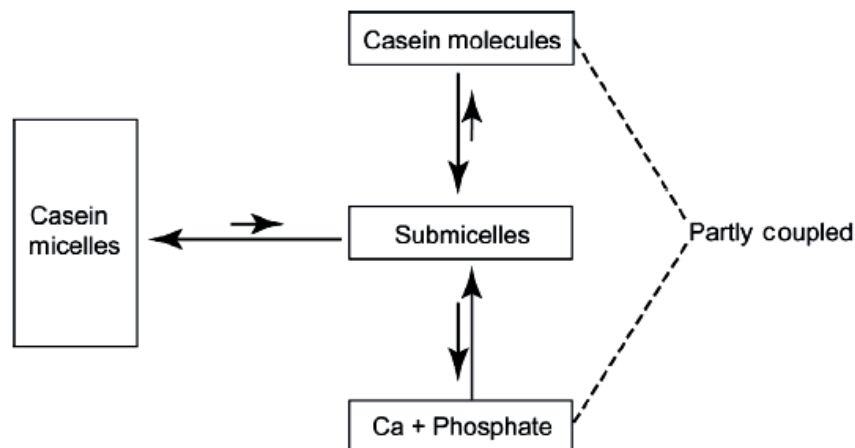


Figure 2. Proposed scheme of the most important dynamic equilibria between casein micelles and milk serum (Qi, 2007).

Factors affecting on casein micelle properties

Food protein networks have the ability to interact with a wide range of active compounds by functional groups of their polypeptides. The casein micelles have a strong trend to aggregate due to entropically driven hydrophobic interactions. Hence, if this steric and repulsive stabilization are damaged, attractive Van der Waals interactions appear and the aggregation of casein micelles occurs. Casein micelle structure is not fixed, but it's dynamic. In various ways, it responds to changes in micellar environment such as pH, temperature and cations (Horne, 2014).

- pH

Caseins are linear protein polymers and therefore the charge distribution both sign and magnitude change with pHs. The isoelectric point of the caseins is around pH 4.6 where they precipitate out of solution (De Kruif et al., 2002). If an acid is added to the caseins, the pH is decreased. This influence changes the environment of the casein micelles in two ways. Firstly, colloidal calcium phosphate in the casein dissolves and forms ionized calcium, which can enter the micelle structure and create strong internal calcium bonds. Secondly, the pH of the solution approaches the isoelectric points of the individual species. These changes initiate within the micelles. The influences of pH are illustrated in Figure 3. In salt solutions, the range for optimal precipitation is pH 4.5 to 4.9. If a large excess of sodium hydroxide is added to the precipitated isoelectric casein, the redissolved casein can be converted into sodium caseinate, partly dissociated into ions (Bylund, 1995).

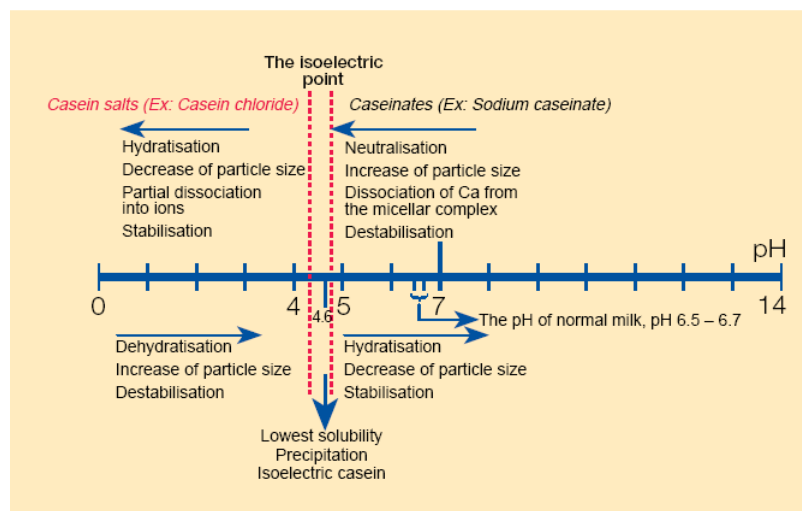


Figure 3. Effect of pH on characteristics of casein dispersion (Bylund, 1995)

Casein micelles are formed at high pH, event at pH 12.0 (Lui and Guo, 2008). Because the strong electrostatic repulsive might lead to the dissociation of casein micelles. The hydrophilic interaction between the hydrophobic fractions of casein molecules still plays an essential role in the self-association of casein molecules, and consequently the formation of casein micelles at higher pH. The radius of casein micelles increases smoothly with pH in the pH range of 6.0 to 12.0. Under pH 3.0, the radius is very similar to that at pH 7.0. In conclusion, casein molecules can self-assemble into casein micelle in pH range of 2.0 to 3.0 and 5.5 to 12.0. In addition to the hydrophobic interaction, hydrogen bond and electrostatic action are the main interactions in the formation of casein micelles that more compact at low pH and looser at high pH.

- Enzymes

Precipitation of casein micelles can be caused by enzymes as well. The amino acid chain of κ -casein comprises 169 amino acids. Many proteolytic enzymes can cleavage the bond between amino acids 105 (phenylalanine) and 106 (methionine), where are easily attack. The soluble amino end contains amino acids 106 to 169, which are dominated by polar amino acids. The remaining part of the κ -casein, consisting of amino acids 1 to 105, is insoluble and remains in the curd together with α S- and β -casein. The splitting of the 105-106 bond in the κ -casein molecules is often called the primary phase of the rennet (proteolytic enzymes) action, whereas coagulation is referred to as the secondary phase. In addition, the secondary phase is strongly affected by the calcium ion concentration and by the condition of micelles with regard to absence or presence of denatured milk serum proteins on the surfaces of the micelles (Bylund, 1995).

- Denaturalizing agents

The stability of casein micelles derives from the layer of κ -casein molecules, extending their C-terminal parts into the solution. The influence of ethanol on the stability of casein micelles was studied by relation between renneting time (times that casein exposed proteolytic enzymes) and ethanol level. The micelles flocculate if the level of ethanol accesses 35 vol%. Ethanol can break the layer of κ -casein and form a weak gel immediately prior to flocculation (De Kruif, 1999).

- Temperatures

Temperature strongly affects properties of caseins. At low temperature, casein can dissociate from micelles and β -casein is the predominant protein released. At high temperature, size of casein micelles increased from aggregation of casein (Lui et al., 2013).

- Cations

Casein can also interact with other macromolecules to form complexes and conjugates with synergistic combinations (Elzoghby et al., 2011). The stability of the casein micelles obtains from the layer of κ -casein molecules. If the layers on the surface are collapsed, the stability of casein is reduced (De Kruif, 1999). Calcium chelators are often used to improve the heat stability of milk products. Chelators shift protein-mineral equilibria lead

to a decrease in the concentration of free calcium ions and deficiency of colloidal of calcium phosphate. This effect causes an increase in repulsion interaction between the negative charged of amino acids in the casein micelles (De Kort et al., 2011). Mechanism of cation association with casein micelles suspended in the aqueous phase of milk has been studied. The association of cations with casein micelle are 82%, 25%, 95%, 52% and 99% for calcium, magnesium, zinc, copper and ferric ion, respectively (Philippe et al., 2005). The order of cation association with micelles is: $\text{Cu}^{2+} > \text{Zn}^{2+} > \text{Ca}^{2+} > \text{Mg}^{2+} > \text{Fe}^{3+}$. These decreases were in agreement with a direct binding of cations to casein and may be formed by electrostatic (Ca^{2+} , Mg^{2+} and Zn^{2+}) or coordination (Fe^{3+} and Cu^{2+}) bonds with oxygen atoms of phosphoserine, aspartyl and glutamyl residues.

Applications of casein micelle for poorly soluble drugs

Casein micelle has a hydrophobic interior of those phosphoproteins held together by hydrophobic interaction whereas the micelle surface is covered by a hydrophilic layer of κ -casein. Thus, casein micelles are used as a natural alternative to synthetic block copolymers for delivery of poorly soluble drugs. But effects of casein micelle on solubility depend on drug loading, casein form, i.e. salt or free acid, and preparation method.

Sodium caseinate can enhance solubility and dissolution of chlorothiazide and hydrochlorothiazide (Millar and Corrigan, 1991). The solubility of chlorothiazide and hydrochlorothiazide in pH 7.4 phosphate buffer increases when increasing sodium caseinate content. Similarly, solubility of hydrochlorothiazide in distilled water relates to increasing sodium caseinate content. Increasing sodium caseinate content has a small change of dissolution rate of chlorothiazide and hydrochlorothiazide in pH 7.4 phosphate buffer. The release profiles of drug from the mixtures are lower than that of pure drug in acidic medium. However, dissolution studies on hydrochlorothiazide/sodium caseinate freeze dried systems are performed in pH 7.4 phosphate buffer. The relative enhancement in dissolution rate from the hydrochlorothiazide/sodium caseinate (25:75 and 50:50) system are about 1.5. The 75/25 system disintegrates very rapidly. Therefore, the process of freeze drying with sodium caseinate has much less effect to hydrochlorothiazide. On the other hand, the release profile of pure drug is lower than that of drug mixtures dried by using freeze-drying because freeze drying process can make molecule of chlorothiazide became to amorphous form. While physical mixture provides crystalline and amorphous forms of chlorothiazide. Thus, freeze drying process increases the dissolution rate of chlorothiazide.

In the case of ibuprofen, the solubility of ibuprofen increases with increasing sodium caseinate concentration (Millar and Corrigan, 1993). The increase in solubility at high sodium caseinate concentration indicates a weak binding of ibuprofen to sodium caseinate. However, ibuprofen release rate decreases with increasing proportion of sodium caseinate. This suggests that the increase in solubility does not seem to be accompanied by an increase in dissolution rate. It appears as if the presence of sodium caseinate has a slight retarding effect on the

dissolution rate of ibuprofen. This may be related to the increased viscosity of diffusion layer of mixed discs, which seem to reduce the diffusion coefficient of ibuprofen.

Sodium caseinate is used as a solubilizer of flutamide, antiandrogen, for intravenous administration (Elzoghby et al., 2013). When flutamide solution (flutamide dissolves in 95% ethanol) is added to aqueous solution, precipitation of flutamide occurs because their poor aqueous solubility. While flutamide solution is added to casein solution, the mix solution become to clear solution. These results indicate that strong hydrophobic interactions lead to association of the drug with the casein micelle. For confirmation, flutamide solubility is increased with increasing casein concentration. The higher concentration of micelles contribute to increase hydrophobic interaction. Spray-drying technique is employed for conversion of flutamide-casein micelle dispersion into solid redispersible micelles with no need for drying adjuvant depending on the stabilizing properties and thermal stability of casein itself. Increasing casein ratio from 1:5 to 1:20 decrease drug release. These results show that casein micelle can not only solubilize the poorly soluble drug, but also sustain drug release. For pharmacokinetic study, the longer half-life and blood residence time of flutamide-loaded casein micelles are the result of a reduced clearance rate. This study suggests that the hydrophobic core of casein micelles can also retain drug concentration in plasma for a long time

Characteristics of sodium caseinate films

Sodium caseinate films are natural materials that are considered for food packaging and applications for pharmaceuticals because of biodegradability and biocompatibility of sodium caseinate (Pereda et al., 2011a). Although synthetic polymers present more benefit than natural polymers, but natural polymers are lesser toxicity than synthetic polymers. In food industry, sodium caseinate films are interesting for food application because they are high nutritional quality and potential to provide food products with suitable protection from their surrounding environment. Besides, appearances of sodium caseinate films are transparent and soft nature. For pharmaceuticals, the most important biodegradable sodium caseinate films are used in controlled drug delivery systems. Sodium caseinate are proteins that have the ability to interact with other molecules via functional group. For example, sodium caseinate can interact with calcium ion to form complexes and lead to improve properties of sodium caseinate (Walstra et al., 2006; Elzoghby et al., 2011).

Moreover, sodium caseinate films are generally prepared by a casting method. However, proteins based films have two major problems: poor mechanical properties and high water sensitivity due to the highly hydrophilic of sodium caseinate (Audic and Chaufer, 2005). Thus, improvement of sodium caseinate films properties is required.

Factors affecting on sodium caseinate films properties

-Effect of plasticizers

Sodium caseinate films prepared without plasticizers are cracked and brittle during drying. So, plasticizers, such as glycerin and sorbitol, are used to improve mechanical properties of protein films, which include an increase of flexibility. Mostly, plasticizers cause an increase in material flexibility by decreasing intermolecular forces between polymer coils. However, the values of tensile strength of the films with glycerin have lower than those of the film with sorbitol. On the other hand, the values of elongation of the films with glycerin have higher than those with sorbitol. Thus, sodium caseinate films with glycerin are more flexible and more stretchable than those with sorbitol (Fabra et al., 2008). This phenomenon can explain that glycerol molecule is smaller than sorbitol molecule and higher hydrophilic part compared to sorbitol. Due to the smaller glycerin molecule, it can easily attach with protein molecules when comparison with sorbitol. Glycerin interacts with protein by hydrogen bonding. Moreover, when increasing glycerol content, water vapor permeability of sodium caseinate films increases (Khwaldia et al., 2004). This suggests that glycerol is hydrophilic molecules which is favorable to adsorption of water molecules, lead to increase water vapor permeability of sodium caseinate films.

Polyols, such as ethylene glycol, and di-, tri- and tetra-ethylene glycol are often used as plasticizers for protein based films (Audic and Chaufer, 2005). Series of ethylene glycol have two hydroxyl groups, and tetra-ethylene glycol has the longest structure in series of ethylene glycol. Increasing repeating unit decreases film strength, but enhances elongation of the films. This suggests that increasing for longer molecules in the ethylene glycol series contributes to plasticizer efficiency by increase in steric of plasticizers to proteins. This can lead to an increase in the sodium caseinate free volume and bring about to improve properties of films. Besides, the sodium caseinate films with low plasticizers contents present poor critical elongation. Elongation at break of sodium caseinate films is depended on plasticizer content, and the best tensile properties of sodium caseinate films is obtained when using 50% plasticizer.

-Effect of crosslinking agents

Aldehydes have been preferred to achieving a stronger polymeric protein structure (Audic and Chaufer, 2005; Perada et al., 2010). Aldehydes, such as formaldehyde and glutaraldehyde, can promote crosslinking with protein by covalent bonds¹¹. Due to properties of glutaraldehyde, it has advantage to react with a large number of available amino groups. Moreover, glutaraldehyde is largely the most generally used owing to high efficiency in the stabilization of protein-based materials and high solubility in aqueous solutions. Glutaraldehyde concentration up to 1.5 wt% can be used for film cross-linking (Bigi et al., 2001). Elastic modulus values and tensile strength enhance when glutaraldehyde content increases. These results are correlated with the increase in covalent bonds formed between the polypeptide chains as the glutaraldehyde content increases. However, the water vapor permeability values increase as the crosslinking content increases. It is suggested that the

increase in permeability with increased concentration of glutaraldehyde influences by the molecular structure between the glutaraldehyde-crosslinked protein chains. This effect can separate the protein molecules through relatively long distances and can decrease intermolecular forces along the protein chains. This lead to an increase free volume and promoting water molecules diffuse through the sodium caseinate films. Then, they are a higher permeability when compared without glutaraldehyde.

-Effect of water insoluble additives

Cellulose fibers, such as carbomethoxy cellulose and cellulose acetate, are attractive as reinforcing fillers in sodium caseinate films due to their good mechanical properties with very high bending strength and stiffness (Perada et al., 2011a, b). Moreover, lipids, for example oleic acid and bee wax, are alternative materials for moisture barrier properties of sodium caseinate film (Fabra et al., 2008). However, incorporation of oleic acid causes a decrease of film strength that the films show more brittle and crack during drying.

Magnesium aluminum silicate (MAS)

MAS is a mixture of colloidal montmorillonite and saponite (Rowe et al., 2006) that has been washed with water to optimize purity and performance and is employed as a pharmaceutical excipient due to its non-toxicity and non-irritation at levels used in drug formulations (Rowe et al., 2006). MAS is composed of three-lattice layers, a central octahedral sheet of aluminum or magnesium and two external silica tetrahedron layers (Alexandre and Dubois, 2000). The silicate layer surface of clay has a negative charge, but weakly positive charges are presented on the edges of the silicate layers. The silicate layers of clay can be separated and form three-dimensional structures when they are hydrated in water. The negatively charged faces bring about a strong electrostatic interaction with amine drugs (Suksri and Pongjanyakul, 2008; Pongjanyakul et al., 2009; Rojtanatanya and Pongjanyakul, 2010), leading to a prolonged release of drug. The positively charged edges of MAS can interact with anionic polymers, such as xanthan gum (Ciullo, 1981), carbomer (Ciullo and Braun, 1991), and sodium alginate (Pongjanyakul et al., 2005b; Pongjanyakul and Puttipipatkachorn, 2007), resulting in viscosity synergism of the composite dispersions. Moreover, hydrogen bonding between MAS and anionic polymers is a crucial mechanism for changing the composite dispersion properties. Furthermore, sodium alginate-MAS films are fabricated for tablet film coating (Pongjanyakul et al., 2005a) and buccal drug delivery (Pongjanyakul and Suksri, 2009).

MAS can also interact with a positively charged polysaccharide, such as chitosan, resulting in an improvement of rheology of composite dispersions and a formation of positively charged flocculates (Khunawattanakul et al., 2008). The chitosan-MAS composite films are successfully prepared and characterized (Khunawattanakul et al., 2010). The mechanical properties, particularly % elongation, of the chitosan films can be improved by nanocomposite formation of chitosan and MAS. Additionally, the chitosan-MAS films provide lower drug permeability than chitosan films. In addition, the chitosan-MAS films also

show a sustained-release pattern of nicotine for buccal delivery (Pongjanyakul et al., 2013). Recently, chitosan microparticles added with MAS are prepared by a spray-drying method. The chitosan-MAS microparticles display better flowability than the chitosan microparticles, and offer to use as a matrix forming agent for sustaining drug release (Khlisuwan and Pongjanyakul, 2015).

Halloysite

Halloysite is a hydrated polymorph of kaolinite. It has a tubular morphology in nanoscale (2–50 nm). It is consisting of the oxygen-sharing tetrahedral SiO_4 sheet and the adjacent octahedral AlO_6 sheet in the 1:1 and this layer has been wrapped to a tubular structure. Generally, tubular halloysite is approximately 0.02–30 μm long and has an external diameter of 30–190 nm and an internal diameter of 10–100 nm (Tan et al., 2013). The nano-sized tubular structure of halloysite makes it suitable for use as an adsorbent for pollutant (Zhao and Liu, 2008), an additive for polymer nanocomposites (Hedicke-Höchstötter et al., 2009), and a carrier for sustaining drug release. It can be used as a drug carrier for furosemide, dexamethasone, nifedipine, and ibuprofen because the surface hydroxyl groups and external surface siloxane (Si–O–Si) groups of halloysite have weak interactions with guest molecules through hydrogen bonding or Van der Waals forces (Aguzzi et al., 2007). Due to the weak interaction between halloysite and drugs, a low drug loading capacity (5 mass%) is found. Moreover, the advantages of the use of halloysite are a high level of biocompatibility and low cytotoxicity. In addition, halloysite has been also used to modify characteristic of polymeric films (Liu et al., 2012; Oiao et al., 2012; He et al., 2012) and to combine with polymeric films for controlled-release of drug (Wang et al., 2010).

Fluconazole

Fluconazole is a triazole antifungal drug that acts by inhibition of the ergosterol component of the fungal cell membrane. It is active against a broad spectrum of yeast and other fungal pathogens and is available for both oral and parenteral use (Dollery, 1999). Fluconazole has molecular weight of 306.3 Da. It shows a slightly soluble drug with pK_a of 2.03 (Clarke, 2004). The solubility of fluconazole in water was reported to be 5 mg/mL (Park et al., 2010). Thus, many researchers investigated the methods for enhancement fluconazole solubility. Several approaches, such as solid dispersion with polymers (Papageorgiou et al., 2008), complexation with cyclodextrins (Yurtdaş et al., 2011; Li et al., 2016) and micellization using surfactants (Bhardwaj et al., 2014), are used to enhance water solubility of this drug.

Oral candidiasis caused by *Candida albicans* is the most common opportunistic fungal infection in human immunodeficiency virus-infected patients and other immunocompromised hosts. (Pelletier et al., 2000). The current treatment regimen for this infection is clotrimazole lozenges or torches, which is available in Thailand. However, the use of clotrimazole is discontinued because the relapses of oral candidiasis in the patients

usually occur that may be an emergence of resistance to this drug ((Pelletier et al., 2000). For this reason, other antifungal agent, such as fluconazole, is alternative drug for use in this disease. Fluconazole used clinically for the treatment of oral candidiasis is commercially available as oral conventional tablets. However, high dose and long term regimen for treatment of oral candidiasis cause disturbances in GI tract and hepatotoxicity (Dollery, 1999). Thus, local delivery of fluconazole is considered to minimize the adverse effects and the risk of drug resistance. Moreover, minimum inhibitory concentration of fluconazole for *C. albicans* is reported in the range of 2-16 µg/ml (Rathod et al., 2012), which is low concentration of drug. For these reasons, local fluconazole delivery systems have been prepared and evaluated, such as films (Yehia et al., 2009; Patel et al., 2015), gels (Suresh and Manhar, 2014) and tablets (Pathak et al., 2016). Polymers, such as chitosan, carbomer, hydroxypropyl methylcellulose, and sodium alginate were used as matrix- or film-forming agents.

Surface modification of drug delivery system by polymers

Surface modification of drug delivery systems can be performed in order to improve some properties such as biocompatibility (Cai et al., 2002) and mucoadhesion (Surassmo et al., 2015). Carbopol, an anionic polymer, has been used to modify the surface of poly (lactic-co-glycolic acid) nanoparticles, leading to an enhancement of the mucoadhesion between nanoparticles and mucin particles (Surassmo et al., 2015). Chitosan, a positively charged biopolysaccharide, is widely used to modify the surface of drug delivery systems for improving mucoadhesive properties because it can interact with a negatively charged mucin on mucosa, indicative of good mucoadhesive properties (Grabovac et., 2005). Surface-modified films show good affinity with cells and promote cell proliferations (Cai et al., 2002; Cai et al., 2008). Moreover, chitosan adsorbed on the surface of microparticles can enhance mucoadhesive properties and increase drug permeation across mucosa (Kanjanaakawinkul et al., 2013).

From these reviews, it is known that the basic knowledge about the preparation and characterization of sodium caseinate films blended with MAS or halloysite are not available in the literatures. Due to micellar solubilization and film-forming agent of sodium caseinate, it may enhance fluconazole solubility and use for preparing a film containing fluconazole. It is possible to prepare and evaluate the fluconazole films surface modified with chitosan. And the sodium caseinate and sodium caseinate-clay films in this study may have a strong potential to use for fluconazole delivery in oral cavity.

Objectives of this study

General objective

- To investigate physicochemical properties and application of sodium caseinate or sodium caseinate-clay composite films containing fluconazole for local delivery of oral candidiasis.

Specific objective

- To study effect of clays on characteristics of sodium caseinate films.
- To prepare and evaluate fluconazole-loaded films using sodium caseinate and sodium caseinate-clay composites as film-forming agents.
- To prepare and characterize surface-modified fluconazole-loaded films using chitosan.

บทคัดย่อ

รหัสโครงการ: BRG6080016

ชื่อโครงการ: การศึกษาคุณลักษณะของฟิล์มผสมโซเดียมเคซีเนต-เคลย์สำหรับการนำส่งฟลูโคนาโซลเฉพาะที่
ในแคนติติเอซิสช่องปาก

ชื่อนักวิจัย: ศ.ดร. ธเนศ พงศ์จรรยากุล คณะเภสัชศาสตร์ มหาวิทยาลัยขอนแก่น

E-mail Address: thaned@kku.ac.th

ระยะเวลาโครงการ: 15 พฤษภาคม 2560 – 14 พฤษภาคม 2562

วัตถุประสงค์ของงานวิจัยนี้เพื่อศึกษาคุณลักษณะฟิล์มผสมของโซเดียมเคซีเนตและเคลย์ เช่นแมกนีเซียมอะลูมิเนียมซิลิเกตและฮัลลอยไซต์ เพื่อประโยชน์ทางเภสัชกรรม และเพื่อเตรียมและประเมินฟิล์มฟลูโคนาโซลโดยใช้สารผสมโซเดียมเคซีเนต-เคลย์เป็นสารก่อเมทริกซ์ นอกจากนี้ ฟิล์มโซเดียมเคซีเนตที่เติมฟลูโคนาโซลที่ดัดแปรผิวด้วยไคโตแซนก็ทำการศึกษาด้วย ผลการทดลองพบว่าหมู่เอไมด์และอะมิโนของโซเดียมเคซีเนตสามารถเกิดอันตรกิริยากับหมู่ไฮดรอกซิลของเคลย์โดยพันธะไฮโดรเจน เคลย์ที่เติมสามารถเพิ่มเสถียรภาพด้านความร้อนให้กับฟิล์มโซเดียมเคซีเนต ความต้านแรงเจาะและการยืดของฟิล์มโซเดียมเคซีเนตลดลงเมื่อเพิ่มอัตราส่วนของเคลย์ในสภาวะแห้ง ในทางตรงกันข้าม การเพิ่มอัตราส่วนเคลย์ทำให้ความต้านแรงเจาะมากขึ้นในฟิล์มเปียกด้วยตัวกลางกรด ฟิล์มโซเดียมเคซีเนต-เคลย์ไม่ได้ยับยั้งการซึมผ่านของไอน้ำอย่างชัดเจน แต่การซึมผ่านและสัมประสิทธิ์การแพร่ของยาในสภาวะกรดลดลงเมื่อเพิ่มอัตราส่วนของเคลย์ ยิ่งไปกว่านั้น สารกระจายโซเดียมเคซีเนต-เคลย์สามารถใช้เป็นวัสดุเคลือบฟิล์มยาเม็ดสำหรับการดัดแปรการปลดปล่อยยา ฟิล์มโซเดียมเคซีเนต-เคลย์ที่บรรจุฟลูโคนาโซลสามารถเตรียมได้ด้วยวิธีการพ่น การผสมเคลย์สามารถเพิ่มเพิ่มเสถียรภาพด้านความร้อนและคุณสมบัติเชิงกลของฟิล์ม นอกจากนี้ ฟิล์มสามารถปลดปล่อยยาช้าลงเมื่อเปรียบเทียบกับฟิล์มที่ไม่มีเคลย์เนื่องจากฟิล์มมีโครงสร้างที่แน่นขึ้น ฟลูโคนาโซลในฟิล์มมีพหุสัณฐานที่แตกต่างจากผงฟลูโคนาโซล แสดงให้เห็นการเปลี่ยนแปลงสัณฐานของยาเมื่อมีการก่อผลึกอีกครั้งในระหว่างการเตรียมฟิล์ม อย่างไรก็ตาม ฟิล์มโซเดียมเคซีเนต-เคลย์ที่บรรจุฟลูโคนาโซลยังคงมีฤทธิ์ต้านเชื้อราและมีคุณสมบัติการยึดติดเยื่อเมือก ฟิล์มสองชั้นโซเดียมเคซีเนต-ไคโตแซนที่บรรจุฟลูโคนาโซลแสดงการปลดปล่อยยาช้าลงเมื่อเทียบกับฟิล์มโซเดียมเคซีเนต เพราะการเกิดอันตรกิริยาของโซเดียมเคซีเนตกับไคโตแซนด้วยพันธะไฮโดรเจน โครงสร้างที่ซับซ้อนของฟิล์มสองชั้นทำให้ฟิล์มแข็งแรงขึ้นและยังมีคุณสมบัติยึดติดเยื่อเมือก ด้วยยาที่ปลดปล่อยออกจากฟิล์มสองชั้นยังคงมีฤทธิ์ต้านเชื้อแคนดิดา การศึกษานี้แสดงให้เห็นว่า ฟิล์มโซเดียมเคซีเนต-เคลย์และฟิล์มสองชั้นโซเดียมเคซีเนต-ไคโตแซนมีศักยภาพดีสำหรับใช้เป็นระบบนำส่งแบบใหม่สำหรับยาต้านเชื้อราในการรักษาแคนติติเอซิสช่องปาก

คำสำคัญ: โซเดียมเคซีเนต, เคลย์, ฟลูโคนาโซล, ฟิล์ม, ไคโตแซน

Abstract

Project Code: BRG6080016

Project Title: Characterization of sodium caseinate-clay composite films for local fluconazole delivery in oral candidiasis

Investigator: Prof.Dr. Thaned Pongjanyakul, Faculty of Pharmaceutical Sciences, Khon Kaen University

E-mail Address: thaned@kku.ac.th

Project Period: 15 May 2017 – 14 May 2019

The objectives of this work were to characterize the composite films of sodium caseinate (SC) and clays, such as magnesium aluminum silicate (MAS) and halloysite (HS), for pharmaceutical uses and to prepare and evaluate fluconazole (FZ) films by using the SC-clay composite as a matrix former. Moreover, the FZ-loaded SC films surface modified by chitosan (CS) were also investigated. The results showed that the amide and amino groups of SC could molecularly interact with the hydroxyl groups of clays via hydrogen bonding. Clays added could enhance thermal stability of the SC films. The puncture strength and elongation of the SC films decreased with increasing clay ratios in the dry state. On the other hand, increasing clay ratios caused an increase of puncture strength of the wet films in acidic medium. The SC-clay films did not obviously retard the water vapor permeation, but the drug permeability and diffusion coefficient across the films in acidic medium remarkably decreased when increasing clay ratios. Furthermore, the SC-clay dispersions could be employed as a film coating material for modifying drug release. The SC-clay films containing FZ could be prepared using a spray method. Incorporation of clay can enhance thermal and mechanical properties of the films. Besides, the FZ-loaded SC-clay films presented slower release when compared with the film without clay due to denser structure of the films. The FZ in the films showed the different polymorphism when compared with FZ powder, suggesting the polymorphism change of FZ during recrystallization in film preparation. However, the FZ-loaded SC-clay films still possessed antifungal activity and mucoadhesive property. The SC-CS bilayer film added with FZ showed slower drug release when compared with the SC films because SC and CS are able to form the molecular interaction via hydrogen bonding. The complex structure of the SC-CS bilayer film could enhance the strength of the films, and also provided good mucoadhesive properties. The FZ released from the SC-CS bilayer films still had an anticandidal activity. These findings suggested that the SC-clay films and the SC-CS bilayer films have a good potential for use as a novel delivery system for antifungal drug in treatment of oral candidiasis.

Keywords (3-5 words) sodium caseinate, clay, fluconazole, film, chitosan

Executive summary

การดัดแปรวัสดุทางเภสัชกรรมมีการทำวิจัยมากขึ้นเพื่อให้วัสดุผสมสามารถใช้งานตามวัตถุประสงค์ที่ต้องการ คุณสมบัติเคมีฟิสิกส์เชิงกลและการซึมผ่านของยาของเมทริกซ์พอลิเมอร์สามารถดัดแปรได้โดยการเติมเคลย์ เคซีนเป็นโปรตีนที่ได้จากน้ำนม สามารถใช้เป็นสารก่อเมทริกซ์และสารช่วยละลายโดยการเกิดไมเซลล์ ในงานวิจัยนี้ได้ใช้โซเดียมเคซีเนตซึ่งเป็นเกลือโซเดียมของเคซีนมาใช้ในการก่อฟิล์มเมทริกซ์และดัดแปรคุณสมบัติโดยการเติมเคลย์เพื่อใช้เป็นสารเคลือบฟิล์มยาเม็ดและเตรียมเป็นระบบนำส่งฟลูโคนาโซลเพื่อใช้เฉพาะที่ในการรักษาแคนดิดิเอซิสช่องปาก ผลการทดลองพบว่าหมูเอไมด์และอะมิโนของโซเดียมเคซีเนตสามารถเกิดอันตรกิริยากับหมูไฮดรอกซิลของเคลย์โดยพันธะไฮโดรเจน เคลย์ที่เติมสามารถเพิ่มเสถียรภาพด้านความร้อนและเปลี่ยนแปลงคุณสมบัติเชิงกลของฟิล์มโซเดียมเคซีเนต ความต้านแรงเจาะและการยืดของฟิล์มโซเดียมเคซีเนตแห้งลดลงเมื่อเพิ่มอัตราส่วนของเคลย์ ขณะที่การเพิ่มอัตราส่วนเคลย์ทำให้ความต้านแรงเจาะมากขึ้นในฟิล์มเปียกด้วยตัวกลางกรด ฟิล์มโซเดียมเคซีเนต-เคลย์สามารถลดอัตราการซึมผ่านและสัมประสิทธิ์การแพร่ของยาในสภาวะกรดเมื่อเพิ่มอัตราส่วนของเคลย์ ยิ่งไปกว่านั้น ฟิล์มโซเดียมเคซีเนต-เคลย์สามารถเคลือบยาเม็ดและชะลอการปลดปล่อยยาได้ โดยขึ้นกับอัตราส่วนของเคลย์และความหนาของฟิล์มเคลือบ ฟิล์มโซเดียมเคซีเนต-เคลย์ที่บรรจุฟลูโคนาโซลสามารถปลดปล่อยยาช้าลงเมื่อเปรียบเทียบกับฟิล์มที่ไม่มีเคลย์และฟลูโคนาโซลในฟิล์มมีพหุสัณฐานที่แตกต่างจากผงฟลูโคนาโซล แสดงให้เห็นการเปลี่ยนแปลงสัณฐานของยาเมื่อมีการก่อผลึกอีกครั้งในระหว่างการเตรียมฟิล์ม อย่างไรก็ตาม ฟิล์มโซเดียมเคซีเนต-เคลย์ที่บรรจุฟลูโคนาโซลยังคงมีฤทธิ์ต้านเชื้อราและมีคุณสมบัติการยึดติดเยื่อเมือก ฟิล์มสองชั้นโซเดียมเคซีเนต-โคโตแซนที่บรรจุฟลูโคนาโซลมีความแข็งแรงเพิ่มขึ้นและยังมีคุณสมบัติยึดติดเยื่อเมือก การปลดปล่อยยาจากฟิล์มสองชั้นสามารถควบคุมได้ดีขึ้นเมื่อเทียบกับฟิล์มโซเดียมเคซีเนตและตัวยาที่ปลดปล่อยออกจากฟิล์มสองชั้นยังคงมีฤทธิ์ต้านเชื้อราแคนดิดา ผลลัพธ์ของการศึกษานี้ คือ การได้องค์ความรู้พื้นฐานของการเกิดอันตรกิริยาระดับโมเลกุลระหว่างโซเดียมเคซีเนตและเคลย์ และนำมาซึ่งความรู้ใหม่ของคุณสมบัติของฟิล์มผสม นอกจากนี้ ยังได้ต้นแบบของยาเม็ดเคลือบฟิล์มผสมที่สามารถเตรียมได้ด้วยเครื่องมือจำลองในระดับอุตสาหกรรมยา และฟิล์มผสมสามารถใช้ประโยชน์ในการดัดแปรรูปแบบการปลดปล่อยยาฟลูโคนาโซลสำหรับการนำส่งเฉพาะที่ในการรักษาแคนดิดิเอซิสช่องปาก

Contents

	Page
บทคัดย่อ	i
Abstract	ii
Executive summary	iii
Contents	iv
Introduction	1
Literature review	3
Objective of this study	14
Methodology, results and discussion	
Part I: Sodium caseinate-magnesium aluminum silicate films	15
Part II: Sodium caseinate-halloysite films	39
Part III: Sodium caseinate-clay films containing fluconazole	56
Part IV: Sodium caseinate-chitosan bilayer films containing fluconazole	74
<u>Additional work</u>	
Part V: Alginate-sodium caseinate beads for anticandidal delivery	93
Part VI: Alginate-starch beads for drug delivery	113
Conclusions	130
References	131
Outputs	136
Appendix	138

Part I: Sodium caseinate-magnesium aluminum silicate films

1. Introduction

Thin film technology is very important for pharmaceutical manufacturing, for example film coating for masking the unpleasant taste and odor of drugs, and for sustaining drug release in tablets (Nagai et al., 1997). The films loaded with drugs have been used as drug delivery systems (Karki et al., 2016). Furthermore, the application of thin films is extended to food industry, which they are developed and used for food packaging and wrapping. Natural polymers have been widely employed for these purposes because of their biocompatibility and biodegradability. Polysaccharides, such as chitosan, have been used in tablet film coatings (Nunthanid et al., 2002) and food packaging (Van Den Broek et al., 2015; Cazón et al., 2017). In addition, protein-based films, which were prepared from gelatins (Nur Hanani et al., 2014) and caseins (Bonnaillie et al., 2014), have been applied as a packaging material. Moreover, casein film coatings for fruits show a minimum lose of weight and juice level during storage under ambient conditions (Alam and Paul, 2001).

Caseins, biomacromolecules from milk, are composed of 94% protein and 6% colloidal calcium phosphate (Walstra et al., 2006). Their molecule weights are in the range of 19 and 25 kDa. The average of isoelectric point of caseins is about 4.6 to 4.8. Caseins in an acidic form (casein salt) have a low aqueous solubility, but sodium caseinate (SC), sodium salt of casein, is freely soluble in water except the pH is close to isoelectric point (Elzoghby et al., 2011). Because SCs have distinct hydrophobic and hydrophilic domains, self-assemble into stable micellar structures in aqueous solutions can be formed when their concentration are higher than critical micelle concentration, 1.0 mg mL^{-1} (Horne and Euston, 2005). For this characteristic, SCs are used as emulsifying and foaming agents in food industry. Furthermore, they have been pharmaceutically applied as a solubilizing agent for poorly soluble drugs (Millar and Corrigan, 1991; Millar and Corrigan, 1993). SCs also have a potential use as drug delivery systems, particularly beads (Bani-Jaber et al., 2009), microparticles (Knepp et al., 1993; Magee et al., 1993; Santinho et al., 1999) and nanoparticles (Elzoghby et al., 2013a, 2013b; Pan et al., 2013, 2014).

One of the crucial properties of SC is a film forming agent. It can be used for tablet film coatings (Abu Diak et al., 2007; Elzoghby et al., 2011) and food packaging (Bonnaillie et al., 2014). Unfortunately, the SC films have the disadvantages about mechanical properties and water vapor permeability (Wihodo and Moraru, 2013). Therefore, it is necessary to modify the film properties of SC by adding plasticizers, such as glycerin and sorbitol (Khwaldia et al., 2004; Audic and Chaufer, 2005), cross-linking agents, such as aldehydes (Audic and Chaufer, 2005; Perada et al., 2010) and water insoluble additives such as fatty acid and wax (Fabra et al., 2008), and celluloses (Perada et al., 2011a, 2011b). Among them, the addition of water-insoluble substances is the interesting approach to modify physicochemical, mechanical, permeability properties of the SC films. From the literature reviews, clays have been potentially used to modify the polymeric film properties and molecular interaction between

polymer and clay can create a new type of films that so called nanocomposite materials (Khunawattanakul et al., 2010; Rongthong et al., 2013; Shakil et al., 2017). Thus, it is interesting that incorporation of clays may improve SC film properties for using in pharmaceutical film coating.

Montmorillonite clay, magnesium aluminum silicate (MAS), is employed as a pharmaceutical excipient due to its non-toxicity and non-irritation at levels used in drug formulations (Rowe et al., 2006). MAS is composed of many silicate layers, which each silicate layer consists a central octahedral sheet of aluminum or magnesium and two external silica tetrahedron layers (Alexandre and Dubois, 2000). The silicate layers of MAS can be separated when hydrated with water, and the silanol groups (-SiOH) on the surface of the silicate layers show a negative charge that bring about a strong electrostatic interaction with a positively charged polymer, such as chitosan (Khunawattanakul et al., 2008). Moreover, the silanol groups can interact with anionic polymers, such as xanthan gum (Ciullo, 1981), carbomer (Ciullo and Braun, 1991), and sodium alginate (Pongjanyakul et al., 2005; Pongjanyakul 2009), via hydrogen bonding. Molecular interaction of polymeric molecules and MAS can possibly create two types of nanocomposites (Alexandre and Dubois, 2000). The first is an exfoliated nanocomposites that the silicate layers of MAS can be completely dispersed in the polymer's matrix. The latter is an intercalated nanocomposites that the space between two silicate layers of MAS can be inserted by polymeric molecules. The formation of nanocomposites had a significant influence on the key properties of the films, resulting in decreased water absorption, swelling and drug permeability when compared to native polymeric films (Khunawattanakul et al., 2010).

Therefore, the aims of this work were to prepare and investigate the SC films incorporated with MAS for use in tablet film coating. The composite dispersions with various SC-MAS ratios were prepared using a simple mixing. The particle size and zeta potential of the dispersed phase as well as the viscosity of the dispersions were determined before film casting. Film properties, such as thermal behavior, crystallinity, mechanical properties, water uptake and erosion, and water vapor and drug permeabilities were characterized. Molecular interaction and nanocomposite formation between SC and MAS were also examined. Additionally, the SC-MAS dispersions were evaluated as a film coating material. Film morphology, water uptake and drug release of the coated tablets were investigated as well.

2. Materials and methods

2.1. Materials

SC (sodium salt from bovine milk) and MAS in granular form (Veegum[®] HV) were purchased from Sigma-Aldrich Company (St. Louis, MO) and R.T. Vanderbilt Company, Inc. (Norwalk, CT), respectively. Glycerin and acetaminophen was obtained from Namsiang Co., Ltd. (Bangkok, Thailand) and Pharma Thai Co., Ltd. (Bangkok, Thailand), respectively. Spray-dried lactose (Flowlac[®]100, Thai Meochems Co., Ltd., Bangkok, Thailand), Microcrystalline cellulose (Ceolus[®] PH102, SiamChem-Pharm (1997) Co., Ltd., Bangkok,

Thailand), magnesium stearate (Mallinckrodt Inc., USA), and colloidal silicon dioxide (Aerosil® 200, Degussa, Japan) were used for preparing core tablets. All other reagents were of analytical grade and were used as received.

2.2. Preparation of SC-MAS dispersion

SC (5 g) was dispersed in 80 mL of distilled water. MAS (0, 0.25, 0.5, or 1 g) was dispersed in a hot water (10 mL), and then the MAS dispersion was mixed with the SC dispersion to get a SC-MAS ratios of 1:0, 1:0.05, 1:0.1, or 1:0.2 by weight, respectively. pH of the SC and SC-MAS dispersions was adjusted to 6.8 using 0.1 M HCl or 0.1 M NaOH. All dispersions were adjusted to the final volume (100 mL) using distilled water prior to testing. Additionally, MAS dispersion (1 %w/v) at pH 6.8 was also prepared and examined for comparison.

2.3. Characterization of SC-MAS dispersion

2.3.1. Particle size determination

The particle size of the MAS and SC-MAS dispersions was measured by using a laser diffraction particle size analyzer (Mastersizer2000 Model Hydro2000SM, Malvern Instrument Ltd., UK). The dispersions were dispersed in 70 mL of distilled water in a small volume of sample dispersion unit, and stirred at a rate 50 Hz for 30 s before measurement. The volume weighted mean diameters were determined and reported.

2.3.2. Zeta potential measurement

The zeta potential of the dispersions was measured using a laser Doppler electrophoresis analyzer (Zetasizer Model ZEN 2600, Malvern Instrument Ltd., UK). Temperature of the samples was controlled at 25 °C. The dispersions were diluted to obtain appropriate concentrations (count rates >20,000 counts s⁻¹) prior to the measurements.

2.3.3. Viscosity determination

The viscosity of the dispersions was determined using a Brookfield digital rheometer (Model DV-III, Brookfield Engineering Laboratories Inc., Middleboro, MA, USA). The small sample adaptor with spindle no.31 was used. Temperature of the dispersions was controlled at 35.0 ± 1.0 °C. The single point viscosity of the dispersions at a shear rate of 20.40 s⁻¹ was reported.

2.4. Preparation of SC-MAS films

SC and SC- MAS films were prepared by using a casting/solvent evaporation method. SC (5 g) was dispersed in 80 mL of distilled water, and glycerin (30% w/w based on SC content) used as a plasticizer was added into the SC dispersion. MAS (0, 0.25, 0.5, 1, or 2.5 g) was dispersed in a hot water (10 mL), and the MAS dispersion was mixed with the SC dispersion to get a SC-MAS ratios of 1:0, 1:0.05, 1:0.1, 1:0.2, or 1:0.5 by weight, respectively. pH of the SC and SC-MAS dispersions was adjusted to 6.8 using 0.1 M HCl or 0.1 M NaOH. All dispersions were adjusted to the final volume (100 mL) using distilled water and stirred for 30 min at room temperature (27 ± 2 °C). After that, 20 mL of the SC and SC-MAS dispersions was casted onto a plastic mold (6.0 cm × 9.5 cm), and dried at 60 °C for 24 h. The dry films were peeled off and kept in desiccators prior to characterization.

2.5. Characterization of SC-MAS films

2.5.1. Thickness determination

Thickness of the dry and wet films was measured at different places using a microprocessor coating thickness gauge (Minitest600B, ElektroPhysik, Germany). The dry films were cut and placed on a control plate. The probe, which had been connected to the measurement gauge and calibrated using a standard film, gently moved down-ward to touch the film, and the film thickness was then measured. To determine the film thickness in wet state, the films were subsequently placed in a small beaker containing 0.1 M HCl or pH 6.8 phosphate buffer, which was shaken occasionally in a water bath at 37.0 ± 0.5 °C for 5 min. The samples were taken and blotted to remove excess water. The thickness of the wet films was immediately determined following the procedure mentioned above.

2.5.2. SEM and DSC studies

Surface and film matrix morphologies of the films were observed by scanning electron microscopy (SEM). The films and cross-sections of films were mounted onto stubs, coated with gold in a vacuum evaporator, and investigated using scanning electron microscope (Hitachi S-3000N, Tokyo, Japan). The thermal behavior of the films was investigated using differential scanning calorimetry (DSC). The DSC thermogram of the samples was recorded using a differential scanning calorimeter (DSC822°, Mettler Toledo, Switzerland). An accurately weighed sample (2.5-3.5 mg) was placed into a 40- μ l aluminum pan without an aluminum cover. The measurements were taken over a temperature range of 30-450 °C at a heating rate of 10 °C min⁻¹.

2.5.3. Molecular interaction studies

Molecular interaction between SC and MAS in the SC-MAS films were investigated using FTIR spectroscopy (Spectrum One, Perkin Elmer, Norwalk, CT) and KBr disc method. All films were crashed and triturated with KBr powder and then pressed with 10 tons of a hydrostatic press for 10 min. The samples were placed in a sample holder and scanned from 4000 to 450 cm⁻¹ at the resolution rate of 4 cm⁻¹. Nanocomposite formation and crystallinity of the SC-MAS films were studied by a powder X-ray diffractometry (PXRD) using Cu α radiation generated at 40 kV and 40 mA as the X-ray source, an angular of 2-30 °2 θ and a step angle of 0.02 °2 θ s⁻¹ (Bruker D8 Advance diffractometer, Bruker BioSpin AG, Germany). The thickness of the silicate MAS layers was calculated using Bragg's equation:

$$n\lambda = 2d \sin \theta \quad \text{Eq. 1}$$

where n is 1 (the first order reflection was used), λ is the X-ray wavelength (1.54 Å), θ is the angle of the basal spacing peak of MAS, and d is the thickness of the MAS silicate layer.

2.5.4. Determination of mechanical properties

Mechanical properties of the films including puncture strength and elongation were investigated by using a texture analyzer (TA-XT2, Stable Micro system, Ltd., UK) equipped with a 500 N load cell. In dry condition, the films (2 × 2 cm) were cut and kept in a chamber with 55% RH at room temperature (27.0 ± 2.0 °C) for 3 days before testing. In wet condition, the films were cut and shaken in 0.1 M HCl or pH 6.8 phosphate buffer for 5 min. After that,

the excess water of the wet films was removed by a filter paper. Dry and wet films were fixed using a film holder between two mounting plates. A 5 mm diameter spherical stainless puncturing probe was fixed at the load cell and moved downwards at 0.1 mm s^{-1} . The applied force and displacement were recorded. The puncture strength and %elongation at break were calculated as follows (Rongthong et al., 2013):

$$\text{Puncture strength} = \frac{F}{A} \quad \text{Eq. 2}$$

where F is the maximum force for puncture, A is the cross-sectional area of the edge of the films located in the path of cylindrical opening of the film holder.

$$\text{Elongation (\%)} = \frac{\sqrt{r^2 + D^2} - r}{r} \times 100 \quad \text{Eq. 3}$$

where r is radius of the film exposed in the cylindrical hole of the film holder and D is the displacement of the probe from the point of contact to the point of film puncture.

2.5.5. Water vapor permeability studies

Discs were punched from the films, placed on open 5-mL glass vials containing 3.5 g silica gel beads and held in place with a screw lid having a test area of 0.58 cm^2 . The vials were placed in a dessiccator containing a saturated aqueous sodium chloride solution (75% RH). The dessiccator was kept in a room temperature ($26.0 \pm 2.0 \text{ }^\circ\text{C}$) with $50 \pm 2\%$ RH. The weight change of the vials was recorded periodically over 72 h. The WVP rate was obtained from the slope of relationship between the amount of water vapor permeated and time. The WVP coefficient of the films was calculated using the following equation (Pongjanyakul et al., 2005):

$$\text{WVP coefficient} = \frac{Mh}{A\Delta P_v} \quad \text{Eq. 4}$$

where M is the WVP rate, h is the mean thickness of the film, A is the area of the exposed film, and ΔP_v is the vapor pressure difference.

2.5.6. Water uptake and erosion studies

Water uptake and erosion of the films were investigated using a gravimetric method. Films ($1.5 \text{ cm} \times 1.5 \text{ cm}$ size) were weighed (W_0) and then soaked in 0.1 M HCl that had been incubated at $37.0 \pm 0.5 \text{ }^\circ\text{C}$ and shaken occasionally. After a predetermined time interval, each film was withdrawn, blotted to remove excess water, immediately weighed (W_t), and then dried in a hot air oven at $50 \text{ }^\circ\text{C}$ to constant weight (W_d). The water uptake and erosion can be calculated from the following equation (Tuovinen et al., 2003; Pongjanyakul, 2009):

$$\text{Water uptake (\%)} = \frac{W_t - W_d}{W_d} \times 100 \quad \text{Eq. 5}$$

$$\text{Erosion (\%)} = \frac{W_0 - W_d}{W_0} \quad \text{Eq. 6}$$

2.5.7. Drug permeability studies

Acetaminophen permeability across the films was investigated by using a side-by-side diffusion cell. The donor and acceptor compartments had a volume of 3 mL each; the film surface area for drug diffusion was 0.66 cm^2 . The permeation fluid was 0.1 M HCl and temperature was controlled at $37 \text{ }^\circ\text{C}$. The films were cut into circular pieces and gripped

between donor and receptor compartment. Acetaminophen in the concentration of 4 mg mL⁻¹ (3 mL) was filled into the donor compartment and 3 ml of medium was placed in receptor compartment. Both compartments were continuously stirred throughout the tests. At predetermined intervals, 2.7 mL of medium in the receptor compartment was collected and replaced with an equal volume of fresh medium. The amount of acetaminophen in the collected samples was measured by UV-visible spectrophotometer (Shimadzu UV1201, Japan) at a wavelength of 265 nm, respectively.

Drug permeation through the films was determined under steady state conditions by means of Fick's first law (Flynn et al., 1974), which can be expressed as:

$$\frac{dQ}{Adt} = P_{app}C_0 \quad \text{Eq. 7}$$

where dQ/Adt is the permeation flux (the slope calculated using linear regression analysis of the relationship between the amount of drug permeated per surface area of the films (A) and time). C₀ is the concentration of drug in the donor compartment and P_{app} is apparent permeability coefficient. The apparent diffusion coefficient (D_{app}) was estimated from the following equation:

$$t_L = \frac{h^2}{6D_{app}} \quad \text{Eq. 8}$$

where t_L is the lag time, obtained from the x-intercept of the permeation profiles, and h is the mean thickness of the wet films.

2.6. Preparation of SC-MAS coated tablets

Core tablets containing acetaminophen was prepared using a direct compression method. The core tablets contained acetaminophen powder (16 % w/w), spray-dried lactose (54.75 %w/w), microcrystalline cellulose (28 % w/w), colloidal silicon dioxide (0.25 %w/w), and magnesium stearate (1 %w/w). The drug powder, microcrystalline cellulose, spray-dried lactose and colloidal silicon dioxide were mixed using a Y-shape mixer for 30 min. Then, magnesium stearate was added and mixed into the mixture for 5 min before tablet compression. The mixtures were compressed into tablets using a single punch machine (YeoHeng Co., Ltd, Bangkok, Thailand), and a biconvex punch and die in 8-mm diameter was used. Average weight of the core tablets obtained was 253.8 ± 4.0 mg per tablet (n=20) with 112.4 ± 13.3 N (n=10) of hardness. Friability of the core tablets was 0.25 ± 0.09 % (n=3). The drug content in the core tablets was extracted by using 0.1M HCl and measured by UV-visible spectrophotometer (Shimadzu UV1201, Japan) at a wavelength of 265nm. The core tablets had 39.6 ± 0.2 mg each of acetaminophen content (n=3).

The 5 %w/v SC dispersion and SC-MAS dispersions at the ratios of 1:0.05, 1:0.1, and 1:0.2, which were prepared following the method in Section 2.4, were used as a coating material. The core tablets obtained were coated using a side-vented pan coating machine (Thai Coater Model FC15, Pharmaceuticals and Medical Supply, Thailand). The core tablets (900 g) were warmed in the coating pan under an inlet temperature of 70–75 °C and the coating pan was rotated at a rate of 10 revolutions min⁻¹. The spray rate of the coating

dispersions was 4 mL min^{-1} under spray pressure of 0.38 mPa. After the coating process, the coated tablets were stored in a dessicator prior to further examination

The effect of SC–MAS ratio on characteristics of the coated tablets was investigated. The core tablets were coated with SC film and SC–MAS films at the ratios of 1:0.05, 1:0.1, and 1:0.2 at a mean weight gain 3.3 %w/w. To investigate the effect of coating level, the core tablets were coated with the SC-MAS (1:0.1) films at the mean weight gains of 3.3, 6.1, and 8.2 %w/w.

2.7. Evaluation of SC-MAS coated tablets

2.7.1. SEM studies

Surface and film matrix morphology of the coated tablet were observed by scanning electron microscopy (SEM). The coated tablets and cross-sections of tablets were mounted onto stubs, coated with gold in a vacuum evaporator, and investigated using scanning electron microscope (Hitachi S-3000N, Tokyo, Japan)

2.7.2. In vitro drug release studies

In vitro drug release from the coated tablets was studied by using the USP dissolution apparatus I (basket) with 900 mL of medium. The dissolution mediums were 0.1 M HCl and pH 6.8 phosphate buffer, and the temperature of system were controlled at $37.0 \pm 1.0^\circ\text{C}$. The baskets were rotated at a rate of $50 \text{ revolution min}^{-1}$. The simulated gastro-intestinal conditions used to test drug release were performed using 0.1M HCl (900 mL) for 2 h, followed by pH 6.8 phosphate buffer (900 mL). At predetermined intervals, samples were collected and replaced with an equal volume of fresh medium. The concentration of drug released was analyzed by UV-visible spectrophotometer (Shimadzu UV1201, Japan) at wavelength of 265 nm.

2.7.3. Water uptake studies

Water uptake of the coated tablets in both 0.1 M HCl and pH 6.8 phosphate buffer was determined using USP dissolution apparatus I (basket) and the test conditions were the same as in the drug release study. The coated tablets were weighted (W_i), placed into baskets and immersed into the medium. At predetermined intervals, wet coated tablets were collected, carefully blotted with filter paper to remove surface water and weighted (W_c). Water uptake of the coated tablets could be calculated as follows ([Sunghongjeen et al., 2004](#)):

$$\text{Water uptake (\%)} = \frac{W_c - W_i}{W_i} \times 100$$

3. Results and discussion

3.1. Characteristics of SC-MAS dispersions

The SC dispersion was milky with viscosity of 2.34 mPa s as shown in [Table 1](#). SC possessed a negative charge with zeta potential value of -18.36 mV because pH of the dispersion (pH=6.8) was higher than the SC isoelectric point (4.6 to 4.8) that carboxyl groups of SC could be ionized. Unfortunately, particle size of SC could not be determined due to its very small size. The MAS dispersion (1 %w/v) showed a negative charge with 4.60- μ m particle size, and the viscosity was found to be 22.7 mPa s. Incorporation of MAS into the SC dispersion resulted in greater particle size, and higher zeta potential value of the dispersed phase. Moreover, the viscosity of the SC-MAS dispersions was higher than that of the SC dispersion, and increased with increasing MAS content. However, the SC-MAS (1:0.2) composite dispersion (contained MAS equivalent to 1% w/v) gave remarkably lower viscosity than the 1 %w/v MAS dispersion.

The silicate layers of MAS could be separated in water and then the three-dimension structure of the silicate layers could be created, resulting in higher viscosity of MAS dispersion ([Cruz and Peng, 2016](#)). When MAS was incorporated into SC dispersion, the three dimension structure of MAS could not be formed, leading to lower viscosity of the SC-MAS (1:0.2) dispersion when compared to the 1% w/v MAS dispersion. However, adding the MAS into the SC dispersion caused a viscosity synergism that could be observed from the increase of the viscosity of the SC dispersion when adding MAS. In addition, larger particle size of the dispersed phase with higher density of negative charges was formed because of the feasibility of the formation of the SC-MAS flocculates ([Khunawattanakul et al., 2008](#); [Rongthong et al., 2013](#)). These finding indicated that molecular interaction between SC and MAS in the dispersion could be readily occurred after simple mixing.

3.2. Appearance and thickness of the SC-MAS films

The SC films were prepared using a casting/solvent evaporation method. Actually SC could not form a good continuous film, so plasticizers were needed, which glycerin in 30 %w/w of SC content was used in this study. Thus, the SC films (with glycerin) obtained were quite transparent and good homogeneous sheet for further investigation. In the case of the SC-MAS films, the SC-MAS dispersions prepared had no sedimentation of the dispersed phase when allowing to settle for 12 h, so the SC-MAS films obtained after drying process showed opaque continuous sheet at all SC-MAS ratios used. However, the SC-MAS films in the ratio of 1:0.5 had a high brittleness that liable to break easily, leading to an exclusion of this film ratio (1:0.5) from this study. Using SEM, the SC films had quite smooth surface ([Fig. 1a](#)), whereas a rougher film surface was observed when adding MAS ([Fig. 1b](#)). Moreover, the incorporation of MAS resulted in a different matrix structure of the films. The dry thickness of the SC films was 133.0 μ m, which incorporation of MAS into the films resulted in an increase of the film thickness ([Table 2](#)). The wet thickness of the films was also determined after immersing in 0.1 M HCl for 5 min. The results showed that the thicknesses of the wet films were greater than those of the dry thickness, indicative of swelling property of the films

in an acidic condition. However, the wet film thickness in pH 6.8 phosphate buffer was not determined because the wet films could not be handled due to very high swelling property in this medium.

3.3. Thermal properties of the films

DSC thermograms of the films are displayed in Fig. 2. MAS showed a broad endothermic peak around 75 °C due to a dehydration of water residue, whereas SC powder presented two exothermic degradation peaks at 290 and 357 °C. The formation of the SC films without glycerin caused a shift of exothermic peaks to 296 and 358 °C. Addition of glycerin, a plasticizer, obviously affected thermal behavior of the SC films, which the small exothermic peak showed at 308 °C for the SC film with glycerin. Furthermore, MAS incorporated resulted in a shift of the exothermic peak to higher temperature, and peak intensity decreased with increasing MAS ratios. The thermal patterns of the SC-MAS films were remarkably different from those of SC-MAS physical mixtures. The results showed that MAS could enhance thermal stability of the SC films.

3.4. Molecular interaction and nanocomposite formation of the films

Molecular interaction of the components in the films was investigated using FTIR-spectroscopy and PXRD. FTIR spectrum of MAS showed the O–H stretching of SiOH (3610 cm^{-1}), the O–H stretching of H₂O (3434 cm^{-1}), the O–H bending of H₂O (1638 cm^{-1}), and the Si–O–Si stretching (1016 cm^{-1}) (Pongjanyakul et al., 2005), as shown in Fig. 3. SC presented the N–H stretching overlapped with the O–H stretching at 3399 cm^{-1} , the C–H stretching at 2934 and 2963 cm^{-1} , the C=O stretching (amide I) at 1657 cm^{-1} , the N–H bending (amide II) at 1536 cm^{-1} and the C–N stretching at 1237 cm^{-1} (Santinho et al., 1999; Pereda et al., 2010; Demirbaş et al., 2015). The film formation of SC (without glycerin) caused a shift of the N–H stretching (with the O–H stretching), amide I and amide II because of hydrogen bonding with water residues. Incorporation of glycerin had an impact to the FTIR pattern of the SC films that the N–H stretching (with the O–H stretching) showed a sharper peak and moved to lower wavenumber (3429 cm^{-1}), and the C–H stretching peak of SC was also shifted to lower wavenumber, suggesting the formation of intermolecular hydrogen bonding and more flexibility of the main structure of SC molecules. In addition, the SC film with glycerin also presented the new peak at 1134 cm^{-1} that was the C–O stretching peak of glycerin. The SC-MAS films showed different FTIR pattern when compared with the SC-MAS physical mixtures. MAS added into the SC films caused a shift of the N–H stretching (with O–H stretching), and the peaks of amide I and amide II. These changes could be clearly observed in the SC-MAS (1:0.2) films. This result indicated that the silanol groups of MAS could mainly interact with the amide and amino groups of SC via intermolecular hydrogen bonding mechanism. These interactions could be occurred when mixing MAS with SC in the dispersion, leading to viscosity synergism that was mentioned above.

The nanocomposite formation of the SC-MAS films was investigated using PXRD. The PXRD pattern of MAS showed the basal spacing peak at $7.0^\circ 2\theta$ (Fig. 4) that the space or thickness of the silicate layers was 1.26 nm when calculated using Eq. 1 (Pongjanyakul et al., 2005). The crystallinity of the SC powder showed broad peaks around 8 and $20^\circ 2\theta$, which similar to that of the SC film with glycerin, indicative of an amorphous form of the SC powder and film. Addition of MAS at all ratios in the SC films brought about disappearance of the basal spacing peak of the MAS silicate layers, whereas this peak of MAS located around $7^\circ 2\theta$ in the SC-MAS physical mixtures at the ratios of 1:0.1 and 1:0.2. These results suggested that the SC-MAS films were exfoliated nanocomposites that could be formed when low amount of clay added (Alexandre and Dubois, 2000; Rongthong et al., 2013). Additionally, glycerin could interact with MAS by hydrogen bonding, and it could induce a formation of intercalated nanocomposites in alginate-MAS films when using as a plasticizer (Pongjanyakul and Puttipipatkachorn, 2007). So, glycerin may involve the nanocomposite formation of the SC-MAS films. However, FTIR data could prove that SC could strongly interact with MAS in the films by hydrogen bonding after incorporating MAS, which was the main interaction for hindering the rearrangement of the MAS silicate layers, leading to the formation of exfoliated nanocomposites in this study.

3.5. Water uptake and erosion of the films

The water uptake and erosion of the films were tested in both 0.1 M HCl and pH 6.8 phosphate buffer. When the films were immersed in acidic medium, they still provided a continuous sheet because sodium caseinate was changed to casein salt that had water-insoluble property (Elzoghby et al., 2011). Therefore, both parameters could be determined in acidic condition. Unfortunately, the wet films in pH 6.8 phosphate buffer could not be properly handled and blotted to remove excess water due to very high swelling and some matrix dissolutions of the films, leading to a lack of the data of water uptake and matrix erosion in this medium. Figure 5 presents the water uptake and erosion of the films in 0.1 M HCl. The SC films provided the highest water uptake at 15 min of the test because casein in the acidic form in the hydrated films may had a weak intermolecular bonding, leading to a large aqueous pore in the films' matrix. However, the wet SC films at 60 and 120 min could not be handled due to very high water imbibition. The water uptake of the SC films decreased with increasing MAS ratios (Fig. 5a). Apart from film water uptake, the SC films showed 21.3 % erosion at 15 min of the test, whereas erosion of the SC-MAS films was found over the range of 21-26 % (Fig. 5b). It is possible to explain that film erosion occurred by leaching of water-soluble plasticizer added, such as glycerin (Pongjanyakul and Puttipipatkachorn, 2007). This finding suggested that addition of MAS into the SC films retarded water absorption process of the films and resulted in denser matrix structure that could be attributed to SC-MAS nanocomposite formation, reflecting aqueous-filled channels in the film matrix and matrix strength of the wet films in acidic condition.

3.6. Mechanical properties of the films

The puncture strength and %elongation of the films in dry and wet stages are illustrated in Fig. 6. The SC films in dry state provided the highest puncture strength and % elongation. Both parameters decreased with increasing MAS ratios in the films. These results were in agreement with the previous reports about the effect of solid materials added into polymeric films (Okhamafe and York, 1984; Felton and McGinity, 2002; Rongthong et al., 2013). This could probably be attributed to the fact that the presence of the MAS particles hindered the formation of a continuous three-dimensional SC network.

The mechanical properties of the wet films tested in 0.1 M HCl are also shown in Fig. 6. The puncture strength of the wet SC films was remarkably lower than that of the dry state, whereas the %elongation of the SC film in both states were comparable. Increasing MAS ratios in the SC films resulted in increase of puncture strength. This was due to the decrease of water uptake of the SC-MAS films with higher MAS ratios (Fig. 5a). However, the %elongation of the SC-MAS films was lower than that of the SC film, but they still had 11-15 % elongation at all MAS ratios. The results were similar to the effect of clay additive on mechanical properties of wet polymethacrylate films (Rongthong et al., 2013). These findings suggested that the molecular interaction and nanocomposite formation of SC with MAS could enhance films' strength when exposed to acidic medium. This could be a crucial advantage when used as sustained release film coatings for tablets in an acidic condition. In addition, these films provided good strength for mechanical stress within the gastro-intestinal tract.

3.7. Water vapor and drug permeability of the films

Water vapor permeation (WVP) rate and coefficient of the films are listed in Table 2. WVP rate of the SC films obviously decreased with increasing MAS ratios. However, the WVP coefficients were calculated using Eq. 4 that had no effect of dry film thickness. This parameter presented that MAS added did not influence WVP properties of the SC films. The result suggested that the SC-MAS nanocomposite formation did not clearly increase tortuosity of water vapor pathways in the film matrix.

Drug permeability of the films in 0.1 M HCl was performed using acetaminophen as a model drug. The drug permeation profiles obtained presented good linearity ($R^2 > 0.98$) of relationship between drug permeated and time. This indicated that the drug permeation reached a steady state with high drug concentration in the donor compartment, and could be described using Fick's first law. The drug permeation parameters are listed in Table 2. The drug permeation flux and P_{app} value were obviously reduced when increasing MAS ratios in the films, whereas the longer lag time for drug permeation was found. Decreasing of the D_{app} values occurred when MAS added in the SC films was increased.

The diffusive transport of drug in a polymeric film can be described using two mechanisms (Thacharodi and Panduranga Rao, 1993; Pongjanyakul, 2009). The first is the partition mechanism of drug into polymeric films, which is dependent upon drug affinity with film polymer, and the diffusion process in the polymer fraction progressed across the films. The other is pore mechanism that drug diffuses within the structure of hydrated films via

aqueous-filled channels. In this study, both mechanisms could be applied to describe the diffusion of acetaminophen across the SC-MAS films in acidic medium. The partition mechanism possibly predominated in the initial stage of the permeation process, which could be observed from a longer lag time when MAS added was increased. However, acetaminophen had weak affinity with MAS (Pongjanyakul et al., 2005) because it was a non-electrolyte molecule (Nakano et al., 1984; Terzyk et al., 2003), which caused less partition process of drug with the SC-MAS films in the steady state of permeation process. Thus, the film permeation of acetaminophen was mainly diffused through aqueous-filled channels of the films. Increase of MAS ratios resulted in lower water uptake in the films that meant smaller aqueous-filled channels (or higher tortuosity) in the films' matrix, leading to reduction of drug diffusivity in the matrix network under the same concentration gradient (Lecomte et al., 2003; Rongthong et al., 2015). Thus, decrease of D_{app} values of drug was obtained in this study.

3.8. Use of SC-MAS films for tablet film coatings

The SC and SC-MAS films at different ratios were applied as a coating material for tablets. The appearance of the SC and SC-MAS coated tablets is shown in Fig. 7. A few defects of the coated tablets were found by visible observations. The surface and cross-sectional morphology of the SC coated films showed similar feature with those of the SC-MAS coated films (Fig. 7). Effect of SC-MAS ratios on drug release and water uptake of the coated tablets was investigated in this study. The acetaminophen core tablets were coated with SC and SC-MAS films at the mean weight gain 3.3 %w/w. The drug release and water uptake using 0.1 M HCl are shown in Fig. 8a and 8c, respectively. The core tablets displayed a fast release and complete release was found within 30 min. The SC coated tablets showed slower drug release than the core tablets. This suggested that the SC films possessed a stable wet film around the tablets when SC was change to casein salt, water-insoluble property, in acidic condition, after that the wet coated films could retard the diffusion of drug dissolved. Incorporation of MAS into the coated films could modulate the drug release pattern. The higher the MAS ratios in the coated films, the slower the drug released in acidic medium was obtained. Moreover, the water uptake of the coated tablets displayed that the coated tablets with SC-MAS films at the ratios of 1:0.05 and 1:0.1 had similar %water uptake when compared with the SC coated tablets, while the lowest water uptake was obtained from the SC-MAS (1:0.2) coated tablets (Fig. 8c). The results showed that the SC-MAS coated films could possibly slow down the water penetration process into the coated tablets before drug dissolution and drug release. Additionally, the lower drug diffusivity across the SC-MAS films with higher ratios of MAS (Table 2) also led to slower drug release from the coated tablets.

Effects of film coating level on drug release and water uptake of the coated tablets in 0.1 M HCl are presented in Fig. 8b and 8d, respectively. The drug release from the SC-MAS (1:0.1) coated tablets decreased with increasing film coating levels (Fig. 8b). The 8.2 % weight gain coating provided sustained-release pattern of drug for 10 h. Increasing film

coating level could obviously retard water absorption process of the coated tablets (Fig. 8d). This finding suggested that the higher coating level of the SC-MAS (1:0.1) coated tablets could retard drug release from the coated tablets due to slower water uptake for drug dissolution and longer pathway lengths for drug diffusion.

Apart from acidic condition, the water uptake and drug release of the coated tablets were also tested in pH 6.8 phosphate buffer as shown in Fig. 9. It could be observed that the drug release and water uptake of the coated tablets in pH 6.8 phosphate buffer were greater than those in acidic medium. The SC and SC-MAS (1:0.05) coated tablets showed fast release comparable to the core tablets (Fig. 9a). Increasing MAS ratios caused more sustain drug release, while the coated tablets with 6.1 and 8.2 % weight gain gave similar drug release profile, but slower than those with 3.3 % weight gain. The water uptake study could be only tested within 5 min due to very fast swelling of the coated films. The results showed that the presence of MAS in the coated films provided greater water uptake than the SC coated tablets, and increasing of film coating levels led to higher water uptake of the coated tablets (Fig. 9b). It could be explained that SC could still have swelled in neutral medium although it interact and create nanocomposites with MAS. Swelling of SC loosened the film matrix structure and increased the matrix volume for absorbing water, leading to higher water uptake when increasing the film coating level. Moreover, MAS had water absorption capacity as well, therefore the presence of MAS could promote water uptake of the coated tablets. The other factor after swelling of the coated films was dissolution or erosion of SC from the films. This phenomenon may result in faster drug release from the coated tablets, irrespective of the MAS ratios and film coating levels.

The simulated gastro-intestinal conditions starting with 0.1 M HCl for 2 h followed by pH 6.8 phosphate buffer were used to test the drug release from the SC-MAS (1:0.1) coated tablets, which is shown in Fig. 10. It could be seen that the drug release from the SC-MAS coated proceeded continuously when the dissolution medium was changed from acidic medium to pH 6.8 phosphate buffer. The drug release patterns obtained in this test was similar to those using 0.1 M HCl (Fig. 8b). The results suggested that SC in the coated films, which had been changed to casein salt in acidic condition, did not readily hydrate and swell when passing to pH 6.8 phosphate buffer. Thus, the drug released from the coated tablets was controlled by the drug diffusion process across the coated films throughout 8 h of the tests. This finding suggested that the release of drug could possibly take place continuously when the SC-MAS coated tablets were transferred from the stomach to the small intestine in the gastro-intestinal tract.

4. Conclusions

This study demonstrates that SC can molecularly interact with MAS in the dispersions after simple mixing, resulting in SC-MAS flocculation and viscosity synergism. The SC-MAS films can successfully prepared by casting method. Molecular interaction between the amide and amino groups of SC and the silanol groups of MAS via intermolecular hydrogen bonding

results in the formation of exfoliated nanocomposites. MAS added can enhance thermal stability of the SC films. The puncture strength and elongation of the SC films decrease with increasing MAS ratio in the dry state. On the contrary, increasing MAS ratio causes an increase of puncture strength of the wet SC-MAS films in acidic medium. The SC-MAS films do not obviously retard the water vapor permeation, but the drug permeability and diffusivity across the films in acidic medium remarkably decrease when increasing MAS ratios because nanocomposite matrix structure possesses smaller water-filled channels with higher tortuosity. The SC-MAS dispersions can be employed as a film coating material. The SC-MAS coated tablets present a few film defect and smooth surface morphology. The drug release from the coated tablets in acidic medium can be modified by varying MAS ratios and film coating levels. The SC-MAS coated tablets also display sustained-release pattern of drug in simulated gastro-intestinal condition. This finding indicates that the SC-MAS nanocomposite films can be used in oral modified-release tablet coatings.

References

- Abu Diak, O., Bani-Jaber, A., Amro, B., Jones, D., Andrews, G.P., 2007. The manufacture and characterization of casein films as novel tablet coating. *Food Bioprod. Process.* 85: 284-290.
- Alam, S., Paul, S., 2001. Efficacy of casein coating on storage behavior of kinnow. *J. Food Sci. Technol.* 38, 235-238.
- Alexandre, M., Dubois, P., 2000. Polymer-layered silicate nanocomposites: preparation, properties and uses of a new class of materials. *Mater. Sci. Eng.* 28, 1-63.
- Audic, J.L., Chaufer, B., 2005. Influence of plasticizers and crosslinking on the properties of biodegradable films made from sodium caseinate. *Eur. Polym. J.* 41, 1934-1942.
- Bani-Jaber, A., Aideh, K., Hamdan, I., Maraqa, R., 2009. Drug-loaded casein beads: influence of different metal-types as cross-linkers and oleic acid as a plasticizer on some properties of the beads. *J. Drug Deliv. Sci. Technol.* 19, 125-131.
- Bonnaillie, L.M., Zhang, H., Akkurt, S., Yam, K.L., Tomasula, P.M., 2014. Casein films: The effects of formulation, environmental conditions and the addition of citric pectin on the structure and mechanical properties. *Polymers* 6, 2018-2036.
- Cazón, P., Velazquez, G., Ramírez, J.A., Vázquez, M., 2017. Polysaccharide-based films and coatings for food packaging: A review. *Food Hydrocolloids* 68, 136-148.
- Ciullo, P.A., 1981. Rheological properties of magnesium aluminum silicate/xanthan gum dispersions. *J. Soc. Cosmet. Chem.* 32, 275-285.
- Ciullo, P.A., Braun, D.B., 1991. Clay/carbomer mixtures enhance emulsion stability. *Cosmet. Toilet.* 106, 89-95.
- Cruz, N., Peng, Y., 2016. Rheology measurements for flotation slurries with high clay contents – A critical review. *Miner. Eng.* 98, 137-150.
- Demirbaş, Ö., Alkan, M., Demirbaş, A., 2015. Adsorption of casein onto some oxide minerals and electrokinetic properties of these particles. *Micropor. Mesopor. Mater.* 204, 197-203.

- Elzoghby, A.O., El-Fotoh, W.S., Elgindy, N.A., 2011. Casein-based formulations as promising controlled release drug delivery systems. *J. Control. Release* 153, 206–216.
- Elzoghby, A.O., Helmy, M.W., Samy, W.M., Elgindy, N.A., 2013a. Novel ionically crosslinked casein nanoparticles for flutamide delivery: formulation, characterization, and in vivo pharmacokinetics. *Int. J. Nanomed.* 8, 1721-1732.
- Elzoghby, A.O., Helmy, M.W., Samy, W.M., Elgindy, N.A., 2013b. Spray-dried casein-based micelles as a vehicle for solubilization and controlled delivery of flutamide: formulation, characterization, and in vivo pharmacokinetics. *Eur. J. Pharm. Biopharm.* 84, 487-496.
- Fabra, M.J., Talens, P., Chiralt, A., 2008. Tensile properties and water vapor permeability of sodium caseinate films containing oleic acid-beeswax mixtures. *J. Food Eng.* 85, 393-400.
- Felton, L.A., McGinity, J.W., 2002. Influence of insoluble excipients on film coating systems. *Drug Dev. Ind. Pharm.* 28, 225– 243.
- Flynn, G.L., Yalkowsky, S.H., Roseman, T.J., 1974. Mass transport phenomena and models: theoretical concepts. *J. Pharm. Sci.* 63, 479–510.
- Horne, D.S., Euston, S.R., 2005. Simulating the self-association of caseins. *Food Hydrocolloids* 19, 379-386.
- Karki, S., Kim, H., Na, S.-J., Shin, D., Jo, K., Lee, J., 2016. Thin films as an emerging platform for drug delivery. *Asian J. Pharm. Sci.* 11, 559-574.
- Khunawattanakul, W., Puttipipatkachorn, S., Rades, T., Pongjanyakul, T., 2008. Chitosan-magnesium aluminum silicate composite dispersions: Characterization of rheology, flocculate size and zeta potential. *Int. J. Pharm.* 351, 227-235.
- Khunawattanakul, W., Puttipipatkachorn, S., Rades, T., Pongjanyakul, T., 2010. Chitosan-magnesium aluminum silicate nanocomposite films: Physicochemical characterization and drug permeability. *Int. J. Pharm.* 393, 219-229.
- Khwaldia, K., Banon, S., Perez, C., Desobry, S., 2004. Properties of sodium casinate film-forming dispersions and films. *J. Dairy Sci.* 87, 2011-2016.
- Knepp, W.A., Jayakrishnan, A., Quigg, J.M., Sitren, H.S., Bagnall, J.J., Goldberg, E.P., 1993. Synthesis, properties, and intratumoral evaluation of mitoxantrone-loaded casein microspheres in Lewis lung carcinoma. *J. Pharm. Pharmacol.* 45, 887-891.
- Lecomte, F., Siepmann, J., Walther, M., MacRae, R.J., Bodmeier, R., 2003. Blends of enteric and GIT-insoluble polymers used for film coating: physicochemical characterization and drug release patterns. *J. Control. Release* 89, 457-471.
- Magee, G.A., Willmott, N., Halbert, G.W., 1993. Development of a reproducible in vitro method for assessing the biodegradation of protein microspheres. *J. Control. Release* 25, 241-248.
- Millar, F.C., Corrigan, O.I., 1991. Influence of sodium caseinate on the dissolution rate of hydrochlorothiazide and chlorothiazide. *Drug Dev. Ind. Pharm.* 17, 1593-1607.
- Millar, F.C., Corrigan, O.I., 1993. Dissolution mechanism of ibuprofen-casein compacts. *Int. J. Pharm.* 92, 97-104.

- Nagai, T., Obara, S., Kokubo, H., Hoshi, N., 1997. Application of HPMC and HPMCAS to aqueous film coating of pharmaceutical dosage forms. In: McGinity, J.W. (Ed.), *Aqueous Polymeric Coatings for Pharmaceutical Dosage Forms*. Marcel Dekker Inc., New York, pp. 177–226.
- Nakano, N.I., Shimamori, Y., Umehashi, M., Nakano, M., 1984. Preparation and drug adsorption characteristics of activated carbon beads suitable for oral administration. *Chem. Pharm. Bull.* 32, 699–707.
- Nunthanid, J., Wanchana, S., Sriamornsak, P., Limmatavapirat, S., Luangtanaanan, M., Puttipipatkachorn, S., 2002. Effect of heat on characteristics of chitosan film coated on theophylline tablets. *Drug Dev. Ind. Pharm.* 28, 919–930.
- Nur Hanani, Z.A., Roos, Y.H., Kerry, J.P., 2014. Use and application of gelatin as potential biodegradable packaging materials for food products. *Int. J. Biol. Macromol.* 71, 94–102.
- Okhamafe, A.O., York, P., 1984. Effect of solids-polymer interaction on the properties of some aqueous-based tablet film coating formulation: II. Mechanical characteristics. *Int. J. Pharm.* 22, 273–281.
- Pan, K., Chen, H., Davidson, P.M., Zhong, Q., 2014. Thymol nanoencapsulated by sodium caseinate: physical and antilisterial properties. *J. Agric. Food Chem.* 62, 1649–1657.
- Pan, K., Zhong, Q., Baek, S.J., 2013. Enhanced dispersibility and bioactivity of curcumin by encapsulation in casein nanoparticles. *J. Agric. Food Chem.* 61, 6036–6043.
- Perada, M., Aranguren, M.I., Marcovich, N.E., 2010. Effect of crosslinking on the properties of sodium caseinate films. *J. Appl. Polym. Sci.* 116, 18–26.
- Pereda, M., Amica, G., Racz, I., Marcovich, N.E., 2011a. Preparation and characterization of sodium caseinate films reinforced with cellulose derivatives. *Carbohydr. Polym.* 86, 1014–1021.
- Pereda, M., Amica, G., Racz, I., Marcovich, N.E., 2011b. Structure and properties of nanocomposite films based on sodium caseinate and nanocellulose fibers. *J. Food Eng.* 103, 76–83.
- Pereda, M., Aranguren, M.I., Marcovich, N.E., 2010. Caseinate films modified with tung oil. *Food Hydrocolloids* 24, 800–808.
- Pongjanyakul, T., 2009. Alginate–magnesium aluminum silicate films: Importance of alginate block structures. *Int. J. Pharm.* 365, 100–108.
- Pongjanyakul, T., Priprem, A., Puttipipatkachorn, S., 2005. Investigation of novel alginate–magnesium aluminum silicate microcomposite films for modified-release tablets. *J. Control Release* 107, 343–356.
- Pongjanyakul, T., Puttipipatkachorn, S., 2007. Alginate–magnesium aluminum silicate films: Effect of plasticizers on film properties, drug permeation and drug release from coated tablets. *Int. J. Pharm.* 333, 34–44.
- Rongthong, T., Sungthongjeen, S., Siepmann, F., Siepmann, J., Pongjanyakul, T., 2015. Quaternary polymethacrylate–magnesium aluminum silicate films: Water uptake kinetics and film permeability. *Int. J. Pharm.* 490, 165–172.

- Rongthong, T., Sungthongjeen, S., Siepmann, J., Pongjanyakul, T., 2013. Quaternary polymethacrylate–magnesium aluminum silicate films: Molecular interactions, mechanical properties and tackiness. *Int. J. Pharm.* 458, 57–64
- Rowe, R.C., Sheskey, P.J., Owen, S.C., 2006. *Handbook of Pharmaceutical Excipients*. Fifth ed. Pharmaceutical Press and American Pharmaceutical Association, Washington.
- Santinho, A.J.P., Pereira, N.L., Freitas, O.D., Collett, J.H., 1999. Influence of formulation on the physicochemical properties of casein microparticles. *Int. J. Pharm.* 186, 191-198.
- Shakil, O., Masood, F., Yasin, T., 2017. Characterization of physical and biodegradation properties of poly-3-hydroxybutyrate-co-3-hydroxyvalerate/sepiolite nanocomposites. *Mater. Sci. Eng. C* 77, 173-183
- Sungthongjeen, S., Puttipatkhachorn, S., Paeratakul, O., Dashevsky, A., Bodmeier, R., 2004. Development of pulsatile release tablets with swelling and rupturable layers. *J. Control. Release* 95, 147–159.
- Terzyk, A.P., Rychlicki, G., Biniak, S., Łukaszewicz, J.P., 2003. New correlations between the composition of the surface layer of carbon and its physicochemical properties exposed while paracetamol is adsorbed at different temperature and pH. *J. Colloid Interface Sci.* 257, 13–30.
- Thacharodi, D., Panduranga Rao, K., 1993. Release of nifedipine through crosslinked chitosan membranes. *Int. J. Pharm.* 96, 33–39.
- Tuovinen, L., Peltonen, S., Järvinen, K., 2003. Drug release from starch-acetate films. *J. Control. Release* 91, 345–354.
- Van Den Broek, L.A.M., Knoop, R.J.I., Kappen, F.H.J., Boeriu, C.G., 2015. Chitosan films and blends for packaging material. *Carbohydr. Polym.* 116, 237-242.
- Walstra, P., Wouters, J., Geurts, T., 2006. *Dairy Science and Technology*. Second ed. Taylor & Francis Group, Boca Raton.
- Wihodo, M., Moraru, C.I., 2013. Physical and chemical methods used to enhance the structure and mechanical properties of protein films: A review. *J. Food Eng.* 114, 292-302.

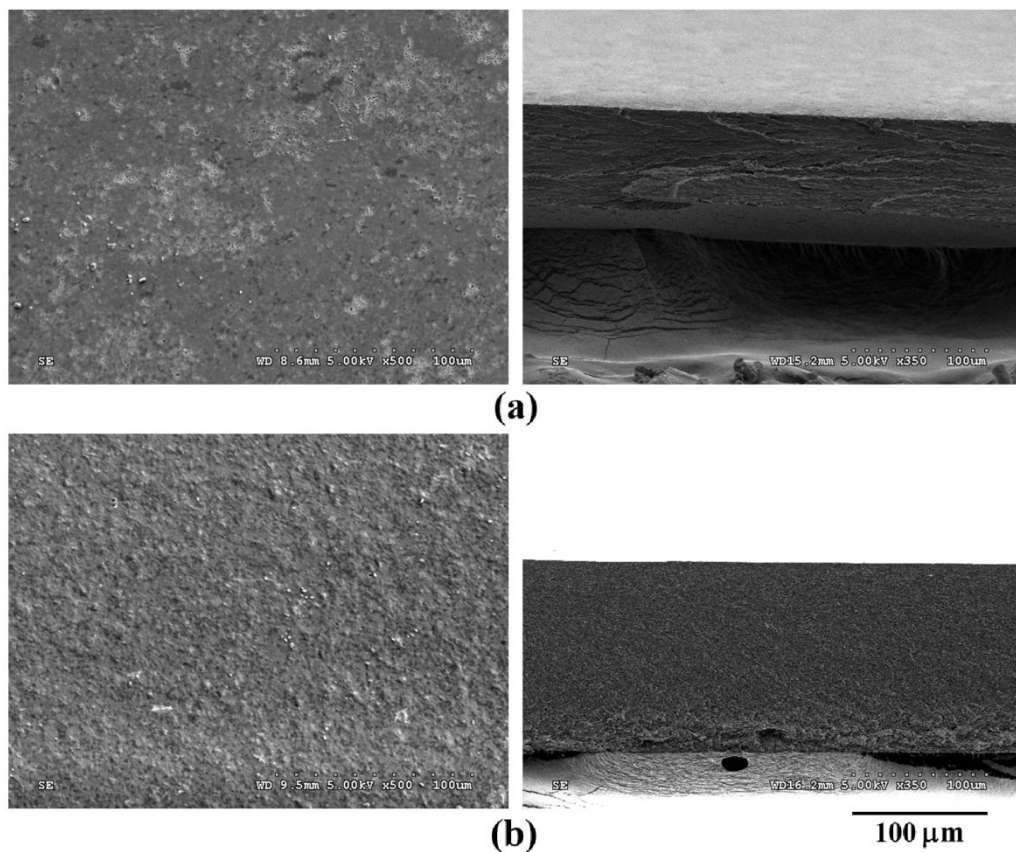


Figure 1. Surface and cross-section morphology of SC film (a) and SC-MAS (1:0.2) film (b).

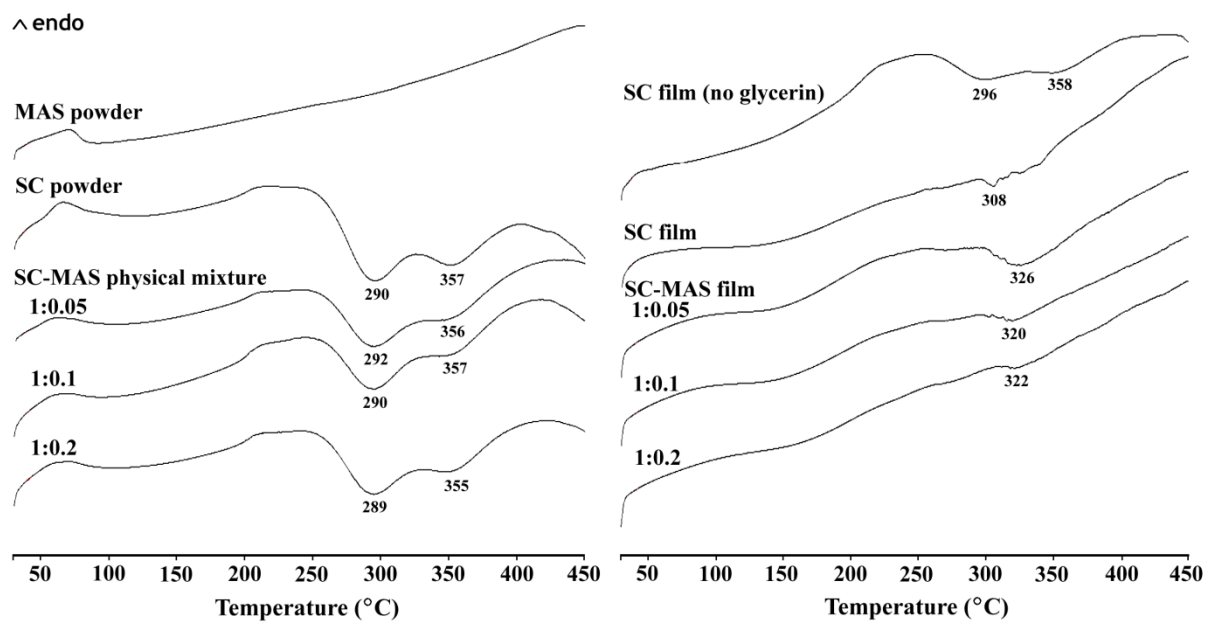


Figure 2. DSC thermograms of MAS, SC, SC-MAS physical mixture, SC film, and SC-MAS films.

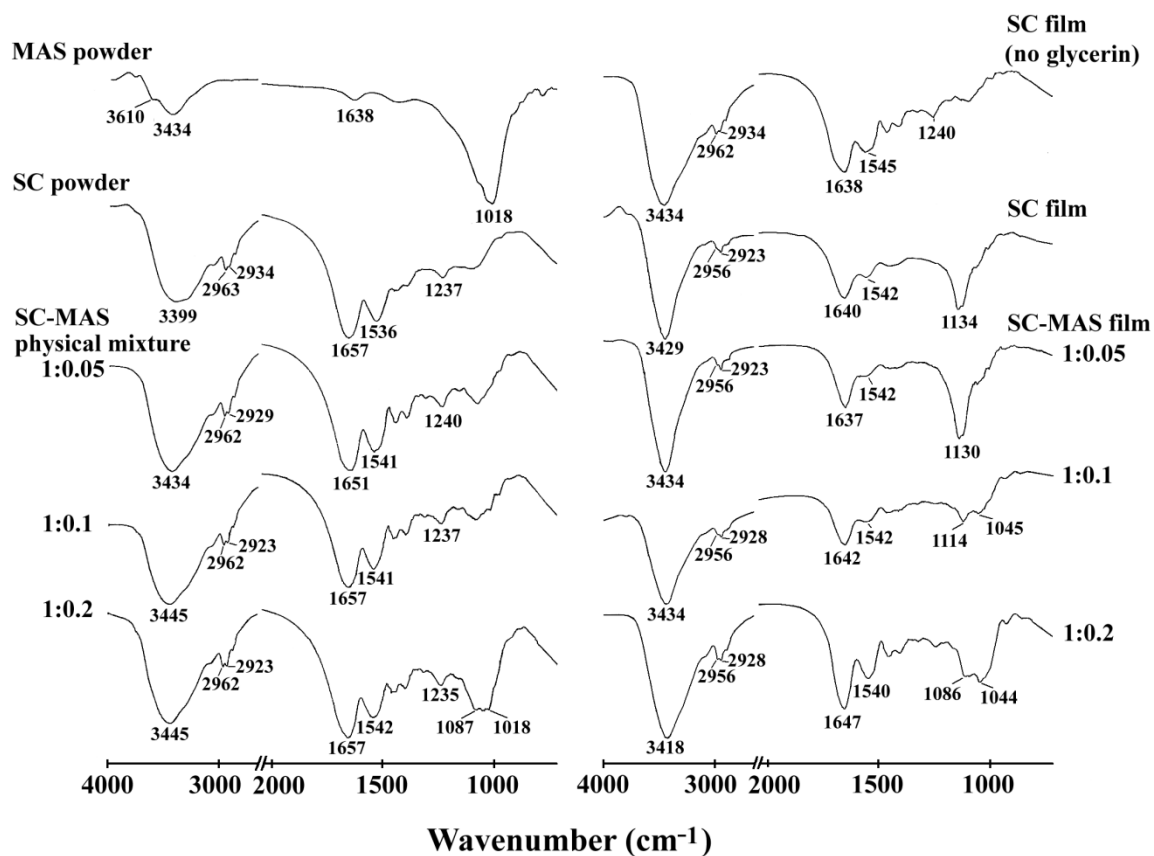


Figure 3. FTIR spectra of MAS, SC, SC-MAS physical mixture, SC film, and SC-MAS films.

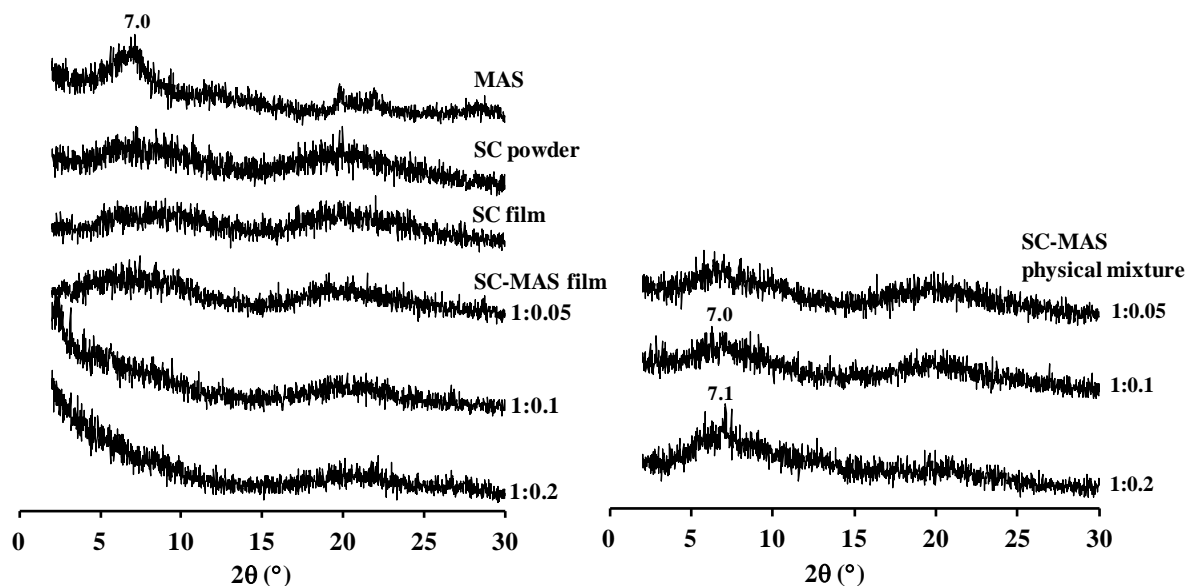


Figure 4. PXRD patterns of MAS, SC, SC-MAS physical mixture, SC film, and SC-MAS films.

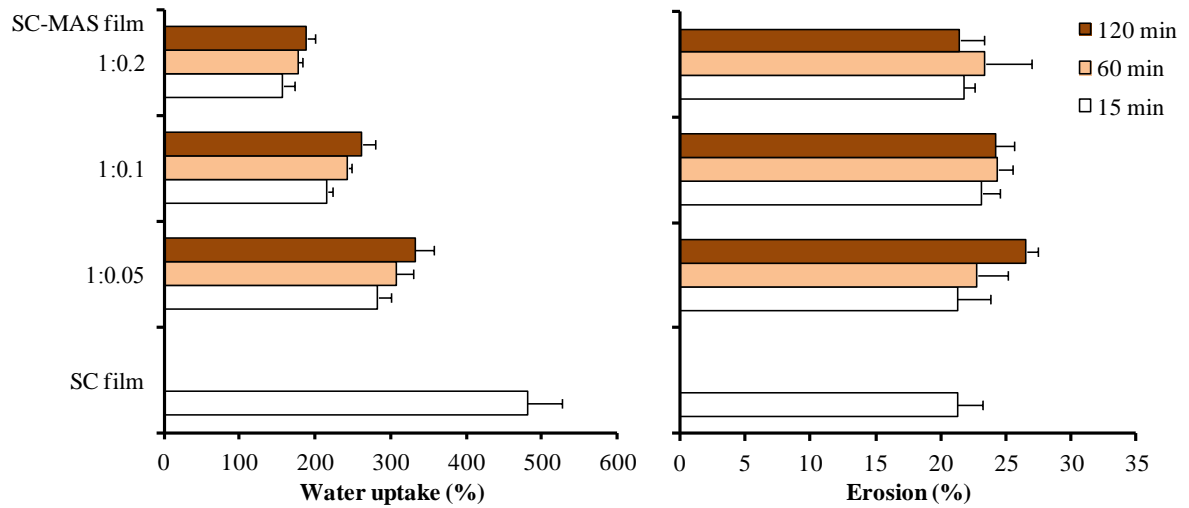


Figure 5. Water uptake and erosion of SC film and SC-MAS films at various ratios in 0.1 M HCl. Each value indicates mean \pm SD, n=4-5.

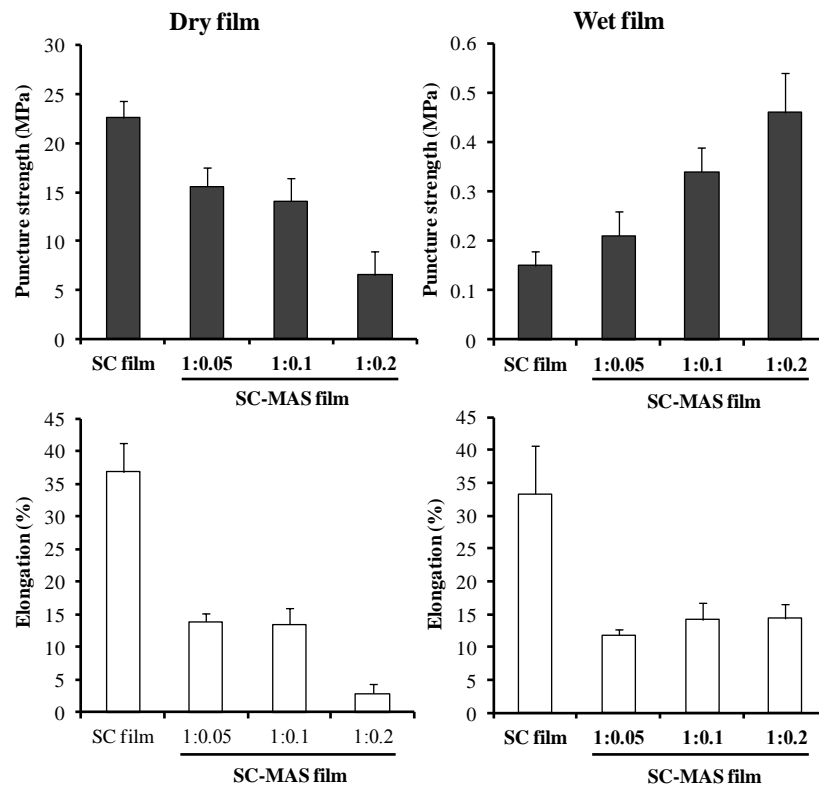


Figure 6. Puncture strength and elongation of SC films and SC-MAS films at different ratios in dry and wet states. Each value indicates mean \pm SD, n=4.

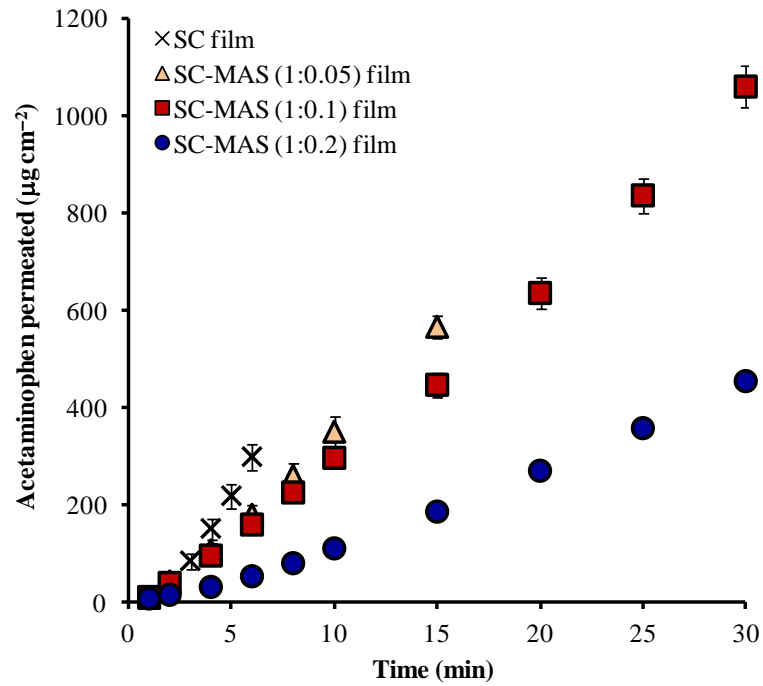


Figure 7. Permeation profiles of acetaminophen across SC film and SC-MAS films at different SC-MAS ratios. Each value indicates mean \pm SD, n=3.

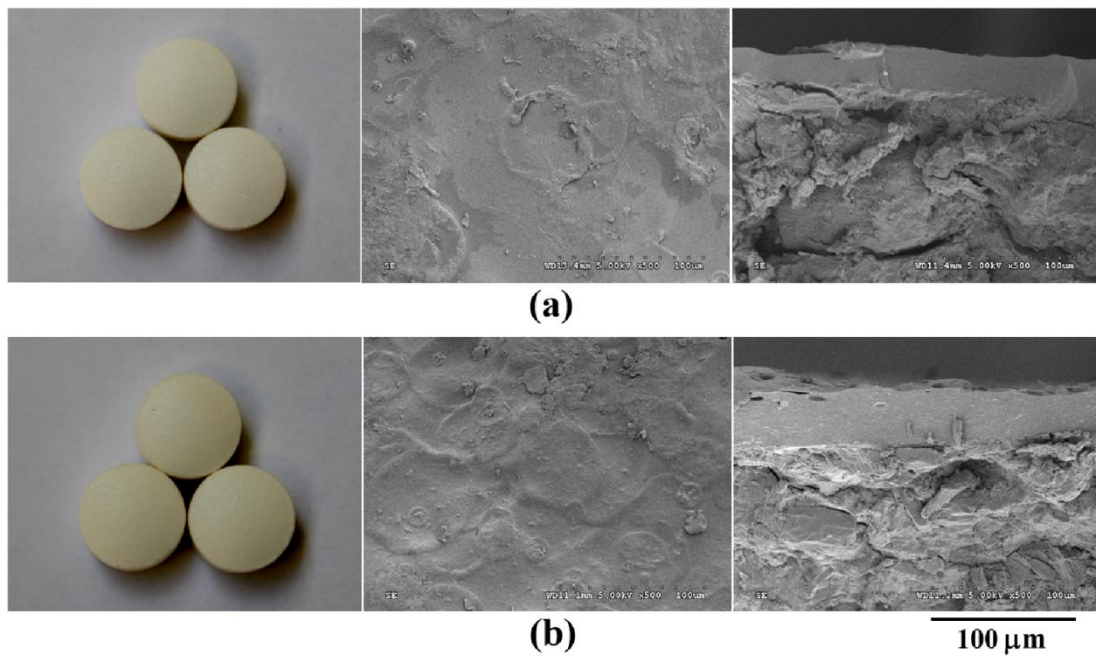


Figure 8. Appearance and surface and cross-section morphology of acetaminophen tablets coated with SC film (a) and SC-MAS (1:0.1) film (b) at 3.3 %w/w coating level.

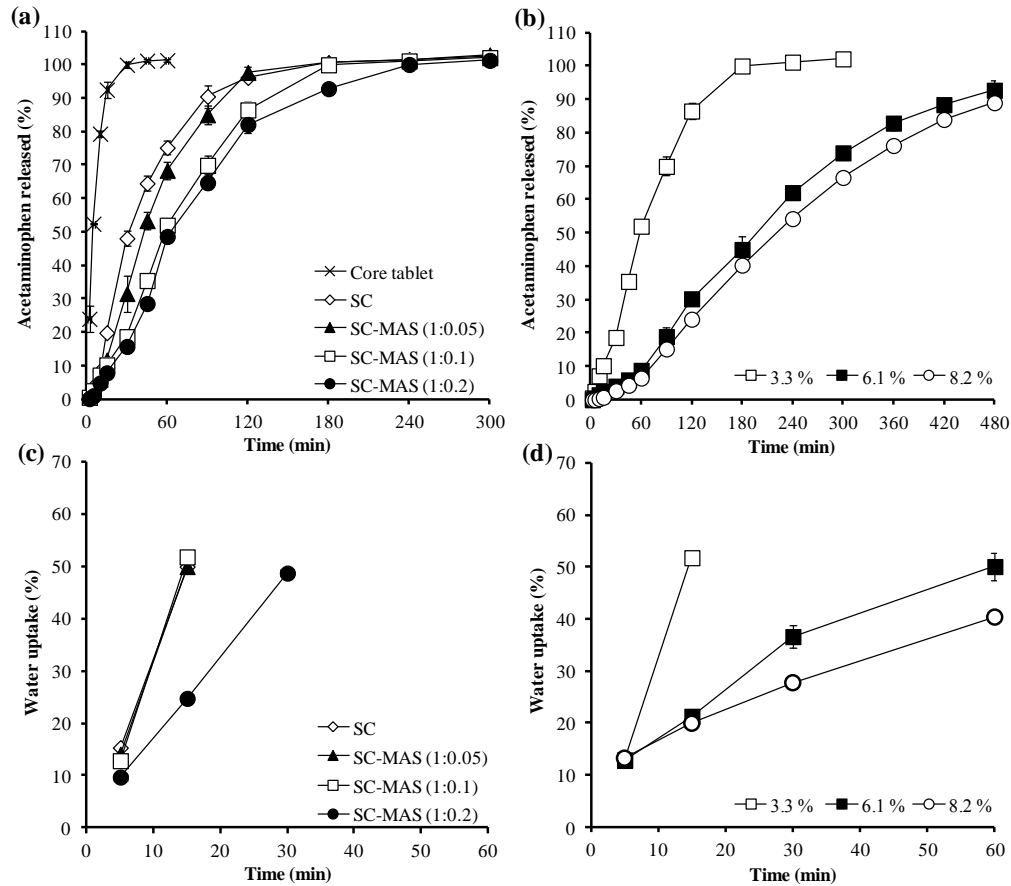


Figure 9. Effect of SC-MAS ratios (a,c) and film coating levels (b,d) on drug release (a,b) and water uptake (c,d) of acetaminophen coated tablets in 0.1 M HCl. Each point indicates mean \pm SD, n=3.

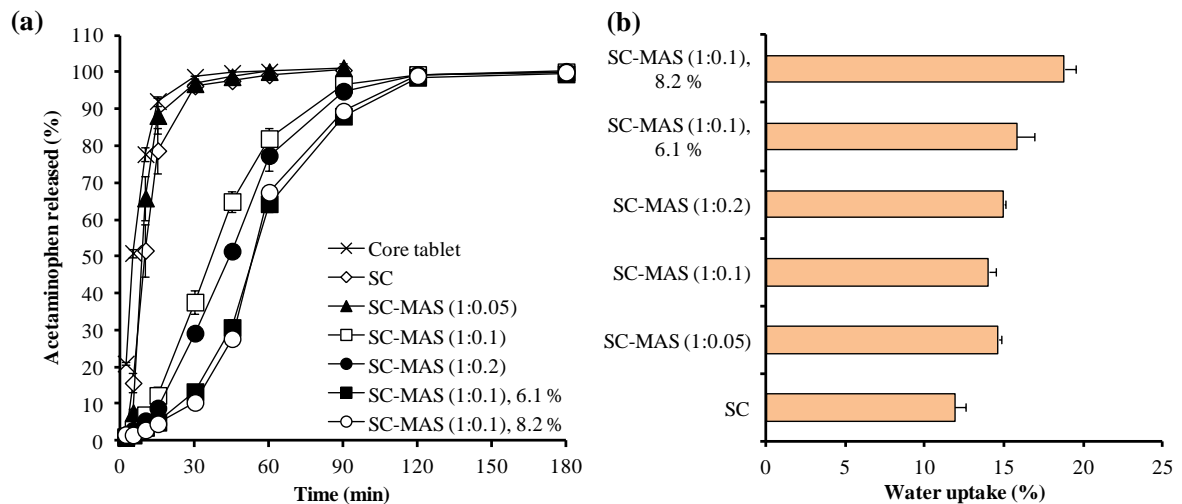


Figure 10. Effect of SC-MAS ratios and film coating levels on drug release (a) and water uptake at 5 min (b) of acetaminophen coated tablets in pH 6.8 phosphate buffer. Each value indicates mean \pm SD, n=3.

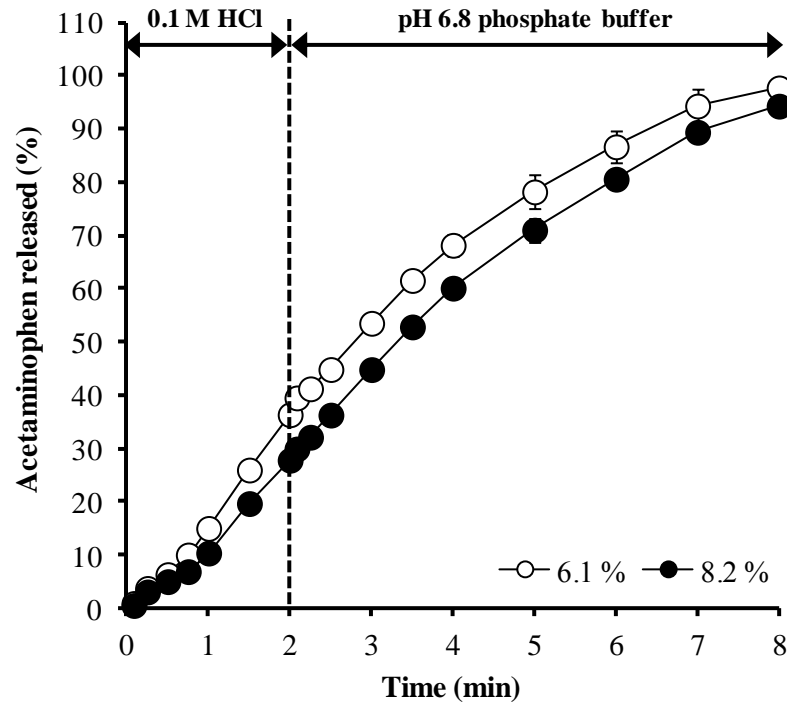


Table 1. Characteristics of SC-MAS dispersions

Component	Particle size (μm)	Zeta potential (mV)	Viscosity (mPa s)
5 % w/v SC dispersion	ND	-18.36 ± 1.63	2.34 ± 0.06
1 %w/v MAS dispersion	4.60 ± 0.01	-19.16 ± 1.80	22.7 ± 0.46
SC-MAS dispersion			
1:0.05	30.24 ± 2.89	-33.23 ± 2.46	3.66 ± 0.06
1:0.1	26.71 ± 5.06	-31.21 ± 2.42	4.17 ± 0.16
1:0.2	23.29 ± 2.78	-33.34 ± 2.13	6.32 ± 0.38

Viscosity at shear rate of 20.4 s^{-1}

pH of all dispersions was controlled at 6.8.

ND=could not be determined.

Table 2. Thickness and film permeability of SC and SC-MAS films.

Film	Dry thickness (μm)	Wet thickness (μm)	WVP rate ($\text{mg cm}^{-2} \text{h}^{-1}$)	WVP coefficient $\times 10^4$ ($\text{mg mm}^{-1} \text{h}^{-1} \text{mmHg}^{-1}$)	Acetaminophen permeation			
					Flux	Lag time	$P_{\text{app}} \times 10^4$	$D_{\text{app}} \times 10^7$
					($\mu\text{m cm}^{-2} \text{min}^{-1}$)	(min)	(cm s^{-1})	($\text{cm}^2 \text{s}^{-1}$)
SC film	133.0 ± 6.8	220.8 ± 27.7	2.44 ± 0.20	4.12 ± 0.33	71.0 ± 3.6	1.87 ± 0.20	2.96 ± 0.15	7.29 ± 0.72
SC-MAS film								
1:0.05	128.8 ± 2.2	195.3 ± 17.0	2.31 ± 0.19	4.25 ± 0.35	42.2 ± 0.8	1.71 ± 0.44	1.76 ± 0.44	6.50 ± 1.76
1:0.1	141.2 ± 4.8	197.7 ± 4.0	2.05 ± 0.29	4.12 ± 0.58	36.5 ± 1.3	1.94 ± 0.24	1.52 ± 0.05	5.66 ± 0.66
1:0.2	169.4 ± 8.1	250.0 ± 16.4	1.65 ± 0.37	4.74 ± 1.06	16.7 ± 0.6	3.40 ± 0.03	0.69 ± 0.03	5.11 ± 0.04

Part II: Sodium caseinate-halloysite films

1. Introduction

Sodium caseinate (SC), a sodium salt of casein, is the major milk protein that composed four different peptides - αS_1 , αS_2 , β and κ casein in the ratio of 4:1:4:1 (Walstra et al., 2006). Their molecular weights are in the range of 19 and 25 kDa. The isoelectric point (pI) of caseins is about 4.6 to 4.8. They are amphiphilic proteins, which are able to self-association into micelle structures in aqueous solution by hydrophobic interaction and by bridging of calcium phosphate nanoclusters. The core of micelle consists of αS_1 -, αS_2 - and β -casein with very little κ -casein, whereas the micelle surface is covered with κ -casein that provides a hydrophilic layers (Neha et al., 2012).

SC has widely used in food and pharmaceutical application such as film-coating tablet, improve drug solubility, and modified drug release². However, the nature of SC films is transparent and brittle during drying (Fabra et al., 2008; Audic and Chaufer, 2005). Moreover, it has two major problems: poor mechanical properties and high water vapor sensitivity (Audic and Chaufer, 2005). Plasticizers and lipids were used to enhance SC film properties (Fabra et al., 2008; Audic and Chaufer, 2005). Glycerin or polyols are good plasticizers for protein based films because it can reduce intermolecular hydrogen bonding of proteins (Audic and Chaufer, 2005). Additives, such as lipids, can reduce moisture permeability of films (Fabra et al., 2008). Moreover, celluloses are used as reinforcing fillers of sodium caseinate films (Pereda et al., 2011). So, it is interesting to seek a natural material to modify SC film properties for use in pharmaceutical applications.

Natural clays have been used to improve polymeric film properties (Alexandre and Dubois, 2000). Halloysite (HS) is a natural clay that has been used in pharmaceuticals such as adsorbents and additives in polymers (Rowe et al., 2009). HS is composed of aluminum oxide octahedrons and silicon dioxide tetrahedrons. Aluminum octahedrons and silicon tetrahedrons are compounded into the tubular structure. The surface of HS is silicon that had negative charge, but the inner is the positive charge of aluminum (Yuan et al., 2015; Lvov and Abdullayev, 2013). In pharmaceuticals, HS was used to improve polymeric film properties and used to develop drug delivery system (Yuan et al., 2015; Lvov and Abdullayev, 2013). In addition, HS was used to adsorb both the negative and positive charge of molecules (Lvov and Abdullayev, 2013). So, it is interesting to improve the SC film properties with HS. Effect of HS on the SC film properties including molecular interaction, mechanical properties, water uptake, water vapor permeability and drugs permeability were investigated.

2. Materials and methods

2.1. Materials

Casein sodium salt or sodium caseinate (SC) from bovine milk, and halloysite (HS) were purchased from Sigma-Aldrich Company (St. Louis, MO). Acetaminophen (ACT) and glycerin were obtained from Pharma Thai Co., Ltd. (Bangkok, Thailand) and Namsiang Co.,

Ltd. (Bangkok, Thailand), respectively. Methylparaben and ethylparaben were purchased from Sigma-Aldrich Company (St. Louis, MO). Propylparaben was obtained from Fluka (Dorset, England). All other reagents and solvents were of analytical grade.

2.2. Preparation of SC-HS dispersions

SC (5% w/v) was dispersed in distilled water, and glycerin (30% w/w based on SC content) was used as a plasticizer. Various amounts of HS (0.0, 2.5%, 5%, 10%, 20%, or 25 % w/w based on SC content) were dispersed in small volume of hot water, and then HS dispersions were mixed with SC dispersion to achieve SC-HS ratios of 1:0.025, 1:0.05, 1:0.1, 1:0.2, or 1:0.25 by weight, respectively. Then the pH of the SC and SC-MAS dispersions was adjusted to 6.8 using 0.1 M HCl or 0.1 M NaOH. All dispersions were adjusted to the final volume (100 mL) using distilled water and stirred for 30 min at room temperature (27 ± 2 °C). Then, the SC and SC-HS dispersions (20 mL) was cast onto a plastic plate (6.0 cm \times 9.5 cm) and dried at 60 °C for 24 h. The films were peeled off and stored in silica gel bead desiccators prior to use.

2.3. Characterization of SC-HS films

2.3.1. Thickness and transparency determinations

Thickness of the dry and wet films was measured at 6 different places using a microprocessor coating thickness gauge (Minitest600B, ElektroPhysik, Germany). The dry films were cut and placed on a control plate. The probe, which had been connected to the measurement gauge and calibrated using a standard film, gently moved downward to touch the film, and the film thickness was subsequently measured. To measure the wet thickness of the films, the films were subsequently placed in a small beaker containing 0.1 M HCl, which was shaken occasionally in a water bath at 37.0 ± 0.5 °C for 5 min. The samples were taken and blotted to remove excess water. The thickness of the wet films was immediately determined following the method mentioned above.

Transparency of the dry films was examined by measuring transmittance of the films using an UV-visible spectrophotometer (Shimadzu UV1201, Japan). The films were cut to a length of 4 cm and 1 cm in width and fixed to the measuring cell with adhesive tape. Then, the transmittance value was recorded at the wavelength of 500 nm. The thickness of the films was also determined using the method mentioned above. The transparency value could be computed using Eq. 1 (Merino et al., 2018; Woggum et al., 2014)

$$\text{Transparency value} = \frac{-(\log T_{500})}{h} \quad \text{Eq.1}$$

where T_{500} is the transmittance value at 500 nm and h is the mean thickness of the films.

The transparency values of the SC-HS films were compared with those of the SC films added with montmorillonite clay (magnesium aluminum silicate) that were prepared using the same method in the Section 2.2.

2.3.2. Surface and matrix morphology

Surface and matrix morphology of films were observed by using a scanning electron microscopy (SEM). The samples were placed on stubs, coated with gold in vacuum evaporator, and investigated using scanning electron microscope (S-3000N, Hitachi, Japan).

2.3.3. FTIR spectroscopy

Molecular interaction between SC and HS in SC-HS films were investigated using FTIR spectroscopy (Spectrum One, Perkin Elmer, Norwalk, CT) and KBr disc method. All films were crashed and triturated with KBr powder and then press with 10 tons of a hydrostatic press for 10 min. The samples were placed in a sample holder and scanned from 4000 to 450 cm^{-1} at the resolution rate of 4 cm^{-1} .

2.3.4. Powder X-ray diffraction (PXRD)

PXRD patterns of the samples in the forms of powders and films were studied by a powder x-ray diffractometer (Bruker D8 Advance diffractometer, Bruker BioSpin AG, Germany). A Cu radiation at 40 kV and 40 mA is an X-ray source, $2\theta = 2-30^\circ$ and step angle $= 0.02^\circ$. The interlayer distance of HS was calculated using Bragg's equation:

$$n\lambda = 2d\sin\theta \quad \text{Eq.2}$$

where n is 1 (the first order reflection was used). λ is the X-ray wavelength (1.54). θ is the angle of the basal spacing peak of HS, and d is the interlayer distance of HS.

2.3.5. Differential scanning calorimetry (DSC)

The thermal properties of the samples in the forms of powders and films were measured by a differential scanning calorimeter (DSC822, Mettler Toledo, Switzerland). The films were cut into small pieces and weighted (3-3.5 mg) in 40- μL aluminium pan without an aluminum cover. After that, the samples were heated at $10^\circ\text{C}/\text{min}$ and performed over $30-450^\circ\text{C}$.

2.3.6. Mechanical properties

Mechanical properties of the films including puncture strength and %elongation were investigated by using a texture analyzer (TA-XT2, Stable Micro system, Ltd., UK). In dry condition, the films were cut into $2\text{ cm} \times 2\text{ cm}$ and kept in 55% RH at room temperature for controlling the humidity of the films before to testing for 3 days. In the wet condition, the films were cut into $2 \times 2\text{ cm}$ and shaken in 0.1 M HCl for 5 min. After that, the excess water of the wet films was removed by a filter paper. The dry and wet films were fixed on the holder and penetrated by spherical stainless puncture probe (diameter 0.5 cm). The maximum force and displacement were recorded. The puncture strength and %elongation were calculated as follow:

$$\text{Puncture strength} = \frac{F}{A} \quad \text{Eq.3}$$

where F is the maximum force for puncture and A is the cross-sectional area of the edge of the films located in the path of cylindrical opening of the film holder.

$$\text{Elongation (\%)} = \frac{\sqrt{r^2 + D_T^2} - r}{r} \times 100 \quad \text{Eq. 4}$$

where D_T is the displacement of the probe from the point of contact to the point of film puncture.

2.3.7. Water uptake and matrix erosion determinations

Films (1.5 cm × 1.5 cm) were cut, and soaked in 0.1 M HCl at 37 °C for 5 and 15 min. The wet films were blotted to remove excess water, weighed, and dried at 50 °C to constant weight. The water uptake of films was calculated from the different wet and dried weight of films. The erosion of films was measured from weight before the test and dried constant weight of films.

$$\text{Water uptake (\%)} = \left(\frac{W_t - W_i}{W_i} \right) \times 100 \quad \text{Eq.5}$$

$$\text{Matrix erosion (\%)} = \left(\frac{W_i - W_d}{W_d} \right) \times 100 \quad \text{Eq.6}$$

where W_i , W_t , and W_d are the initial, wet and dry weight of the films, respectively.

2.3.8. Water vapor and drug permeabilities

Films were cut into a disc with a diameter of 1 cm, placed on open glass vials containing silica gel beads, and held in place using a screw lid with 0.58 cm² test area. The vials were placed in a desiccator containing a saturated sodium chloride solution (75% RH) at room temperature (20 °C, 45 %RH). The weight change of the samples was recorded periodically over 72 h. The relationship between water vapor permeated per area and time was plotted, and the slope of this relationship was water vapor permeation (WVP) rate. The WVP coefficient could be calculated by using the following equation:

$$\text{WVP coefficient} = \frac{Mh}{A\Delta P_v} \quad \text{Eq.7}$$

where M is WVP rate, h is the mean thickness of the films, A is the area of the exposed film, and ΔP_v is the vapor pressure difference.

The drug permeability of films was investigated by using a side-by-side diffusion cell. The films were cut and gripped between donor and receptor compartment with a diffusion area of 0.66 cm². The donor and receptor compartments had a volume of 3 mL, and the permeation medium used in this study was 0.1 M HCl. Acetaminophen (ACT) in concentration of 4 mg/mL was placed in donor compartment and refresh medium was replaced in receptor compartment. The amount of ACT in the samples collected at a given time was analyzed using a UV-visible spectrophotometer at wavelength of 265 nm. Parabens (methylparaben; MP, ethylparaben; EP, and propylparaben; PP) were used to characterize permeability of the SC and SC-HS films. An excess amount of parabens was exposed to 20 mL of 0.1 M HCl in Erlenmeyer flasks that were shaken at 37 °C for 3 days. The obtained suspensions were placed into the donor compartments. The concentration of parabens in the saturated solution and the samples collected from the receptor compartments were analyzed using a UV-visible spectrophotometer at wavelength of 256 nm.

The parameters of drug permeation across the films under steady state could be calculated by using the Fick's first law that could be shown as follows:

$$\frac{dM}{Adt} = PC_0 \quad \text{Eq.8}$$

where dM/dt is permeation flux that calculated using linear regression analysis of the relationship between cumulative amount of drug permeated and time, A is the diffusion area

of the film that the drug permeated, C_0 is the concentration of the drug in donor compartment, and P is apparent permeability coefficient. The apparent diffusion coefficient (D) elucidating the diffusivity of drug molecules across the film without thickness effects was calculated using the following equation:

$$D = \frac{h^2}{6t_L} \quad \text{Eq.9}$$

where t_L is the lag time which obtained from the x-intercept of the permeation profiles, and h is the mean thickness of the wet films. Thus, the apparent partition coefficient (K) is obtained as follows:

$$K = \frac{Ph}{D} \quad \text{Eq.10}$$

3.Results and discussion

3.1.Thickness, morphology and transparency of the films

The SC film without glycerin was cracked and brittle. Glycerin was used as a plasticizer for enhancing flexibility of the films and the continuous films were formed. The mean thickness of the dry films was over the range of 133-160 micron (Table 1). When increasing HS ratios, the thickness of the films was increased due to higher solid content of the cast dispersion. The wet thickness of the films after immersing in 0.1 M HCl for 5 min was determined and the data is listed in Table 1. The SC films gave obviously greater wet thickness than the dry thickness because of water absorption property of SC (Bajpai and Tiwari, 2014). Incorporation of HS in the ratios of 1:0.025-1:0.2 caused a lower wet thickness when compared with the dry thickness, whereas the HS ratio of 1:0.25 gave the highest wet thickness. It was visibly observed that the SC-HS films could swell when exposed with acidic medium, but the horizontal swelling of the films was possibly higher than the vertical swelling. This may lead to the lower wet thickness of the SC-HS films. The surface and matrix morphologies of the films are presented in Fig. 1. The smooth surface of SC film and SC-HS films in the ration of 1:0.1 were found, whereas increasing the ratio of HS to 1:0.2 caused a rough surface. This may be cracking of the surface region of the films during drying process. However, all films possessed a similar matrix structure.

The SC film with glycerin displayed a quite transparent, while addition of HS resulted in more opaqueness of the films. However, it was surprising that the SC-HS films had more visibly transparent than the SC films added with MMT that were characterized in the previous study (Kajthunyakarn et al., 2018). This led to the transparency study of the films, which the results are illustrated in Fig. 2. The higher the transparency values, the greater the opaqueness of the films was obtained. Addition of HS brought about a similar transparency value even though the highest ratio of HS was used. On the other hand, the SC-MMT films provided obviously greater transparency values than the SC-HS films at the ratios of 1:0.1, 1:0.2 and 1:0.25. These results suggested that the SC and SC-HS films showed similar transparent properties, whereas the SC-MMT films had more opacity than the SC-HS when adding at the

higher ratios. Thus, the characteristics of the SC-HS films were interesting to investigate for comparison with the SC-MMT films in the previous study.

3.2. Thermal behavior of the films

DCS thermograms of HS powder, SC powder, and the films are presented in Fig. 3. HS powder had no peak at the investigation temperature range. SC powder showed broad endothermic peak at 240 °C and following with two exothermic degradation peaks at 290 °C and 353 °C, respectively. The SC-HS physical mixture at the ratio of 1:0.25 showed the same DCS pattern when compared with that of the SC powder. When the SC film was formed, the thermal properties of the SC films was different with the SC powder, which the SC films showed small exothermic peak at 308 °C. Addition of HS into the SC films caused a shift of the exothermic peak to higher temperature that the highest ratio of HS (1:0.25) gave the exothermic peak at 323 °C. This result suggested that the thermal stability of the SC films could enhance by adding HS.

3.3. Molecular interaction between SC and HS in the films

HS powder showed the spectra at 3694 cm^{-1} and 3620 cm^{-1} , 1028 cm^{-1} , and 911 cm^{-1} (Fig. 4) that indicating the O–H stretching of inner-surface hydroxyl groups, Si–O stretching, and Al–O bending, respectively (Sakloetsakun and Pongjanyakul, 2017; Liu et al., 2015). FTIR spectra of SC powder presented the N–H stretching overlapped with the O–H stretching at 3368 cm^{-1} , the C=O stretching (amide I) at 1657 cm^{-1} and the N–H bending (amide II) at 1535 cm^{-1} (Pereda et al., 2008). The outstanding peaks of SC powder were shifted after film preparation due to hydrogen bond formation with water residues. Moreover, the SC films also displayed the C–O stretching peak (1045 cm^{-1}) of glycerin that was used as a plasticizer. The FTIR spectrum of the SC-HS (1:0.25) films could be compared with that of the SC-HS physical mixture at the same ratio. An obvious shift of the N–H stretching overlapped with the O–H stretching and amide I peaks was observed from the SC-HS films, suggesting the formation of hydrogen bond between amine and amide groups of SC and hydroxyl groups on the outer surface of tubular HS. Furthermore, the free O–H stretching peaks of inner-surface hydroxyl groups of HS at 3695 cm^{-1} were still found. This result indicated that SC could not interact with the OH groups in the inner surface of tubular HS.

PXRD pattern of HS showed the first order basal reflection at $2\theta=11.4^\circ$ with 7.75 Å interlayer distance, suggesting the dehydrated form of HS (Fig. 5). Moreover, the peaks at $2\theta=20.0^\circ$ (4.43 Å), and $2\theta=24.8^\circ$ (3.59 Å) corresponded to the tubular HS structure, and the second order basal reflection, respectively (Lvov and abdullayev, 2013). The SC powder displayed two broad peaks at approximately $2\theta=9^\circ$, and 20° , which the same pattern was found in the SC films. Incorporation of HS did not affect the PXRD pattern of the SC films, although the highest ratio of HS was used. On the other hand the SC-HS physical mixture clearly showed the peaks at $2\theta=11.4$ and 20.0° since the SC-HS ratio of 1:0.2 was used. In the previous report, HS incorporated in gellan gum film showed small two peaks of PXRD when

adding 40% of HS (Sakloetsakun and Pongjanyakul, 2017). It can be described that the HS dispersed homogeneously in the SC matrix had too low content for detecting by PXRD.

Taken together, the SC in the form of micelles is covered with κ -caseins. The outer parts of the surface are known as caseinomacropeptide chains (Dalgleish and Corredig, 2012), and the amine and amide I groups of amino acids in this chain could molecularly interact with the hydroxyl groups on the outer tubular structure of HS via the hydrogen bonding. The SC micelles could not intercalate into the tubular lumen or the silicate layer of HS because the SC micelle size was bigger than the internal lumen of HS. The average diameter of SC micelles is approximately 120 nm (Horne and Euston, 2005), whereas the diameter of the internal lumen of HS is 10-20 nm, and its outside diameter is in the range of 50-100 nm (Lvov and Abdullayev, 2013). Thus, the tubular HS could disperse in the SC films, and the nanocomposite formation between both substances could not be occurred.

3.4. Mechanical properties of the films

The puncture strength and % elongation of the dry films are displayed in Fig. 6. Addition of HS into the SC films resulted in decrease of both parameters, particularly the lowest of both parameters was found in the SC-HS films at the ratios of 1:0.2 and 1:0.25 (Fig. 6a and 6b). These results were similar to the polymeric films added with solid materials (Felton and McGinity, 2002; Rongthong et al., 2013), and were in agreement with the SC films incorporated with MAS (Kajthunyakarn et al., 2018). It could be explained that the HS particles could partially obstruct three-dimensional SC network of film formation. The wet films that were immersed in 0.1 M HCl for 5 min were also investigated for the puncture strength and % elongation. The wet films gave remarkably lower puncture strength than the dry films (Fig. 6a). However, the puncture strength of the wet SC-HS films was obviously greater than that of the wet SC films, and the highest puncture strength of the SC-HS (1:0.025) films was found. The dry and wet SC films showed similar % elongation, but the SC-HS films in wet state had remarkably higher %elongation than those in dry state (Fig. 6b). Moreover, decreasing of the %elongation of the wet SC films occurred when increasing HS ratios. These results indicated that the molecular interaction between SC and HS could improve the strength and flexibility of the films when the films were exposed to 0.1 M HCl.

The mechanical properties of the SC-HS could be compared with those of the SC-MAS films at the ratio of 1:0.1 that was reported previously. The SC-HS and SC-MAS films in dry state provided a similar puncture strength and % elongation. The puncture strength of the wet SC-HS films was lower than that of the wet SC-MAS films, but the wet SC-HS films gave better flexibility than the SC-MAS films.

3.5. Water uptake and erosion of the films

Water uptake and matrix erosion could be investigated in 0.1 M HCl because SC could be changed to insoluble caseins salt in acidic form, leading to a continuous sheet for testing. In contrast, SC could swell and dissolve in pH 6.8 phosphate buffer, resulting that the wet films could not be handled properly and blotted the excess water. Thus, a lack of the data was obtained in the neutral medium. Furthermore, the water uptake of the SC films could be tested

for 15 min because this film showed very high water absorption after 15 min and the wet films could not be handled properly. It was different from the SC-HS films at investigated ratios which possessed a continuous sheet for 120 min. The water uptake of the films in acidic medium at 5 and 15 min is shown in Fig. 7a. The water uptake of the SC films seemed to decrease when adding small amount of HS, and the SC-HS films in the ratios of 1:0.2 and 1:0.25 presented obviously lower water uptake than the SC films. These results suggested that a denser structure of the SC-HS films may be formed because of the molecular interaction between SC and HS that was described above, leading to lower water absorption capacity of the SC-HS films. Moreover, the similar results were found in the case of the gellan gum added with HS (Sakloetsakun and Pongjanyakul, 2017). Apart for water uptake studies, the matrix erosion of the SC films was found to be 21-26%, whereas SC-HS films seemed to show higher matrix erosion when compared with the SC films (Fig. 7b). The matrix erosion of the films could be possibly found because of leaching of water-soluble plasticizer, such as glycerin (Pongjanyakul and Puttipipatkachorn, 2007). Moreover, other water-soluble substances in HS powder may be leached from the films after exposed to the medium. These results suggested that decreasing of water uptake of the SC films occurred by incorporation of HS at higher ratios. This resulted in a denser matrix structure of the SC-HS film formed, reflecting water-filled channels and matrix strength of the wet films under acidic condition.

3.6. Film permeability studies

The permeability of the dry films could be tested by permeation of water vapor across the films. Thus, water vapor permeability of the films was determined and computed as WVP coefficient for regarding the effect of film thickness. The WVP coefficient of the films is presented in Table 1. The values of WVP coefficient of the SC films tended to decrease when adding HS to 10% and more than. This phenomena may be caused by increasing of tortuosity of water vapor pathway due to denser matrix formation of the SC-HS films.

Effect of HS ratios on the drug permeability of the SC films was tested using ACT as a drug model and 0.1 M HCl was used as a permeation medium. The ACT permeation profiles, which were the relationship between drug permeated and time, showed good linearity with R^2 more than 0.98, suggesting the permeation of drug achieved a steady state with very high concentration of drug. Thus, the Fick's first law could be used for describing the drug permeation process. Increase of HS ratios in the SC films resulted in a decrease of permeation flux and shorter lag time was found (Table 1). Moreover, the P values decreased because of the slower drug permeation fluxes. For elimination of the film thickness effects, the D was computed following the Eq. It can be seen that the D values of the SC-HS films were lower than that of the SC films, but not related to the ratios of HS added. The highest ratios of HS (1:0.25) in the SC films caused an increase of the D when comparing with the films with lower ratios of HS. These results suggested that incorporation of HS at low content could retard drug diffusivity due to denser matrix structure of the wet films in acidic medium. However, higher content of HS added could disturb matrix structure of the casein salt films formed after exposed to acidic medium, leading to higher D value was obtained.

Effects of parabens on film permeability were characterized using the SC and SC-HS (1:0.1) films in 0.1 M HCl. MP (MW=152.15 Da), EP (MW=166.18 Da), and PP (MW=10.20 Da) were used, and their solubilities in 0.1 M HCl at 37 °C were 4.03 ± 0.52 , 1.40 ± 0.12 , and 0.57 ± 0.05 mg/ml, respectively, which was similar to the previous report (Rongthong et al., 2015). The permeation profiles of parabens through the films are illustrated in Fig. 8. It can be seen that the higher the molecular weight of paraben, the lower permeation flux and the longer lag time were found. The parabens permeated across the SC films showed shorter lag time than using the SC-HS films. However, the permeation fluxes of parabens through the SC-HS films were greater than those through the SC films. This may be due to the thinner thickness of the wet SC-HS film (Table 1). These results caused higher P values of the SC-HS films as shown in Fig. 9a. The D values of parabens across the SC-HS films were lower than those across the SC films (Fig. 9b), and increasing MW of parabens brought about the lower D values that was the influence of number of alkyl chain of parabens (Rongthong et al., 2015). Furthermore, addition of HS into the SC films created higher tortuosity of water-filled channels, leading to lower diffusivity of parabens through the SC-HS films. The last parameter was partition coefficient (K). Figure 9c shows the K values of parabens when permeating through the SC and SC-HS films. The SC-HS films possessed higher K values of parabens than the SC films, and this parameter increased with increasing MW (longer alkyl chain) of parabens. These results suggested that parabens had higher affinity with the SC-HS films when compared with the SC films. It was possibly to explain that the OH and C=O groups of parabens may molecularly interact with the hydroxyl groups in the inner or outer tubular HS. Moreover, longer alkyl chain of parabens may also involve a hydrophobic interaction with HS, leading to greater K values of the SC-HS films for parabens.

4. Conclusions

This study shows that SC and HS can molecularly interact with HS by formation of hydrogen bond between amine and amide groups of SC and hydroxyl groups on the outer surface of tubular HS. SC micelles can not intercalate into the tubular lumen or the silicate layer of HS, thus nanocomposite between SC and HS can not be formed. However, the SC-HS films show continuous sheets and provide the similar transparency with the SC films. HS added results in a reduction of puncture strength and elongation of the dry SC films, whereas it can enhance film strength of the wet SC films in acidic medium. Addition of the HS at low content can retard drug diffusivity across the films in acidic medium, but 25% HS causes higher D value because HS can disturb matrix structure of the casein salt films formed after exposed to acidic medium. Furthermore, the drug permeations across the SC and SC-HS films are dependent on MW or alkyl chain of permeants, which affect on drug diffusion and partition processes in the films. These findings suggest that the SC-HS films could offer potential in the development for modulating drug release from coated tablets.

References

- Alexandre M, Dubois P. Polymer-layered silicate nanocomposites: preparation, properties and uses of a new class of materials. *Mater Sci Eng* 2000; 28: 1-63.
- Audic JL and Chaufer. Influence of plasticizers and crosslinking on the properties of biodegradable films made from sodium caseinate. *Eur Polym J* 2005; 41: 1934-42.
- Bajpai SK, Tiwari P. Investigation of moisture sorption behavior of soluble sodium caseinate. *Emir J Food Agric* 2014; 26: 399-408.
- Dalgleish DG, Corredig M. The structure of the casein micelle of milk and its changes during processing. *Annu Rev Food Sci Technol* 2012;3:449–467.
- Fabra MJ, Talens P and Chiralt A. Tensile properties and water vapor permeability of sodium caseinate films containing oleic acid-beeswax mixtures. *J Food Eng* 2008; 85: 393-400.
- Felton LA, McGinity JW. Influence of insoluble excipients on film coating systems. *Drug Dev Ind Pharm* 2002;28:225–243.
- Horne DS and Euston SR. Simulating the self-association of caseins. *Food hydrocolloids* 2005; 19: 379-386.
- Kajthunyakarn W, Sakloetsakun D, Pongjanyakul T. Sodium caseinate-magnesium aluminum silicate nanocomposite films for modified-release tablets *Mater Sci Eng C* 2018;92:827–839.
- Liu M, Dai L, Shi H, Xiong S, Zhou C. In vitro evaluation of alginate/halloysite nanotube composite scaffolds for tissue engineering. *Mater Sci Eng C* 2015;49:700-712.
- Lvov Y, Abdullayev E. Functional polymer-clay nanotube composite with sustained release of chemical agents. *Prog Polym Sci* 2013; 38: 1690-1719.
- Merino D, Mansilla AY, Gutiérrez TJ, Casalongué CA, IvarezVA. Chitosan coated-phosphorylated starch films: Water interaction, transparency and antibacterial properties. *React Funct Polym* 2018;131:445–453.
- Neha A, Tarun G, and Ajay B. Review on casein production and casein based nano-formulations. *Int Res J Pharm* 2012; 3(1): 41-45.
- Pereda M, Amica G, Racz I and Marcovich NE. Structure and properties of nanocomposite films based on sodium caseinate and nanocellulose fibers. *J Food Eng* 2011; 103: 76-83.
- Pereda M, Aranguren MI, Marcovich NE. Characterization of chitosan/caseinate films. *J Appl Polym Sci* 2008; 107: 1080-1090.
- Pongjanyakul T, Puttipipatkachorn S. Alginate-magnesium aluminum silicate films: effect of plasticizers on film properties, drug permeation and drug release from coated tablets. *Int J Pharm* 2007; 333: 34–44.
- rice starch based biodegradable films. *Int J Biol Macromol* 2014;67:490–502.
- Rongthong T, Sungthongjeen S, Siepmann F, Siepmann J, Pongjanyakul T. Quaternary polymethacrylate-magnesium aluminum silicate films: Water uptake kinetics and film permeability. *Int J Pharm* 2015; 490: 165-172.

- Rongthong T, Sungthongjeen S, Siepmann J, Pongjanyakul T. Quaternary polymethacrylate-magnesium aluminum silicate films: Molecular interactions, mechanical properties and tackiness. *Int J Pharm* 2013; 458: 57-64.
- Rowe RC, Sheskey PJ, and Quinn ME. Handbook of pharmaceutical excipients, 6th ed. American Pharmaceutical Association, Washington; 2009. 352-354.
- Sakloetsakun D, Pongjanyakul T. Modification of gellan gum by halloysite: physicochemical evaluation and drug permeation properties. *Drug Dev Ind Pharm* 2017; 43(3): 492-501.
- Walstra P, Wouters JT, Geurts TJ. Dairy science and technology. 2nd ed. Wageningen: Taylor & Francis Group; 2006.
- Woggum T, Sirivongpaisal P, Wittaya T. Properties and characteristics of dual modified
- Yuan P, Tan D, Annabi-Bergaya F. Properties and applications of halloysite nanotubes: recent research advances and future prospects. *Appl Clay Sci* 2015; 112-113: 75-93.

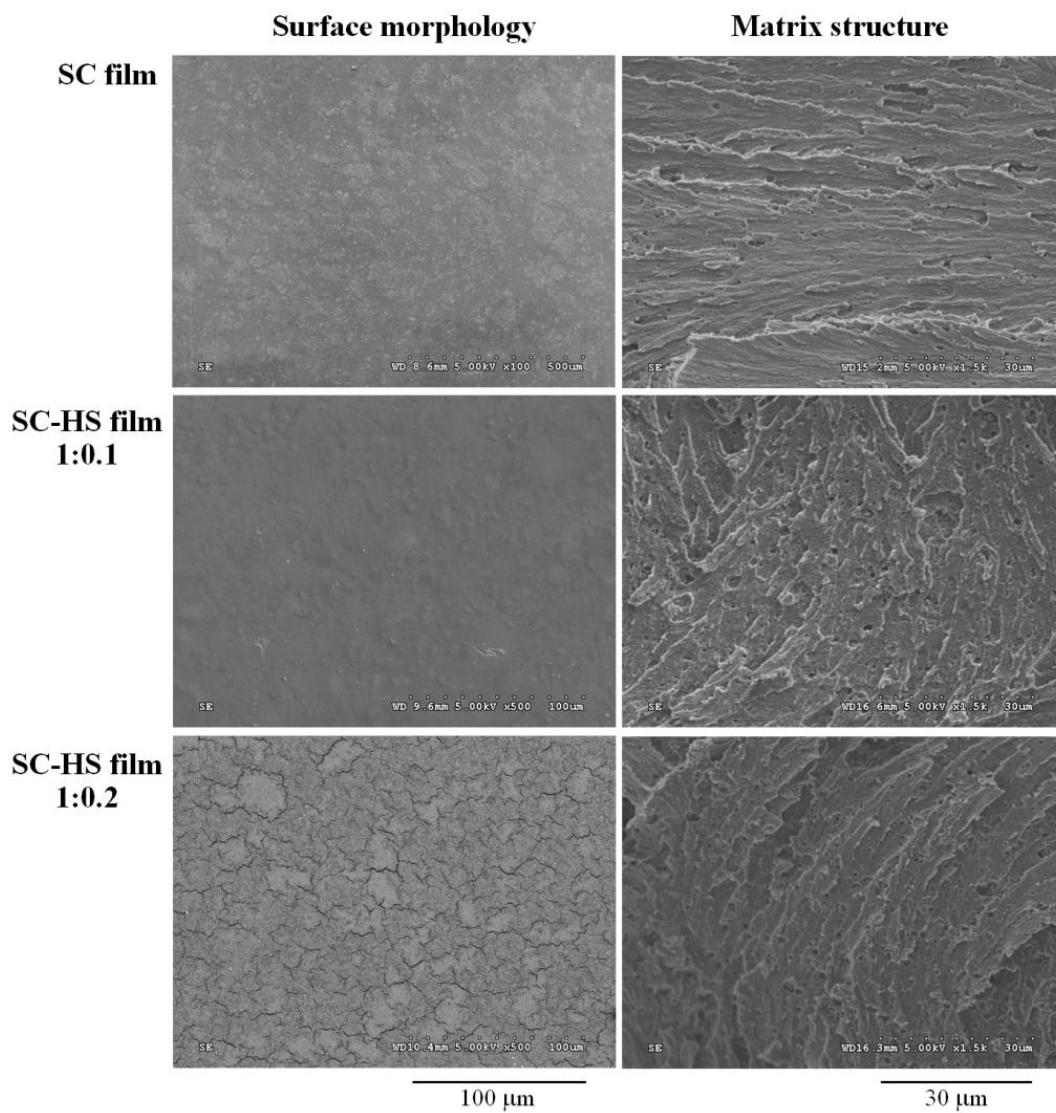


Figure 1. Surface and matrix morphologies of SC film and SC-HS films at the ration of 1:0.1 and 1:0.2.

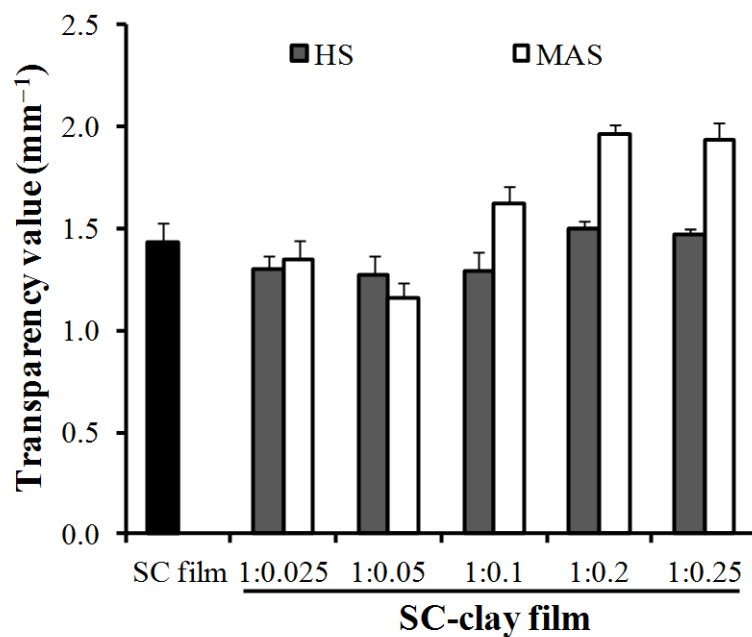


Figure 2. Transparency value of the SC, SC-HS, and SC-MAS films at the wavelength of 500 nm. Each value indicates mean \pm SD, n=3.

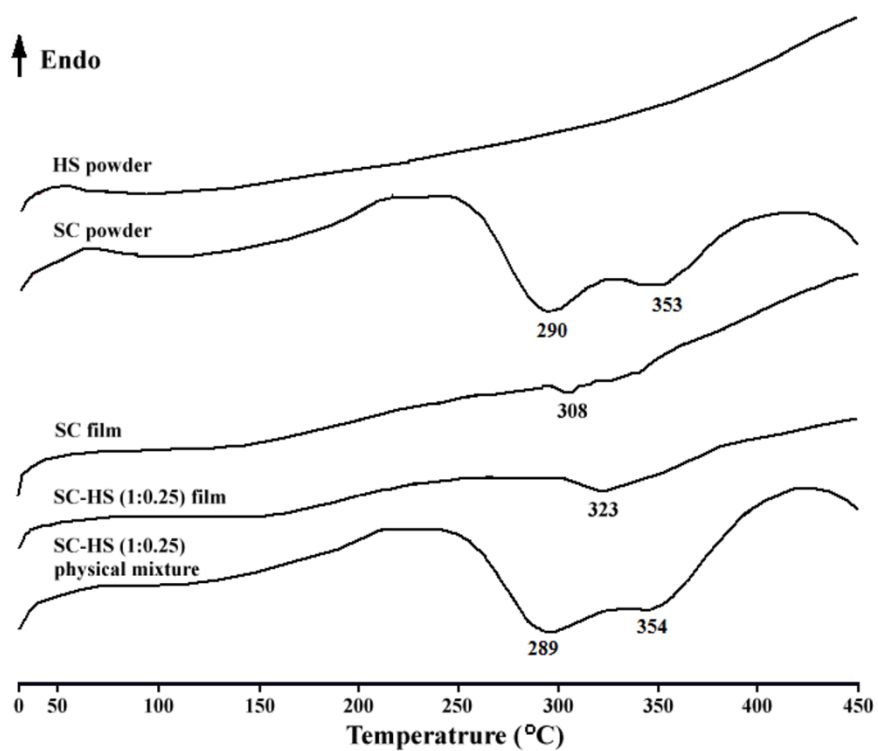


Figure 3. DSC thermograms of HS powder, SC powder, SC film, and SC-HS film.

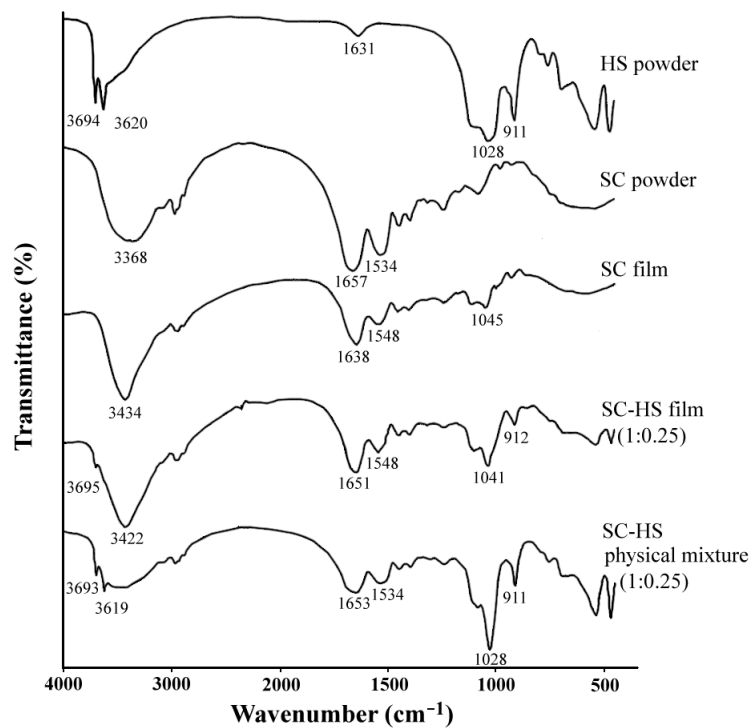


Figure 4. FTIR spectra of HS powder, SC powder, SC film, and SC-HS film.

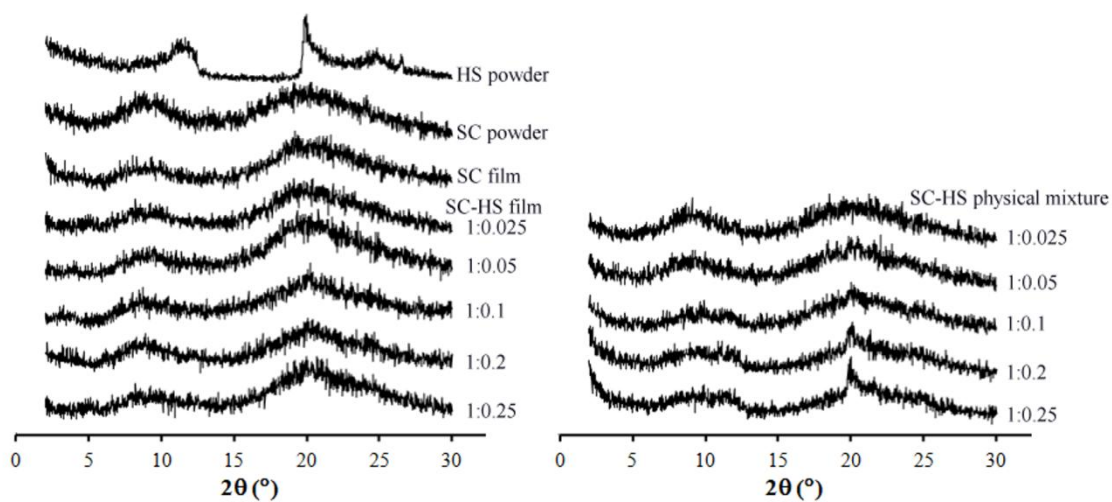


Figure 5. PXRD pattern of HS powder, SC powder, SC film, SC-HS physical mixtures, and SC-HS films.

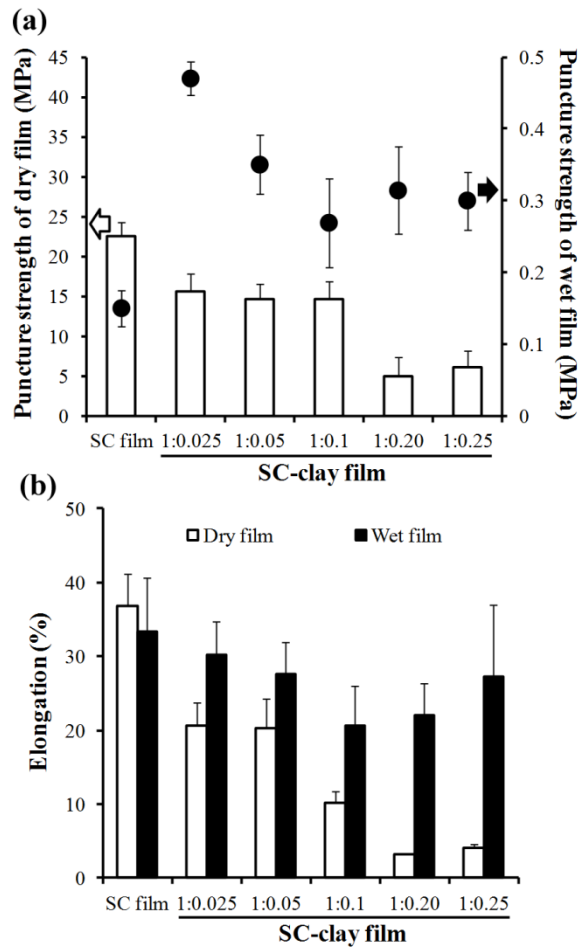


Figure 6. Puncture strength and elongation of SC, and SC-HS films in dry and wet states. Each value indicates mean \pm SD, $n=4$.

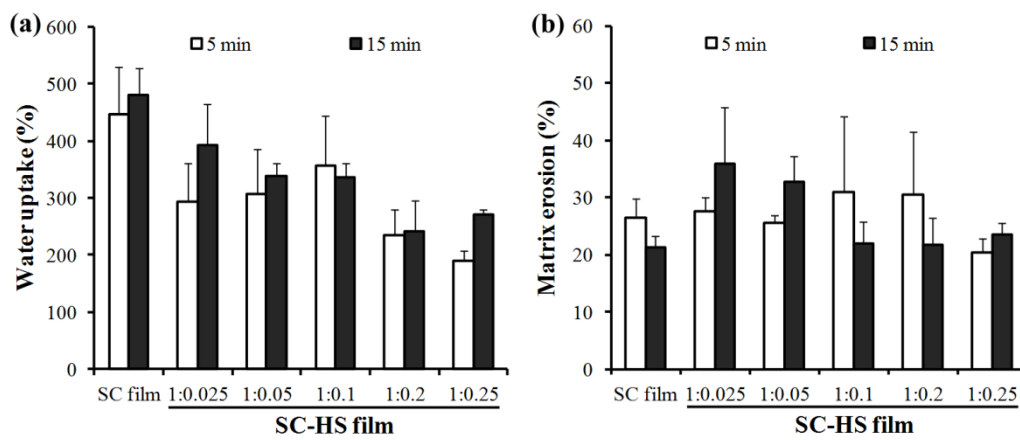


Figure 7. Water uptake (a) and matrix erosion (b) of SC and SC-HS films in 0.1 M HCl. Each value indicates mean \pm SD, $n=5$.

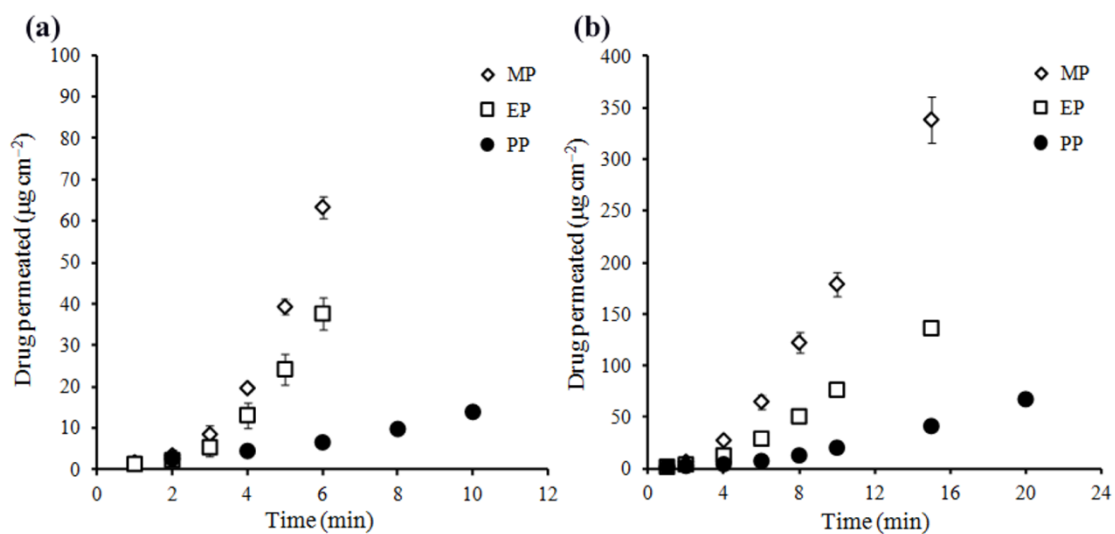


Figure 8. Permeation profiles of parabens across SC (a) and SC-HS (1:0.1) (b) films using 0.1 M HCl as a permeation medium. Each value indicates mean \pm SD, $n=3$.

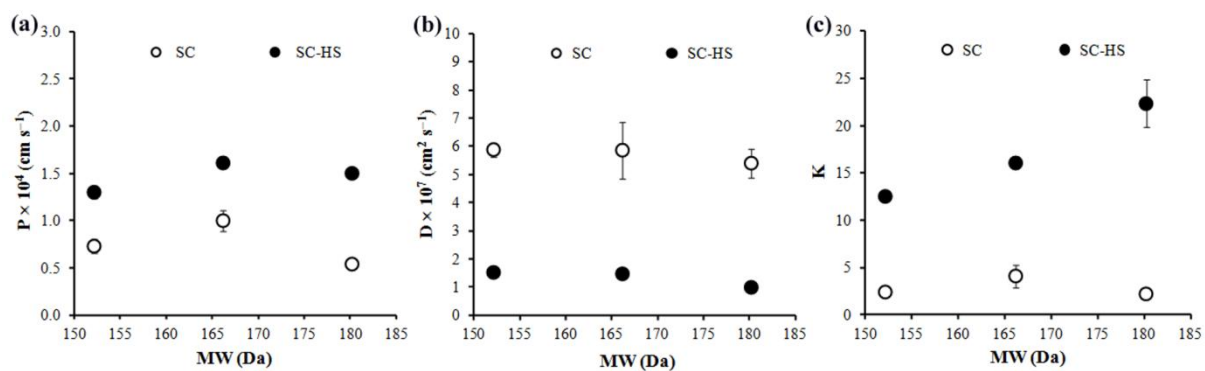


Figure 9. Permeability coefficient (a), diffusion coefficient (b), and partition coefficient (c) of parabens in SC and SC-HS (1:0.1) films. Each value indicates mean \pm SD, $n=3$.

Table 1. Thickness and film permeability of SC and SC-HS films.

Film	Dry thickness ^a (μm)	Wet thickness ^a (μm)	WVP coefficient ^b $\times 10^4$ ($\text{mg mm}^{-1} \text{h}^{-1} \text{mmHg}^{-1}$)	ACT permeation ^c			
				Flux	Lag time	$P_{\text{app}} \times 10^4$	$D_{\text{app}} \times 10^7$
				($\mu\text{m cm}^{-2} \text{min}^{-1}$)	(min)	(cm s^{-1})	($\text{cm}^2 \text{s}^{-1}$)
SC film	133.0 ± 6.8	220.8 ± 27.7	4.12 ± 0.33	71.0 ± 3.6	1.87 ± 0.20	2.96 ± 0.15	7.29 ± 0.72
SC-HS film							
1:0.025	160.9 ± 18.6	109.0 ± 9.54	4.13 ± 0.49	53.9 ± 0.73	2.03 ± 0.21	2.25 ± 0.03	1.62 ± 0.02
1:0.05	156.4 ± 11.9	125.3 ± 32.0	4.38 ± 0.43	42.5 ± 1.29	1.74 ± 0.01	1.77 ± 0.05	2.51 ± 0.01
1:0.1	149.7 ± 6.8	146.3 ± 35.7	3.64 ± 0.94	38.9 ± 0.84	2.30 ± 0.05	1.62 ± 0.03	2.58 ± 0.05
1:0.2	152.4 ± 11.6	138.0 ± 21.9	3.43 ± 0.53	40.2 ± 1.42	1.91 ± 0.12	1.67 ± 0.06	2.77 ± 0.18
1:0.25	160.6 ± 7.9	224.0 ± 20.9	3.54 ± 0.49	26.6 ± 0.86	2.74 ± 0.15	1.11 ± 0.04	5.10 ± 0.28

^a Data are mean \pm S.D., n=6.^b Data are mean \pm S.D., n=5.^c Data are mean \pm S.D., n=3.

Part III: Sodium caseinate-clay films containing fluconazole

1.Introduction

Sodium caseinate (SC), a casein salt, is the major milk protein (Walstra et al., 2006; Elzoghby et al., 2011). SC is composed of αS_1 , αS_2 , β and κ casein in the ratio of 4:1:4:1 (Walstra et al., 2006; Neha et al., 2012). Casein micelle has a hydrophobic interior of phosphoproteins held together by hydrophobic interaction, whereas the micelle surface is covered by a hydrophilic layer of κ -casein (Walstra et al., 2006). It is a biodegradable polymer that has been used in food industry and pharmaceuticals as films coating for tablets (Diak et al., 2007), drug solubilizers (Millar and Corrigan, 1991), and drug delivery systems (Elzoghby et al., 2013). The appearances of SC films are transparent and brittle in nature. So, modification of the SC film properties is required with plasticizer (Audic and Chaufer, 2005; Fabra et al., 2008). Mostly, plasticizers, such as glycerin and sorbitol, cause an increase in material flexibility by decreasing intermolecular forces between polymers coils (Fabra et al., 2008). However, they have two major problems: poor mechanical properties and high water vapor sensitivity (Audic and Chaufer, 2005). Thus, it is interesting to seek a natural material to modify SC film properties for use in drug delivery systems.

Recently, natural clays have been widely used in pharmaceuticals, for example, adsorbent, stabilizing agents, and additives in polymers (Kibbe, 2000). Addition of clay, such as magnesium aluminum silicate (MAS) and halloysite (HS), could modify physical properties and drug permeability of the SC films. MAS is composed of three-lattice layers, a central octahedral sheet of aluminum or magnesium and two external silica tetrahedron layers (Alexandre and Dubois, 2000). Several studies showed that MAS can improve film properties. The composite films of chitosan and MAS have good film properties including well-behaved tensile strength, flexible films. Besides, the chitosan-MAS films can modify release of drug because chitosan interacted with MAS by electrostatic interaction (Khunawattanakul et al., 2010). In addition, films of quaternary polymethacrylate with MAS have fine film properties and can modify release of drugs as well (Rongthong et al., 2013; Rongthong et al., 2015). HS is composed of aluminum oxide octahedrons and silicon dioxide tetrahedrons. Aluminum octahedrons and silicon tetrahedrons are compounded into the tubular structure. The surface of HS is silicon that had negative charge, but the inner is the positive charge of aluminum (Yuan et al., 2015; Lvov and Abdullayev, 2013). In pharmaceuticals, HS was used to improve polymeric film properties and used to develop drug delivery system (Yuan et al., 2015; Lvov and Abdullayev, 2013). In addition, HS was used to adsorb both the negative and positive charge of molecules (Lvov and Abdullayev, 2013). So, it is interesting to use the SC-clay film for drug delivery system.

Oral candidiasis is the most common disease from fungal infection of patients who used long term steroid drugs. *Candida albican* is a primarily pathogen of this disease. Additionally, it is rapid and more progress in patients with human immunodeficiency (HIV) because they are immune compromised function (Bachhaav et al., 2011). The use of topical antifungal

medications is the standard treatment of oral candidiasis, and imidazole derivative drugs were firstly selected for treatment oral candidiasis. However, the imidazole drugs are short half-life when administrated via oral route due to first pass metabolism (Yang et al., 2008). Nowadays, developments of topical imidazole drugs were widely reported for local treatment, for example, fluconazole (FZ) buccal films (Yehia et al., 2009) and clotrimazole (CLZ) buccal tablets (Khanan et al., 1996). FZ is the first of synthesis azole derivative and has activity against *Candida* sp (Correa and Salgado, 2011). It is an antifungal drug that had hydrophobic structure. However, the concentration of FZ at the site of infection is low because of high volume distribution especially topical infection (Correa and Salgado, 2011). So, it is interesting to study alternative materials for enhancing FZ solubility and use for fabricating local drug delivery systems. This may result in an improvement of antifungal activity of FZ.

The aim of this study was to prepare the SC-clay films loaded with FZ by a spray method. The films were characterized including film thickness, crystallinity, drug content, drug release, mucoadhesive properties, and antifungal activity. Thus, the FZ-loaded SC-clay films may be used as a local delivery system in oral candidiasis.

2. Methodology

2.1. Preparation of FCZ-loaded SC-clay dispersions

SC (5% w/v) was dispersed in distilled water, and clay both MAS and HS (5%, 10%, or 20% based on SC content) were dispersed in hot water. Then, clay dispersion was mixed with SC dispersion. After that, FCZ powder (20% w/v based on SC content) was added into the SC-clay dispersions and the mixtures of dispersions were continuously stirred at room temperature.

2.2. Characterization of dispersions

2.2.1. pH and Particle size

The pH of all dispersions was measured by pH meter (Minitest 600B, ElectroPhysik, Germany). Particle size of dispersions was measured by using a laser diffraction particle size analyzer (mastersizer2000, Malvern Instrument Ltd., UK). The dispersions were dispersed in 70 mL of distilled water in a small volume of sample dispersion unit. Before measurement, the samples were stirred at a rate 50Hz for 30 second. Particle size was reported as volume weight mean particle size ($D_{4,3}$), polydispersity index (PI), and particle size dispersion. PI was calculated from the following equation:

$$PI = \frac{d(0.9) - d(0.1)}{d(0.5)} \quad (1)$$

Where $d(0.9)$, $d(0.5)$, and $d(0.1)$ are the particle diameters determined at the 90th, 50th and 10th percentile of undersized particles, respectively.

2.2.2. Zeta potential

Zeta potential of all samples was determined by laser Doppler electrophoresis analyzer (Zetasizer Model ZEN 2600, Malvern Instrument Ltd., UK). It was controlled temperature at 25 °C. Each sample was diluted to obtain appropriate concentration before testing.

2.3. Preparation of FZ-loaded SC-clay film

The FZ-loaded SC-clay films were prepared by spray method. SC (5% w/v) was dispersed in distilled water at room temperature. Various amounts of clay (0%, 5%, 10% or 20% based on SC content) were dispersed in hot water, and then clay dispersion was mixed with SC dispersion. In this study, glycerin (30% based on SC content) was used as a plasticizer. After that, FZ powder (20% w/v based on SC content) was added into the SC- clay dispersions and the mixtures of dispersions were stirred overnight at room temperature. Then the mixture dispersions were sprayed on a plastic sheet that was attached in the tablet coating pan to get drug-loaded SC-clay films. The films were kept in the refrigerator before testing.

2.4.Characterization of the films

2.4.1.Film thickness and morphology

The film thicknesses were measured at fifteen different positions by a microprocessor coating thickness gauge (Minitest 600B, ElectroPhysik, Germany). The probe was touched to the films placed on a control plate. The mean thickness was reported. Surface morphology and cross-sectional morphology of the films were observed by using scanning electron microscopy (SEM).

2.4.2. FTIR spectroscopy

Molecular interactions between SC and FCZ in the films were investigated using FTIR spectroscopy (Spectrum One, Perkin Elmer, Norwalk, CT) and KBr disc method. All films were crashed and triturated with KBr powder and then press with 8 tons of a hydrostatic press for 10 min. The samples were placed in a sample holder and scanned from 4000 to 400 cm^{-1} at the resolution rate of 4 cm^{-1} .

2.4.3.Powder X-ray diffractometry (PXRD)

The crystallinity of FCZ in the films was studied by a powder x-ray diffractometry (Bruker D8 Advance diffractometer, Bruker BioSpin AG, Germany). A Cu radiation at 40 kV and 40 mA is an X-ray source, $2\theta = 2-30^\circ$ and step angle = 0.02 2θ s^{-1} .

2.4.4. Differential scanning calorimetry (DSC)

The thermal properties of the films were measured by a differential scanning calorimeter (DSC822, Mettler Toledo, Switzerland). The films were cut into small pieces and weighted (3-3.5 mg) in aluminium pan. After that, the samples were heated at $10^\circ\text{C}/\text{min}$ and performed over $30-450^\circ\text{C}$.

2.4.5.Mechanical properties

Mechanical properties of the films including puncture strength and elongation were investigated by using a texture analyzer (TA-XT2, Stable Micro system, Ltd., UK). The films were cut into 2 x 2 cm and kept in 55%RH at room temperature for controlling the humidity of the films before to testing for 3 days. After that, the films were fixed on the holder and penetrated by spherical stainless puncture probe (diameter 0.5 cm). The maximum force and displacement were recorded (n=4). The puncture strength and %elongation were calculated as follow:

$$\text{Puncture strength} = \frac{F}{A} \quad (2)$$

where F is the maximum force for puncture and A is the cross-sectional area of the edge of the films located in the path of cylindrical opening of the film holder.

$$\% \text{ Elongation} = \frac{\sqrt{r^2 - D^2} - r}{r} \times 100 \quad (3)$$

where D is the displacement of the probe from the point of contact to the point of film puncture.

2.4.6. Drug content

The films were cut into a disc and weighted accurately, and then the films were added into 50 mL of acetonitrile:water (3:7) mixed solvents in a volumetric flask. Next, the flasks were sonicated until the films dissolved. The medium will be filtered through filter membrane, and then FZ content was measured by HPLC at the wavelength of 210 nm. The FZ content in the films was calculated (n=3).

Fluconazole content was quantitatively analyzed by HPLC method. HPLC analysis was used an octadecyl carbon chain (C18) column (4.6 mm x 15 cm, 5 μ m), and UV detector at 210 nm. A mobile phase system consisting of 3:7 acetonitrile-water was used at flow rate of 1 mL/min and injection volume of 20 μ L.

2.4.7. Drug release

The FZ release was investigated by using a side-by-side diffusion cell. The films were cut into a disc, weighted accurately, and gripped with the cell. The release medium was pH 5.8 Stimulated saliva fluid (SSF). The 3 mL of pH 5.8 SSF was added into the cells at 37 ± 1 °C, then 1 mL of sample was collected and replaced with refresh medium. The FCZ release was analyzed HPLC at the wavelength of 210 nm (n=3).

2.4.8. Antifungal activity

The antifungal activity was studied using agar diffusion assay. A volume of 20 mL of sterile sabouraud dextrose agar was dispersed in sterile petri dish for incubated *C. albican* (ATCC 10231) at 37°C for 24 hr. 10^6 cfu/mL of *C. albican* 200 μ L was spread on surface sabouraud dextrose agar. The agar in each petri dish was bored 4 cavities (0.5 cm diameter), and then 50 μ L of samples collected from drug release studies at 15 minute were added into the cavity. After that, the petri dishes were incubated at 37°C for 24 hr. The diameter of inhibition zone were measured and reported (n=3). Fluconazole at concentration 80 and 100 μ g/mL were positive control. The release medium was a negative control.

2.4.9. Mucoadhesive test

Mucoadhesive properties of the films were studied by using texture analyzer, and porcine esophageal mucosa was used as a bioadhesive membrane. Before testing, the porcine esophageal mucosa was soaked into the pH 7.4 phosphate buffer and pH 5.8 SSF was dropped onto the mucosa tissue. Then, the mucosa tissue was fixed on a platform. The films were cut and attached to the cylinder probe. The probe was moved downward and contacted to the mucosa. Maximum force used to remove the films form mucosa tissue was recorded (n=5).

3. Results and discussion

3.1. Characterization of the dispersions

The dispersions of FZ-loaded SC and FZ-loaded SC-clay are milky dispersions. All ratios of dispersions were presented neutral pH because of the neutral pH of SC and clay dispersions. Moreover, when adding clay ratio, average of particle size was decreased and the size distribution were double mode with different polydispersity indexes due to the aggregation. The SC dispersion showed negative charge around -24.37 mV and MAS and HS dispersions were also presented negative charge around -34.42 mV and -28.14 mV respectively, so all dispersions of SC-clay ratio were exhibited a negative charge too. In addition, FZ dispersion also presented a negative charge. The particle size and zeta potential of all dispersions were showed in Table 1.

3.2. Appearance of the films

The FZ-loaded SC film and FZ-loaded SC-clay film were prepared by a spray method and glycerin was used as a plasticizer. Since SC film without plasticizer were cracked. The appearance of the films was yellow thin films and thickness of the films was between $91.03 \pm 4.40 \mu\text{m}$ to $128.50 \pm 2.78 \mu\text{m}$. The thickness was increased when increasing clay ratio due to higher solid content in the films. Furthermore, incorporation of clay into the films, led to the films had stronger. The surface of SC film without clay and FZ had a smooth film (Figure 1), while the films with clay and FZ had unrefined surface. Moreover, association of clay and FZ resulted in the dense matrix structure of the films (Figure 2-4).

3.3. FTIR

Molecular interaction of components in the films was studied by FTIR spectroscopy. The major spectra of SC powders presented N-H stretching of NH_2 at 3399 cm^{-1} , C=O stretching of amide I and N-H bending of amide II at 1657 cm^{-1} and 1536 cm^{-1} , respectively. Moreover, the C-H stretching of SC showed at 2963 cm^{-1} and 2929 cm^{-1} (Pereda et al., 2008). The spectra peak of MAS at 1640 cm^{-1} indicated the hydroxyl bending and Si-O-Si stretching of MAS showed spectra peak at 1015 cm^{-1} (Rongthong et al., 2013). The main spectra of HS at 3694 cm^{-1} and 3620 cm^{-1} indicated the Al-OH stretching, and Si-O-Al stretching of HS presented at 1028 cm^{-1} and 539 cm^{-1} . Besides, the Al-OH bending of HS displayed at 911 cm^{-1} , and the Si-O stretching showed at 692 cm^{-1} (Sakloetsakun and Pongjanyakul, 2017). When HS was combined into the films, the Al-OH stretching was lost, led to the destroyed of the octahedral sheet of HS. The FTIR spectrum of FZ powder displayed the C-H stretching of triazole group (3122 cm^{-1} and 1254 cm^{-1}), the C=C stretching of difluorobenzyl group (1621 cm^{-1}), the C-F stretching of difluorobenzyl group (1272 cm^{-1}), the C-H deforming of difluorobenzyl group (1075 cm^{-1}), and the C-C stretching of propane backbone (1117) (Alkhamis et al., 2002; Park et al., 2007). These spectra of FZ could be reported that FCZ powder was two mixture polymorphs: hydrate form I and monohydrate. The FZ-loaded SC-MAS films showed different FTIR spectra peak when compared with the physical mixture of SC-MAS-FZ. Addition FZ into the films resulted in a miss of triazole group peak (3122 cm^{-1} and 1254 cm^{-1}). Moreover, the C=C stretching of difluorobenzyl group at 1621 cm^{-1} and the

C-H deforming of difluorobenzyl group at 1075 cm^{-1} were also disappeared. In addition, propane backbone peak was shifted to lower wavenumber (1111 cm^{-1}) with the addition of FZ. However, the C-F stretching of difluorobenzyl group was moved to a higher wavenumber (1276 cm^{-1}). This result suggested that incorporation of FCZ into the films led to the changed of polymorphism from mixture of hydrate form I and monohydrate to monohydrate. Nevertheless, the FTIR spectra of physical mixture still exhibited the characteristic peak of FZ.

3.4. PXRD

The crystallinity of FCZ in the films was studied by a powder x-ray diffractometry. The PXRD profiles of the FCZ-loaded SC-MAS films are showed in Figure 3 and Figure 4, and the FCZ-loaded SC-HS films are showed in Figure 5 and Figure 6. The basal spacing of MAS was showed at 7.0° (2θ) that indicated a thickness of the MAS silicate layers at 1.26 nm^{14} . The basal spacing of HS is presented at $2\theta = 12.08^\circ$ that indicated the dehydrated form of HS (Sakloetsakun and Pongjanyakul, 2017). The SC powder presented broad peaks, similar to the SC film, revealing of an amorphous of SC both SC powder and SC film. However, FCZ powder was two mixture polymorphs such as anhydrate form I and monohydrate. The PXRD patterns of the FCZ-loaded SC-MAS film did not show the basal spacing peak of MAS at 7.0° 2θ , indicating a formation of nanocomposite material. For the films with HS, the HS basal spacing was disappeared when HS was added into the films, indicated that the bonds between kaolinite layers were disrupted (Sabahi et al., 2018; Souri et al., 2015). Furthermore, when FCZ powder was added into the films, the polymorphs of FCZ were changed to the mixtures of monohydrate and amorphous. These results suggest that the recrystallization of FCZ caused a different polymorphism during film formation. However, the physical mixture of FCZ was performed the crystallinity of anhydrate form I and monohydrate.

3.5. DSC

The thermal property of the films was investigated by using a differential scanning calorimeter or DSC and results are shown in Figure 7-10. The DSC thermograms of FZ exhibited the melting point at 142°C and MAS showed only endothermic peak around 77°C that is indicated the evaporation of water (Rongthong et al., 2013). Whereas SC powder presented endothermic peak around 70°C and exothermic peak around 290°C and 350°C . The endothermic peak of SC referred to water evaporation, while exothermic peak mentioned to decompose of SC. As previous study showed that endothermic peak of HS was around 435°C , bring about to the de-hydroxylation of HS (Zhang et al., 2012). Incorporation of clay into the film, the melting point of FZ and exothermic peak of SC were disappeared. Nevertheless, the mixture of SC-MAS-FZ and SC-HS-FZ by physical mixture still showed the melting point of FZ and exothermic peak of SC. The results showed that clay could be improved the thermal property of the films.

3.6. Mechanical properties

Mechanical properties of the films such as puncture strength and elongation were studied using a Texture analyzer as shown in Figure 11. The SC film without FCZ and clay had the

highest mechanical properties including puncture strength and elongation. The mechanical properties were decreased when increasing clay ratios. These results can describe from obstruction of clay particles. Clay particles may be hinder the formation of SC films and contributed to hard and brittle films (Rongthong et al., 2013). However, the mechanical properties of the films were good properties for pharmaceutical applications.

3.7. *In vitro* drug release

In vitro drug release of the films was studied in pH 5.8 SSF. The FZ-loaded SC film and FZ-loaded SC-clay films were reported FZ content in the range of 11.06-13.43 %w/w because FZ content in the films was fixed in the ratio SC-FZ of 5:1. The FZ content seemed to decrease when adding clay into the films due to adsorption of drug on clay particles. The release profiles of FZ from the films with MAS and HS are showed in Figure 12 and Figure 13, respectively. The FZ release from FZ-loaded SC film was faster than the films with MAS and complete release was found within 3 h. This was due to the denser structure of SC-MAS film and adsorption of FZ onto the MAS silicate layer. On the other hand, FZ release from the films with HS had no different when compared with the film without clay. Moreover, % release of FZ seemed to decrease when increasing clay content. These results caused from lower FZ content in the films with higher clay content.

3.8. *Antifungal activity*

The antifungal activity of FZ after release from the films was studied using an agar diffusion assay and inhibition zone is report in Figure 14. The FZ in the concentration of 100 µg/mL was used as a positive control and showed the inhibition zone of 13.98 ± 0.32 mm. The FZ released from the films at 15 minute could inhibit *C. albican* with diameter of inhibition zone in the range 13.84-15.08 mm. However, incorporation of clay had no effect to diameter of inhibition zone. This result like to other previous study, for example, FZ released from FZ-loaded alginate-SC beads had effective against *C. albican* (Khlibsuwan et al., 2018).

3.9. *Mucoadhesive properties*

The porcine esophageal membrane was used as a bioadhesive membrane for testing mucoadhesive properties. The results showed that FZ-loaded SC film and FZ-loaded SC-clay films were presented mucoadhesive properties. Moreover, addition of clay into the films did not affect the detachment force of the films (Figure 15). This result was in agreement with previous study about the effect of clay on mucoadhesive properties of polymeric film (Pongjanyakul et al., 2013). The silicate layer surface of MAS and silicon dioxide of HS were contained hydroxyl groups that could be interacted with mucus via hydrogen bonding. So, the FZ-loaded SC-clay films had mucoadhesive properties.

4. Conclusion

The FZ-loaded SC-clay films were prepared using a spray method and the effect of clay on the films properties was investigated. Incorporation of clay can enhance thermal and mechanical properties of the films. Besides, the FZ-loaded SC-clay films presented slower release when compared with the film without clay due to denser structure of the films. FZ powder was reported as mixture polymorphisms of anhydrate form I and monohydrate. Furthermore, the films loaded with FZ were showed the recrystallization of FZ during film preparation. However, the FZ-loaded SC-clay films still possess antifungal activity and mucoadhesive property. So, the films display a potential use as a local delivery system in oral candidiasis.

References

- Walstra P, Wouters JT, and Geurts TJ. Dairy Science and Technology. 2nd ed. Wageningen: Taylor & Francis Group; 2006.
- Elzoghby AO, El-Fotoh WS, and Elgindy NA. Casein-based formulations as promising controlled release drug delivery systems. *J Contr Release* 2011; 153: 206–216.
- Neha A, Tarun G, and Ajay B. Review on casein production and casein based nano-formulations. *Int Res J Pharm* 2012; 3(1): 41-45.
- Elzoghby AO, Helmy MW, Samy WM and Elgindy NA. Spray-dried casein-based micelles as a vehicle for solubilization and controlled delivery of flutamide: formulation, characterization, and in vivo pharmacokinetics. *Eur J Pharm Biopharm* 2013; 84: 487-496.
- Diak OA, Jaber AB, Amro B, Jones D, Andrews GP. The manufacture and characterization of casein films as novel tablet coatings. *Food Bioprod Process* 2007; 85: 284-290.
- Millar FC and Corrigan OI. Influence of sodium caseinate on the dissolution rate of hydrochlorothiazide and chlorothiazide. *Drug Dev Ind Pharm* 1991; 17(21): 1593-1607.
- Audic JL and Chaufer. Influence of plasticizers and crosslinking on the properties of biodegradable films made from sodium caseinate. *Eur Polym J* 2005; 41: 1934-42.
- Fabra MJ, Talens P and Chiralt A. Tensile properties and water vapor permeability of sodium caseinate films containing oleic acid-beeswax mixtures. *J Food Eng* 2008; 85: 393-400.
- Kibbe HA. Handbook of pharmaceutical excipients, 3rd ed. American Pharmaceutical Association, Washington; 2000. 295–298.
- Alexandre M, Dubois P. Polymer-layered silicate nanocomposites: preparation, properties and uses of a new class of materials. *Mater Sci Eng* 2000; 28: 1-63.
- Khunawattanakul W, Puttipipatkachorn S, Rades T, Pongjanyakul T. Chitosan-magnesium aluminum silicate nanocomposite films: Physicochemical characterization and drug permeability. *Int J Pharm* 2010; 393: 219-229.
- Rongthong T, Sungthongjeen S, Siepmann F, Siepmann J, Pongjanyakul T. Quaternary polymethacrylate-magnesium aluminum silicate films: Water uptake kinetics and film permeability. *Int J Pharm* 2015; 490: 165-172.

- Rongthong T, Sungthongjeen S, Siepmann J, Pongjanyakul T. Quaternary polymethacrylate-magnesium aluminum silicate films: Molecular interactions, mechanical properties and tackiness. *Int J Pharm* 2013; 458: 57-64.
- Yuan P, Tan D, Annabi-Bergaya F. Properties and applications of halloysite nanotubes: recent research advances and future prospects. *Appl Clay Sci* 2015; 112-113: 75-93.
- Lvov Y, Abdullayev E. Functional polymer-clay nanotube composite with sustained release of chemical agents. *Prog Polym Sci* 2013; 38: 1690-1719.
- Bachhav YG, Mondon K, Kalia YN, Gurny R and Möller M. Novel micelle formulations to increase cutaneous bioavailability of azole antifungals. *J Contr Release* 2011; 153: 126-132.
- Yang W, Wiederhold NP and Williams RO. Drug delivery strategies for improved azole antifungal action. *Expert Opin Drug Deliv* 2008; 5(11): 1199-216.
- Yehia SA, El-Gazayerly ON, Basalious EB. Fluconazole mucoadhesive buccal films: *In vitro*/*In vivo* performance. *Curr Drug Deliv* 2009; 6: 17-27.
- Khanna R, Agarwal SP and Ahuja A. Preparation and evaluation of bioerodible buccal tablets containing clotrimazole. *Int J Pharm* 1996; 138: 67-73.
- Correa JCR, Salgado HRN. Review of fluconazole and analytical methods for its determination. *Crit Rev Anal Chem* 2011; 41: 124-132.
- Pereda M, Aranguren MI, Marcovich NE. Characterization of chitosan/caseinate films. *J Appl Polym Sci* 2008; 107: 1080-1090.
- Sakloetsakun D, Pongjanyakul T. Modification of gellan gum by halloysite: physicochemical evaluation and drug permeation properties. *Drug Dev Ind Pharm* 2017; 43(3): 492-501.
- Alkhamis KA, Obaidat AA, Nuseirat AF. Solid-state characterization of fluconazole. *Pharm Dev Technol* 2002; 7(4): 491-503.
- Park HJ, Kim MS, Lee S, Kim JS, Woo JS, Park JS, and et al. Recrystallization of fluconazole using the supercritical antisolvent (SAS) process. *Int J Pharm* 2007; 328: 152-160.
- Sabahi H, Khorami M, Rezayan AH, Jafari Y, Karami MH. Surface functionalization of halloysite nanotubes via curcumin inclusion. *Colloids Surf A* 2018; 538: 834-840.
- Souri A, Golestani-Fard F, Naghizadeh R, Veisheh S. An investigation on pozzolanic activity of Iranian kaolins obtained by thermal treatment. *Appl Clay Sci* 2015; 103: 34-39.
- Zhang Y, Fu L, Yang H. Insights into the physicochemical aspects from natural halloysite to silica nanotubes. *Colloids Surf A Physicochem Eng Asp* 2012; 414: 115-119.
- Khlibsuwan R, Khunkitti W, and Pongjanyakul T. Alginate-caseinate composites: Molecular interactions and characterization of cross-linked beads for the delivery of anticandidals. *Int J Biol Macromo* 2018; 115: 483-493.
- Pongjanyakul T, Khunawattanakul W, Strachan CJ, Gordon KC, Puttipipatkachorn S, and Rades T. Characterization of chitosan-magnesium aluminum silicate nanocomposite films for buccal delivery of nicotine. *Int J Biol Macromo* 2013; 55: 24-31.

Table 1 Characteristics of FZ-loaded SC-clay dispersions

Dispersions	pH	Particle size D4,3 (μm)	Zeta potential (mV)
1. SC dispersion	6.50	0.391 ± 0.01	-24.37 ± 0.87
2. MAS dispersion	8.73	2.39 ± 0.08	-34.42 ± 3.76
3. HS dispersion	5.42	21.71 ± 0.43	-28.14 ± 1.54
4. FZ dispersion	6.55	ND	-27.46 ± 0.89
5. FZ-loaded SC-clay 5:0	6.68	115.31 ± 1.74	-19.87 ± 1.64
6. FZ-loaded SC-MAS 5:0.25	6.73	65.39 ± 9.80	-30.14 ± 1.43
7. FZ-loaded SC-MAS 5:0.5	6.89	43.85 ± 1.74	-31.87 ± 0.62
8. FZ-loaded SC-MAS 5:1	6.90	37.62 ± 3.03	-34.45 ± 1.31
9. FZ-loaded SC-HS 5:0.25	6.70	74.69 ± 4.70	-28.66 ± 1.32
10. FZ-loaded SC-HS 5:0.5	6.71	64.21 ± 5.97	-30.48 ± 1.23
11. FZ-loaded SC-HS 5:1	6.77	39.57 ± 2.61	-29.31 ± 0.71

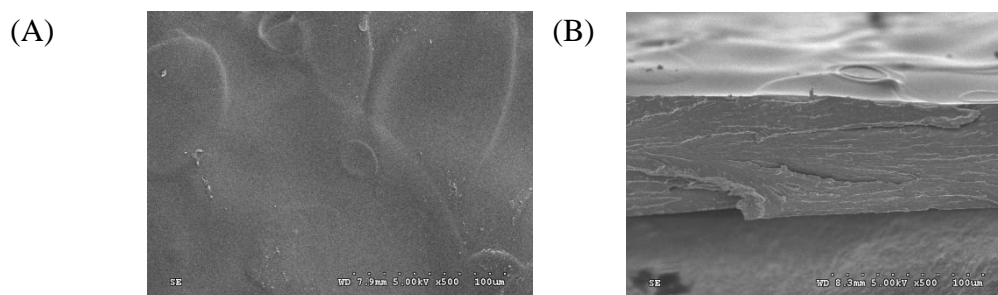


Figure 1 Morphology of SC film (A) Surface and (B) Matrix

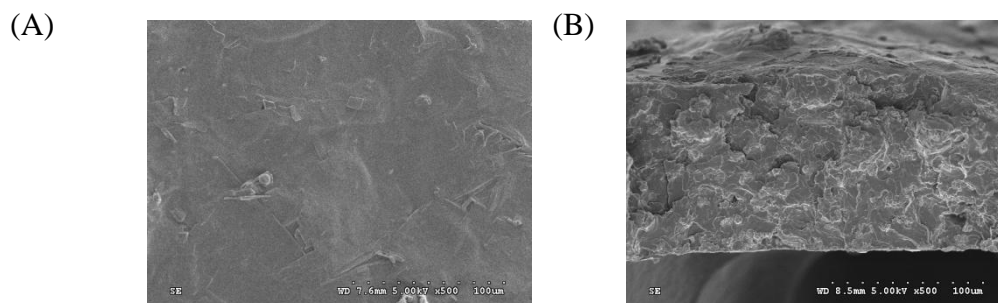


Figure 2 Morphology of FZ-loaded SC film (A) Surface and (B) Matrix

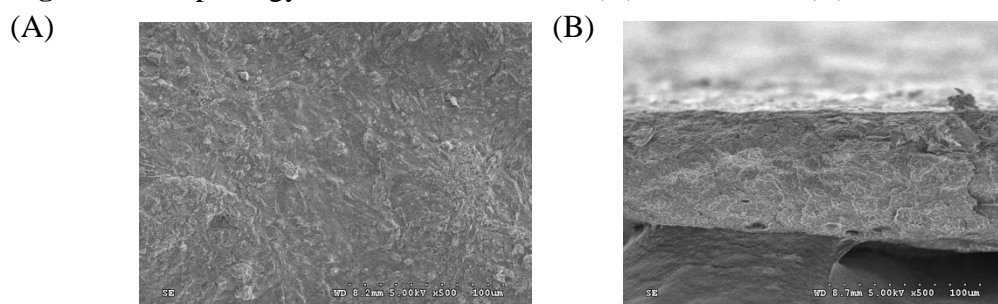


Figure 3 Morphology of FZ-loaded SC-20%MAS film (A) Surface and (B) Matrix

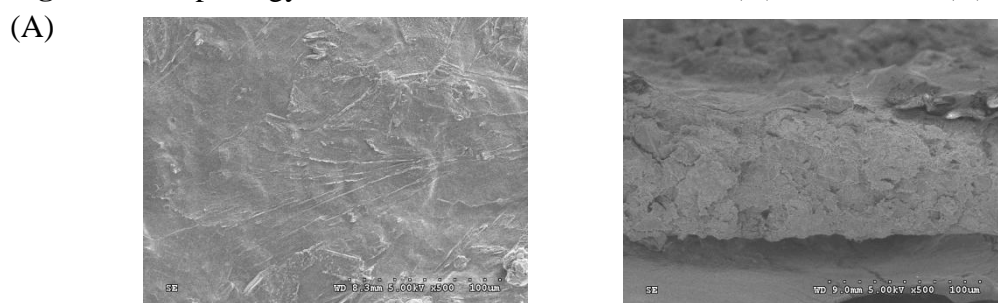


Figure 4 Morphology of FZ-loaded SC-20%HS film (A) Surface and (B) Matrix

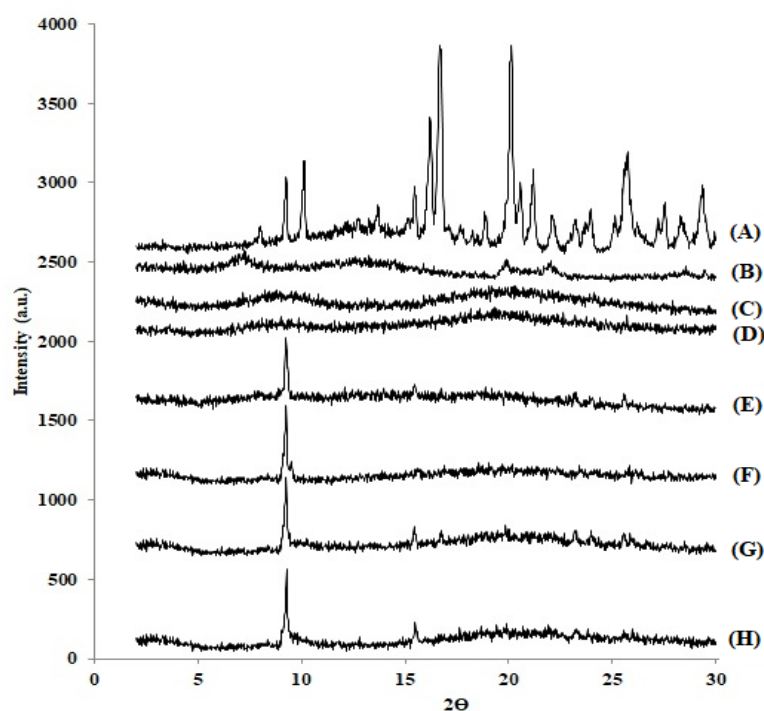


Figure 3 PXRD of FZ-loaded SC-MAS films: (A) FZ powder, (B) MAS powder, (C) SC powder, (D) SC film, (E) FZ-loaded SC-0%MAS film, (F) FZ-loaded SC-5%MAS film, (G) FZ-loaded SC-10%MAS film, and (H) FZ-loaded SC-20%MAS film

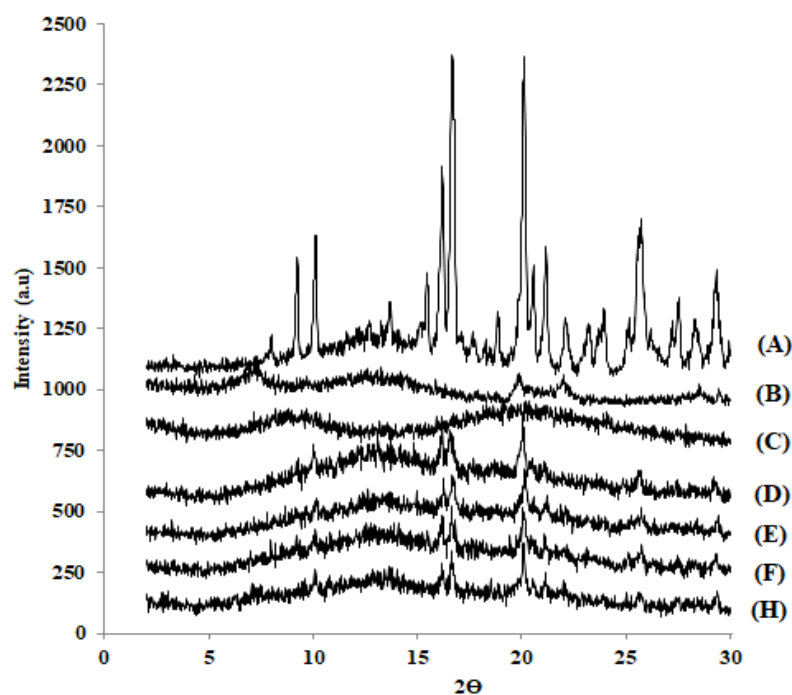


Figure 4 PXRD of physical mixture of SC-MAS-FZ in different ratio: (A) FZ powder, (B) MAS powder, (C) SC powder, (D) SC-MAS-FZ 5:0:1, (E) SC-MAS-FZ 5:0.25:1, (F) SC-MAS-FZ 5:0.5:1, and (H) SC-MAS-FZ 5:1:1

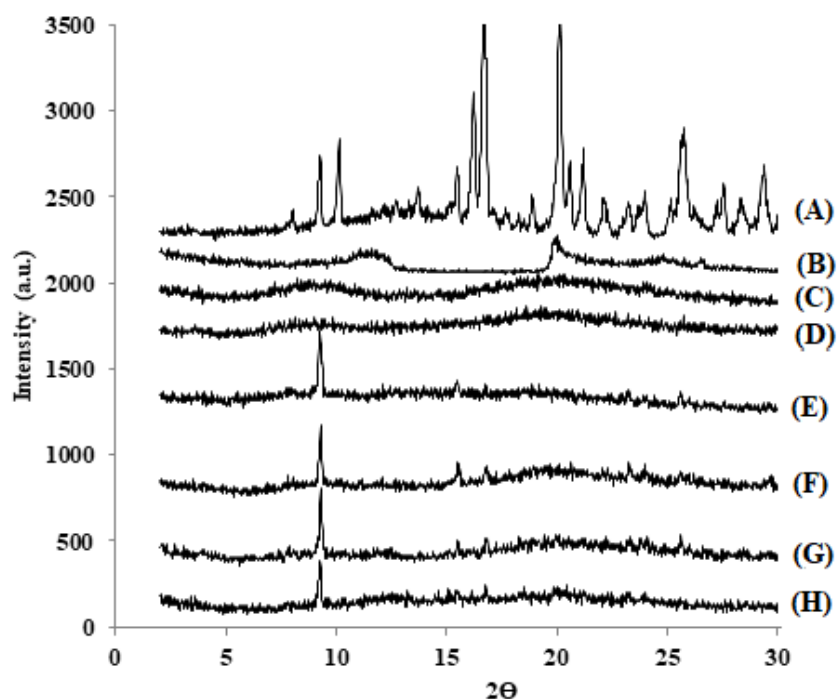


Figure 5 PXRD of FZ-loaded SC-HS films: (A) FZ powder, (B) HS powder, (C) SC powder, (D) SC film, (E) FZ-loaded SC-0% HS film, (F) FZ-loaded SC-5% HS film, (G) FZ-loaded SC-10% HS film, and (H) FZ-loaded SC-20% HS film

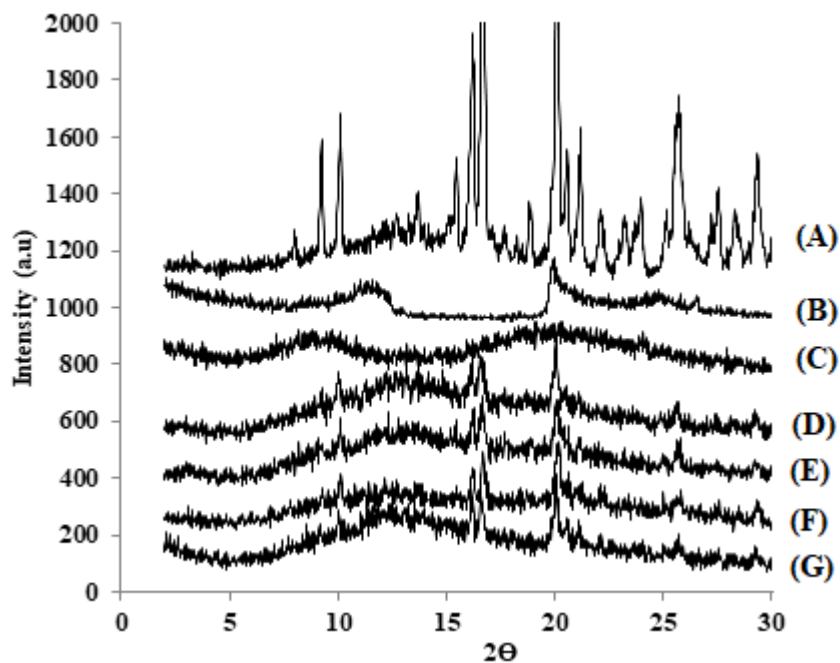


Figure 6 PXRD of physical mixture of SC-HS-FZ in difference ratio: (A) FZ powder, (B) HS powder, (C) SC powder, (D) SC-HS-FZ 5:0:1, (E) SC-HS-FZ 5:0.25:1, (F) SC-HS-FZ 5:0.5:1, and (H) SC- HS-FZ 5:1:1

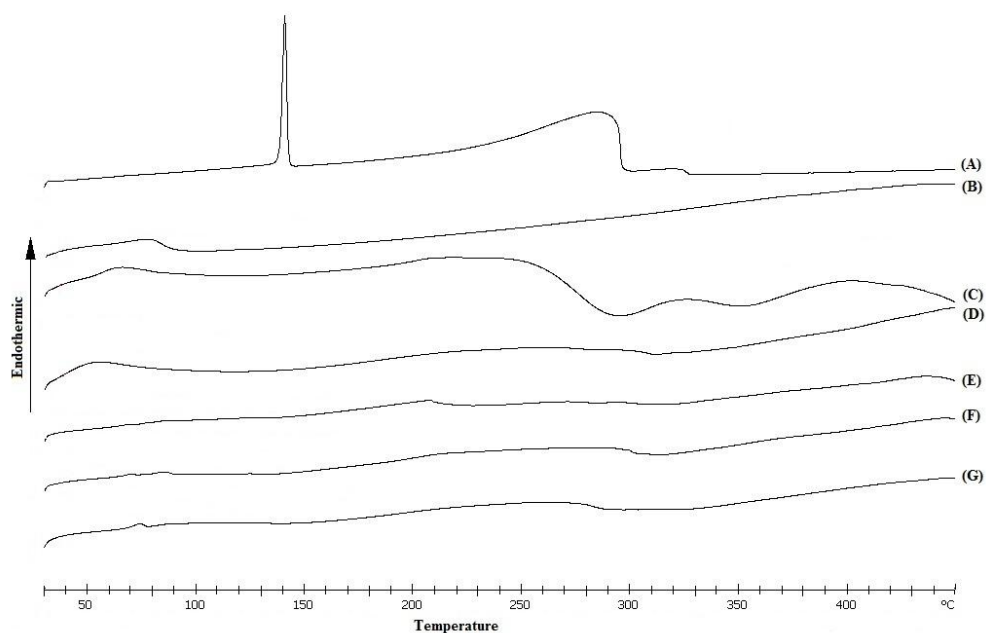


Figure 7 DSC of FZ-loaded SC-MAS films (A) FZ powder, (B) MAS powder, (C) SC powder, (D) SC film, (E) FZ-loaded SC-MAS film 5:0.25, (F) FZ-loaded SC-MAS film 5:0.50, and (G) FZ-loaded SC-MAS film 5:1.0

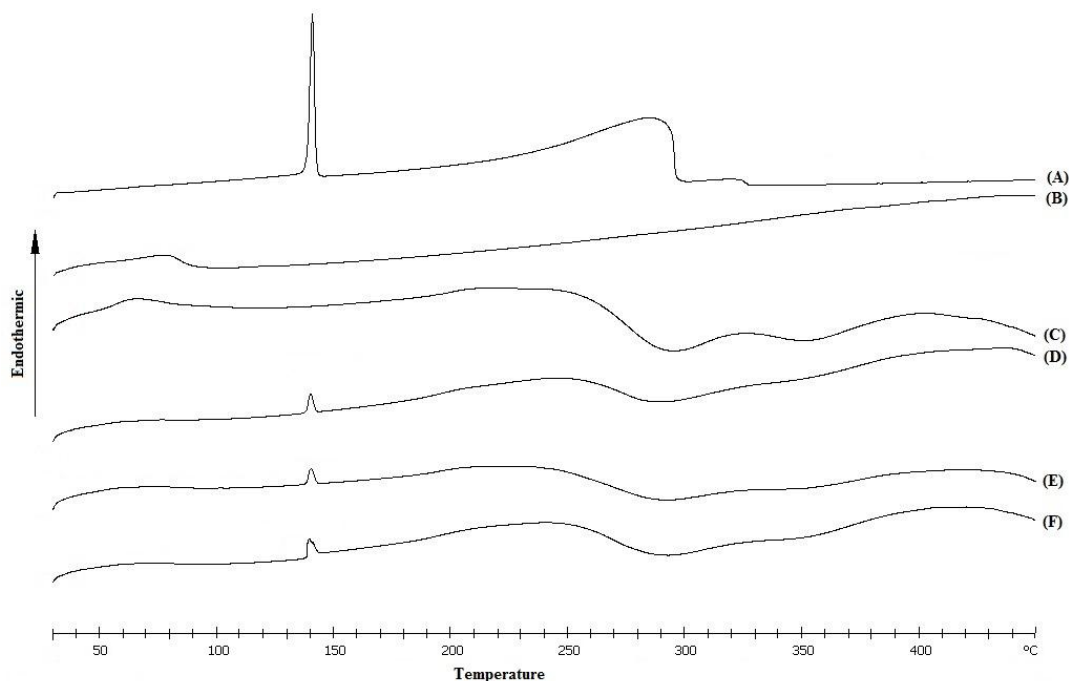


Figure 8 DSC of FZ-MAS physical mixture (A) FZ powder, (B) MAS powder, (C) SC powder, (D) SC-MAS-FZ 5:0.25:1, (E) SC-MAS-FZ 5:0.50:1, and (F) SC-MAS-FZ 5:1:1

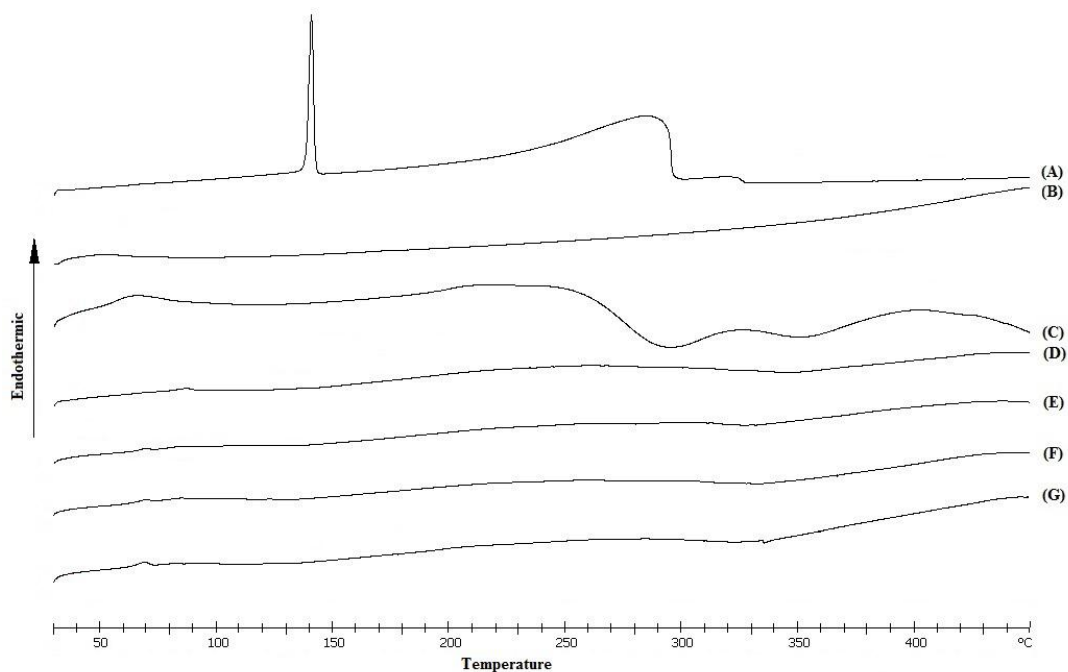


Figure 9 DSC of FZ-loaded SC-HS films (A) FZ powder, (B) HS powder, (C) SC powder, (D) SC film, (E) FZ-loaded SC-HS film 5:0.25, (F) FZ-loaded SC-HS film 5:0.50, and (G) FZ-loaded SC-HS film 5:1.0

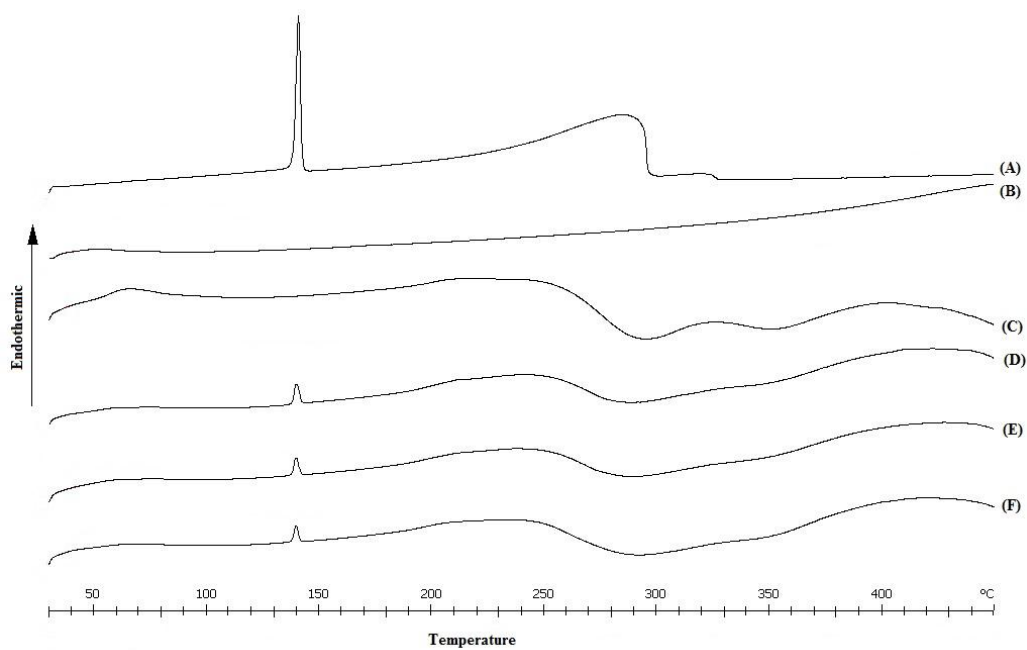


Figure 10 DSC of FZ-HS physical mixture (A) FZ powder, (B) HS powder, (C) SC powder, (D) SC-HS-FZ 5:0.25:1, (E) SC-HS-FZ 5:0.50:1, and (F) SC-HS-FZ 5:1:1

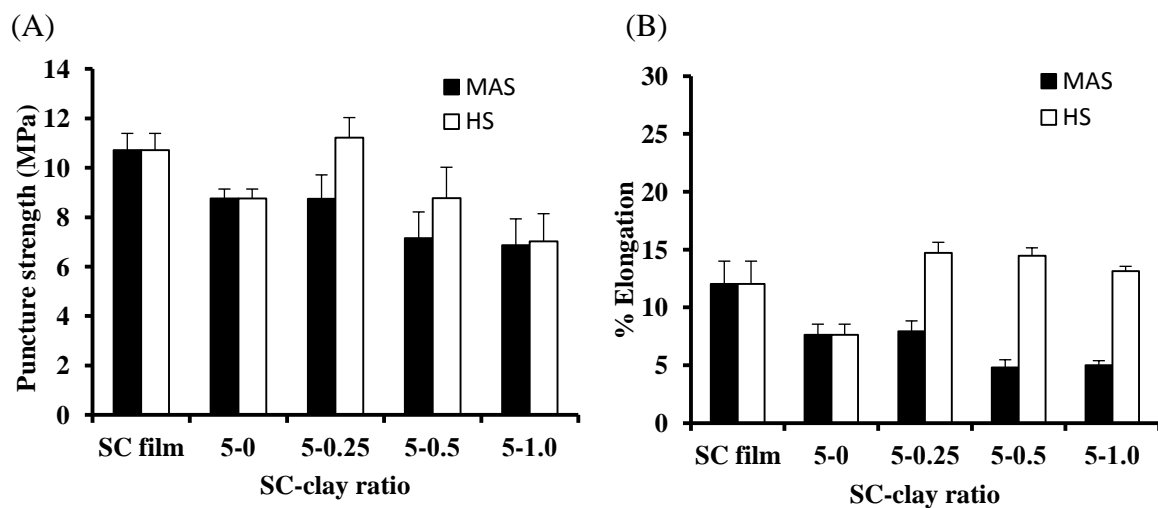


Figure 11 Mechanical properties of FZ-loaded SC-clay film (A) Puncture strength, and (B) Elongation

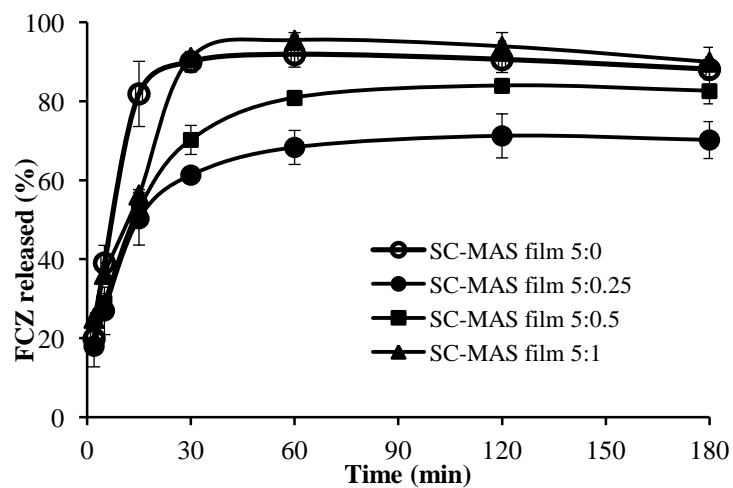


Figure 12 FZ released from FZ-loaded SC-MAS films

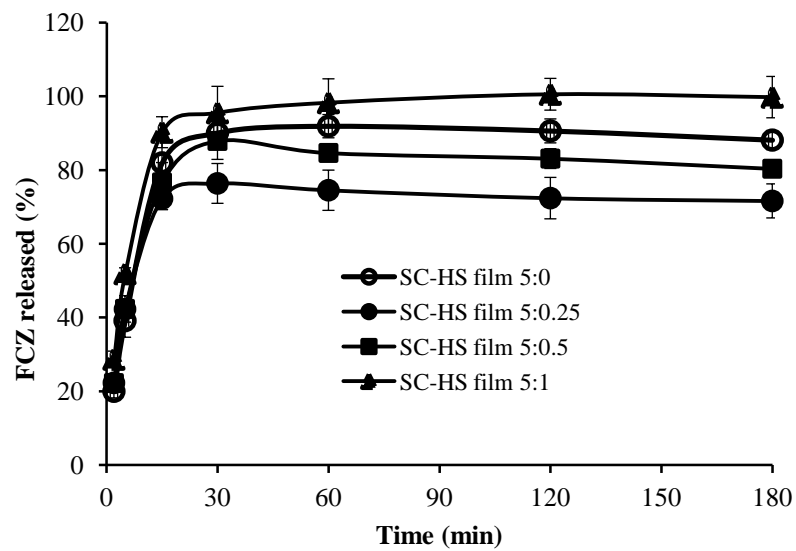


Figure 13 FZ released from FZ-loaded SC-HS films

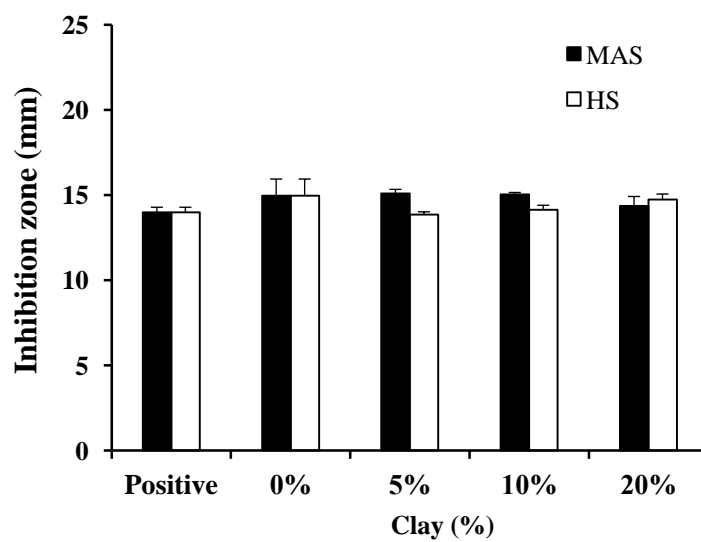


Figure 14 Antifungal activity of FZ released from the films

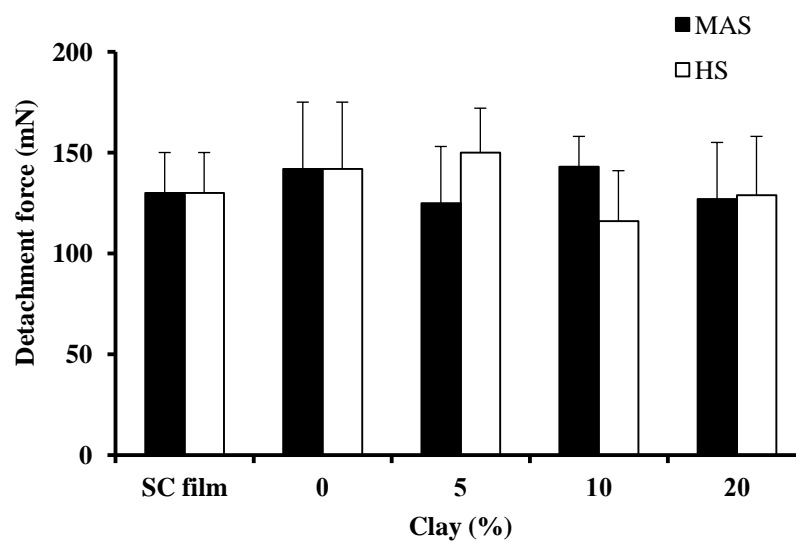


Figure 15 Detachment force of FZ-loaded SC-clay films

Part IV: Sodium caseinate-chitosan bilayer films containing fluconazole

1. Introduction

In the present, many polymers have been developed for use as pharmaceutical material. Especially in the composite of polymer with other substances is interesting to apply for drug formulation and drug delivery system. The interaction between different types of polymer can be obtained the new composite material which is able to enhanced the physic-chemical properties of primitive material, and use in pharmaceutical field (Ates et al., 2017). Sodium caseinate (SC) is biomaterial which obtained from milk, comprising of 94% protein and 6% colloidal calcium phosphate (Walstra et al., 2006). The structure of SC consist of hydrophilic part and hydrophobic part which is able to use as surfactant, and also self-assembly into micelle (De Kruif and Grinberg, 2002; Qi, 2007). So, SC is able to use as emulsifying and foaming agents in food industry, solubilizing agent for poorly insoluble drug (Millar and Corrigan, 1991; 1993), film forming agent (Abu Diak et al., 2007; Elzoghby et al., 2011) and microparticle in drug delivery system for pharmaceutical application. SC, a negatively charge protein, could interact with polysaccharides via many mechanisms, which was dependent upon molecular charge of polysaccharides. The film properties of SC is able to modify by addition of plastisizer (Audic and Chaufer, 2005), cross-linking agent (Audic and Chaufer, 2005; Perada et al., 2010) and insoluble material (Fabra et al., 2008), etc. Accordingly, the composite between polysaccharide with SC is interesting combination to apply as drug reservoir in composite film for drug delivery system.

Chitosan was a positively charged polysaccharide that could be interacted with SC by electrostatic force, whereas hydrogen bonding mechanisms occurred between SC and sodium alginate due to the same charge of both substances. These interactions may cause a change of characteristics of sodium caseinate-polysaccharide films, which could be applied for tablet film coating and drug delivery system. In this study, chitosan was used for surface modification of sodium caseinate films containing fluconazole. This film may be used for local delivery of oral candidiasis. The outputs of this study will be the new basic knowledge of characteristics and applications of the sodium caseinate-polysaccharide films in pharmaceuticals.

2. Materials and methods

2.1. Materials

SC (sodium salt from bovine milk) and CS (85% degree of deacetylation with a molecular weight of 800 kDa chitosan) were purchased from Sigma-Aldrich Company (St. Louis, MO) and Bio21 Co., Ltd. (Chonburi, Thailand), respectively. Glycerin was obtained from Namsiang Co., Ltd. (Bangkok, Thailand). FZ was purchased from Hubei Yuancheng Gongchuang Technology Co., Ltd.

(Wuhan, China). Sodium lauryl sulfate (SLS) was obtained from S. Tong Chemicals Co., Ltd. (Bangkok, Thailand). *Candida albicans* ATCC 10231 was a gift from the Biofilm Research Group, Faculty of Dentistry, Khon Kaen University (Khon Kaen, Thailand). All other reagents were of analytical grade and were used as received.

2.2 Preparation of SC-CS bilayer films

SC (25 g) was dispersed in purified water (400 mL) at 26 ± 1 °C. The SC dispersion was stirred using a magnetic stirrer and stored for overnight. Then SC dispersions were adjusted to the final volume (500 mL). The SC dispersion was sprayed on plastic board which arranged inside the pan of conventional coating machine (YeoHeng Co., Ltd, Bangkok, Thailand). Before spraying, the pan was heated at 75 ± 5 °C for 30 min and then thin films was conducted using an air-assist spray nozzle of coating machine (Thai Coater Model FC15, Pharmaceuticals and Medical Supply, Thailand). The spray rate of the spraying dispersions was 5 ml/min under spray pressure of 0.38 mPa. After the spraying process, the thin film was continue dried in the pan for 15 min. The thin film was peeled out of the plastic board and stored in a desiccator prior to further examination. For bilayer film, the dried SC film was covered with other dispersions such as 1% w/v acetic acid (AcOH), various volume of 1% CS (50, 100, 150 and 200 ml). The sandwich structure SC/CS/SC was prepared follow the same step as a bilayer film. The dried SC bilayer film which covered with 1% CS 200 ml was peeled out and stitched again on the plastic plate. The CS dispersion (200 ml) was sprayed on the SC surface and followed the same step as bilayer film preparation.

The FZ loaded film was prepares by adding FZ powder (5 g) into SC dispersion (25 g in 400 ml of purified water) at 26 ± 1 °C. Next, the FZ loaded SC dispersion was stirred using a magnetic stirrer for overnight. The FZ loaded SC dispersions were then adjusted to the final volume (500 mL). The film was prepared following the procedure mentioned above.

2.3. Characterization of SC-CS bilayer films

2.3.1. Morphology and thickness of SC-CS bilayer films

The surface morphology and cross-section of film was observed using scanning electron microscopy (SEM). The samples were mounted on dummies, coated with gold in a vacuum evaporator, and then viewed using a scanning electron microscope (Hitachi Se3000 N, Tokyo, Japan).

Thickness of the dry films was measured at different places using a microprocessor coating thickness gauge (Minitest600B, ElektroPhysik, Germany). The probes, which had been connected to the measurement gauge and calibrated using a standard film, gently touch on the film, and the film thickness was subsequently measured.

2.3.2 FZ content determination

The FZ loaded film were cut to disc, weight accurately and then dissolved in acetonitrile:water (30:70) in a volumetric flask. The solution was ultrasonicated for 4 hour and stored in shaking water bath for overnight. Then, the solution was added with the mobile phase and ultrasonicated for 15 min, adjusted the volume to 50 ml. The solution was filtered

with nylon membrane filter (0.20 micron). The amount of drug was measured by using HPLC analysis as Section 2.8. The drug content was calculated from the following equation:

$$((\text{FCZ amount in the film})/\text{FCZ added}) \times 100$$

2.4 Molecular interaction of SC-CS bilayer films

2.4.1 DSC

The thermal behavior of pure substance powder, blank films and FZ loaded film the films were investigated using differential scanning calorimetry (DSC). The DSC thermogram of the samples was recorded using a differential scanning calorimeter (DSC822e, Mettler Toledo, Switzerland). An accurately weighed sample (2.5–3.5 mg) was placed into a 40- μL aluminum pan without an aluminum cover. The measurements were taken over a temperature range of 30 to 450 $^{\circ}\text{C}$ at a heating rate of 10 $^{\circ}\text{C min}^{-1}$.

2.4.2 FTIR spectroscopy

FTIR spectra of the blank film and drug loaded bead were determined using the KBr disc method. Each sample was gently triturated with KBr powder at a weight ratio of 1:100 and then pressed with a hydrostatic press at 10 tons for 10 min. The discs were placed in a sample holder and scanned from 4000 to 400 cm^{-1} at a resolution of 4 cm^{-1} (Spectrum One, Perkin Elmer, Norwalk, CT).

2.5 Mucoadhesive property studies

The mucoadhesive properties of the films were measured using a texture analyzer (TA.XT.plus, Stable Micro Systems Ltd., UK). Porcine esophageal mucosa was used in this study. The esophageal tube was opened longitudinally and cut to a size of 2 cm \times 2 cm. The porcine esophageal mucosa was fixed on a platform with the mucosal surface facing up. The films were cut to disc with a surface area of 0.785 cm^2 and attached to the 10 mm diameter cylindrical probe using double-sided adhesive tape. Before testing, 20 μL of pH 6.8 phosphate buffer was dropped onto the mucosa. The probe attached to the film was moved down toward the mucosal tissue at the rate of 1 mm min^{-1} and made contact with the tissue with a contact force of 100 g for 30 sec. The probe was then withdrawn from tissue at the rate of 1 mm min^{-1} . The relationship between force and film displacement was plotted. Maximum detachment force and force max area were computed using the Texture Exponent 32 program (Stable Micro Systems, UK).

2.6 Mechanical properties studies

Puncture strength and elongation studied refer to mechanical properties of the films. The value of puncture strength and elongation were examined by using a texture analyzer (TA.XT2, Stable Micro System, Ltd., UK) equipped with a 500 N load cell. The dry films (2 \times 2 cm) were cut and kept in a chamber with 55% RH at room temperature (25.0 ± 1.0 $^{\circ}\text{C}$) for 3 days before testing. Then, the dried films were fixed using a film holder between two mounting plates. A 5-mm-diameter spherical stainless steel puncturing probe was fixed at the load cell and moved downwards at 0.1 mm s^{-1} . The applied force and displacement were recorded. The puncture strength and % elongation at the break were calculated as follows:

$$\text{Puncture strength} = F/A$$

where F is the maximum force for puncture, and A is the cross-sectional area of the edge of the film located in the path of cylindrical opening of the film holder.

$$\text{Elongation (\%)} = \left(\frac{\sqrt{r^2 + D^2} - r}{r} \right) \times 100$$

where r is the radius of the film exposed in the cylindrical hole of the film holder, and D is the displacement of the probe from the point of contact to the point of film puncture.

2.7 *In vitro* drug release studies

The FZ-loaded films were investigated about *In vitro* release studies on using modified side-by-side diffusion cell (Crown Glass Co., Inc., Somerville, NJ). The disc of FZ-loaded films with a surface area of 0.785 cm² and accurately weighed before being placed on the one side of diffusion cell. The diffusion cell was filled with release medium (3 ml of pH 5.5 simulated salivary fluid), tested at a controlled temperature of 37.0 ± 0.1 °C, and stirred at 600 rpm. The cells were then fixed and tightly fastened with a screw. The samples (1 ml) were collected and replaced with fresh medium. The amount of FZ released was analyzed using high performance liquid chromatography (HPLC).

2.8 HPLC analysis

The HPLC system consisted of Waters 1525 binary pumps, 2489 dual absorbance detector and Waters Breeze Software, 2.0 version (Waters, MA, USA). The FCZ measurements were determined using the Waters HPLC system with a Mightysil RP-18 GP column (4.6×150 mm, 5 µm particle size; Kanto chemical co., inc, Tokyo, Japan). The mobile phase consisting of acetonitrile:water in the ratio of 30:70 for determination amount of FZ at a flow rate of 1 ml/min. The retention time of FZ was approximately 4.55 min. The detection wavelength was set at 210 nm.

2.9 Anticandidal activity study

The activity of FCZ from drug loaded films was tested against *Candida albicans* by an agar dilution method using Sabouraud dextrose agar. *C. albicans* were inoculated into 20 ml of Sabouraud dextrose broth. The exponential period of growth and the culture broth was diluted. The concentration of *C. albicans* was diluted to 10⁶ CFU/ml.

Then, the Sabouraud dextrose agar (20 ml) plates were prepared, in which 200 µl solution of microbe suspension was added and spread uniformly with sterile cotton swabs and then punched with a Pasteur pipet to make holes 6 mm in a diameter. Four sets of holes were made on each plates. The 45 µl solution of negative control, positive control and release solution from Section 2.8 were dropped into the hole. All the plates were incubated at 32 ± 1 °C for 18 h. Then the plates were taken out and the diameters of the inhibitory zones were measured in millimeter. Negative control was pH 5.5 simulated salivary fluids. Positive control was 100, 200 and 400 µg/ml of FZ solution. The FZ release solution was selected at 60 min of dissolution studies to test the microbial activity.

3. Results and discussion

3.1 The morphology of SC-CS bilayer films

The morphology of control film is shown in Fig. 1a. The pure SC and CS films had some drying marks on the surface. The shapes of mark were oval and circle. These seem occurred by the fast evaporation of water from dispersion droplet. The bilayer of SC film which covered with AcOH 100 ml showed more roughness surface than monolayer of SC film whereas the bi-layer of SC-CS 100 ml was the smoothest surface film. The cross-section of film showed that the mono-layer of SC and CS had a dense structure (Fig. 2a, 2d). After covered SC film with CS 100 ml, the bi-layer film still had dense matrix without separation to each layer of polymer (Fig. 2c). In contrast to bi-layer of SC-AcOH film showed loose matrix structure. The layer was divided into two regions (Fig. 2b). Thickness of monolayer CS film was $11.9 \pm 1.8 \mu\text{m}$, which is the lowest when compared with other formulation. The thickness of mono-layer SC film was $102.5 \pm 18.3 \mu\text{m}$. After prepared to bi-layer film by covered with AcOH and CS 100 ml, thickness of SC film were increased to 114.8 ± 26.5 and $117.4 \pm 11.0 \mu\text{m}$, respectively.

The different morphology was observed when adding FZ particle into formulation. All formulation of FZ loaded film showed more roughness and higher particulates on the surface of film (Fig 3.) These may be occurred from saturated FZ particle in the dispersion. The same matrix structures of films were observed in all formulation of SC-CS bilayer film, even increasing amount of CS into the film. However, other properties such as thickness, film weight and FZ were varied depend on content of CS. As shown in Table 1, the increasing content of CS in bi-layer films resulted in increased film thickness (Table 1).

3.2 Molecular interaction of SC-CS bilayer films

Thermal property of films was investigated by using differential scanning calorimeter. The DSC thermogram showed that the exothermic peak of monolayer SC film without glycerin approximately 321°C (Fig. 5a). It will be considered, that the addition of glycerin which is a plasticizer obviously affected the thermal behavior of the SC films. The exothermic peak appeared at 314°C for the SC film with glycerin. The exothermic peak of mono-layer SC film was changed to higher temperature both in control film and FZ-loaded films (Fig. 5b). The higher peak of exothermic degradation of bi-layer SC film was obtained when increasing more amounts of CS. This mean high amount of CS in bilayer SC film is able to enhance the thermal stability of monolayer SC film.

The molecular interaction between SC and CS in the bilayer film was investigated by using FTIR spectroscopy. The FTIR spectra of controlled film are shown in Fig. 6a. The mono-layer SC film showed the band at 3274 cm^{-1} corresponded to the O-H stretching, which overlapped the N-H stretching in the same region. The band at 2926 cm^{-1} assigned to the stretching of C-H groups. The strong peak at 1628 cm^{-1} was due to the C=O stretching vibrations of the amide I groups, and the peak at 1535 cm^{-1} was N-H bending of amide II groups. For CS film, the peak at 2871 cm^{-1} referred to the CH stretching of CS. The carbonyl

stretching (amide I) peak showed at 1636 cm^{-1} . NH_2 bending peak (amide II) of primary amine in CS structure was 1542 cm^{-1} .

After mono-layer SC was covered with 1% w/v CS 100 ml, only the peak of C-H stretching of SC at 2926 cm^{-1} was changed to higher (2945 cm^{-1}). This peak related to C-H group of CS. To confirm the molecular interaction between SC and CS in FZ loaded formulation, the FTIR of FZ loaded SC film was investigated. The bi-layer SC with CS film showed only the band of C-H stretching at 3281 cm^{-1} was moved to lower. At this peak related to O-H stretching, which overlapped the N-H stretching both in SC and CS structure. This may be confirmed that SC and HCS is able to interact together when HCS was sprayed on the surface of SC film via hydrogen bond between O-H group and N-H group. Moreover, the high amount of HCS in sandwich structure CS/SC/CS film showed the peak movement from 1512 to 1542 cm^{-1} . This peak related to NH_2 bending peak (amide II) of primary amine in CS structure. This caused from high content of CS in the formulation.

3.3 Mucoadhesive property of SC-CS bilayer films

The mucoadhesive properties of film were tested using porcine esophageal mucosa as a model membrane. The effect of CS content to bilayer SC film was presented in Fig. 7. The highest maximal detachment force was from monolayer SC film. However, the more content of CS in bilayer SC film showed higher the maximal detachment force. This described by the medium which used during the studies was pH 6.8 phosphate buffer, CS in this environment pH slightly protonated. So, the bi-layer SC-CS had lower maximal detachment force than monolayer SC film.

3.4 Mechanical property of SC-CS bilayer films

Fig. 8 shows the puncture strength and percentage of elongation of the films. It was found that the modification of mono-layer SC films to bi-layer SC-HCS resulted in an enhancement of mechanical properties. The monolayer SC films provided the lowest puncture strength and % elongation. However, both parameters did not depend on the increasing content of HCS to cover SC film. From these results, the presence of the HCS polymer chain in SC film is able to increase mechanical strength of SC film. In addition, these bilayer SC films provided good mechanical strength.

3.5 In vitro drug release studies and anticandidal activity

Profile of FZ release from monolayer SC, bilayer SC and sandwich CS-SC-CS film are shown in Fig. 9. All film formulations presented the fast release for 15 min. The release profile from monolayer and bilayer SC-AcOH were reached a plateau within 30 min. So, theses formulation had faster release rate profile than the bi-layer SC-CS film. This was due to the rapid dissolve of the SC film in the pH 5.5 simulated salivary fluids. All formulations of bi-layer SC-CS film showed the similar FZ release profile. The different release profiles from varied amount of CS were observed after 60 min of immersion. The lowest release profile was obtained from bi-layer SC film covered with CS 200 ml. This related to the mechanical property of bi-layer SC-CS 200 ml film when compared within formulation of bi-

layer SC-CS film. Moreover, the highest thickness of bi-layer SC-CS 200 ml film affected to long distance of fluid to dissolve SC which was covered with HCS.

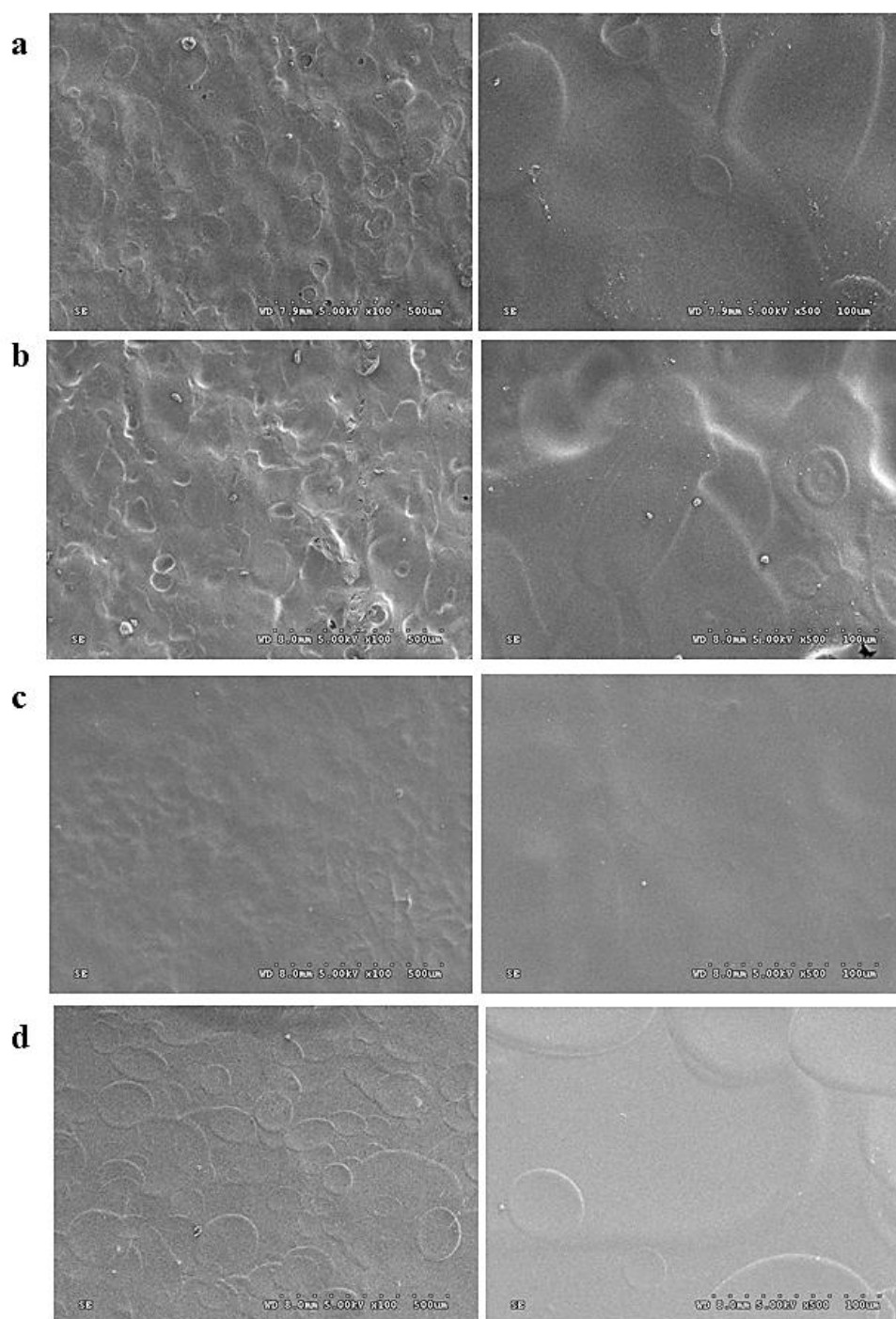
The antimicrobial effect in this study was investigated to confirm the efficacy of FZ after release from carriers. Accordingly, the FZ solution in this study was obtained from dissolution study. For FZ release solution was collected from dissolution test after 60 min which provide FZ concentration more than MIC of FZ for *C. albicans*. The anticandidal activity was measured about the inhibition zone as seen in Fig.10. The FZ release at concentration about 880-1780 µg/ml showed the ability of FZ to inhibit the *C. albicans* growth. These mean that the FCZ which released from the formulation of mono-layer SC, bi-layer SC-CS and sandwich SC-CS films could inhibit the growth of *C. albicans* completely.

4. Conclusion

Bi-layer SC film covered with CS can be successfully formed by using modified method from convention coating machine. SC and CS were able to form the molecular interaction via hydrogen bonding. The complex structure of SC-CS bi-layer film could enhance the strength of the films, and also provide good mucoadhesive properties. The releases of FZ from bi-layer SC-CS were able to provide more sustained profile than the mono-layer. Moreover, FZ release solutions still have an anticandidal activity. These findings suggested that the SC-CS bilayer film have a good potential for use as novel delivery system for antifungal drug in treatment of topical candidiasis.

Reference

- Abu Diak O, Bani-Jaber A, Amro B, Jones D, Andrews GP. The manufacture and characterization of casein films as novel tablet coatings. *Food Bioprod Process* 2007; 85: 284-290.
- Ates B, Koytepe S, Balcioglu S, Ulu A, Gurses C. *Hybrid Polymer Composite Materials: 12 - Biomedical applications of hybrid polymer composite materials* Woodhead Publishing Limited, Cambridge 2017: 343-408.
- Audic JL, Chaufer B. Influence of plasticizers and crosslinking on the properties of biodegradable films made from sodium caseinate. *Eur Polym J* 2005; 41: 1934-1942.
- De Kruif CG, Grinberg VY. Micellation of β -casein. *Colloid Surface A* 2002; 210: 183-190.
- Elzoghby AO, Abo El-Fotoh WS, Elgindy NA. Casein-based formulations as promising controlled release drug delivery systems. *J Control Release* 2011;153: 206-216.
- Fabra MJ, Talens P, Chiralt A. Tensile properties and water vapor permeability of sodium caseinate films containing oleic acid-beeswax mixtures. *J Food Eng* 2008; 85: 393-400.
- Millar FC, Corrigan OI. Dissolution mechanism of ibuprofen-casein compacts. *Int J Pharm* 1993; 92: 97-104.
- Millar FC, Corrigan OI. Influence of sodium caseinate on the dissolution rate of hydrochlorothiazide and chlorothiazide. *Drug Dev Ind Pharm* 1991; 17(21): 1593-607.
- Perada M, Aranguren MI, Marcovich NE. Effect of crosslinking on the properties of sodium caseinate films. *J Appl Polym Sci* 2010; 116: 18-26.
- Qi PX. Studies of casein micelle structure: The past and the present. *Dairy Sci Technol* 2007; 87: 363-383
- Walstra P, Wouters JT, Geurts TJ. *Dairy science and technology*. 2nd ed. Wageningen: Taylor & Francis Group; 2006.



Surface morphology of SC (a), SC – acetic acid (b), SC – 100 CS (c) and CS (d) film

Fig. 1. Surface morphology of controlled film of SC (a), SC film covered with AcOH (b), 100 ml CS (c) and monolayer of CS film (d).

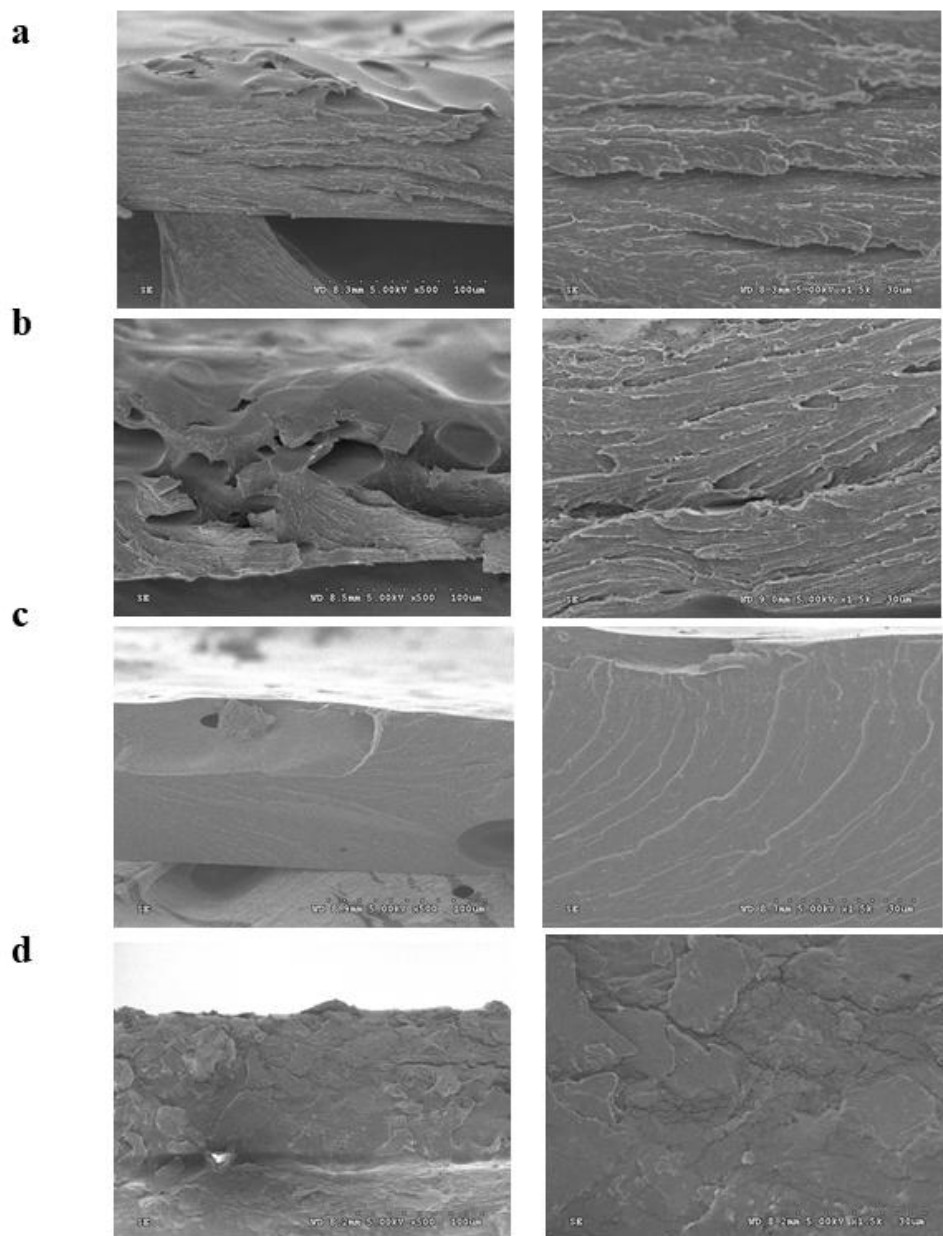
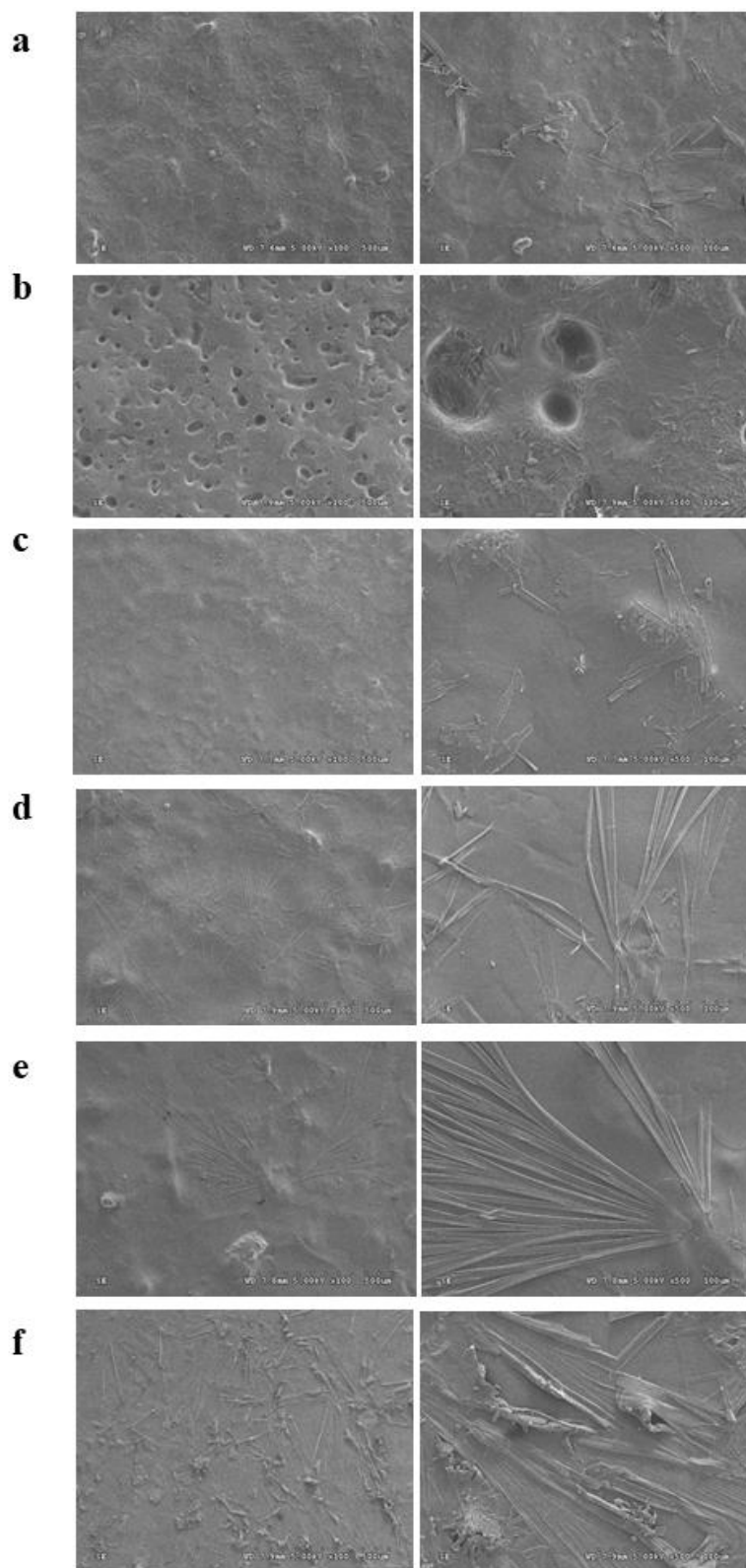
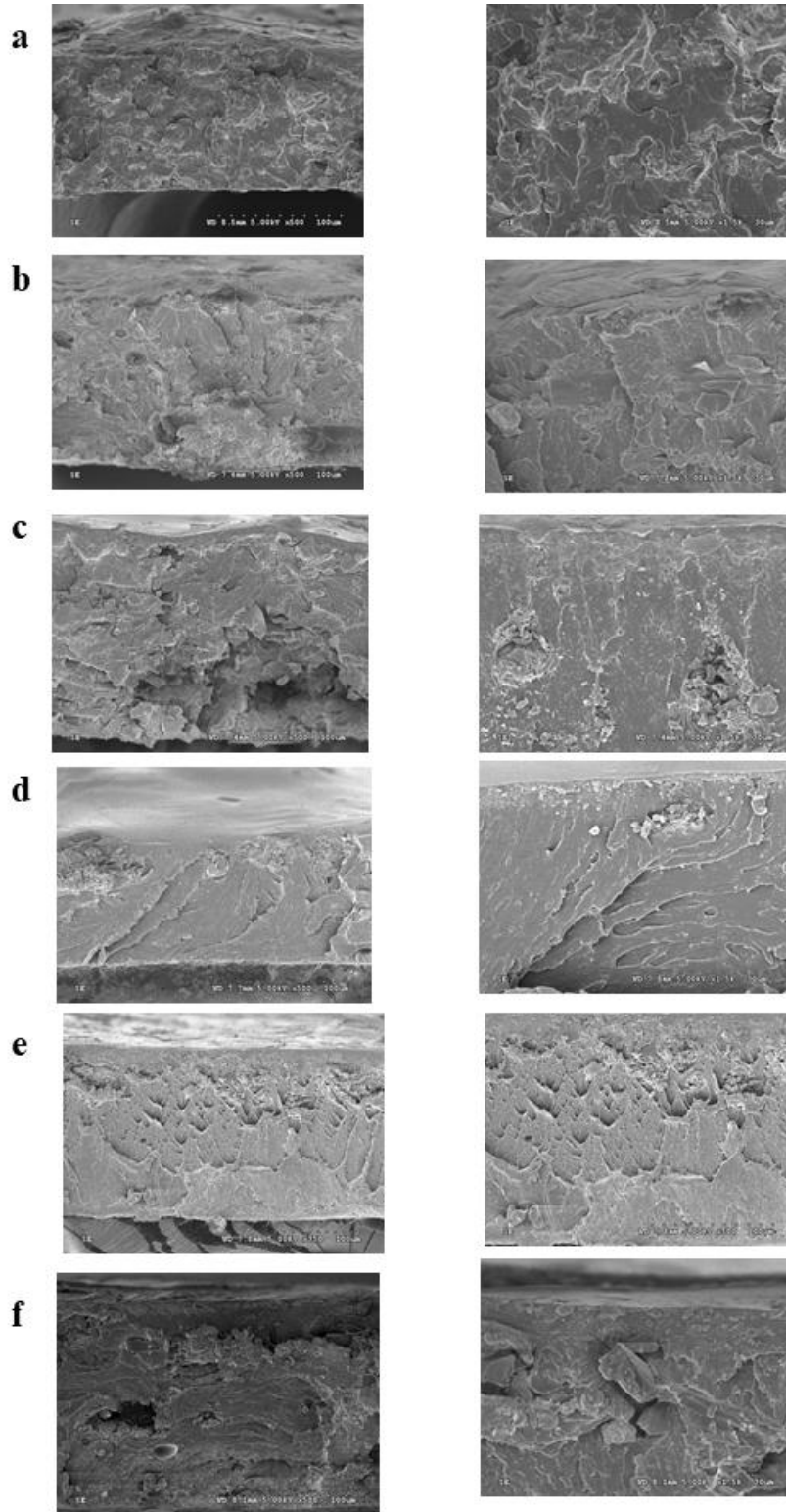


Fig. 2. Cross-section of controlled film of SC (a), SC film covered with AcOH (b), 100 ml CS (c) and monolayer of CS film (d).



Surface morphology of FZ loaded film of SC (a), SC – acetic acid (b), SC – 1% CS 50 ml (c), 100 ml (d), 200 ml (e) and sandwich CS – FZ (f).

Fig. 3. Surface morphology of FZ loaded film of SC (a), SC film covered with AcOH (b), 50 ml CS (c), 100 ml CS (d), 200 ml CS (e) and Sandwich-structured of CS/SC/CS film (f).



Cross-section of FZ loaded film of SC (a), SC – acetic acid (b), SC –1%CS 50 ml (c), 100 ml (d), 200 ml (e) and sandwich CS – FZ (f).

Fig. 4. Cross-section of FZ loaded film of SC (a), SC film covered with AcOH (b), 50 ml CS (c), 100 ml CS (d), 200 ml CS (e) and Sandwich-structured of CS/SC/CS film (f).

Table 1

Properties of FZ loaded SC-CS bilayer films

1% w/v FZ loaded 5% SC films	Thickness (μm, n=10)	Film weight (mg/0.79 cm², n=3)	FZ content (mg/0.79 cm², n=3)	%DC (w/w, n=3)
Monolayer of 5% SC	104.4 \pm 12.6	9.2 \pm 1.2	1.23 \pm 0.16	13.08 \pm 0.18
Bi-layer covered with				
-AcOH	123.9 \pm 14.3	13.3 \pm 2.5	1.72 \pm 0.33	12.82 \pm 0.54
-1% CS 50 ml	150.9 \pm 7.2	17.3 \pm 0.6	2.28 \pm 0.08	12.73 \pm 0.32
-1% CS 100 ml	154.2 \pm 8.9	14.5 \pm 0.4	1.88 \pm 0.05	12.75 \pm 1.23
-1% CS 150 ml	156.0 \pm 13.6	16.1 \pm 2.6	2.06 \pm 0.33	12.21 \pm 0.83
-1% CS 200 ml	170.2 \pm 10.0	18.0 \pm 2.3	2.28 \pm 0.29	12.13 \pm 0.29
Sandwich-structured of CS/SC/CS film	181.0 \pm 6.8	19.25 \pm 0.54	2.32 \pm 0.07	10.31 \pm 0.23

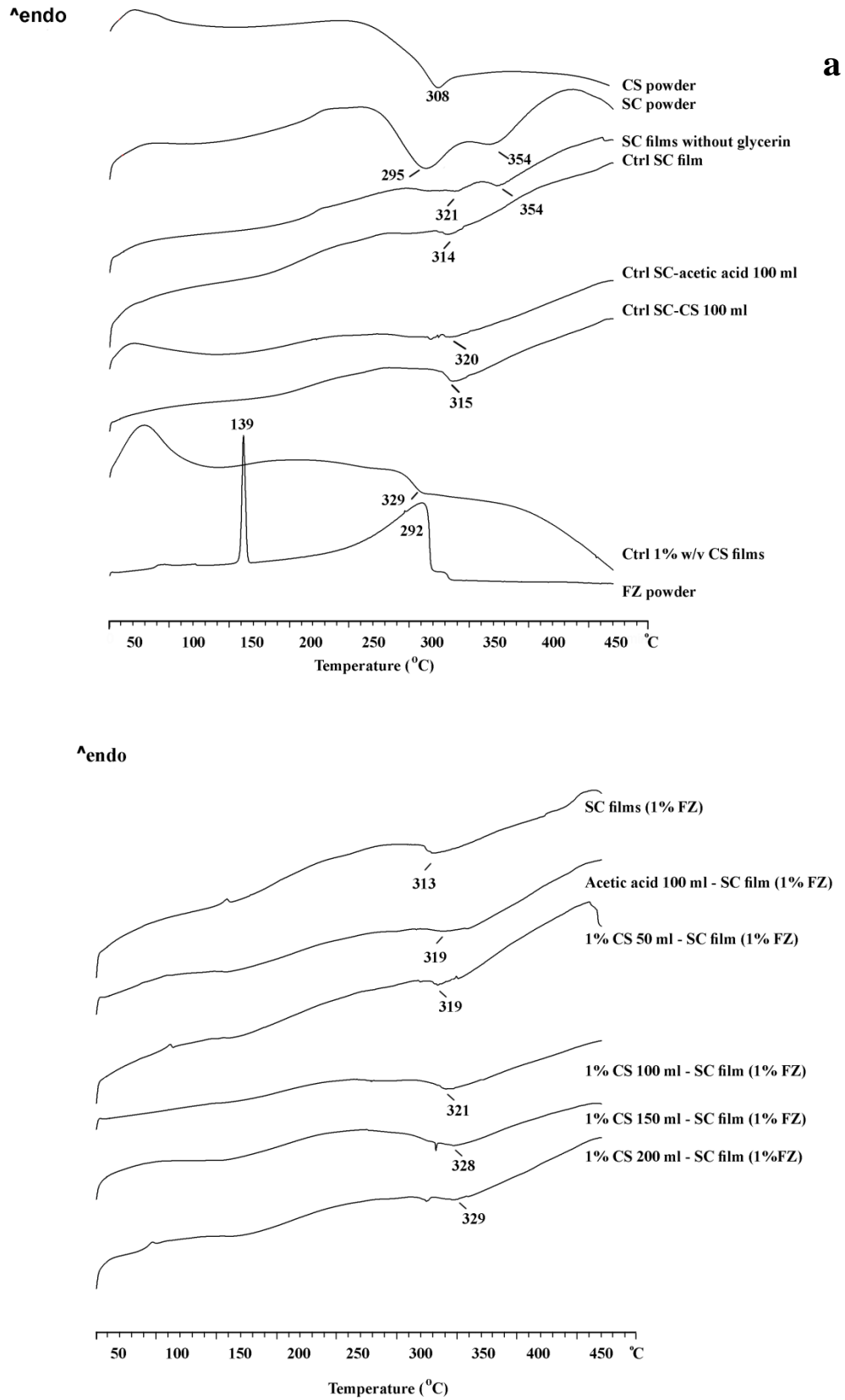


Fig. 5. DSC thermograms of powder, controlled film without FZ (a) and FZ loaded film (b).

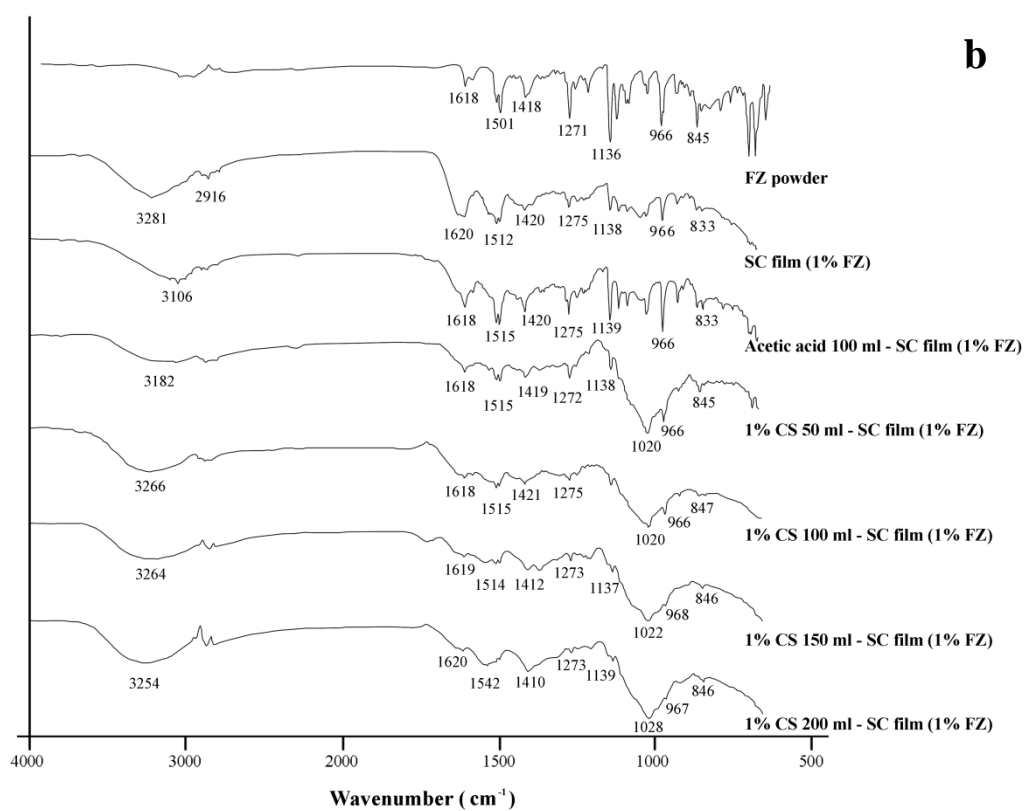
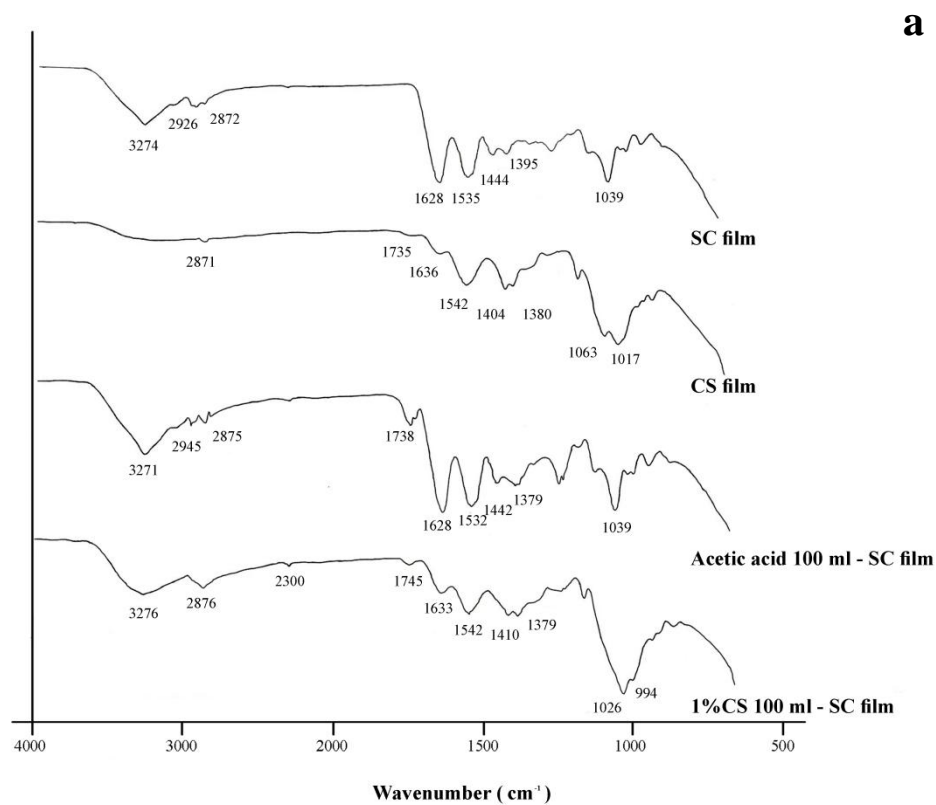


Fig. 6. FTIR spectra of powder, controlled film without FZ (a) and FZ loaded film (b).

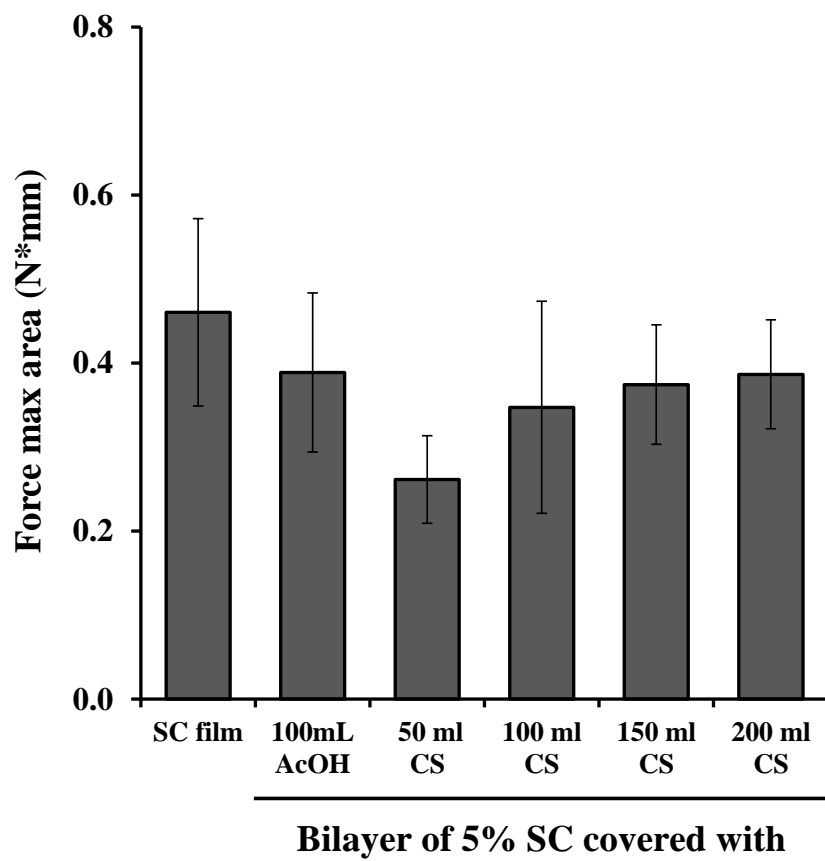


Fig. 7. Mucoadhesive property of SC-CS bilayer films in various contents of CS

Table 2

Mechanical properties of SC films in various types of film formulations

Film formulations	Puncture strength (MPa \pm SD)	Elongation (% \pm SD)
Control films		
- Monolayer of 5% SC	12.28 \pm 0.79	14.16 \pm 2.13
- Monolayer of 1% CS	39.57 \pm 3.85	7.97 \pm 1.33
- Bilayer with AcOH	11.27 \pm 0.59	13.54 \pm 0.43
- Bilayer with CS	18.50 \pm 0.75	14.97 \pm 0.82
1% FZ loaded films		
- Monolayer of 5% SC	8.82 \pm 0.67	7.85 \pm 0.66
- Bilayer covered with AcOH	15.47 \pm 1.27	23.26 \pm 2.52
1% CS 50 ml	10.23 \pm 0.47	15.82 \pm 4.03
1% CS 100 ml	13.18 \pm 0.99	15.36 \pm 2.49
1% CS 150 ml	10.91 \pm 0.20	11.87 \pm 0.73
1% CS 200 ml	13.01 \pm 0.62	19.84 \pm 3.43

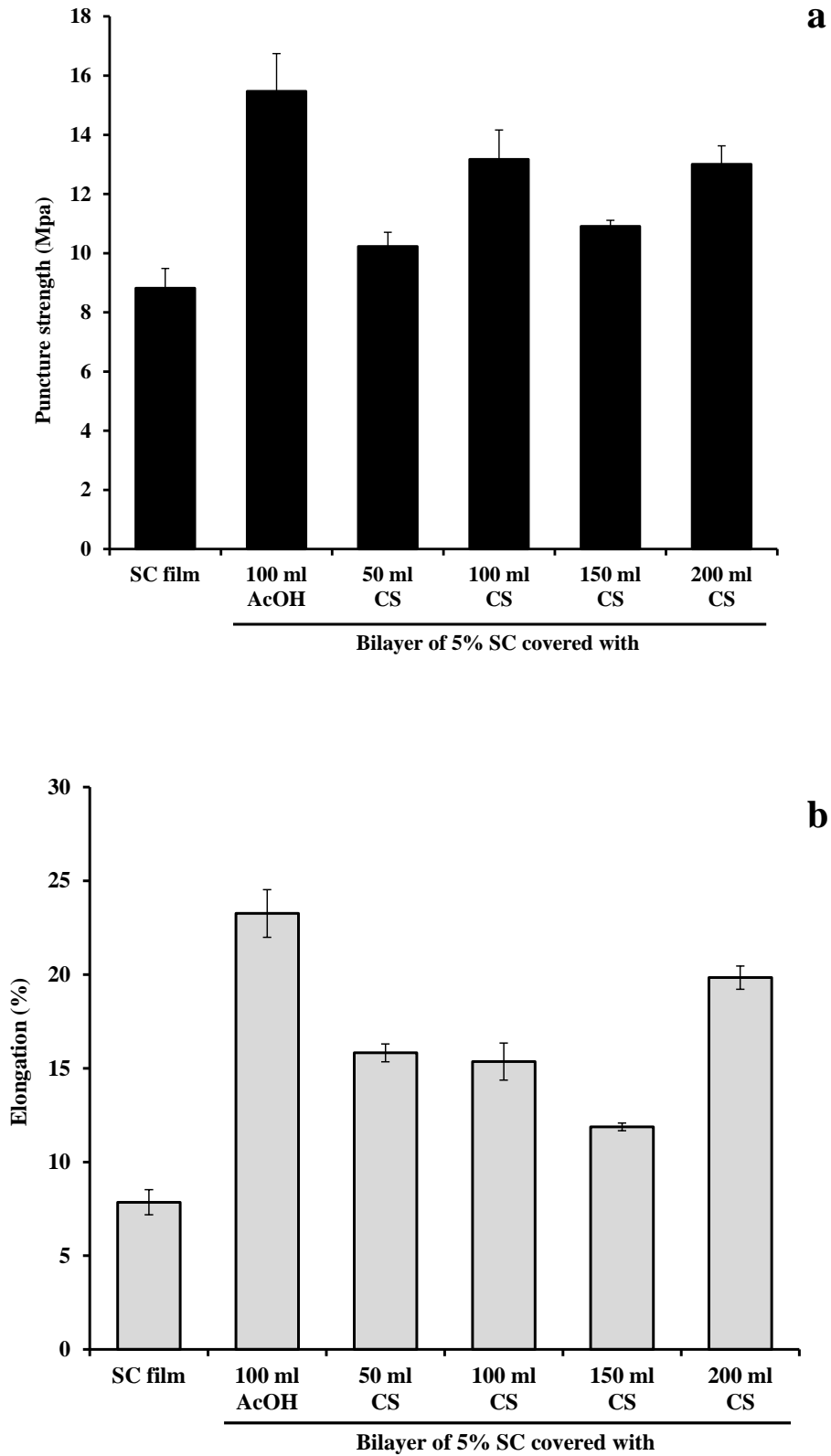


Fig. 8. Puncture strength (a) and % elongation (b) of SC-CS bilayer films at various contents of 1% CS covered on SC film. Each value is the Mean \pm S.D., n =6.

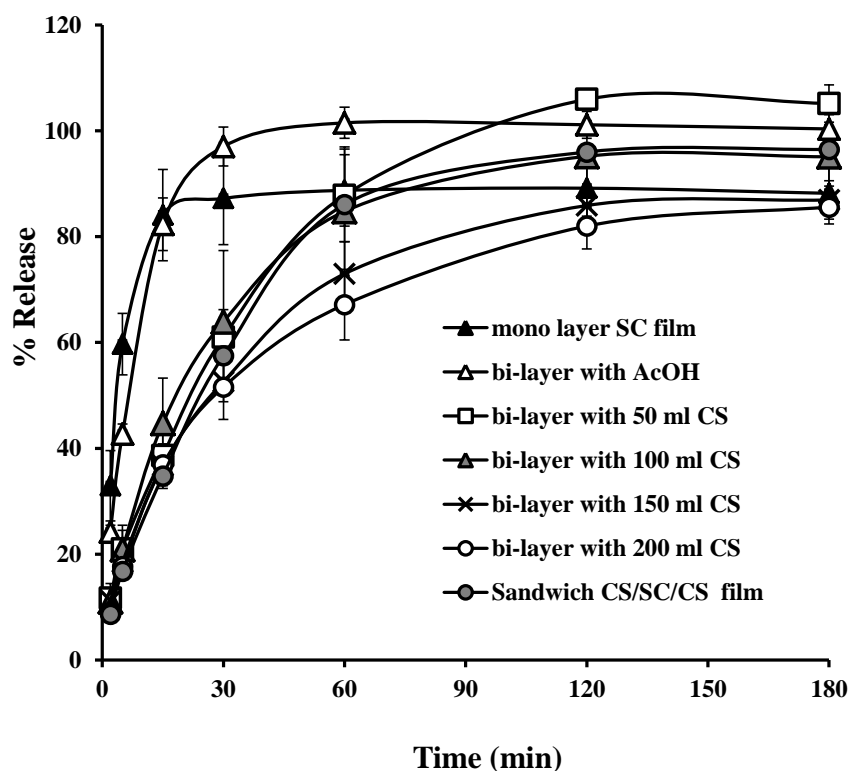


Fig. 9. FZ released from SC-CS bilayer films at different contents of 1% CS covered on SC film. Each value is the Mean \pm S.D., n =4.

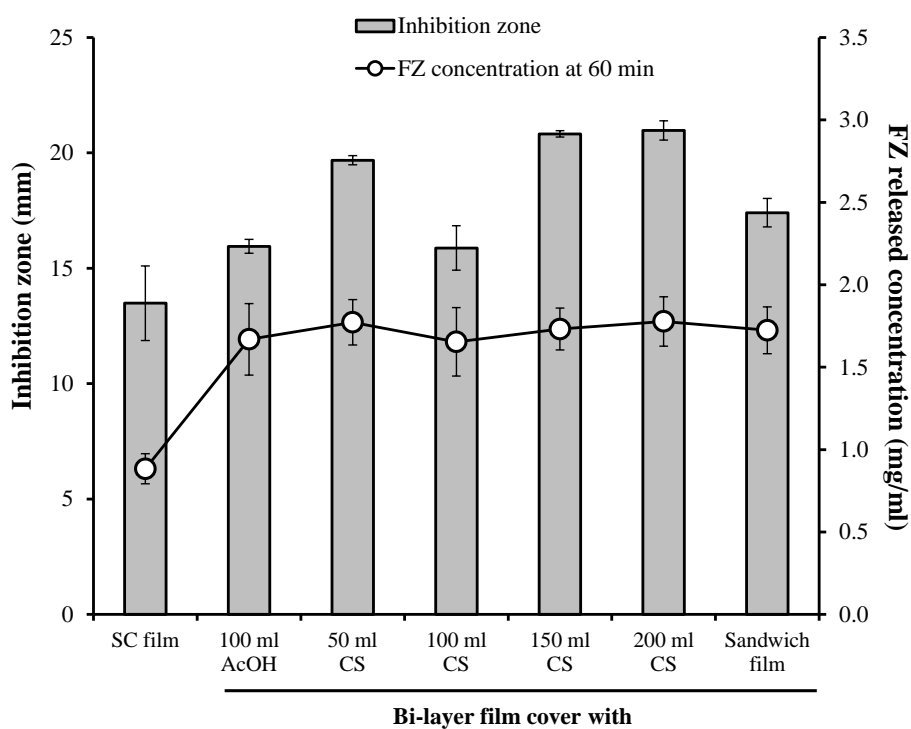


Fig. 10. Anticandidal activity of 1% FZ released from SC film covered with varying amounts of CS. Each value indicates the mean \pm SD, n = 3.

Part V: Alginate-sodium caseinate beads for anticandidal delivery

1.Introduction

Polysaccharide-protein blends offer a great potential for use in food and pharmaceutical technologies. Molecular interactions between polysaccharides and proteins lead to a formation of complexes that depended on type of interaction bonding. Basically, these interactions can be classified as covalent and non-covalent interactions (Dickinson, 2008). Covalent interactions are highly specific by strong binding and irreversible interaction between proteins and polysaccharides. In contrast, non-covalent interactions are non-specific and occurred via electrostatic force, hydrogen bonding, and hydrophobic interactions, leading to a formation of soluble or insoluble complexes that dependent upon weak or strong interactions, respectively (Wijaya et al., 2017). The polysaccharide-protein complexes have been characterized and applied as emulsifiers (Evans et al., 2013), film formers (Mohammadi et al., 2018), and micro/nanomatrix formers used for delivery of drugs and nutrients (Jain et al., 2016; Chang et al., 2017; Shaddel et al., 2018).

Sodium alginate (SA) is a natural anionic polysaccharide found in marine brown algae. SA is composed of (1–4)-linked β -D-mannuronic acid and α -L-guluronic acid (Draget, 2000). It has regions rich in mannuronic acid units, guluronic acid units and regions in which both monomers are equally prevalent. SA can be crosslinked with a divalent cation, such as calcium ions, to form microparticles and beads, which are depended on droplet sizes of dispersions dropped into the divalent ion-rich solution. This method was so-called ionotropic gelation (Pillay et al., 1998). The calcium alginate (CA) in the forms of microparticles or beads has been widely used as a delivery system of drugs (Sugawara et al., 1994; El-Aassar et al., 2014; Ozseker and Akkaya, 2016) and proteins (Haider and Husain, 2007). Reinforcement of the CA beads can be made via incorporation of water-soluble (Puttipipatkachorn et al., 2005; Pongjanyakul and Puttipipatkachorn, 2007) and water-insoluble polymers (Pongjanyakul, 2007), clays (Puttipipatkachorn et al., 2005; Pongjanyakul and Rongthong 2010), and proteins (Almeida and Almeida, 2004) in the drug-loaded SA dispersion before crosslinking process. This approach lead to improvement of drug entrapment efficiency (DEE) and retardation of drug release of the CA beads. Thus, it is interesting to seek a natural substance to modify the characteristics of the CA beads. One of natural proteins is casein that it could interact with several polymers, such as pectin (Maroziene and De Kruif, 2000) and starch (Sun et al., 2016). This may have a potential to interact with SA and to improve CA bead characteristics.

Caseins are composed of 94% protein and 6% colloidal calcium phosphate (Walstra et al., 2006), which molecule weights of caseins are in the range of 19-25 kDa with isoelectric point of 4.6-4.8. They are composed of four different peptides: α S₁, α S₂, β , and κ caseins (Dalglish and Corredig, 2012). Caseins in an acidic form possess a low aqueous solubility, but sodium caseinate (SC), sodium salt of casein, is freely soluble in water (Elzoghby et al., 2011). Due to amphiphilic properties of SC molecules, self-assemble into stable micellar

structures in aqueous solutions can be formed when the SC concentration is higher than 1.0 mg mL^{-1} , a critical micelle concentration (Horne and Euston, 2005). The core of micelles consists of αS_1 , αS_2 , and β caseins, whereas κ caseins locate and cover onto the surface of micelles (Dalgleish and Corredig, 2012). For this characteristic, SC has been pharmaceutically applied as a solubilizing agent for poorly soluble drugs (Millar and Corrigan, 1991; Millar and Corrigan, 1993). Furthermore, SC has a potential use as drug delivery systems, particularly microparticles (Knepp et al., 1993; Santinho et al., 1999) and nanoparticles (Elzoghby et al., 2013; Pan et al., 2013).

Polysaccharide-protein composites between SA and SC have been previously investigated in the form of dispersions and microparticles. Phase separation of SA and SC in the composite dispersion was prepared, and rheology and viscosity of each phase were characterized by Simeone et al. (2004). The SC rich phase and SC solution showed Newtonian flow, whereas a shear thinning system was found in SA rich phase and SA solution. The drug-loaded microparticles were prepared by dropping the SA-casein dispersions at a basic pH into calcium chloride solution (He et al., 2015), resulting in a sustained-release of drug from the microparticles. Moreover, CA microgel particles prepared using a spray aerosol method could interact with SC that was detected by zeta potential studies and dye-binding method (Ching et al., 2015). It can be seen that the viscosity synergism of SA and SC in the composite dispersion after simple mixing is not available in literature reviews. Furthermore, the molecule interaction between SA and SC, and the characteristics of CA beads incorporated with SC for drug delivery are yet unknown.

Therefore, the aims of this study were to examine molecular interaction between SA and SC in composite dispersions and films, and to characterize the SC-CA beads for anticandidals delivery. The composite SA-SC dispersions were prepared, and zeta potential and viscosity of the dispersions were investigated. Solid state molecular interaction between SA and SC in the films was examined using DSC and FTIR spectroscopy. Then, the SA-SC beads were prepared using the ionotropic gelation. Drugs incorporated in the beads were fluconazole (FZ) and clotrimazole (CZ), which were used for candidiasis treatments. Particle size and morphology, DEE, water uptake and erosion, *in vitro* drug release and anticandidal activity of drug released were investigated. The anticandidal-loaded SC-CA beads may utilize as a model delivery system and drug reservoirs in tablets for candidiasis treatment in oral cavity.

2. Materials and methods

2.1. Materials

Alginic acid sodium salt from brown algae (low viscosity, 100-300 cP at 25°C) was purchased from Sigma-Aldrich, Inc. (MO, USA). The ratios of mannuronic acid to guluronic acid residues were 1.6 (Lemoine et al., 1998). Casein sodium salt from bovine milk (MW=19-25 kDa) was also obtained from Sigma-Aldrich, Inc. (MO, USA). FZ and CZ were purchased from Hubei Yuancheng Gongchuang Technology Co., Ltd. (Wuhan, China) and Changzhou Yabang Pharmaceutical Co., Ltd. (Jiangsu, China), respectively. Sodium lauryl sulfate (SLS) was obtained from S. Tong Chemicals Co., Ltd. (Bangkok, Thailand). *Candida albican*

ATCC10231 was a gift from the Biofilm Research Group, Faculty of Dentistry, Khon Kaen University (Khon Kaen, Thailand). All other reagents used were of analytical grade and used as received.

2.2. Preparation of SA-SC dispersions

SC (0, 0.5, 1 and 2 g) was dispersed in purified water (75 mL) at 25 °C. Then, SA (2 g) was gently added and stirred using a magnetic stirrer for 2 h. After that, the SA-SC dispersions were adjusted to the final volume (100 mL). The zeta potential and viscosity of the dispersions obtained were characterized. Moreover, the SC dispersion in the concentration of 2 %w/v was also prepared and characterized for comparison.

2.3. Characterization of SA-SC dispersions

2.3.1. Zeta potential measurement

The zeta potential of the SA-SC dispersions were measured using a laser Doppler electrophoresis analyzer (Zetasizer Model ZEN 2600, Malvern Instrument Ltd., UK). The samples were kept at 25 °C, and the dispersions were diluted using deionized water to obtain the appropriate concentrations (count rates >20,000 counts per second) prior to measurement.

2.3.2. Viscosity determination

Viscosities of the dispersions were determined using a small sample adapter of a Brookfield Digital Rheometer (Model DV-III, Brookfield Engineering Labs Inc., Stoughton, MA) at 30 ± 2 °C. A spindle no 31 was used at shear rate over the range of 6.8-27.2 s⁻¹. The shear stress and viscosity at different shear rate were recorded.

2.4. Solubility of FZ and CZ

Solubility of FZ and CZ were conducted in various media involved at 37 °C. Excess amounts of drug powder were added to 10 mL of medium in a test tube. Then, the mixture was sonicated for 2 h, and shaken in a horizontal water bath shaker at a rate of 80 oscillations min⁻¹ at 37 °C for 5 days to achieve a solubility equilibrium of drug. A clear supernatant (1 mL) was collected, and the concentration of drug in saturated solution (solubility value) was analyzed using HPLC.

2.5. Molecular interaction studies between SA and SC

2.5.1. Preparation of films

Molecular interaction between SA and SC in solid state was investigated. SA, SC and SA-SC films were prepared using a casting/solvent evaporation method. The 2 %w/v SA, 2 %w/v SC, and 2%w/v SA-2%w/v SC dispersions were prepared following the method mentioned above, and then the dispersions (20 mL) were poured in a plastic plate (6 cm × 9.5 cm) and dried using a hot air oven at 50 °C. The dry films were peeled off, and kept in a desiccator prior to use.

2.5.2. Fourier transform infrared (FTIR) spectroscopy

FTIR spectra of the films were determined using the KBr disc method. Each sample was gently triturated with KBr powder at a weight ratio of 1:100 and then pressed with a hydrostatic press at 10 tons for 10 min. The discs were placed in a sample holder and scanned from 4000 to 450 cm⁻¹ at a resolution of 4 cm⁻¹ (Spectrum One, Perkin Elmer, Norwalk, CT).

2.5.3. Differential scanning calorimetry (DSC)

DSC thermogram of the films were recorded using a differential scanning calorimeter (DSC822, Mettler Toledo, Switzerland). Samples (2.5-3.0 mg) was accurately weighed and placed in a 40- μ L aluminum pan without an aluminum cover. The samples were heated from 30 to 450 °C at a heating rate of 10 °C min⁻¹.

2.6. Preparation of drug-loaded beads

SC (0, 0.5, 1 or 2 g) was dispersed in purified water (75 mL) at 25 °C. Then, FZ (0.25 g) or CZ (0.25 g) was gently added into the SC dispersion, and the SC dispersions containing drugs were stirred and incubated at 25 °C for overnight. After that, SA (2 g) was added to the SC dispersions containing drugs. The composite dispersions were stirred at 25 °C for 2 h and adjusted the final volume to 100 mL. The composite dispersions obtained were dropped through a nozzle (0.8 mm inner diameter) into 2 % w/v calcium chloride solution (240 mL) with gentle agitation. The gel beads were cured in calcium chloride solution for 30 min, washed with 240 mL of purified water, blotted to remove excess water, and dried at 50 °C using a hot air oven for 24 h.

2.7. Characterization of beads

2.7.1. Particle size and morphology

Particle size of the drug loaded beads was determined using an optical microscope (Olympus CH300RF200, Olympus Optical Co., Ltd, Japan). Three hundred beads were randomized and their Feret's diameters were measured and the mean diameters of the beads were calculated. The particle morphology of the beads was also observed using scanning electron microscopy (SEM). The samples were mounted on dummies, coated with gold in a vacuum evaporator, and then viewed using a scanning electron microscope (Hitachi Se3000 N, Tokyo, Japan).

2.7.2. Drug content and entrapment efficiency

The drug-loaded beads (50 mg) were immersed in pH 6.8 phosphate buffer (10 ml) in order to completely disintegrate of the beads. The mixture was sonicated for 4 h and incubated in a shaking water bath for overnight. Then, the mixture was mixed with the mixed solvent (acetonitrile:water (7:3) for FZ and acetonitrile:dipotassium phosphate (3:1) at pH 5.8 for CZ), sonicated for 15 min, and adjusted the final volume to 50 mL. The mixture was filtered using a 0.2- μ m nylon membrane before HPLC analysis. The amount of drug was determined using HPLC analysis. The ratio of the actual to the theoretical drug contents in the beads was termed as DEE ([Wang and He, 2002](#)).

2.7.3. DSC and FTIR spectroscopy

The FTIR spectra and DSC thermogram of the beads were investigated using the same procedure that mentioned in Section 2.5.2 and 2.5.3, respectively.

2.7.4. In vitro drug release studies

FZ released from the beads was investigated using pH 5.8 simulated salivary fluid (SSF) as a release medium. The SSF consisted of 2.38 g Na₂HPO₄, 0.19 g KH₂PO₄ and 8 g NaCl₂ per liter of purified water, and the final pH was adjusted to 5.8 using phosphoric acid. The

beads equivalent to 50 mg of FZ were weighed and placed in an Erlenmeyer flask containing 100 mL of release medium. The flasks were incubated in a water bath at 37 °C with shaking at 90 oscillations min⁻¹. At different time intervals, samples (5 mL) were collected and replaced with a fresh medium. The amount of FZ released was analyzed by using HPLC.

Due to very low solubility of CZ, the release system testing was changed to use the USP dissolution apparatus 2, paddle method, (Hanson Research, Northridge, USA) because it is necessary to increase both release medium volume and stirring efficiency in order to maintain a sink condition. Moreover, the release medium used was SSF added with 0.1 %w/v SLS for dissolution enhancement of CZ. The beads were equivalently weighed to 5 mg of CZ, and placed in the vessel containing 350 mL of release medium at 37.0 ± 1° C. The paddles were rotated at a rate of 50 revolution min⁻¹. Samples (7 ml) were collected and replaced with fresh media at various time intervals. The amount of CZ released was analyzed by using HPLC.

2.7.5. Water uptake and erosion studies

The drug loaded beads were placed in a small basket, immersed in SSF, and shaken occasionally in a water bath at 37 °C. After a predetermined time interval, each basket was withdrawn, blotted to remove excess water and immediately weighed on an analytical balance. The wet beads after soaking for 60 min were dried at 50 °C by using a hot air oven until a constant weight of the beads was obtained. The water uptake and erosion of the beads were determined according to the following equations (Sutananta et al., 1995):

$$\text{Water uptake (\%)} = \frac{(W_w - W_i)}{W_i} \times 100$$

$$\text{Erosion (\%)} = \frac{W_i - W_d - R_c}{W_i} \times 100$$

where W_w is the weight of the wet beads, W_i is the initial weight of the beads, W_d is the weight of the beads after drying process, and R_c is the mean amount of drug released at 60 min obtained from in vitro release studies.

2.7.6. Anticandidal activity study

FZ and CZ released from the beads were tested antimicrobial activity against *C. albicans* using by an agar diffusion method. *C. albicans* were inoculated into 20 mL of Sabouraud dextrose broth. The exponential period of growth and the culture broth was diluted. The concentration of *C. albicans* was diluted to 10⁶ CFU mL⁻¹. Then, plates with Sabouraud dextrose agar (20 ml) were prepared, in which 200 µL solution of microbe suspension was added and spread uniformly with sterile cotton swabs. The agar was punched using a Pasteur pipet to make 6-mm diameter holes, which four holes were made on each plate. The 45-µL solution of negative control, positive control and release medium from drug release testing were dropped into the holes. All plates were incubated at 32.0 ± 1.0 °C for 24 h. Then, the diameters of the inhibition zones were measured. The negative controls were SSF with or without 0.1% w/v SLS for CZ or FZ, respectively. The positive control was 80 and 2.0 µg mL⁻¹ of FZ and CZ in SSF without or without 0.1% w/v SLS, respectively. The FZ and CZ release media at 60 and 240 min of the release studies, respectively, were selected to test the anticandidal activities.

2.8. HPLC analysis

The concentration of FZ or CZ in the samples was analyzed using a HPLC system that consisted of Waters 1525 binary pumps, 2489 dual absorbance detector and Waters Breeze Software 2.0 versions (Waters Corporation, MA, USA). A reversed-phase HPLC using a C-18 column (Mightysil RP-18 GP, 4.6 mm \times 150 mm, 5- μ m particle size; Kanto Chemical Co., Inc., Tokyo, Japan) was employed. The mobile phases of FZ and CZ were acetonitrile:water (30:70) and acetonitrile:0.025 M dipotassium phosphate (K_2HPO_4) (3:1) at pH 5.8, respectively. The flow rate of the mobile phases was 1 mL min⁻¹. The detection wavelength was set at 210 nm. The retention times of FZ and CZ were approximately 3.1 and 4.5 min, respectively. Under these conditions, good linearity and reproducibility were shown over the range 10-120 μ g mL⁻¹ for FZ and 0.2-100 μ g mL⁻¹ for CZ.

3. Results and discussion

3.1. Molecular interaction between SA and SC

The molecular interaction between SA and SC was investigated in the forms of dispersions and films. The SA-SC dispersions showed white turbid liquids because of a milky appearance of SC when dispersing in water. The pH of all dispersions in this study was found in the range of 5.9-6.5. The zeta potential of 2 %w/v SC dispersion was -13.3 ± 0.87 mV (n=3), whereas that of 2 %w/v SA dispersion was found to be -96.6 ± 3.75 mV (n=3). It can be described that the pH of the SA-SC dispersions was higher than the pK_a (3.38-3.65) of SA (Draget, 2000) and the isoelectric point (4.6-4.9) of SC (Elzoghby et al., 2011). This led to ionization of carboxyl groups on SA and SC molecules to display a negative charge. The 2 %w/v SA dispersions incorporated with 0.5, 1, and 2 %w/v SC also presented a negative charge of zeta potential values that were determined to be -56.5 ± 3.12 , -46.7 ± 1.06 , and -41.4 ± 0.15 mV (n=3), respectively. Increase of SC content caused a decrease of zeta potential values of the SA-SC dispersions. Apart from zeta potential, viscosity of dispersions was also reported and relationship between shear rate and viscosity of the dispersions is shown in Fig. 1. The 2 %w/v SC dispersion showed very low viscosity, but it still presented a shear thinning system because the viscosity value decreased with increasing shear rate (Lee et al., 2009). The 2 % SA dispersion presented obviously higher viscosity than the 2% SC dispersion, and possessed a shear thinning behavior as well. Addition of SC resulted in increasing of viscosity of SA dispersion that the greater the SC addition, the higher the viscosity of the SA-SC dispersion was found (Fig. 1). These results suggested that the viscosity synergism effect was able to explain by a molecular interaction between both components.

DSC and FTIR spectroscopy were used to investigate solid state molecular interaction of SA and SC in this study. The SA films showed a small exothermic peak at 224 °C and followed an endothermic peak at around 230 °C (Fig. 2a). This may be due to a recrystallization and a phase transition of SA after heat induction (Pongjanyakul et al., 2005; Pongjanyakul, 2009). The first and second exothermic degradation peaks were found at 251 and 367 °C, respectively. The SC films presented two exothermic peaks at 297 and 353 °C

(Fig. 2a). The SA-SC films showed the exothermic peak at 225 °C and followed the endothermic peak at around 230 °C, and the first degradation peak of SA was slightly shifted to higher temperature (253 °C). Moreover, both exothermic peaks at 343 and 381 °C were found for the composite films. The changes of the thermal property of the SA-SC films suggested molecular interaction occurred after simple mixing of both components.

FTIR spectra of the SA, SC, and SA-SC films are illustrated in Fig. 2b. SA films showed absorption peaks at 3445 cm^{-1} (O–H stretching), 1617 cm^{-1} (COO^- asymmetric stretching), 1412 cm^{-1} (COO^- symmetric stretching) and 1030 cm^{-1} (C–O–C stretching), which were similar to the previous studies (Pongjanyakul et al., 2005; Pongjanyakul, 2009). For SC films, the peak at 3436 cm^{-1} corresponded to the O–H stretching, which overlapped the N–H stretching. The strong peak at 1638 cm^{-1} was due to the C=O stretching vibrations of the amide I groups, and the peaks at 1535 and 1242 cm^{-1} was N–H bending (amide II) and C–N stretching, respectively (Santinho et al., 1999; Pereda et al., 2010). The spectra of the SA-SC films showed the O–H stretching couple with the N–H stretching was moved to lower wavenumber, and the peaks of amide I and II were shifted to higher wavenumber. Moreover, the C–O–C stretching of SA also shifted to 1038 cm^{-1} . These results suggested that the carboxyl and hydroxyl groups of SA could strongly interact with the amide I and II groups of SC via an intermolecular hydrogen bonding.

According to all data investigated, the presentation model of the SA-SC composites is illustrated in Fig. 3. SA side chains could possibly interact with SC micelles that covered with κ -caseins. The outer parts of the surface were so-called the caseinomacropeptide chains (Dalglish and Corredig, 2012) that amino acids in this chain possibly interacted with SA. For example, the ending three amino acids sequence of κ -caseins were threonine, alanine and valine (Fox and McSweeney, 1998). The amide I and II groups of these amino acids could interact with hydroxyl and carboxyl groups of SA via hydrogen bonding, resulting in the formation of SA-SC soluble complexes and the more complexity of matrix network in the dispersions. This may lead to hindering negative charge and decreasing zeta potential value, but enhancing viscosity of the composite dispersions. In addition, the SA-SC complexes influenced the thermal behavior of the composite films.

3.2. Particle characteristics and DEE of the beads

Particle sizes of the beads are listed in Table 1. The CA beads loaded with FZ or CZ showed a comparable particle size approximately 825-855 μm . The CA beads showed quite spherical shape with a few fracture on the particle surface. However, the CZ-loaded CA bead presented rougher surface than the FZ-loaded CA beads (Fig. 4). The particle size of the SC-CA beads tended to increase with increasing SC content (Table 1) because higher density and more viscous of the SC-SA dispersion in the droplets may cause a lower shrinkage during cross-linking with calcium ions. SEM picture also presented that the 2%SC-CA beads containing FZ or CZ was bigger than the CA beads with drugs, but the different surface morphology was observed (Fig. 4).

The drug content of the beads containing for FZ or CZ decreased with increasing SC contents (Table 1) because of increasing of the polymer content for the bead preparation. The DEE of the CA and SC-CA beads with FZ was in the range of 19.3-23.3 %. Increase of 0.5 and 1% SC seemed to decrease %DEE, but adding 2% SC resulted in an increase of %DEE (Table 1). The loss of FZ from the beads was due to water leakage from the beads during the preparation period (Dashevsky, 1998). Moreover, FZ had a slightly soluble in water that the water solubility value of FZ was found to be $6.69 \pm 0.08 \text{ mg mL}^{-1}$ (n=3) in this study. The complete dissolution of 0.25% FZ in the dispersions before cross-linking process brought about the loss of FZ in the water leakage process. Incorporation of 2 %SC could increase %DEE of the CA beads because interaction between SA and SC created denser matrix network that was a barrier for preventing water leakage from the beads.

The %DEE of the CA or SC-CA beads for CZ was remarkably greater than that for FZ (Table 1) because water solubility of drug mainly influence the DEE values (Lee et al., 1999). CZ was practically insoluble in water that was found to be $3.47 \pm 0.44 \text{ } \mu\text{g mL}^{-1}$ (n=3). Thus, CZ particles was suspended in the dispersion before cross-linking, leading to very low CZ loss in the water leakage process of the wet beads. However, addition of SC in the dispersion could enhance CZ solubility, which the CZ solubility in 0.5, 1, and 2 %w/v SC dispersions was 4.13 ± 0.23 , 7.75 ± 1.31 , and $19.20 \pm 1.12 \text{ } \mu\text{g mL}^{-1}$ (n=3). These results presented the micellization property of SC that was reported previously with many hydrophobic drugs (Millar and Corrigan, 1991; 1993; Esmaili et al., 2011; Elzoghby et al., 2013). Enhancement of CZ solubility may cause a decrease of %DEE in the CA beads using 0.5 and 1 %SC. However, denser matrix network of the 2%SC-CA beads could prevent drug loss during cross-linking. Thus, higher %DEE was obtained.

3.3. DSC and FTIR patterns

Molecular interaction of the CA or 2%SC-CA beads loaded with drugs was investigated using FTIR spectroscopy as shown in Fig. 5. The CA beads without drug presented a change of FTIR spectrum from the SA films (Fig. 2). The higher wavenumber shift of COO^- (asymmetric) and COO^- (symmetric) stretching peaks to 1626 and 1435 cm^{-1} , respectively, and lower wavenumber shift of O–H stretching peak to 3436 cm^{-1} was observed. The 2%SC-CA beads without drug caused a shift of amide I (1643 cm^{-1}) and amide II (1544 cm^{-1}) peak of SC, and the FTIR spectrum of this beads were similar to that of a freeze-dried casein-CA microparticle reported previously (He et al., 2015). Addition of FZ into the CA beads resulted in a shift of COO^- (symmetric) stretching peak to 1425 cm^{-1} . Moreover, the amide II peak of SC in the SC-CA beads moved to higher wavenumber when adding FZ. In the case of CZ, the 2%SC-CA beads loaded with CZ showed a shift of COO^- (symmetric) stretching peak of SA. However, the SA-CA beads loaded with FZ or CZ did not present the peak characteristics of FZ or CZ. This is likely to be due to very low amount of drug in the beads when compared with SC and CA. These results suggested that the SC-CA beads still showed the FTIR characteristics of the molecular interaction between SC and SA after cross-linking with

calcium ions, and FZ and CZ loaded into the beads could possibly interact with SA or SC via hydrogen bonding.

DSC thermograms of the CA and 2%SC-CA beads with drugs are presented in [Fig. 6](#). The thermal behavior of the CA beads without drug showed an endothermic peak followed with exothermic peak around 190-210 °C, and an exothermic degradation peak at 297 °C. Incorporation of SC did not affect the DCS thermogram of the CA beads. FZ had a sharp melting peak at 142 °C. The SC-CA beads loaded with FZ did not show the melting peak of FZ. This result suggested that FZ was completely dissolved and dispersed as an amorphous form in the bead matrix. In contrast, the CA and SC-CA beads presented a small melting peak of CZ at around 142-148 °C, suggesting that some CZ crystals were embedded in the bead matrix due to low solubility of CZ.

3.4. Water uptake and erosion

The SSF without or with 0.1 %SLS was used to test water uptake and erosion of the CA or SC-CA beads containing FZ or CZ, respectively, which the medium used was the same with that of drug release testing. The % water uptake of the beads increased when increasing the testing time. The water uptake and erosion of the CA and SC-CA beads loaded with FZ and CZ at 1 h of the test are presented in [Fig. 7](#). It can be seen that % water uptake of the CA beads gradually decreased when adding SC in the contents of 0.5 and 1%, and then the 2%SC-CA beads showed higher % water uptake than the 1%SC-CA beads. The beads with FZ and CZ showed the similar effect of SC added on water uptake results, but the % water uptakes of the beads with CZ was obviously greater than those with FZ ([Fig. 7a and 7b](#)). The use of 0.1% SLS for CZ led to the question about the effect of this surfactant on water uptake values. To prove the effect of SLS, the water uptake of the CA beads containing CZ in SSF without 0.1% SLS was examined, and the result was $1,114.72 \pm 75.08$ % water uptake at 1 h. This result indicated that the SLS did not affect the water uptake of the CA beads with CZ. For erosion results, incorporation of SC decreased % erosion of the beads. The % erosion of the beads with FZ was higher than that with CZ.

The water uptake of the CA beads occurred because CA could be changed to SA when exposing a medium containing monovalent cations ([Østberg et al., 1994](#)), for example SSF used in this study. The water absorption properties of the CA beads decreased when increasing SC content, suggesting that molecular interaction between SA and SC brought about a denser matrix structure of the beads. This also led to decreasing of dissolution of soluble substances in the matrices, such as SA, SC, and SC micelles. Moreover, this study showed that incorporation of 1%SC in the beads could create the densest matrix structure of the beads, which the lowest % water uptake was obtained. However, the % water uptakes of the beads containing FZ were remarkably lower than those of the beads containing CZ, whereas the opposite results of % erosion was found. It is possible to explain that the CZ particle suspended in the SA or SA-SC dispersions may hinder cross-linking process of SA via calcium ions when compared with FZ that was completely dissolved in the concentration of 0.25 %w/v used. This may lead to higher free SA remaining in the beads containing CZ

that caused greater water uptake at the investigation time. Furthermore, the gel formation of SA and SC embedded in the beads containing CZ possibly acted as a barrier of the soluble substances eroded out of the beads. Thus, lower % erosion of the beads containing CZ was obtained.

3.5. *In vitro* drug release

The SSF was used as a release medium for the beads containing FZ. For the beads loading CZ, 0.1 % SLS was added for enhancing CZ solubility. The CZ solubility in SSF without and with 0.1% SLS was 3.04 ± 0.52 and $159.81 \pm 2.13 \mu\text{g mL}^{-1}$ ($n=3$). The use of 0.1 % SLS gave 52.3-time increase of CZ solubility in SSF. For FZ, it had $6.16 \pm 0.03 \text{ mg mL}^{-1}$ ($n=3$) for solubility value in SSF. Thus, the expected maximum of drug concentration in the release system was lower than 10% of drug solubility (Rapedius and Blanchard, 2001), leading to a perfect sink condition of the release testing system.

The FZ release profiles showed a complete release after testing within 60 min (Fig. 8a). $T_{50\%}$, the time to achieve release of 50% of drug content, was calculated as a drug release rate for comparison. The higher the $T_{50\%}$ value, the slower the drug release rate was obtained. The results showed that the CA beads presented the fastest drug release, whereas the drug release seemed to slower (higher $T_{50\%}$ value) when adding SC into the beads (Table 1). The higher the SC added, the greater the $T_{50\%}$ value was obtained. The FZ release from the beads was faster than the release of CZ as shown in Fig. 8b. Less than 50 % of CZ amount in the beads was released within 240 min of the test. Thus, $T_{25\%}$ was used for comparison (Table 1). Increase of SC amount added resulted in higher $T_{25\%}$ values, meaning that SC added in the beads could possibly retard CZ release, although it provided solubility enhancement of CZ. These results suggested that addition of SC into the CA beads could slow down the release of drug due to denser matrix structure and lower water uptake of the SC-CA beads.

3.6. Anticandidal activity

The anticandidal activity of FZ and CZ after release from the beads was investigated in this study. The concentration of FZ or CZ in the samples and inhibition zone are presented in Fig. 9. The FZ in the concentration of $80 \mu\text{g mL}^{-1}$ (positive control) provided an inhibition zone diameter of $9.57 \pm 0.94 \text{ mm}$ ($n=3$). The concentrations of FZ released from the CA and SC-CA beads were over the range of $80.1\text{-}89.8 \mu\text{g mL}^{-1}$ that could inhibit *C. albicans* for the diameter of $9.0\text{-}12.9 \text{ mm}$ (Fig. 9a). The inhibition zone seemed to increase with increasing FZ concentration of the release testing. It can be seen that SC loaded in the beads did not obviously affect antimicrobial activity of FZ.

For CZ, the $2 \mu\text{g mL}^{-1}$ of CZ, which was the positive control, showed a $19.89 \pm 0.08 \text{ mm}$ ($n=3$) inhibition zone (Fig. 9b). The CA beads gave a similar inhibition zone with the positive control, but CZ concentration had 3.5-times higher than the positive control. This result suggested a lower efficiency of CZ released from the CA beads. However, the decrease of CZ concentration with increasing SC in the CA beads caused a small increase of inhibition zone, suggesting higher efficiency of CZ released. It is possible to explain that some of CZ released may be in the form of CZ-loaded SC micelles, which was likely a nanoparticle. The SC

nanoparticles could enhance antimicrobial activity of lipophilic substances, for example thymol-loaded SC nanoparticles (Pan et al., 2014). Moreover, CZ loaded in lipid nanoparticles showed more active against *C. albicans* than a CZ solution (Esposito et al., 2013). These results were different with that of FZ because FZ was a hydrophilic molecule that showed low affinity with a hydrophobic core of SC micelles. This led to a low chance to form FZ-loaded SC micelles. However, this anticandidal activity studies suggested that CZ and FZ loaded in the CA or SC-CA beads were still effective against *C. albicans*.

4. Conclusions

SA can interact with SC by simple mixing in the dispersions. Complexation between SA and SC occurs due to intermolecular hydrogen bonding between carboxyl or hydroxyl groups of SA and amide I or II groups of SC, leading to viscosity synergism in the composite dispersions. The SC-CA beads added with FZ or CZ can be prepared using calcium ions as a cross-linking agent. FZ is an amorphous form, whereas crystalline form of CZ is found in the beads, which is dependent upon water solubility of drugs. The CA beads can be reinforced by incorporating SC, resulting in increase of %DEE when using 2%SC, decrease of water uptake and erosion, and retardation drug release. Moreover, solubility of CZ can be enhanced by micellization of SC, leading to more effective against *C. albicans* of CZ released from the SC-CA beads. This study shows that molecular interaction between SA and SC can reinforce the CA beads, and the SC-CA beads show good potential for anticandidals delivery in oral candidiasis.

References

- Almeida, P.F., Almeida, A.J. 2004. Cross-linked alginate-gelatine beads: A new matrix for controlled release of pindolol. *Journal of Controlled Release* 97(3), pp. 431-439
- Chang C, Wang T, Hu Q, Luo Y. Caseinate-zein-polysaccharide complex nanoparticles as potential oral delivery vehicles for curcumin: Effect of polysaccharide type and chemical cross-linking. *Food Hydrocolloids*, Volume 72, November 2017, Pages 254-262
- Ching SH, Bhandari B, Webb R, Bansal N. Visualizing the interaction between sodium caseinate and calcium alginate microgel particles. *Food Hydrocolloids*, Volume 43, January 2015, Pages 165-171
- Dagleish DG, Corredig M, 2012. The structure of the casein micelle of milk and its changes during processing. *Annu. Rev. Food Sci. Technol.* 2012, 3, 449-467.
- Dashevsky, A., 1998. Protein loss by the microencapsulation of an enzyme (lactase) in alginate beads. *Int. J. Pharm.* 161, 1–5.
- Draget, K.I., 2000. Alginates. In: Philips, G.O., Williams, P.A. (Eds.), *Handbook of Hydrocolloids*. Woodhead Publishing, Cambridge, pp. 379–395.
- El-Aassar M.R., Hafez EE, El-Deeb NM, Fouda MMG. Microencapsulation of lectin anti-cancer agent and controlled release by alginate beads, biosafety approach. *International Journal of Biological Macromolecules*, Volume 69, August 2014, Pages 88-94

- Elzoghby AO, Helmy MW, Samy WM, Elgindy NA. Spray-dried casein-based micelles as a vehicle for solubilization and controlled delivery of flutamide: formulation, characterization, and in vivo pharmacokinetics. *Eur J Pharm Biopharm* 2013; 84: 487-96.
- Elzoghby, A.O., El-Fotoh, W.S., Elgindy, N.A., 2011. Casein-based formulations as promising controlled release drug delivery systems. *J. Control. Release* 153, 206–216.
- Elzoghby, A.O., Helmy, M.W., Samy, W.M., Elgindy, N.A., 2013a. Novel ionically crosslinked casein nanoparticles for flutamide delivery: formulation, characterization, and in vivo pharmacokinetics. *Int. J. Nanomed.* 8, 1721-1732.
- Esmaili, M., Ghaffari, S.M., Moosavi-Movahedi, Z., Atri, M.S., Sharifizadeh, A., Farhadi, M., Yousefi, R., Chobert, J.-M., Haertlé, T., Moosavi-Movahedi, A.A., 2011. Beta casein-micelle as a nano vehicle for solubility enhancement of curcumin; food industry application. *LWT - Food Science and Technology* 44(10), pp. 2166-2172.
- Esposito E, Ravani L, Contado C, Costenaro A, Drechsler M, Rossi D, Menegatti E, Grandini A, Cortesi R. Clotrimazole nanoparticle gel for mucosal administration. *Materials Science and Engineering C* 33 (2013) 411–418
- Evans M, Ratcliffe I, Williams PA. Emulsion stabilisation using polysaccharide–protein complexes. *Current Opinion in Colloid & Interface Science*, Volume 18, Issue 4, August 2013, Pages 272-282
- Fox PF, McSweeney PLH, Dairy chemistry and biochemistry, First ed., Blackie Academic & Professional, London, 1998.
- Haider T, Husain Q. Calcium alginate entrapped preparations of *Aspergillus oryzae* β galactosidase: Its stability and applications in the hydrolysis of lactose. *International Journal of Biological Macromolecules*, Volume 41, Issue 1, 1 June 2007, Pages 72-80
- He, Z., Zhang, X., Qi, W., Huang, R., Su, R. 2015. Alginate-casein microspheres as bioactive vehicles for nutrients. *Transactions of Tianjin University* 21(5), pp. 383-391
- Horne DS, Euston SR. Simulating the self-association of caseins. *Food hydrocolloids* 2005; 19: 379-86.
- Jain A, Thakur D, Ghoshal G, Katore O.P., Shivhare U.S. Characterization of microcapsulated β -carotene formed by complex coacervation using casein and gum tragacanth. *International Journal of Biological Macromolecules*, Volume 87, June 2016, Pages 101-113
- Knepp, W.A., Jayakrishnan, A., Quigg, J.M., Sitren, H.S., Bagnall, J.J., Goldberg, E.P., 1993. Synthesis, properties, and intratumoral evaluation of mitoxantrone-loaded casein microspheres in Lewis lung carcinoma. *J. Pharm. Pharmacol.* 45, 887-891.
- Lee BJ, Min GH, Cui JH. Correlation of drug solubility with trapping efficiency and release characteristics of alginate beads. *Pharm Pharmacol Commun* 1999, 5, 85-89.
- Lee CH, Moturi V, Lee Y. Thixotropic property in pharmaceutical formulations. *Journal of Controlled Release*, Volume 136, Issue 2, 5 June 2009, Pages 88-98
- Lemoine D, Wauters F, Bouchend'homme S, Pr  at V, 1998. Preparation and characterization of alginate microspheres containing a model antigen. *Int J Pharm* 176, 9-19.

- Maroziene, A., De Kruif, C.G 2000 Interaction of pectin and casein micelles. *Food Hydrocolloids* 14(4), pp. 391-394
- Millar FC, Corrigan OI. Dissolution mechanism of ibuprofen-casein compacts. *Int J Pharm* 1993; 92: 97-104.
- Millar FC, Corrigan OI. Influence of sodium caseinate on the dissolution rate of hydrochlorothiazide and chlorothiazide. *Drug Dev Ind Pharm* 1991; 17(21): 1593-607.
- Mohammadi R, Mohammadifar MA, Rouhi M, Kariminejad M, Mortazavian AM, Sadeghi E, Hasanvand S. Physico-mechanical and structural properties of eggshell membrane gelatin- chitosan blend edible films. *International Journal of Biological Macromolecules*, Volume 107, Part A, February 2018, Pages 406-412
- Østberg, T., Lund, E.M., Graffner, C., 1994. Calcium alginate matrices for oral multiple unit administration. IV. Release characteristics in different media. *Int. J. Pharm.* 112, 241–248.
- Ozseker EE, Akkaya A. Development of a new antibacterial biomaterial by tetracycline immobilization on calcium-alginate beads. *Carbohydrate Polymers*, Volume 151, 20 October 2016, Pages 441-451
- Pan K, Chen H, Davidson PM, Zhong Q. Thymol nanoencapsulated by sodium caseinate: physical and antilisterial properties. *J. Agric. Food Chem.* 2014, 62, 1649–1657
- Pan, K., Zhong, Q., Baek, S.J., 2013. Enhanced dispersibility and bioactivity of curcumin by encapsulation in casein nanoparticles. *J. Agric. Food Chem.* 61, 6036-6043.
- Perada, M., Aranguren, M.I., Marcovich, N.E., 2010. Effect of crosslinking on the properties of sodium caseinate films. *J. Appl. Polym. Sci.* 116, 18-26.
- Pillay V, Dangor CM, Govender T, Moopanar KR, Hurbans N. Ionotropic gelation: encapsulation of indomethacin in calcium alginate gel discs. *J Microencapsul.* 1998 Mar-Apr;15(2):215-26.
- Pongjanyakul T, Puttipipatkachorn S. Xanthan-alginate composite gel beads: molecular interaction and in vitro characterization. *Int J Pharm* 2007; 331: 61-71.
- Pongjanyakul T, Rongthong T. Enhanced entrapment efficiency and modulated drug release of alginate beads loaded with drug-clay intercalated complexes as microreservoirs. *Carbohydr Polym* 2010; 81: 409-419.
- Pongjanyakul T. Alginate–magnesium aluminum silicate films: Importance of alginate block structures. *International Journal of Pharmaceutics* 365 (2009) 100–108
- Pongjanyakul T. Characterization of microcrystalline cellulose loaded diclofenac calcium alginate gel beads in vitro. *Pharmazie* 2007; 62: 493-498.
- Pongjanyakul, T., Pripem, A., Puttipipatkachorn, S., 2005b. Investigation of novel alginate–magnesium aluminum silicate microcomposite films for modified release tablets. *J. Control. Release* 107, 343–356.
- Puttipipatkachorn S, Pongjanyakul T, Pripem A. Molecular interaction in alginate beads reinforced with sodium starch glycolate or magnesium aluminum silicate, and their physical characteristics. *Int J Pharm* 2005; 293:51-62.

- Rapedius M, Blanchard J. Comparison of the Hanson Microette and the Van Kel Apparatus for in vitro release testing of topical semisolid formulations. *Pharm. Res.* 2001; 18: 1440-1447.
- Santinho, A.J.P., Pereira, N.L., Freitas, O.D., Collett, J.H., 1999. Influence of formulation on the physicochemical properties of casein microparticles. *Int. J. Pharm.* 186, 191-198.
- Shaddel R, Hesari J, Azadmard-Damirchi S, Hamishehkar H, Fathi-Achachlouei B, Huang Q. Use of gelatin and gum Arabic for encapsulation of black raspberry anthocyanins by complex coacervation. *International Journal of Biological Macromolecules*, Volume 107, Part B, February 2018, Pages 1800-1810
- Simeone M, Alfani A, Guido S. Phase diagram, rheology and interfacial tension of aqueous mixtures of Na-caseinate and Na-alginate. **Food Hydrocolloids** 2004; 18 (3): 463-470.
- Sugawara, S., Imai, T., Otagiri, M., 1994. The controlled release of prednisolone using alginate gel. *Pharm. Res.* 11, 272–277.
- Sun, N.X., Liang, Y., Yu, B., Tan, C.P., Cui, B. Interaction of starch and casein. *Food Hydrocolloids*. 2016,60, pp. 572-579
- Sutananta, W., Craig, D.Q.M., Newton, J.M., 1995. An evaluation of the mechanisms of drug release from glyceride bases. *J. Pharm. Pharmacol.* 47, 182–187.
- Walstra P, Wouters JTM, Geurts TJ. *Dairy science and technology*, second ed., Taylor & Francis, Boca Raton, 2006.
- Wang, K., He, Z., 2002. Alginate-konjac glucomannan-chitosan beads as controlled release matrix. *Int. J. Pharm.* 244, 117–126.
- Wijaya W, Patel AR, Setiowati AD, Van der Meeren P. Functional colloids from proteins and polysaccharides for food applications. *Trends in Food Science & Technology*, Volume 68, October 2017, Pages 56-69

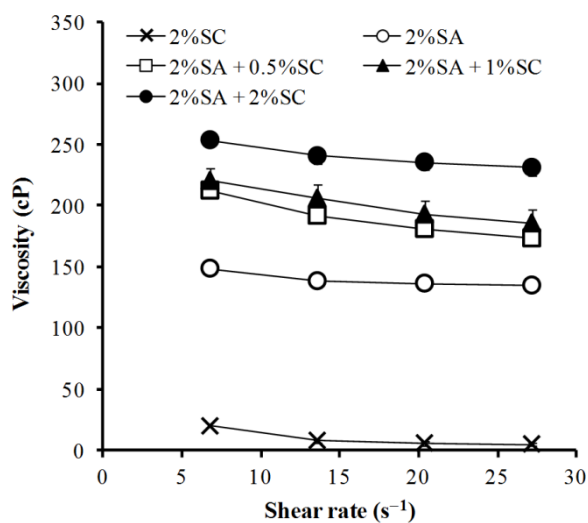


Figure 1. Relationship between shear rate and viscosity of SA, SC, and SA-SC dispersions. Each value indicates mean \pm SD, $n=3$.

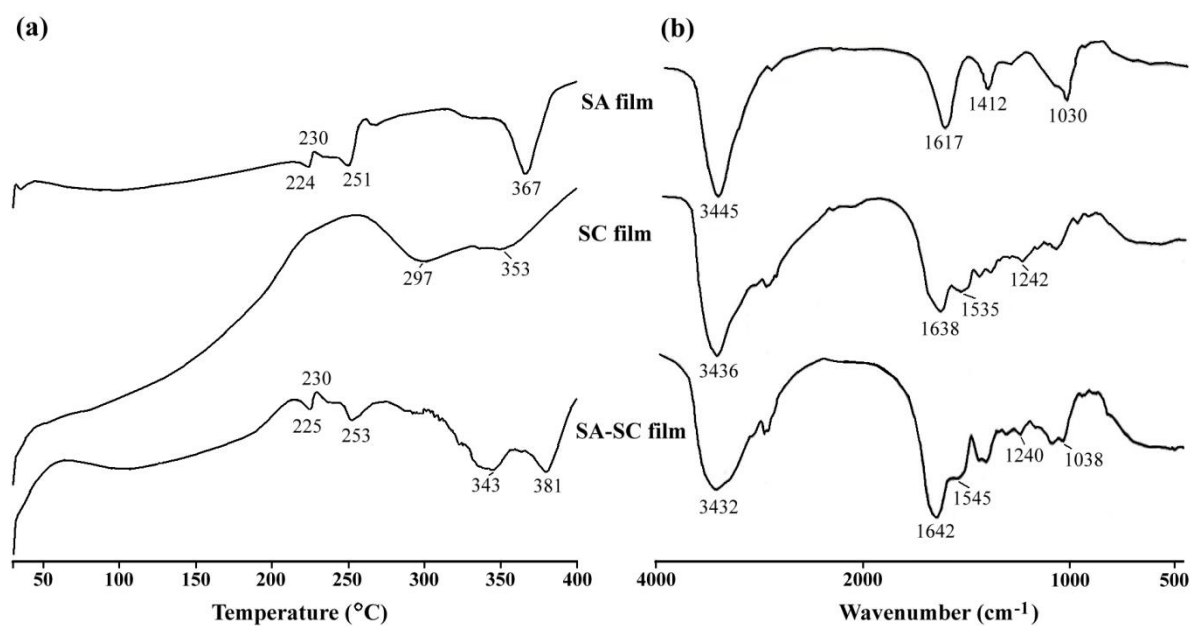


Figure 2. DSC thermogram (a) and FTIR spectra (b) of SA, SC, and SA-SC films.

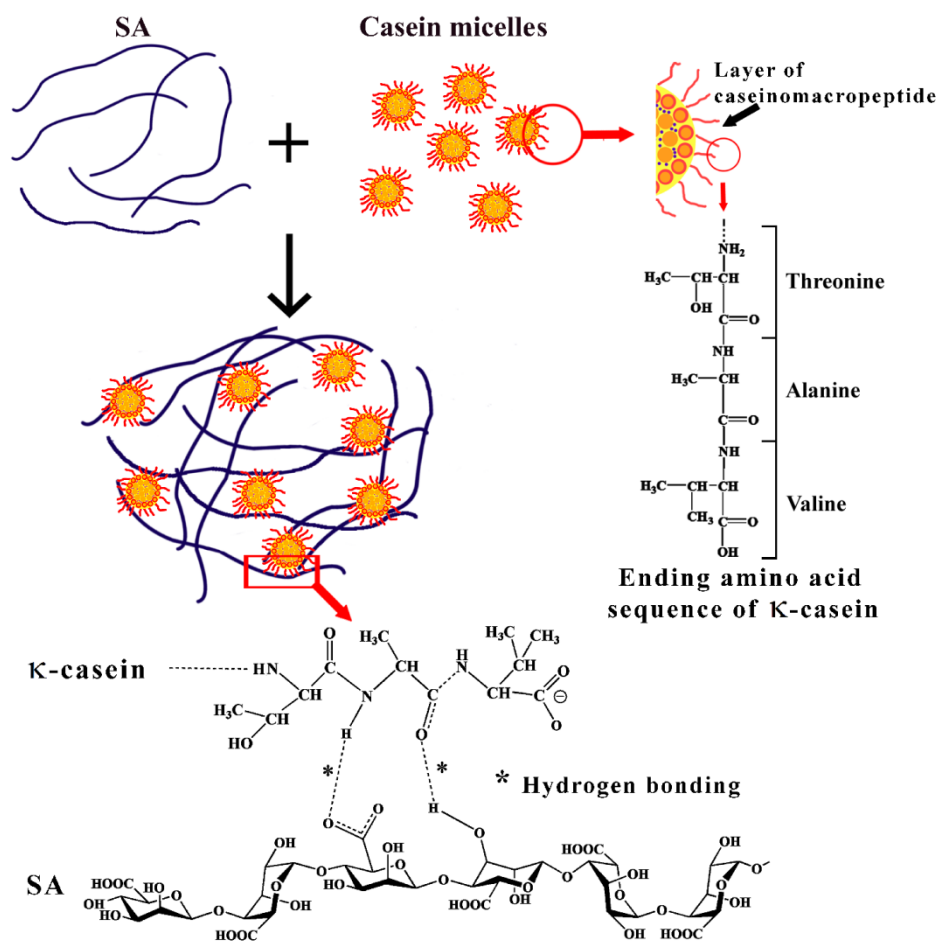


Figure 3. Schematic presentation of molecular interaction between SA and SC.

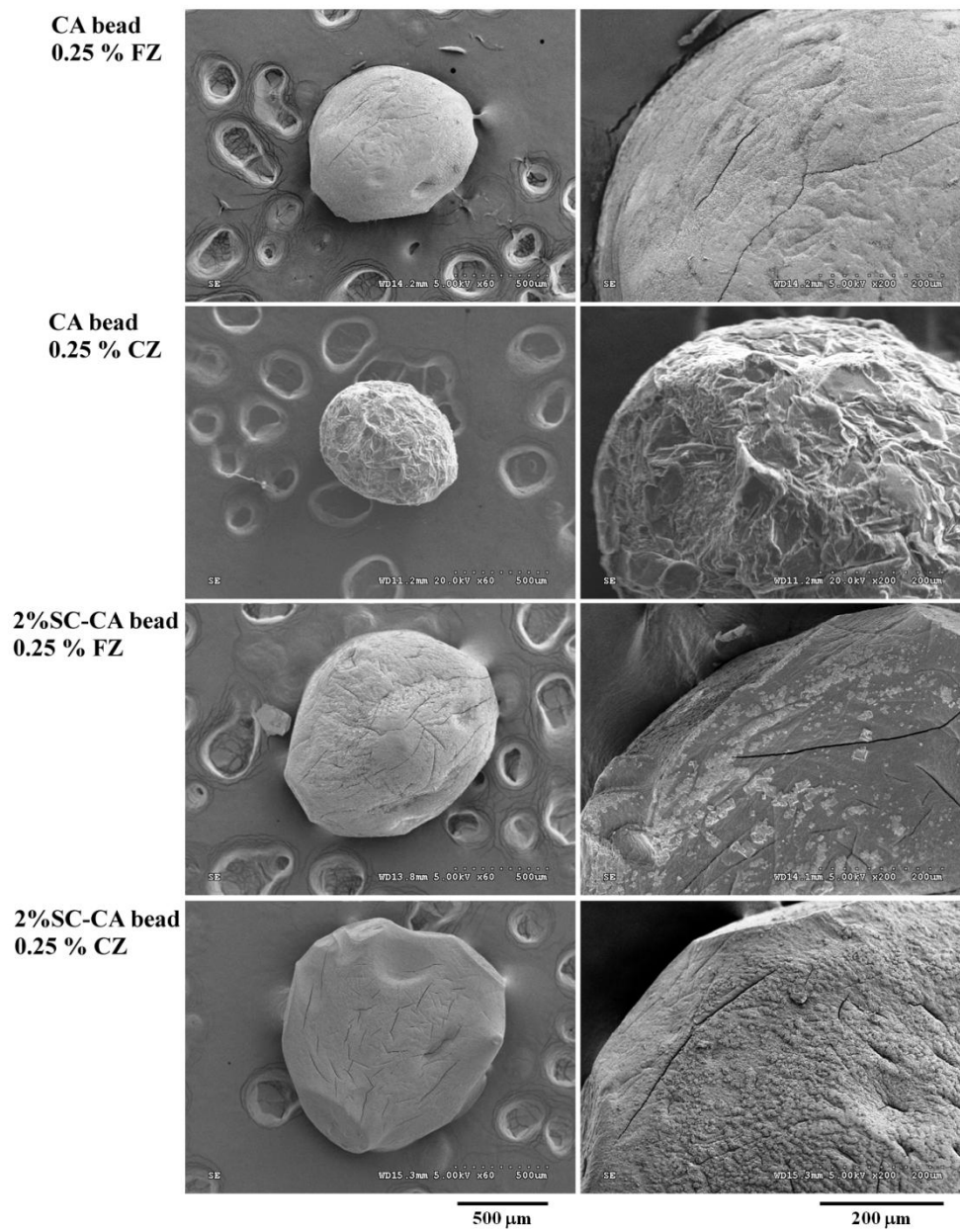


Figure 4. Particle and surface morphology of CA and 2%SC-CA beads prepared using 0.25 % FZ or CZ.

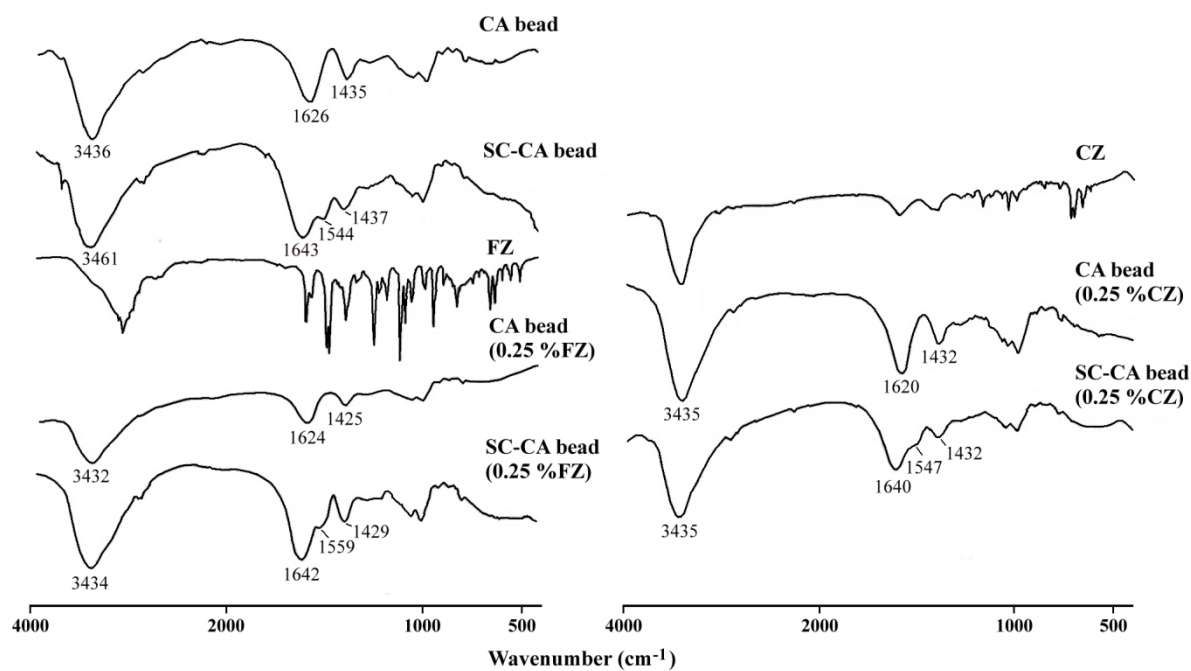


Figure 5. FTIR spectra of CA and 2%SC-CA beads prepared using 0.25 % FZ or CZ.

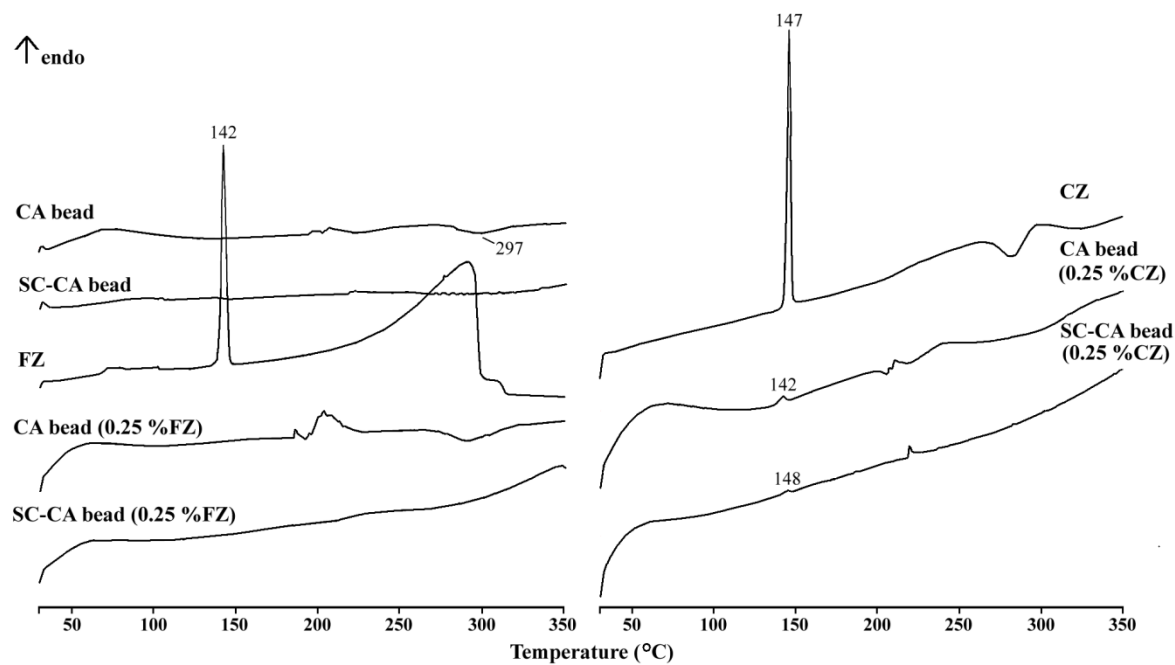


Figure 6. DSC thermograms of CA and 2%SC-CA beads prepared using 0.25 % FZ or CZ.

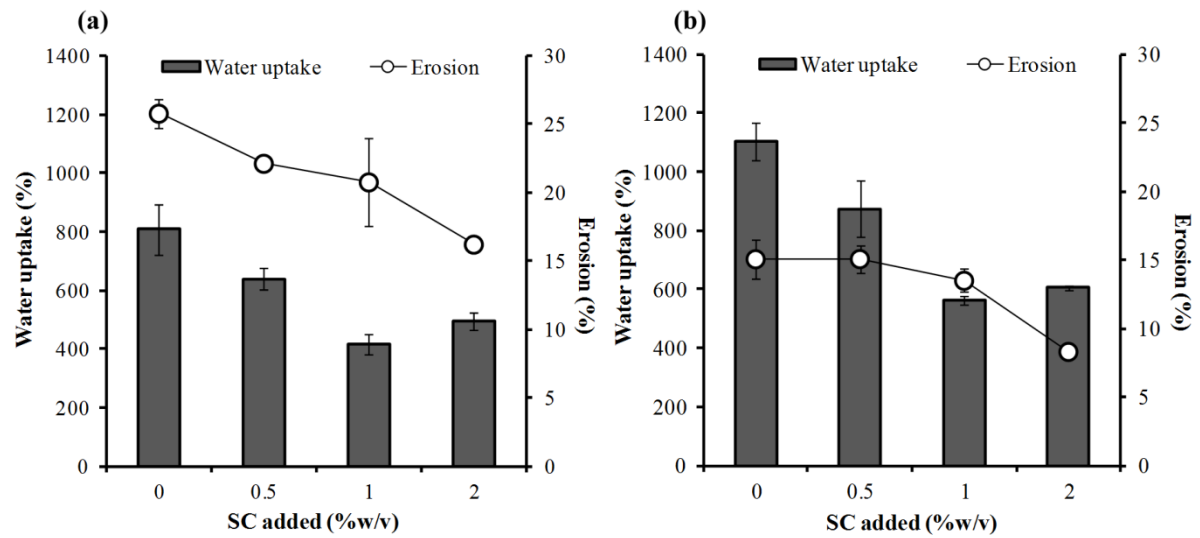


Figure 7. Water uptake and erosion of CA beads prepared using various contents of SC and 0.25 % FZ (a) or CZ (b). Each value indicated mean \pm SD, n=3.

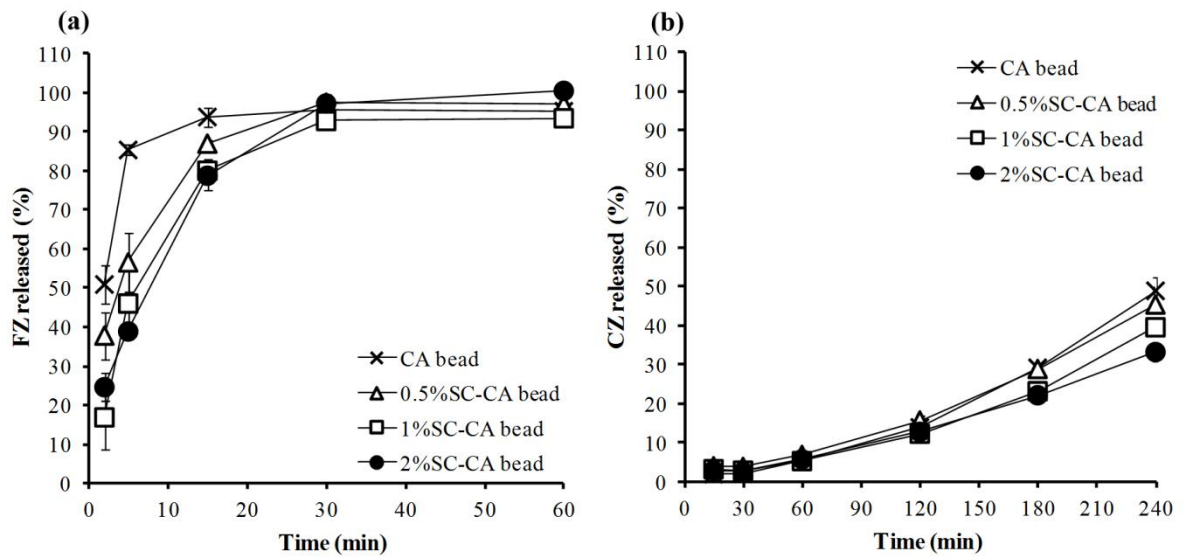


Figure 8. Drug release profiles of CA and SC-CA beads prepared using 0.25 % FZ (a) or CZ (b). Each value indicated mean \pm SD, n=3.

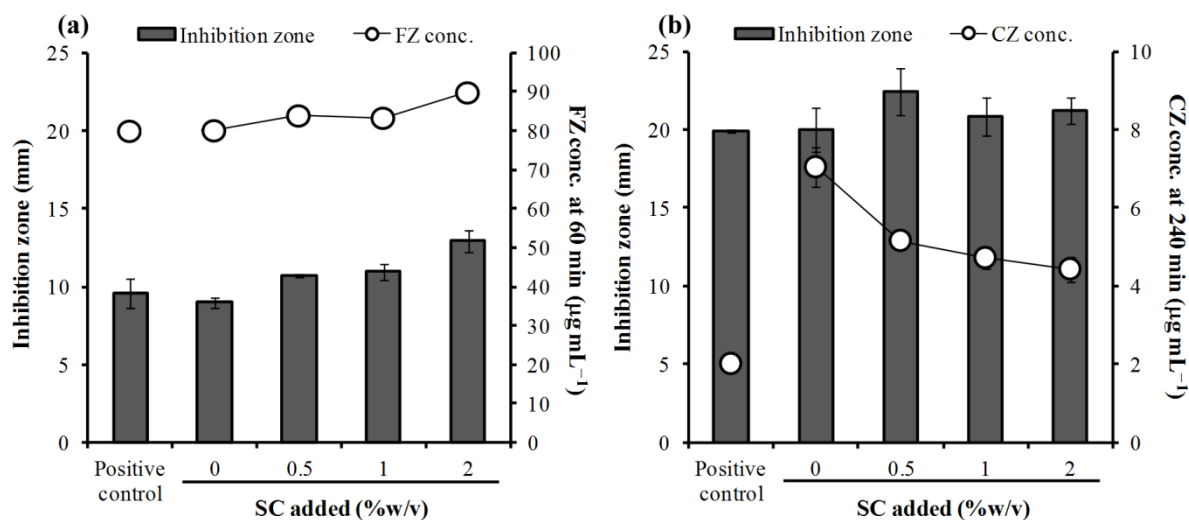


Figure 9. Anticandidal activity of drug released from CA beads prepared using various contents of SC and 0.25 % FZ (a) or CZ (b). Each value indicated mean \pm SD, n=3.

Table 1. Components and characteristics of SC-CA beads loaded with FZ or CZ.

Components	Particle size ^a (μm)	Drug content ^b (%w/w)	DEE ^b (%)	T _{25%} ^b (min)	T _{50%} ^b (min)
0.25 % w/v FZ					
2 % w/v SA	825.2 \pm 123.4	2.19 \pm 0.03	21.91 \pm 0.26	-	< 2
+ 0.5 % w/v SC	855.6 \pm 101.6	1.75 \pm 0.03	19.27 \pm 0.36	-	4.23 \pm 0.99
+ 1.0 % w/v SC	978.1 \pm 125.0	1.53 \pm 0.03	19.86 \pm 0.36	-	6.29 \pm 1.68
+ 2.0 % w/v SC	1117.8 \pm 173.6	1.37 \pm 0.03	23.27 \pm 0.48	-	7.79 \pm 0.63
0.25 % w/v CZ					
2 % w/v SA	849.7 \pm 78.4	10.26 \pm 0.01	93.25 \pm 0.08	163.62 \pm 4.57	> 240
+ 0.5 % w/v SC	832.8 \pm 86.7	7.42 \pm 0.07	81.59 \pm 0.73	161.96 \pm 2.24	> 240
+ 1.0 % w/v SC	896.2 \pm 78.6	6.56 \pm 0.05	85.23 \pm 0.64	186.64 \pm 6.66	> 240
+ 2.0 % w/v SC	1100.3 \pm 114.3	5.64 \pm 0.03	95.59 \pm 0.47	195.76 \pm 8.43	> 240

^a n=300, ^b n=3.

- : Could not be calculated.

Part VI: Alginate-starch beads for drug delivery

1. Introduction

Polysaccharides obtained from natural sources have been widely employed in food, biomedical and pharmaceutical fields. They can be used as an important ingredient and additive in pharmaceutical products because of their biodegradability and biocompatibility (Malafaya, Silva, & Reis, 2007; Shelke, James, Laurencin, & Kumbar, 2014). Among biopolysaccharides, sodium alginate (SA), found in marine brown algae, has been popularly used in pharmaceutical applications, such as a tablet disintegrant, matrix-forming agent, film former and gelling agent (Tønnesen & Karlsen, 2002). It consists of α -L-guluronic and β -D-mannuronic acids, and is composed of homopolymeric blocks and blocks with an alternating sequence (Draget, 2000). Gelation occurs by cross-linking of the uronic acids with divalent cations, for example calcium ion, that is so-called ionotropic gelation (Pillay, Dangor, Govender, Moopanar, & Hurbans, 1998). The formation of calcium alginate (CA) beads is achieved by dropping the drug-containing SA dispersion into a calcium chloride solution (Østberg, Lund, & Graffner, 1994; Sugawara, Imai, & Otagiri, 1994). The CA beads as a matrix system have been investigated as a controlled release system for drugs (Al-Kassas, Al-Gohary, & Al-Faadhel, 2007; Segale, Mannina, Giovannelli, & Pattarino, 2015) and proteins (Hariyadi et al., 2014; Jadhav & Singhal, 2014). Drug released from the CA beads depends on the swelling of the beads and the diffusion of the drug in the gel matrix (Sugawara et al., 1994). They also show a potential for a pulsatile release system of macromolecular drugs (Kikuchi, Kawabuchi, Sugihara, Sakurai, & Okano, 1997). Moreover, they can protect an acid-sensitive drug from gastric juice, and the drug is consequently released from the beads in the small intestine. In addition, the CA beads are suitable for delivery nonsteroidal anti-inflammatory drugs that caused gastric irritation (Hwang, Rhee, Lee, Oh, & Kim, 1995; Fernández-Hervás, Holgado, Fini, & Fell, 1998).

Modification of characteristics of the CA beads can be done by incorporation of some substances in a drug-loaded SA dispersion before cross-linking process, resulting in higher drug entrapment efficiency (DEE) and slower drug release. Water-soluble polymers, such as chondroitin sulfate (Murata, Miyamoto, & Kawashima, 1996), konjac glucomannan (Wang & He, 2002), gelatin (Almeida & Almeida, 2004), sodium starch glycolate (Puttipipatkachorn, Pongjanyakul & Pripem, 2005), xanthan gum (Pongjanyakul & Puttipipatkachorn, 2007), and gum arabic (Nayak, Das, & Maji, 2012; Tsai, Kitamura, & Kokawa, 2017), have been used for this purpose. Furthermore, the addition of water-insoluble substances, such as chitin (Murata, Tsumoto, Kofuji, & Kawashima, 2002) and magnesium aluminum silicate (Puttipipatkachorn et al., 2005; Pongjanyakul & Rongthong, 2010), can enhance DEE and retard drug release from the beads. The achievement of these modifications was because of the molecular interaction between the carboxyl groups of alginate and some functional groups of the additives. Additionally, starch is a potential material for the CA bead modification. Not only starch granules (Chan et al., 2011; Lozano-Vazquez et al., 2015), but also starch gels

(Singh, Sharma, & Gupta, 2009) can be used to modify the CA beads containing drugs and cells. From the literature reviews, comparative studies of the effect of starch granules and gel on characteristics of the CA beads for drug delivery are not available yet.

Starch consists of amylose, a linear polysaccharide of glucose linked via α -1-4 glycosidic bonds, and amylopectin, a branched polysaccharide of glucose with additional linkage of α -1-6 glycosidic bonds, in different contents that are dependent on its source (Masina et al., 2017). In nature, starch is insoluble in water because it has numerous crystalline regions in granules. Hydration of starch can be increased by heat treatment, which appearance of starch dispersion shows a viscous transparent liquid. This phenomenon is so-called gelatinization (Murphy, 2000). In this study, it was focused on one of the traditional starches in Thailand, which was the arrowroot starch extracted from *Tacca leontopetaloides* L. Kuntze (green stem Tacca). This starch has 24.53 % amylose with low protein content of 0.11 %, and the gelatinization temperature is 72.25 °C (Auttapornpitak, 2003). The particle morphology of starch granules is shown in Fig. 1. This arrowroot starch has been used as a main ingredient or additive for some Thai desserts because it provides high viscous and good texture paste after gelatinization. These characteristics showed good potential for modifying the properties of the CA beads.

Therefore, the objective of this study was to investigate the effect of ungelatinized and gelatinized starch (UGS and GS) of *Tacca leontopetaloides* L. Kuntze on characteristics of CA beads containing diclofenac sodium (DS), a nonsteroidal anti-inflammatory drug, as a model drug. The physical properties of the UGS-CA and GS-CA beads, such as particle size, particle and surface morphology, DEE, water uptake and drug release behavior, were investigated. Furthermore, molecular interaction between SA and UGS or GS in the form of dispersions and films was examined for describing the property change of the DS-loaded CA beads when incorporating UGS or GS.

2. Materials and methods

2.1 Materials

SA (viscosity grade of 300 cP and mannuronic acid to guluronic acid ratio=0.59) was obtained from Onimax Co., Ltd. (Bangkok, Thailand). Commercial arrowroot (*Tacca leontopetaloides* L. Kuntze) starch and DS were purchased from Choothin (Bangkok, Thailand) and Bang Trading 1992 Co., Ltd. (Bangkok, Thailand), respectively. All other reagents used were of analytical grade and used as received.

2.2. Characterization of UGS-SA and GS-SA dispersions and films

2.2.1. Preparation of UGS-SA and GS-SA dispersions

SA (1.5 g) was dispersed in 75 mL of purified water. Arrowroot starch (0.25, 0.5, or 1 g) was dispersed in purified water (20 mL). Next, the UGS dispersion was added and mixed into the SA dispersion. The final volume of the UGS-SA dispersions was adjusted to 100 mL using purified water. For GS, the UGS dispersions were incubated and stirred in water bath at 80 °C for 10 min to get clear and viscous dispersion, and the dispersion obtained was cooled down to room temperature. Next, the GS dispersion was mixed into the SA dispersions, then

the GS-SA dispersions were adjusted the final volume to 100 mL. The viscosity of all dispersions was determined, and 1.5 %w/v SA, 1%w/v UGS, and 1 %w/v GS dispersion were prepared and used as the control in this study.

2.2.2. Viscosity determination

Viscosities of the dispersions were measured using a Brookfield Digital Rheometer (Model DV-III, Brookfield Engineering Labs Inc., Stoughton, MA) at 30.0 ± 2.0 °C. A small sample adapter with a spindle no. 31 was used. Apparent viscosity of the dispersions at 13.6 s^{-1} shear rate was reported.

2.2.3. Preparation of UGS-SA and GS-SA films

A 1.5 %w/v SA dispersion containing UGS or GS in the concentrations of 0.25, 0.5 and 1%w/v was prepared using the procedure that mentioned in Section 2.1. Moreover, the 1%w/v UGS and GS dispersions were also prepared. Next, 20 mL of the dispersions was poured into a plastic mold ($5.9 \text{ cm} \times 9.4 \text{ cm}$), and then dried at 50 °C by using hot air oven for 24 h. After drying, the films were kept in desiccators with a relative humidity of 40 ± 2 % before characterization.

2.2.4. Molecular interaction studies

The thermal properties of the films were examined using differential scanning calorimetry (DSC). Sample (2.5-3.0 mg) was weighed and placed in an aluminum pan. The sample was heated over the range of 30-450 °C at a heating rate of 10 °C min^{-1} (DSC822, Mettler Toledo, Switzerland). The DSC thermograms were recorded. Moreover, Fourier transform infrared (FTIR) spectra of the films was also investigated. The sample was gently triturated with KBr powder at a weight ratio of 1:100, and then pressed with a hydrostatic press at 8 tons for 10 min. The discs obtained were placed in a sample holder and scanned from 4000 to 450 cm^{-1} at a resolution of 4 cm^{-1} (Spectrum One, Perkin Elmer, Norwalk, CT).

2.3. Preparation of DS-loaded beads

SA (1.5 g) was dispersed in 75 mL of purified water, and then DS (1 g) was gently added and dissolved in the SA dispersion. Next, arrowroot starch (0.25, 0.5, or 1 g) was dispersed in purified water (20 mL) and prepared as the UGS or GS dispersions using the method mentioned in Section 2.2.1. The UGS or GS dispersions were poured and blended into the DS-loaded SA dispersions. The final volume of the dispersions was adjusted to 100 mL. Then, the resulted dispersion (20 mL) was dropped into 1 %w/v CaCl_2 solution (200 mL) through a nozzle (0.5-mm inner diameter) with gentle stirring. The gel beads were cured in calcium chloride solution for 1 h, rinsed with 50 mL of purified water, blotted to remove excess water, and dried at 50 °C for 8-9 h.

2.4 Characterization of DS-loaded beads

2.4.1 Particle size and morphology

The particle size of the beads was measured by using an optical microscopy (Olympus CH30, Japan). Two hundred beads were randomly selected, and their Feret's diameters were determined. The particle and surface morphology of the beads was observed using scanning electron microscopy. The samples were mounted on dummies, coated with gold in a vacuum

evaporator (Model Emitech K500X, Ashford, Kent, England) at pressure 9×10^{-2} mbar for 4 min, and then viewed using a scanning electron microscope (Hitachi Se3000 N, Tokyo, Japan).

2.4.2 Determination of drug content and entrapment efficiency

The DS-loaded beads (50 mg) were immersed in pH 6.8 phosphate buffer at (75 mL) for complete disintegration of the beads. The mixture was sonicated for 15 min and incubated in a shaking water bath at 37 °C for 12 h. Then, the mixture was adjusted the final volume to 100 mL, and filtered using 0.45- μ m nylon membrane. The concentration of DS in the filtrates was analyzed using UV-visible spectrophotometer (Shimadzu UV1201, Japan) at 260 nm. The DS content was calculated as a percentage by weight of the beads. The DEE was calculated according to the ratio of actual to the theoretical drug content in the beads (Wang & He, 2002).

2.4.3 Water uptake studies

The DS-loaded beads were placed in a small basket, soaked in purified water or pH 6.8 phosphate buffer, and shaken occasionally in a water bath at 37 °C. At 15, 30, or 60 min of the test, each basket was withdrawn, blotted to remove excess water and immediately weighed on an analytical balance. The water uptake of the beads was determined according to the following equations:

$$\text{Water uptake (\%)} = \frac{(W_w - W_i)}{W_i} \times 100 \quad \text{Eq. 1}$$

where W_w is the weight of the wet beads, and W_i is the initial weight of the beads.

2.4.4 In vitro drug release

Due to water-insoluble property of DS in an acidic medium, release media used in this study were purified water and pH 6.8 phosphate buffer. The release of DS from the beads was investigated by using USP dissolution apparatus I (Hanson Research, Northridge, USA). The bead amount equivalent to DS 25 mg was weighed and added to 750 mL of the release medium at 37 °C. The baskets were rotated at the rate of 50 revolution min^{-1} . Samples (7 ml) were collected and replaced with fresh media at various time intervals. The concentration of DS released was analyzed by using UV-visible spectrophotometer at 260 nm. The release data of the DS-loaded beads in purified water or pH 6.8 phosphate buffer were fitted by using the Higuchi model (Eq. 2) or the zero-order model (Eq. 3), respectively, which could be expressed as the following equation (Costa & Lobo, 2001):

$$Q = K_H t^{0.5} \quad \text{Eq. 2}$$

$$Q = K_0 t + B \quad \text{Eq. 3}$$

where Q is the percentage of drug released at a given time (t), K_H is the Higuchi release rate, K_0 is the zero-order release rate, and B is a constant value that was used for computing the lag time of DS released from the beads when Q equals zero.

3. Results and discussion

3.1. Molecular interaction of SA with GS or UGS in dispersions and films

Viscosity of the SA dispersions adding various contents of UGS and GS was determined for preliminary study of molecular interaction between SA and GS or UGS. The SA, GS, and GS-SA dispersions were quite transparent liquid, while a white opaque liquid of the UGS and UGS-SA dispersion was obtained. The viscosity of 1.5 % SA dispersion was determined to be 292.7 ± 2.7 mPa s ($n=3$) at 13.6 s⁻¹ shear rate, whereas that of 1 % GS dispersion showed low viscosity of 3.01 ± 0.74 mPa s ($n=3$). Furthermore, the viscosity of 1% UGS dispersion could not be determined because of its very low viscosity. The effect of UGS and GS on the viscosity of the SA dispersion is shown in Fig. 2. Incorporation of GS into the SA dispersion gave an obviously higher viscosity than the SA dispersion alone, which was related to GS content added. The UGS added at the contents of 0.25 and 0.5 % did not affect viscosity of the SA dispersion, but addition of 1% UGS brought about a slightly increase of SA dispersion viscosity. These results suggested that blending of GS and UGS at higher content with the SA dispersions resulted in a viscosity synergism of the composite dispersions.

The UGS-SA and GS-SA films were prepared and investigated the molecular interaction between SA and GS or UGS in solid state. DSC and FTIR spectroscopy were used for this investigation. The GS and SA films were transparent, whereas the UGS films could be not formed a continuous sheet, and cracking of this film to form a powder was obtained. The GS-SA and UGS-SA films were transparent and opaque in nature, respectively. FTIR spectra of the SA, UGS-SA and GS-SA films are presented in Fig. 3. FTIR spectra of SA films presented the O–H stretching peak at 3439 cm⁻¹, COO⁻ asymmetric stretching peak at 1615 cm⁻¹, the COO⁻ symmetric stretching peak at 1416 cm⁻¹ and the C–O–C stretching peak at 1030 cm⁻¹ (Pongjanyakul, 2009). The native arrowroot starch showed the absorption peaks at 3432 cm⁻¹ (O–H stretching), 1647 cm⁻¹ (O–H bending) due to water residues in amorphous region of starch region, 1371 - 1459 cm⁻¹ (C–H bending), and 1017 - 1160 cm⁻¹ (C–O and C–O–C stretching of glucose structure) (Kizil, Irudayaraj, & Seetharaman, 2002). The UGS films showed the similar FTIR pattern with the native starch, except sharper peak of the O–H stretching of the UGS films was observed. This is likely to be due to water residues in the starch granules. Gelatinization caused a change of FTIR spectra that the O–H bending peak shifted to lower wavenumber, the C–H bending peak at 1372 - 1451 cm⁻¹ disappearance, and the C–O and C–O–C stretching peaks changed with a decreasing of peak intensity. These results suggested that disentanglement of the starch molecules and decrease of crystallinity of the starch occurred after gelatinization by heat treatment. The 1%UGS-SA films showed the same FTIR pattern with the SA films, but an obvious shift of the COO⁻ stretching peak at 1615 cm⁻¹ to higher wavenumber and small shift to lower wavenumber of the O–H stretching peak occurred. These changes could be observed as well when adding 0.25 and 0.5%UGS into the SA films (data not shown). Moreover, it is interesting that the FTIR pattern of the 1% GS-SA films was similar to the 1% UGS-SA films, suggesting that UGS could interact with SA in

the same manner as GS, which hydrogen bonding between carboxyl groups of SA molecules and hydroxyl groups of the granules' surface of UGS and GS molecules could be occurred.

DSC thermograms of the native arrowroot starch, SA and composite films are presented in Fig. 4. The native starch showed an exothermic degradation peak at 351 °C. The UGS films had a new endothermic peak at 291 °C and followed with exothermic peak at 359 °C. Similarly, the endothermic peak of the GS films at 282 °C was also observed and the degradation peak appeared at 353 °C. The endothermic peak at 291 °C of the UGS film and 282 °C of the GS film may be a phase transition after heat induction before film degradation. The SA films showed exothermic degradation peaks at 258 and 366 °C (Pongjanyakul, 2009). The 0.25%UGS-SA and 0.5 %UGS-SA films presented the first degradation peak of SA at 259-260 °C and the second exothermic peak at around 368 °C. Addition of 1% UGS in the films brought about a great degradation peak at 285 °C and the second degradation peak at 411 °C. This phenomenon suggested the first degradation at 260 °C of SA may induce the degradation of UGS embedded in the films, leading to change of thermal behavior at higher temperature. On the other hand, incorporation of GS at various contents caused the similar DSC pattern with the SA films, but the higher temperature of the second degradation peak was observed when increasing GS contents. These finding showed that phase separation of UGS granules embedded in the SA film matrix could be occurred when using higher content of UGS, whereas GS could be completely blended in molecular level in the SA matrix that homogenous GS-SA films was obtained.

Form all results, the present model of molecular interaction between SA and UGS or GS is illustrated in Fig. 5. The carboxyl groups of SA molecules could interact with the hydroxyl groups on the surface of the starch granules. GS had a disentanglement of starch molecules, amylose and amylopectin, which possessed many hydroxyl groups for interaction with the carboxyl groups of SA. Additionally, the branched chain of amylopectin could possibly create numerous contact points, leading to a viscosity synergism and more complexity of matrix network in the composite dispersions. Therefore, the molecular interaction between SA and UGS or GS in the dispersions before calcium ion cross-linking may influence the characteristics of the CA beads containing DS.

3.2. Particle size and DEE of the beads

Average particle sizes of the beads are listed in Table 1. The particle size of the CA beads was 1.17 mm. Addition of GS seemed to increase the size of the CA beads because higher viscosity of the dispersion dropped may bring about smaller shrinkage during cross-linking. The particle and surface morphology of the beads were observed by SEM pictures as shown in Fig. 6 (left and medium panels). All beads displayed a spherical shape with collapsed center. The CA beads had a rough surface and some of DS crystals deposited on the bead's surface. The surface of the UGS-CA beads showed a numerous of starch granules that had a different morphology when compared with the GS-CA beads.

The DS content of the beads was over the range of 19.16-24.36 %w/w (Table 1). The DEE value of the CA beads was 54.25 %. Incorporation of UGS and GS caused obviously

higher DEE than the CA beads. However, the GS-CA beads provided significantly greater DEE than the UGS-CA beads. These results suggested that addition of UGS and GS brought about a denser matrix barrier retarding water leakage from the wet beads during the preparation process (Dashevsky 1998), leading to decrease of drug loss from the beads. However, GS molecules, linear amylose and branched amylopectin, which interacted with SA before cross-linking could create stronger matrix network than the granules of UGS, resulting in higher efficiency for preventing drug molecule leakage from the wet beads. Thus, higher DEE of the GS-CA beads was found in this study.

3.3. Water uptake of the beads

The water uptake of the beads in purified water and pH 6.8 phosphate buffer is shown in Fig. 7a and 7b, respectively. In purified water, the water uptake of the CA beads seemed to decrease when adding 0.25 and 0.5 %UGS, whereas 1 % UGS could increase the water uptake at 1 h of the test. In contrast, the water uptake of the CA beads obviously increased with increasing GS content, and the longer the testing time, the greater the water uptake was found. Effect of the medium used strongly influenced the water uptake properties of the CA beads. The water uptake of the beads in pH 6.8 phosphate buffer was significantly higher than that in purified water. The test in pH 6.8 phosphate buffer could be done at 15 and 30 min, whereas the wet beads could not be handled at 60 min due to very high swelling and disintegration of the beads. The water uptake of the CA beads decreased with increasing UGS contents at 15 min, but the reduction of water absorption properties of the beads at 30 min did not related to UGS contents. On the other hand, GS caused an increase of the water uptake of the beads at 15 min, but the decrease of the water uptake was found in 30 min of the test.

Alginate in the form of calcium salt had water-insoluble property that the CA beads existed as a stable polymer matrix in purifier water, thus a limitation of water absorption of the CA beads was observed. UGS that had a less water absorption properties could retard the water uptake of the CA beads. On the other hand, the addition of GS could promote water absorption of the CA beads in purified water because of higher water absorption properties of GS, which was a hydrophilic polymer. This result was in agreement with that of the previous reports using sodium starch glycolate (Puttipipatkachorn et al., 2005) and xanthan gum Pongjanyakul & Puttipipatkachorn, 2007). Moreover, higher water uptake may also occur when GS could dissolve and erode from the beads in purified water. In contrast with pH 6.8 phosphate buffer, calcium ions cross-linked with alginate were rapidly exchanged with sodium ion-rich medium (Østberg et al. 1994). The partial formation of SA strongly promoted water uptake into the beads. UGS as insoluble particles embedded in the bead's matrix and interacted with SA could retard water uptake of the CA beads. However, the molecules of GS interacted with SA could strengthen and stabilize the wet beads, resulting in decrease of water uptake at 30 min when using 1% GS.

3.4. Drug release of the beads

The DS release of the UGS- and GS-CA beads in purified water is shown in Fig. 8a and 8b, respectively. The relationship between the % drug release and square root of time

provided good linearity with determination coefficient (R^2) greater than 0.99, suggesting that the drug release mechanism was matrix diffusion-controlled. The drug release rate (K_H) of the 0.25%UGS-CA beads was lower than that of the CA beads, whereas increase of UGS content caused slightly higher K_H value when compared with the CA beads (Table 1). The K_H result presented a contradiction on the drug release profile (Fig. 8a) that the UGS-CA beads gave lower % drug release than the CA beads. This could be due to the difference of the %initial drug release of the beads. It could be observed that the initial drug release of the CA beads at 15 min was 9.58 % that was obviously higher than the UGS-CA beads, which the %drug release at 15 min of the 0.25%UGS-, 0.5%UGS-, and 1%UGS-CA beads was found to be 3.35, 5.86, and 3.96 %, respectively. Moreover, the total drug release at 420 min of the UGS-CA beads tended to lower when compared with the CA beads. In contrast, the GS-CA beads gave obviously higher K_H than the UGS-CA and CA beads (Table 1). SEM photographs showed the erosion of the surface of the CA beads after release testing in purified water (Fig. 6, right panel). The erosion of the beads could be occurred because a residual alginate could release from the beads (Murata, Nakada, Miyamoto, Kawashima, & Seo, 1993), which occurred from a small amount of calcium ion released in purified water (Østberg et al., 1994). The surface morphology of the UGS-CA beads after drug release was similar to that before drug release. Therefore, the lower initial drug release and total drug release could be described by the restriction of water uptake of the beads when adding UGS (Fig. 7a). On the other hand, many pores on the surface of the GS-CA beads were observed after drug release testing. This was due to the dissolution of GS from the beads' surface, suggesting that GS was act as a pore-forming agent in this case that the formation of pore channels could accelerate drug release from the beads.

The drug release profile of the UGS- and GS-CA beads in pH 6.8 phosphate buffer showed a sigmoidal curve with a complete release (Fig. 9a and 9b, respectively). The release data showed good fitting with the zero-order model that R^2 value higher than 0.99. This result suggested that the release of drug could be controlled by swelling mechanism. The lag time and drug release rate (K_0) computed using Eq. 3 is listed in Table 1. The UGS-CA beads presented obviously longer lag time than the CA beads, whereas shorter lag time of the GS-CA beads was observed when using 0.5 and 1 %GS. Additionally, the UGS- and GS-CA beads seemed to increase K_0 values when compared with the CA beads. The drug release of the CA beads in pH 6.8 phosphate buffer was depressed by the formation of the gel layer at the initial stage but gradually enhanced by the increasing water content and the erosion of the swollen gel phase at the later stage (Sugawara et al., 1994). This phenomenon was due to the ion exchange process between calcium ion in the beads and sodium ion in the medium. In the initial stage, incorporation of UGS that retarded water uptake of the CA beads (Fig. 7b) led to longer lag time of drug release. On the other hand, GS brought about shorter lag time of drug release, which was attributed to greater water absorption capacity of GS. However, UGS and

GS added into the beads did not clearly influence the drug release rate because of the very high swelling and disintegration of the CA beads in this medium.

4. Conclusions

This study shows that SA could interact with the arrowroot (*Tacca leontopetaloides* L. Kuntze) starch in the form of granules and gels via hydrogen bonding, leading to viscosity synergism in the composite dispersions before cross-linking using calcium ions. The UGS-CA and GS-CA beads loaded with DS present the different surface morphology, and the GS-CA beads provide significantly higher DEE than the UGS-CA beads. Incorporation of UGS tended to retard the water absorption of the CA beads, resulting in lower initial drug release and total drug release of the beads in purified water, and longer lag time of the beads in pH 6.8 phosphate buffer. On the other hand, GS can enhance water uptake process and accelerate drug release of the beads in both media. This finding indicates that this arrowroot starch in the forms of UGS and GS displays strong potential to modify the CA beads for drug delivery.

References

- Al-Kassas, R.S., Al-Gohary, O.M.N., & Al-Faadhel, M.M. (2007). Controlling of systemic absorption of gliclazide through incorporation into alginate beads. *International Journal of Pharmaceutics*, 341, 230–237.
- Almeida, P.F., & Almeida, A.J. (2004). Cross-linked alginate-gelatin beads: a new matrix for controlled release of pindolol. *Journal of Controlled Release*, 97, 431–439.
- Auttapornpitak, T. (2003). Physicochemical properties of arrowroot *Tacca leontopetaloides* Ktze. Starch. Master's thesis, Chulalongkorn University, Bangkok, Thailand.
- Chan, E. S., Wang, S.L., Lee, P.P., Lee, J.S., Ti, T.B., Zhang, Z., Poncelet, D., Ravindra, P., Phan, S.H., & Yim, Z.H. (2011). Effects of starch filler on the physical properties of lyophilized calcium-alginate beads and the viability of encapsulated cells. *Carbohydrate Polymers*, 83, 225–232.
- Costa, P., & Lobo, J.M.S. (2001). Modeling and comparison of dissolution profiles. *European Journal of Pharmaceutical Sciences*, 13, 123–133.
- Dashevsky, A. (1998). Protein loss by the microencapsulation of an enzyme (lactase) in alginate beads. *International Journal of Pharmaceutics*, 161, 1–5.
- Draget, K.I. (2000). Alginates. In G.O. Philips, & P.A. Williams (Eds.), *Handbook of Hydrocolloids* (pp. 379–395). Cambridge: Woodhead Publishing.
- Fernández-Hervás, M.J., Holgado, M.A., Fini, A., & Fell, J.T. (1998). In vitro evaluation of alginate beads of a diclofenac salt. *International Journal of Pharmaceutics*, 163, 23–34.
- Hariyadi, D.M., Ma, Y., Wang, Y., Bostrom, T., Malouf, J., Turner, M.S., Bhandari, B., & Coombes, A.G.A. (2014). The potential for production of freeze-dried oral vaccines using alginate hydrogel microspheres as protein carriers. *Journal of Drug Delivery Science and Technology*, 24, 178–184.

- Hwang, S.J., Rhee, G.J., Lee, K.M., Oh, K.H., & Kim, C.K. (1995). Release characteristics of ibuprofen from excipient-loaded alginate gel beads. *International Journal of Pharmaceutics*, 116, 125–128.
- Jadhav, S.B., & Singhal, R.S. (2014). Pullulan-complexed α -amylase and glucosidase in alginate beads: Enhanced entrapment and stability. *Carbohydrate Polymers*, 105, 49–56.
- Kikuchi, A., Kawabuchi, M., Sugihara, M., Sakurai, Y., & Okano, T. (1997). Pulsed dextran release from calcium–alginate gel beads. *Journal of Controlled Release*, 47, 21–29.
- Kizil, R., Irudayaraj, J., & Seetharaman, K. (2002). Characterization of irradiated starches by using FT-Raman and FTIR spectroscopy. *Journal of Agricultural and Food Chemistry*, 50, 3912–3918.
- Lozano-Vazquez, G., Lobato-Calleros, C., Escalona-Buendia, H., Chavez, G., Alvarez-Ramirez, J., & Vernon-Carter, E.J. (2015). Effect of the weight ratio of alginate-modified tapioca starch on the physicochemical properties and release kinetics of chlorogenic acid containing beads. *Food Hydrocolloids*, 48, 301–311.
- Malafaya, P.B., Silva, G.A., & Reis, R.L. (2007). Natural-origin polymers as carriers and scaffolds for biomolecules and cell delivery in tissue engineering applications. *Advanced Drug Delivery Reviews*, 59, 207–233.
- Masina, N., Choonara, Y.E., Kumar, P., du Toit, L.C., Govender, M., Indermun, S., & Pillay, V. (2017). A review of the chemical modification techniques of starch. *Carbohydrate Polymers*, 157, 1226–1236.
- Murphy, P. (2000). Starch. In G.O. Philips, & P.A. Williams (Eds.), *Handbook of Hydrocolloids* (pp. 41–65). Cambridge: Woodhead Publishing.
- Murata, Y., Miyamoto, E., & Kawashima, S. (1996). Additive effect of chondroitin sulfate and chitosan on drug release from calcium-induced alginate gel beads. *Journal of Controlled Release*, 38, 108–110.
- Murata, Y., Nakada, K., Miyamoto, E., Kawashima, S., & Seo, S.H. (1993). Influence of erosion of calcium-induced alginate gel matrix on the release of brilliant blue. *Journal of Controlled Release*, 23, 21–26.
- Murata, Y., Tsumoto, K., Kofuji, K., & Kawashima, S. (2002). Effect of natural polysaccharide addition on drug release from calcium induced alginate gel beads. *Chemical and Pharmaceutical Bulletin*, 51, 218–220.
- Nayak, A.K., Das, B., & Maji, R. (2012). Calcium alginate/gum Arabic beads containing glibenclamide: Development and in vitro characterization. *International Journal of Biological Macromolecules*, 51, 1070–1078.
- Østberg, T., Lund, E.M., & Graffner, C. (1994). Calcium–alginate matrices for oral multiple unit administration: IV release characteristics in different media. *International Journal of Pharmaceutics*, 112, 241–248.
- Pillay, V., Dangor, C.M., Govender, T., Moopanar, K.R., & Hurbans, N. (1998). Ionotropic gelation: encapsulation of indomethacin in calcium alginate gel discs. *Journal of Microencapsulation*, 15, 215–226.

- Pongjanyakul, T. (2009). Alginate–magnesium aluminum silicate films: Importance of alginate block structures. *International Journal of Pharmaceutics*, 365, 100–108.
- Pongjanyakul, T., & Puttipipatkachorn, S. (2007). Xanthan-alginate composite gel beads: molecular interaction and in vitro characterization. *International Journal of Pharmaceutics*, 331, 61–71.
- Pongjanyakul, T., & Rongthong, T. (2010). Enhanced entrapment efficiency and modulated drug release of alginate beads loaded with drug-clay intercalated complexes as microreservoirs. *Carbohydrate Polymers*, 81, 409–419.
- Puttipipatkachorn, S., Pongjanyakul, T., & Priprem, A. (2005). Molecular interaction in alginate beads reinforced with sodium starch glycolate or magnesium aluminum silicate, and their physical characteristics. *International Journal of Pharmaceutics*, 293, 51–62.
- Segale, L., Mannina, P., Giovannelli, L., & Pattarino, F. (2015). Calcium alginate multi-unit oral dosage form for delayed release of celecoxib. *Journal of Drug Delivery Science and Technology*, 26, 35–43.
- Shelke, N.B., James, R., Laurencin, C.T., & Kumbar, S.G. (2014). Polysaccharide biomaterials for drug delivery and regenerative engineering. *Polymers for Advanced Technologies*, 25, 448–460.
- Singh, B., Sharma, D.K., & Gupta, A. (2009). A study towards release dynamics of thiram fungicide from starch-alginate beads to control environmental and health hazards. *Journal of Hazardous Materials*, 161, 208–216.
- Sugawara, S., Imai, T., & Otagiri, M. (1994). The controlled release of prednisolone using alginate gel. *Pharmaceutical Research*, 11, 272–277.
- Tønnesen, H.H., & Karlsen, J. (2002). Alginate in drug delivery systems. *Drug Development and Industrial Pharmacy*, 28, 621–630.
- Tsai, F.H., Kitamura, Y., & Kokawa, M. (2017). Effect of gum arabic-modified alginate on physicochemical properties, release kinetics, and storage stability of liquid-core hydrogel beads. *Carbohydrate Polymers*, 174, 1069–1077.
- Wang, K., He, Z. (2002). Alginate-konjac glucomannan-chitosan beads as controlled release matrix. *International Journal of Pharmaceutics*, 244, 117–126.

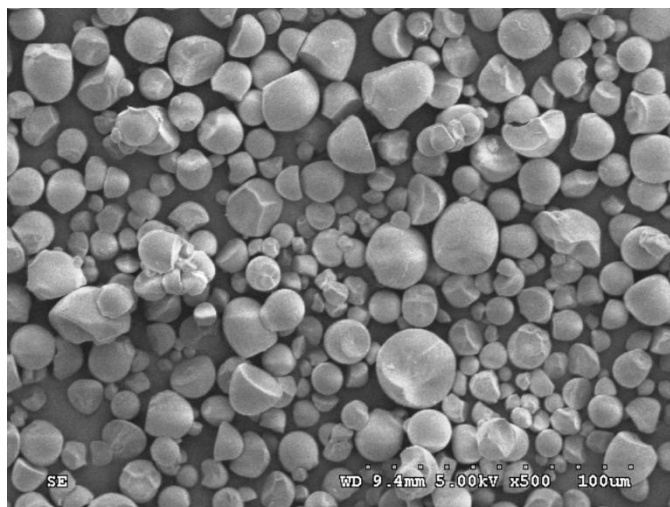


Figure 1. Particle morphology of arrowroot (*Tacca leontopetaloides* L. Kuntze) starch granules.

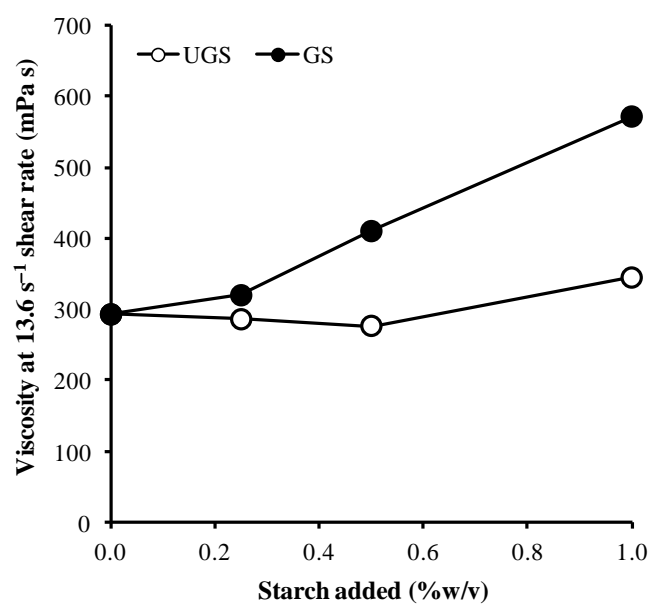


Figure 2. Viscosity of 1.5 %w/v SA dispersion incorporating various concentrations of UGS and GS. Each point is the mean \pm S.D., n=3.

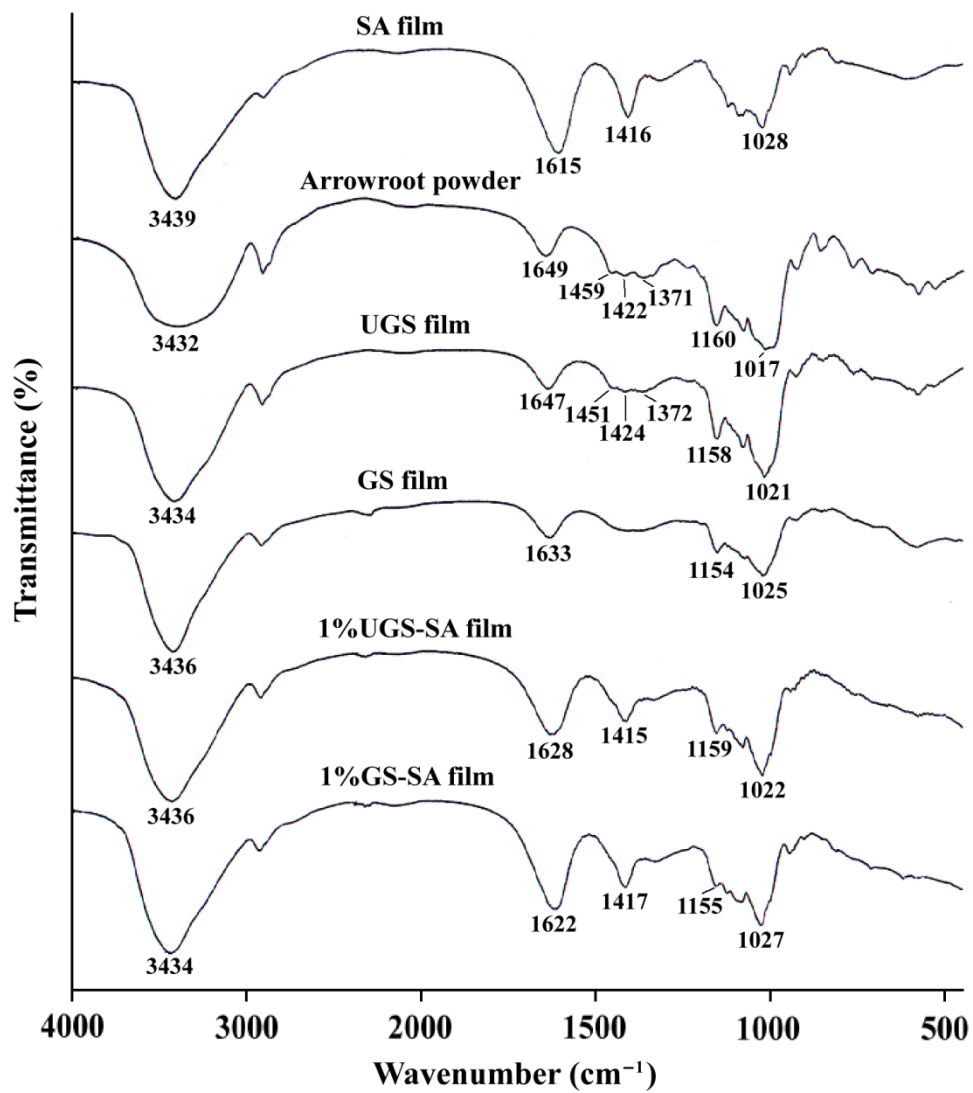


Figure 3. FTIR spectra of SA film, native arrowroot starch, UGS film, GS film, 1%UGS-SA film, and 1%GS-SA film.

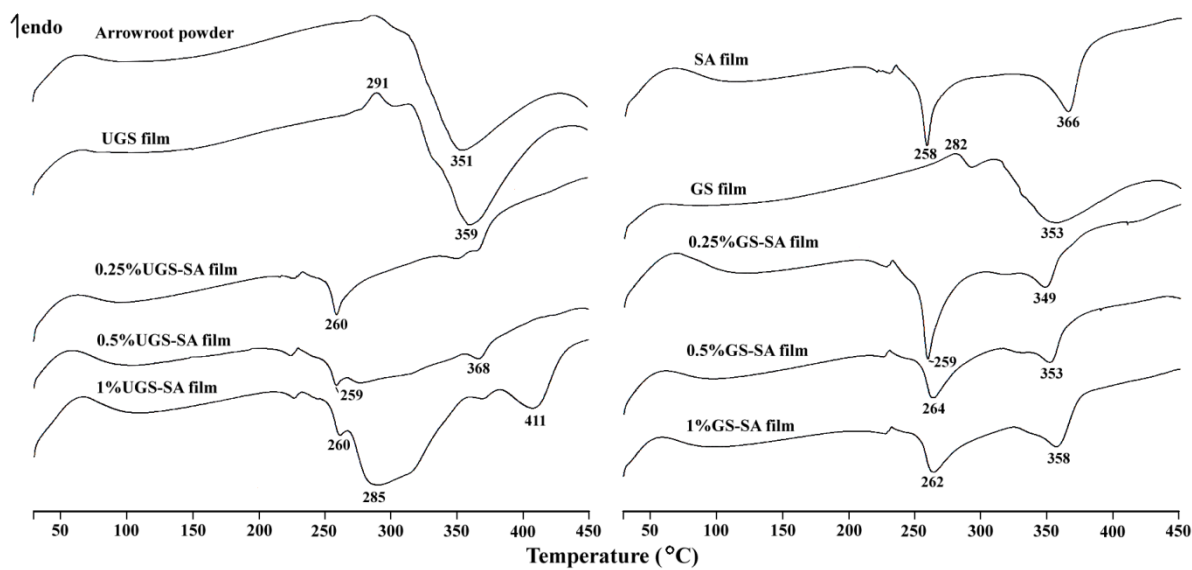


Figure 4. DSC thermogram of SA film, native arrowroot starch, UGS film, GS film, UGS-SA film, and GS-SA film.

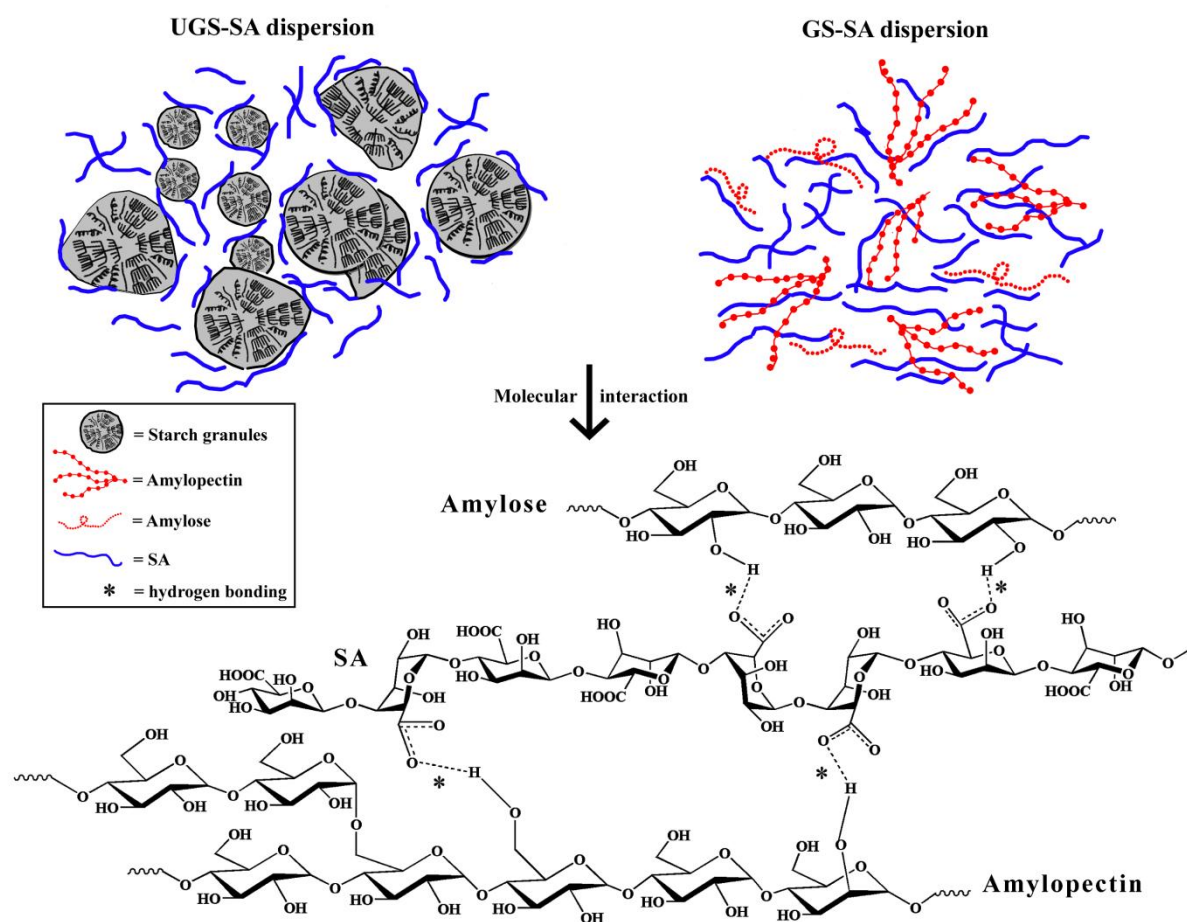
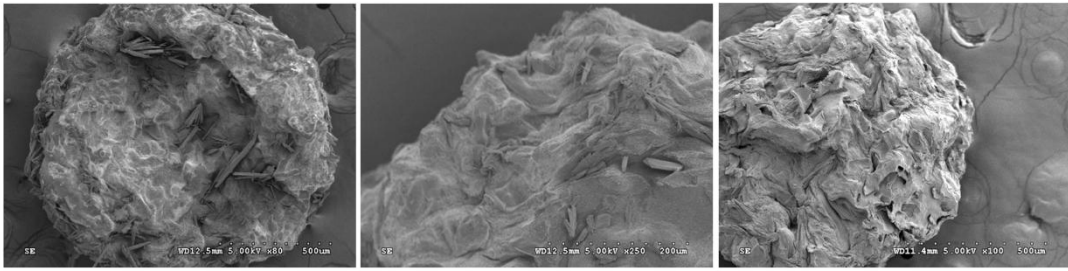
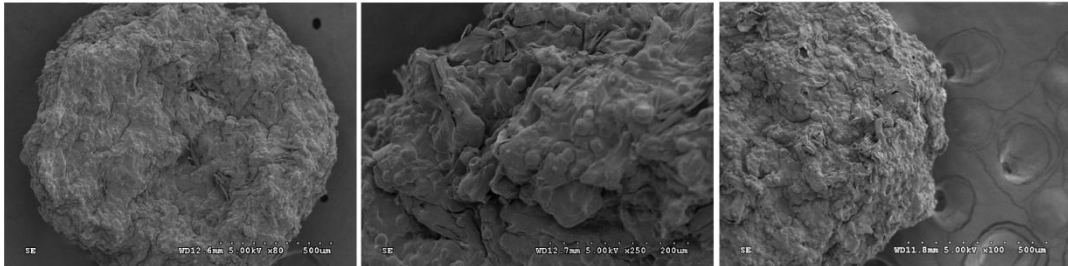
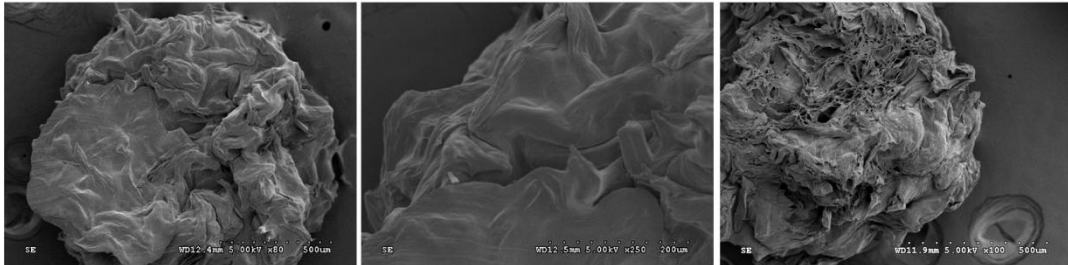


Figure 5. Schematic presentation of the molecular interactions between SA and UGS or GS.

CA bead**UGS-CA bead****GS-CA bead**

500 μm

200 μm

500 μm

Before drug release**After drug release in purified water**

Figure 6. Particle and surface morphology of CA, 1%UGS-CA, and 1%GS-CA beads containing DS before and after drug release testing in purified water.

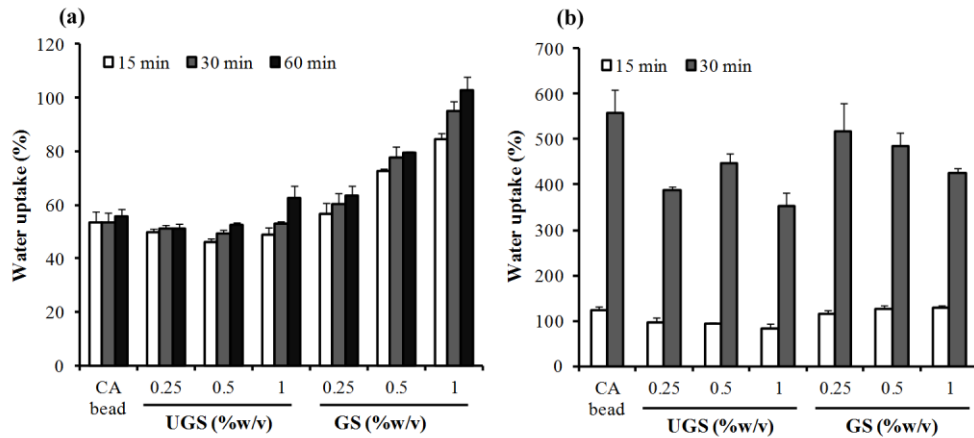


Figure 7. Water uptake of DS-loaded CA beads adding different amount of UGS and GS in purified water (a) and pH 6.8 phosphate buffer (b). Each value is the mean \pm S.D., n=3.

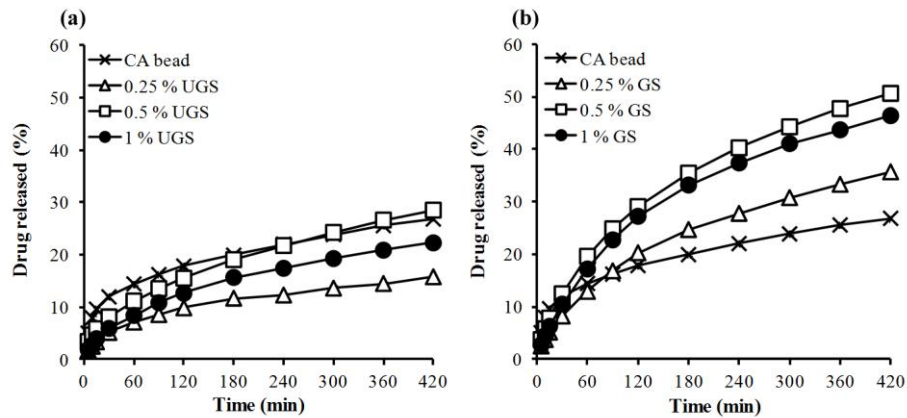


Figure 8. Drug release profiles of CA beads adding different contents of UGS (a) and GS (b) in purified water. Each value is the mean \pm S.D., n=3.

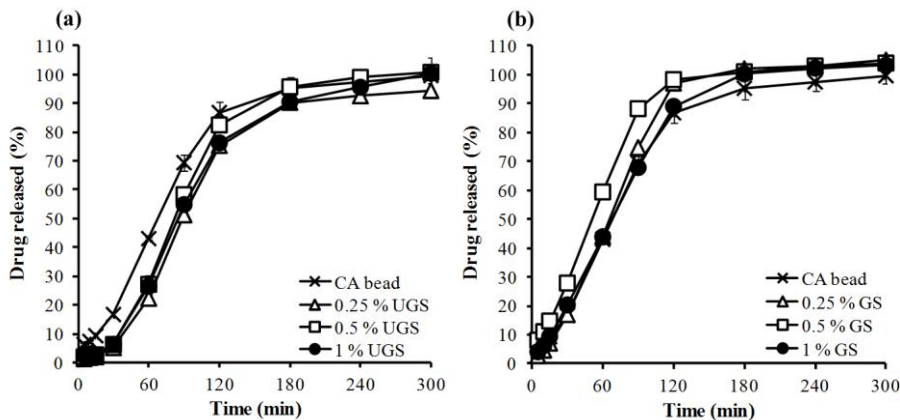


Figure 9. Drug release profiles of CA beads adding different contents of UGS (a) and GS (b) in pH 6.8 phosphate buffer. Each value is the mean \pm S.D., n=3.

Table 1. Characteristics of CA, UGS-CA, and GS-CA beads containing DS.

Components	Particle size ^a (mm)	Drug content ^b (% w/w)	EE ^b (%)	Purified water	pH 6.8 phosphate buffer	
				K _H ^b (% min ^{-0.5})	Lag time ^b (min)	K ₀ ^b (% min ⁻¹)
1.5 % SA	1.17 ± 0.18	21.70 ± 0.54	54.25 ± 0.67	1.05 ± 0.03	4.65 ± 1.09	0.77 ± 0.04
1.5 % SA						
+ 0.25 % UGS	1.02 ± 0.17	22.83 ± 0.57	62.80 ± 0.79	0.75 ± 0.03	26.79 ± 0.40	0.80 ± 0.02
+ 0.5 % UGS	1.07 ± 0.19	22.27 ± 0.04	66.81 ± 0.21	1.38 ± 0.02	24.73 ± 2.80	0.87 ± 0.03
+ 1 % UGS	1.17 ± 0.15	19.16 ± 0.52	67.05 ± 0.91	1.13 ± 0.06	23.33 ± 0.91	0.79 ± 0.03
+ 0.25 % GS	1.16 ± 0.18	24.31 ± 0.51	66.84 ± 0.70	1.87 ± 0.03	7.46 ± 0.28	0.88 ± 0.01
+ 0.5 % GS	1.22 ± 0.18	24.36 ± 0.60	73.07 ± 0.90	2.64 ± 0.03	2.03 ± 0.45	0.99 ± 0.01
+ 1 % GS	1.24 ± 0.16	22.03 ± 0.22	77.11 ± 0.39	2.49 ± 0.05	3.52 ± 0.53	0.78 ± 0.02

^a n=500, ^b n=3.

Conclusions

This study demonstrates that SC can molecularly interact with clays, such as MAS and HS, in the films. Molecular interaction between the amide and amino groups of SC and the silanol groups of MAS via intermolecular hydrogen bonding results in the formation of intercalated or exfoliated nanocomposites. Moreover, hydrogen bonding formation between the amide groups of SC and hydroxyl groups on the surface of tubular HS can be occurred, but no evidences indicates that SC-HS nanocomposite formed. Clays added can enhance thermal stability of the SC films. The puncture strength and elongation of the SC films decrease with increasing clay ratio in the dry state. On the contrary, increasing clay ratio causes an increase of puncture strength of the wet SC-clay films in acidic medium. The SC-clay films do not obviously retard the water vapor permeation, but the drug permeability and diffusivity across the films in acidic medium remarkably decrease when increasing clay ratios. The SC-clay dispersions can be employed as a film coating material. The SC-MAS coated tablets present a few film defect and smooth surface morphology. The drug release from the coated tablets in acidic medium can be modified by varying clay ratios and film coating levels. The SC-clay films can be used in oral modified-release tablet coatings.

The SC-clay films containing fluconazole (FZ) can be prepared using a spray method. Incorporation of clay can enhance thermal and mechanical properties of the films. Besides, the FCZ-loaded SC-clay films presented slower release when compared with the film without clay due to denser structure of the films. The FZ in the films showed the different polymorphism when compared with FZ powder, suggesting the polymorphism change of FZ during recrystallization in film preparation. However, the FZ-loaded SC-clay films still possess antifungal activity and mucoadhesive property. So, the films display a potential use as a local delivery system in oral candidiasis.

The SC film covered with CS can be successfully formed by using a spraying method. SC and CS are able to form the molecular interaction via hydrogen bonding. The complex structure of SC-HCS bilayer film can enhance the strength of the films, and also provide good mucoadhesive properties. The release of FZ from the SC-CS bilayer films provides more sustained-release pattern than that of the SC films. Moreover, FZ released still have an anticandidal activity. These findings suggested that the SC-CS bilayer films have a good potential for use as novel delivery system for antifungal drug in treatment of topical candidiasis.

References

- Abu Diak O, Bani-Jaber A, Amro B, Jones D, Andrews GP. The manufacture and characterization of casein films as novel tablet coatings. *Food Bioprod Process* 2007; 85: 284-290.
- Aguzzi, C., Cerezo, P., Viseras, C., Caramella, C. Use of clays as drug delivery systems: Possibilities and limitations. *Appl Clay Sci* 2007; 36: 22-36.
- Alexandre M, Dubois P. Polymer-layered silicate nanocomposites: preparation, properties and uses of a new class of materials. *Mater Sci Eng* 2000; 28: 1-63.
- Audic JL, Chaufer B. Influence of plasticizers and crosslinking on the properties of biodegradable films made from sodium caseinate. *Eur Polym J* 2005; 41: 1934-1942.
- Bhardwaj T, Bhardwaj V, Sharma K, Gupta A, Cameotra SS, Sharma P. Thermo-acoustical analysis of sodium dodecyl sulfate: Fluconazole (antifungal drug) based micellar system in hydro-ethanol solutions for potential drug topical application. *J Chem Thermodyn* 2014; 78: 1-6.
- Bigi A, Cojazzi C, Panzavolta S, Rubini K, Roveri N. Mechanical and thermal properties of gelatin films at different degrees of glutaraldehyde crosslinking. *Biomaterials* 2001; 22: 763-768.
- Bylund G. *Dairy Processing Handbook*. Lund, Tetra Pak, 1995.
- Cai K, Hu Y, Jandt KD, Wang Y. Surface modification of titanium thin film with chitosan via electrostatic self-assembly technique and its influence on osteoblast growth behavior. *J Mater Sci Mater Med* 2008; 19:499-506.
- Cai K, Yao K, Cui Y, Lin S, Yang Z, Li X, Xie H, Qing T, Luo J. Surface modification of poly (D,L-lactic acid) with chitosan and its effects on the culture of osteoblasts in vitro. *J Biomed Mater Res* 2002; 60: 398-404.
- Clarke EGC. *Clarke's Analysis of Drugs and Poison*, Third edition. Pharmaceutical Press, London, 2004.
- De Kort E, Minor M, Snoeren T, VanHooijdonk T, VanDerLinden E. Effect of calcium chelators on physical changes in casein micelles in concentrated micellar casein solutions. *Int dairy J* 2011; 21: 907-913.
- De Kruif CG, Grinberg VY. Micellation of β -casein. *Colloid Surface A* 2002; 210: 183-190.
- De Kruif CG, Huppertz T, Urban VS, Petukhov AV. Casein micelles and their internal structure. *Adv colloid Interface Sci* 2012; 171-172: 36-52.
- De Kruif CG. Casein micelle interactions. *Int dairy J* 1999; 9: 183-188.
- Dollery C. *Therapeutic Drugs*, Second edition, Churchill Livingstone, Edinburgh, 1999
- Elzoghby AO, Abo El-Fotoh WS, Elgindy NA. Casein-based formulations as promising controlled release drug delivery systems. *J Control Release* 2011;153: 206-216.
- Elzoghby AO, Helmy MW, Samy WM and Elgindy NA. Novel ionically crosslinked casein nanoparticles for flutamide delivery: formulation, characterization, and in vivo pharmacokinetics. *Int J Nanomed* 2013; 8: 1721-32.

- Elzoghby AO, Helmy MW, Samy WM, Elgindy NA. Spray-dried casein-based micelles as a vehicle for solubilization and controlled delivery of flutamide: formulation, characterization, and in vivo pharmacokinetics. *Eur J Pharm Biopharm* 2013; 84: 487-96.
- Fabra MJ, Talens P, Chiralt A. Tensile properties and water vapor permeability of sodium caseinate films containing oleic acid-beeswax mixtures. *J Food Eng* 2008; 85: 393-400.
- Farrell HM, Malin EL, Brown EM, Qi PX. Casein micelle structure: What can be learned from milk synthesis and structure biology. *Curr Opin Colloid Interface Sci* 2006; 11: 135-47.
- Grabovac V, Gugli D, Bernkop-Schnürch A. Comparison of the mucoadhesive properties of various polymers. *Adv Drug Deliv Rev* 2005; 57: 1713 – 1723.
- He, Y., Kong, W., Wang, W., Liu T, Liu Y, Gong, Q., Gao, J. Modified natural halloysite/potato starch composite films. *Carbohydr Polym* 2012; 87: 2706-2711.
- Hedrick-Höchstötter, K., Lim, G.T., Altstädt, V. Novel polyamide nanocomposites based on silicate nanotubes of the mineral halloysite. *Compos Sci Technol* 69 (2009)330-334.
- Horne DS, Euston SR. Simulating the self-association of caseins. *Food hydrocolloid* 2005; 19: 379-86.
- Horne DS. Casein micelle structure and stability. In: Singh H, Boland M, Thompson A, Eds. *Milk Protein*. London: Elsevier 2014, pp. 169-200.
- Kanjanakawinkul W, Rades T, Puttipipatkachorn S, Pongjanyakul T. Nicotine–magnesium aluminum silicate microparticle surface modified with chitosan for mucosal delivery. *Mater Sci Eng C* 2013; 33: 1727–1736.
- Khlibsuwan R, Pongjanyakul T. Spray-dried chitosan-magnesium aluminum silicate microparticles as matrix formers in controlled release tablets. *J Drug Deliv Sci Technol* 2015; 30: 114-122.
- Khunawattanakul W, Puttipipatkachorn S, Rades T, Pongjanyakul T. Novel chitosan-magnesium aluminum silicate nanocomposite film coatings for modified-release tablets. *Int J Pharm* 2011; 407 (1-2): 132-141.
- Khunawattanakul W, Puttipipatkachorn S, Rades T, Pongjanyakul T. Chitosan–magnesium aluminum silicate nanocomposite films: physicochemical characterization and drug permeability. *Int J Pharm* 2010; 393: 219–229.
- Khunawattanakul W, Puttipipatkachorn S, Rades T, Pongjanyakul T. Chitosan-magnesium aluminum silicate composite dispersions: characterization of rheology, flocculate size and zeta potential. *Int J Pharm* 2008; 351: 227-235.
- Khwalidia K, Banon S, Perez C, Desobry S. Properties of sodium casinate film-forming dispersions and films. *J Dairy Sci* 2004; 87: 2011-16.
- Knepp WA, Jayakrishnan A, Quigg JM, Sitren HS, Bagnall JJ, Goldberg EP. Synthesis, properties, and intratumoral evaluation of mitoxantrone-loaded casein microspheres in Lewis lung carcinoma. *J Pharm Pharmacol* 1993; 45: 887-891.
- Levis SR, Deasy PB. Characterisation of halloysite for use as a microtubular drug delivery system. *Int J Pharm* 2002; 243: 125–134

- Li J, Zhang S, Zhou Y, Guan S, Zhang L. Inclusion complexes of fluconazole with β -cyclodextrin and 2-hydroxypropyl- β -cyclodextrin in aqueous solution: Preparation, characterization and a structural insight. *J Incl Phenom Macro* 2016; 84: 209-217.
- Liu, M., Zhang, Y., Wu, C., Xiong, S., Zhou, C. Chitosan/halloysite nanotubes bionanocomposites: Structure, mechanical properties and biocompatibility. *Int J Biol Macromol* 2012; 51:566-575.
- Lui DZ, Weeks MG, Dunstan DE, Martin GJ. Temperature-dependent dynamics of bovine casein micelles in the range 10-40 °C. *Food Chem* 2013; 141: 4081-4086.
- Lui Y, Guo R. pH-dependent structures and properties of casein micelles. *Biophys Chem* 2008; 136: 67-73.
- Magee GA, Willmott N, Halbert GW. Development of a reproducible in vitro method for assessing the biodegradation of protein microspheres. *J Control Release* 1993; 25: 241-248.
- Millar FC, Corrigan OI. Dissolution mechanism of ibuprofen-casein compacts. *Int J Pharm* 1993; 92: 97-104.
- Millar FC, Corrigan OI. Dissolution mechanism of ibuprofen-casein compacts. *Int J Pharm* 1993; 92: 97-104.
- Millar FC, Corrigan OI. Influence of sodium caseinate on the dissolution rate of hydrochlorothiazide and chlorothiazide. *Drug Dev Ind Pharm* 1991; 17(21): 1593-607.
- Millar FC, Corrigan OI. Influence of sodium caseinate on the dissolution rate of hydrochlorothiazide and chlorothiazide. *Drug Dev Ind Pharm* 1991; 17(21): 1593-607.
- Neha A, Tarun G, Ajay B. Review on casein production and casein based nano-formulations. *Int Res J Pharm* 2012; 3(1): 41-5.
- Pan K, Zhong Q, Baek SJ. Enhanced dispersibility and bioactivity of curcumin by encapsulation in casein nanoparticles. *J Agric Food Chem* 2013; 61: 6036-43.
- Papageorgiou GZ, Bikiaris D, Kanaze FI, Karavas E, Stergiou A, Georgarakis E. Tailoring the release rates of fluconazole using solid dispersions in polymer blends. *Drug Dev Ind Pharm* 2008; 34: 336-346.
- Park HJ, Kim MS, Kim JS, Cho W, Park J, Cha KH, Kang YS., Hwang SJ. Solid-state carbon NMR characterization and investigation of intrinsic dissolution behavior of fluconazole polymorphs, anhydrate forms I and II. *Chem Pharm Bull* 2010; 58: 1243-1247.
- Patel SK, Shah DR, Tiwari S. Bioadhesive films containing fluconazole for mucocutaneous candidiasis. *Indian J Pharm Sci* 2015; 77: 55-61.
- Pathak K, Sharma V, Akhtar N, Rastogi P. Localization of fluconazole in oral cavity by preferential coating of buccoadhesive tablets for treatment of oral thrush. *Int J Pharm Invest* 2016; 6: 106-115.
- Pelletier R, Peter J, Antin C, Gonzalez C, Wood L, Walsh TJ. Emergence of resistance of *Candida albicans* to clotrimazole in human immunodeficiency virus-infected children: in vitro and clinical correlations. *J Clin Microbiol* 2000; 38:1563-1568.

- Perada M, Aranguren MI, Marcovich NE. Effect of crosslinking on the properties of sodium caseinate films. *J Appl Polym Sci* 2010; 116: 18-26.
- Pereda M, Amica G, Racz I, Marcovich NE. Preparation and characterization of sodium caseinate films reinforced with cellulose derivatives. *Carbohydr Polym* 2011a; 86: 1014-1021.
- Pereda M, Amica G, Racz I, Marcovich NE. Structure and properties of nanocomposite films based on sodium caseinate and nanocellulose fibers. *J Food Eng* 2011b; 103: 76-83.
- Philippe M, Graet YL, Gaucheron F. The effects of different cations on the physicochemical characteristics of casein micelles. *Food Chem* 2005; 90: 673-683.
- Pongjanyakul T, Khunawattanakul W, Puttipipatkachorn S. Physicochemical characterizations and release studies of nicotine-magnesium aluminum silicate complexes. *Appl Clay Sci* 2009; 44: 242-250.
- Pongjanyakul T, Khunawattanakul W, Strachan CJ, Gordon KC, Puttipipatkachorn, S, Rades T. Characterization of chitosan-magnesium aluminum silicate nanocomposite films for buccal delivery of nicotine. *Int J Biol Macromol* 2013; 55: 24-31.
- Pongjanyakul T, Priprem A, Puttipipatkachorn S. Influence of magnesium aluminium silicate on rheological, release and permeation characteristics of diclofenac sodium aqueous gels in-vitro. *J Pharm Pharmacol*. 2005b; 57: 429-434.
- Pongjanyakul T, Priprem A, Puttipipatkachorn S. Investigation of novel alginate-magnesium aluminum silicate microcomposite films for modified-release tablets. *J Control Release* 2005a; 107: 343-356.
- Pongjanyakul T, Puttipipatkachorn S. Sodium alginate-magnesium aluminum silicate composite gels: Characterization of flow behavior, microviscosity and drug diffusivity. *AAPS PharmSciTech* 2007; 8: Article 72.
- Pongjanyakul T, Suksri H. Alginate-magnesium aluminum silicate films for buccal delivery of nicotine. *Colloid Surface B* 2009; 74: 103-113.
- Pradines B, Gallard JF, Iorga BI, Gueutin C, Ponchel G, Loiseau PM, Bouchemal K. The unexpected increase of clotrimazole apparent solubility using randomly methylated β -cyclodextrin. *J Mol Recognit* 2015; 28: 96-102.
- Qi PX. Studies of casein micelle structure: The past and the present. *Dairy Sci Technol* 2007; 87: 363-383.
- Qiao J, Adams J, Johannsmann D. Addition of halloysite nanotubes prevents cracking in drying latex films. *Langmuir* 2012; 28: 8674-8680.
- Rathod VS, Raut JS, Karuppaiyl SM. In vitro antifungal susceptibility reveals occurrence of azole resistance among clinical isolates of *Candida albicans*. *Asian J Pharm Clin Res* 2012; 5: 171-174.
- Rojtanatanya S, Pongjanyakul T. Propranolol-magnesium aluminum silicate complex dispersions and particles: Characterization and factors influencing drug release. *Int J Pharm* 2010; 383: 106-115.

- Rongthong T, Sungthongjeen S, Siepmann J, Pongjanyakul T. Quaternary polymethacrylate–magnesium aluminum silicate films: molecular interactions, mechanical properties and tackiness. *Int J Pharm* 2013; 458: 57–64.
- Rowe RC, Sheskey PJ, Owen SC. *Handbook of Pharmaceutical Excipients*. 5th ed. Pharmaceutical Press and American Pharmaceutical Association, Washington, 2006.
- Siepmann F, Siepmann J, Walther M, MacRae RJ, Bodmeier R. Polymer blends for controlled release coatings. *J Control Release* 2008; 125: 1–15.
- Suksri H, Pongjanyakul T. Interaction of nicotine with magnesium aluminum silicate at different pHs: characterization of flocculate size, zeta potential and nicotine adsorption behavior. *Colloid Surface B* 2008; 65: 54–60.
- Surassmo S, Saengkrit N, Ruktanonchai UR, Suktham K, Woramongkolchai N, Wutikhun T, Puttipipatkachorn S. Surface modification of PLGA nanoparticles by carbopol to enhance mucoadhesion and cell internalization. *Colloid Surface B* 2015; 130: 229–236.
- Suresh PK, Manhar S. Bioadhesive buccal gels impregnated with fluconazole: Formulation, in vitro and ex vivo characterization. *J Appl Pharma Sci* 2014; 4: 15–19.
- Tan D, Yuan P, Annabi-Bergaya F, Yu H, Liu D, Liu H, He H. Natural halloysite nanotubes as mesoporous carriers for the loading of ibuprofen. *Micropor Mesopor Mat* 2013; 179: 89–98.
- Walstra P, Wouters JT, Geurts TJ. *Dairy science and technology*. 2nd ed. Wageningen: Taylor & Francis Group; 2006.
- Ward CJ, Song S, Davis EW. Controlled release of tetracycline-HCl from halloysite-polymer composite films. *J Nanosci Nanotechnol* 2010; 10: 6641–6649.
- Wihodo M, Moraru CI. Physical and chemical methods used to enhance the structure and mechanical properties of protein films: A review. *J Food Eng* 2013; 114: 292–302.
- Yehia SA, El-Gazayerly ON, Basalious EB. Fluconazole mucoadhesive buccal films: In vitro/in vivo performance. *Curr Drug Deliv* 2009; 6: 17–27.
- Yurtdaş G, Demirel M, Genç L. Inclusion complexes of fluconazole with β -cyclodextrin: Physicochemical characterization and in vitro evaluation of its formulation. *J Incl Phenom Macro* 2011; 70: 429–435.
- Zhao M, Liu P. Adsorption behavior of methylene blue on halloysite nanotubes. *Micropor Mesopor Mat* 2008; 112: 419–424.

Outputs

International publications

1. Kajthunyakarn W, Sakloetsakun D, **Pongjanyakul T***. Sodium caseinate-magnesium aluminum silicate nanocomposite films for modified-release tablets. *Mater Sci Eng C* 2018; 92: 827-839. (Impact factor2017=5.08, Q1 Materials Science, Biomaterials)
2. Khlibsuwan R, Khunkitti W, **Pongjanyakul T***. Alginate-caseinate composites: Molecular interactions and characterization of cross-linked beads for the delivery of anticandidals. *Int J Biol Macromol* 2018; 115: 483-493. (Impact factor2017=3.909, Q1 Polymer Science)
3. Khlibsuwan R, Tansena W, **Pongjanyakul T***. Modification of alginate beads using gelatinized and ungelatinized arrowroot (*Tacca leontopetaloides* L. Kuntze) starch for drug delivery. *Int J Biol Macromol* 2018; 118: 683-692. (Impact factor2017=3.909, Q1 Polymer Science)

Presentations

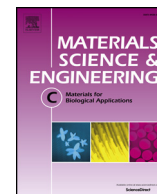
1. **Pongjanyakul T**, Kajthunyakarn W, Sakloetsakun D. Investigation of sodium caseinate-clay nanocomposite films for tablet coating. The 18th TRF-OHEC Annual Congress, Petchaburi 9-11 January 2019. (Oral presentation)
2. **Pongjanyakul T**, Kajthunyakarn W, Sakloetsakun D. Modification of sodium caseinate films using halloysite and montmorillonite for tablet coating. The 3rd European Conference on Pharmaceutics: Bringing science into pharmaceutical practice, Bologna, 25-26 March 2019.
3. Kajthunyakarn W, **Pongjanyakul T**. Investigation of fluconazole-loaded sodium caseinate-clay films for oral candidiasis. The 3rd European Conference on Pharmaceutics: Bringing science into pharmaceutical practice, Bologna, 25-26 March 2019.

Expected international publications

1. Sodium caseinate films modified using halloysite: Molecular interaction, mechanical properties and drug permeability studies. (In preparation)
2. Effect of clays on sodium caseinate films loaded with fluconazole for local delivery of oral candidiasis. (In preparation)
3. Preparation and evaluation of sodium caseinate-chitosan bilayer films for fluconazole delivery. (In preparation)

Connections with other experts within and outside Thailand

1. Assoc.Prof.Dr. Watcharee Khunkitti, Division of Pharmaceutical Technology, Khon Kaen University, Khon Kaen, Thailand
2. Asst.Prof.Dr. Duangkamon Sakloetsakun, Division of Pharmaceutical Technology, Khon Kaen University, Khon Kaen, Thailand
3. Assoc.Prof.Dr. Srisagul Sungthongjeen, Department of Pharmaceutical Technology, Naresuan University, Phitsanulok, Thailand.
4. Prof.Dr. Juergen Siepmann, College of Pharmacy, INSERM U1008, University of Lille, Lille, France.
5. Prof.Dr. Florence Siepmann, College of Pharmacy, INSERM U1008, University of Lille, Lille, France.



Sodium caseinate-magnesium aluminum silicate nanocomposite films for modified-release tablets

Wanassnant Kajthunyakarn, Duangkamon Sakloetsakun, Thaned Pongjanyakul*

Division of Pharmaceutical Technology, Faculty of Pharmaceutical Sciences, Khon Kaen University, Khon Kaen 40002, Thailand

ARTICLE INFO

Keywords:

Sodium caseinate
Magnesium aluminum silicate
Nanocomposites
Films
Tablet coating
Drug release

ABSTRACT

The aim of this study was to investigate the effect of clay, magnesium aluminum silicate (MAS), on the properties of sodium caseinate (SC) dispersions and films. Moreover, the SC-MAS dispersions were evaluated for film coating of modified-release tablets. The results showed that MAS addition led to particle flocculation and viscosity synergism in the SC-MAS dispersions. Exfoliated or intercalated nanocomposites of the SC-MAS films could be formed because of the molecular interaction of both components via hydrogen bonding. The puncture strength and elongation of the dry SC films decreased with increasing MAS ratios. However, MAS added enhanced the puncture strength of the wet films and reduced drug permeability and diffusivity across the films in acidic medium because of lower water uptake and denser matrix structure of the films. The SC-MAS dispersions showed strong potential for use as a film coating material with few defects in the coated acetaminophen (ACT) tablets. The ACT release of the coated tablets in acidic medium was modified by varying the MAS ratios and film coating levels. In addition, the SC-MAS coated tablets possessed sustained-release behavior for the drug under simulated gastrointestinal conditions. This finding indicates that the SC-MAS nanocomposite films can be applied as a tablet coating material to modify drug release.

1. Introduction

Thin film technology is highly important in pharmaceutical manufacturing, being employed in, for example, film coatings for masking an unpleasant taste and odor of drugs and for sustaining drug release in tablets [1]. The films loaded with drugs have been used as drug delivery systems [2]. Furthermore, the application of thin films is extended to the food industry, where the films are developed and used for food packaging and wrapping. Natural polymers have been widely employed for these purposes because of their biocompatibility and biodegradability. Polysaccharides, such as chitosan, have been used as tablet film coatings [3] and food packaging [4]. In addition, protein-based films, which were prepared from gelatins [5] and caseins [6], have been applied as a packaging material. Moreover, casein film coatings for fruits show a minimum loss of weight and juice level during storage under ambient conditions [7].

Caseins, biomacromolecules from milk, are composed of 94% protein and 6% colloidal calcium phosphate [8]. Caseins' molecular weights are in the range of 19 and 25 kDa. The average isoelectric point of caseins is approximately 4.6 to 4.8. Caseins in an acidic form (casein salt) have a low aqueous solubility, but sodium caseinate (SC), the sodium salt of casein, is freely soluble in water, except when the pH is

close to the isoelectric point [9]. Because SCs have distinct hydrophobic and hydrophilic domains, self-assembly into stable micellar structures in aqueous solutions can occur when their concentrations are higher than the critical micelle concentration, 1.0 mg mL^{-1} [10]. Because of this characteristic, SCs are used as emulsifying and foaming agents in the food industry. Furthermore, SCs have been applied in the pharmaceutical industry as a solubilizing agent for poorly soluble drugs [11,12]. SCs also have a potential use as drug delivery systems, particularly hydrogels [13], beads [14], microparticles [15,16] and nanoparticles [17,18].

One of the crucial properties of SC is to act as a film forming agent. SC can be used for tablet film coatings [9,19] and food packaging [6]. Unfortunately, the SC films have several disadvantages, including their mechanical properties and water vapor permeability [20]. Therefore, it is necessary to modify the film properties of SC by adding plasticizers such as glycerin and sorbitol [21,22], cross-linking agents, such as aldehydes [22,23], and water insoluble additives, such as fatty acids and wax [24], and celluloses [25]. Among these modifiers, the addition of water-insoluble substances is the interesting approach to modify physicochemical, mechanical, and permeability properties of the SC films. From the literature reviews, clays could potentially be used to modify the polymeric film properties and molecular interaction between

* Corresponding author.

E-mail address: thaned@kku.ac.th (T. Pongjanyakul).

<https://doi.org/10.1016/j.msec.2018.07.040>

Received 26 January 2018; Received in revised form 29 June 2018; Accepted 17 July 2018

Available online 19 July 2018

0928-4931/ © 2018 Elsevier B.V. All rights reserved.

polymers, and clay can create a new type of films called nanocomposite materials [26–28]. Thus, it is interesting that incorporation of clays may improve the SC film properties for use as a pharmaceutical film coating.

Montmorillonite clay (magnesium aluminum silicate (MAS)), is employed as a pharmaceutical excipient due to its non-toxicity and non-irritation at levels used in drug formulations [29]. MAS is composed of many silicate layers, where each silicate layer consists of a central octahedral sheet of aluminum or magnesium and two external silica tetrahedron layers [30]. The silicate layers of MAS can be separated when hydrated with water, and the silanol groups (-SiOH) on the surface of the silicate layers show a negative charge that brings about a strong electrostatic interaction with a positively charged substances, such as drugs [31], proteins [32], and polymers [33]. Moreover, the silanol groups can interact with anionic polymers such as xanthan gum [34], carbomer [35], and sodium alginate [36,37] via hydrogen bonding. Molecular interaction of polymeric molecules and MAS may create two types of nanocomposites [30]. The first type is an exfoliated nanocomposite in which the silicate layers of MAS can be completely dispersed in the polymer matrix. The latter type is an intercalated nanocomposite in which the space between two silicate layers of MAS can be occupied by polymeric molecules. The formation of nanocomposites has a significant influence on the key properties of the films, resulting in decreased water absorption, swelling and drug permeability compared to native polymeric films [26].

Therefore, the aims of this work were to prepare and investigate the SC films with MAS incorporated for use in tablet film coating. The composite dispersions with various SC-MAS ratios were prepared using simple mixing. The particle size and zeta potential of the dispersed phase, as well as the viscosity of the dispersions, was determined before film casting. Film properties, such as thermal behavior, crystallinity, mechanical properties, water uptake and erosion, and water vapor and drug permeability were characterized. Molecular interaction and nanocomposite formation between SC and MAS were also examined. Additionally, the SC-MAS dispersions were evaluated as a tablet film coating material that acetaminophen (ACT) was used as a model drug in this study. Film morphology, water uptake and ACT release of the coated tablets were investigated, as well.

2. Materials and methods

2.1. Materials

SC (sodium salt from bovine milk) and MAS in granular form (Veegum® HV) were purchased from Sigma-Aldrich Company (St. Louis, MO) and R.T. Vanderbilt Company, Inc. (Norwalk, CT), respectively. Glycerin and ACT were obtained from Namsiang Co., Ltd. (Bangkok, Thailand) and Pharma Thai Co., Ltd. (Bangkok, Thailand), respectively. Spray-dried lactose (Flowlac®100, Thai Meochems Co., Ltd., Bangkok, Thailand), microcrystalline cellulose (Ceolus® PH102, SiamChem-Pharm (1997) Co., Ltd., Bangkok, Thailand), magnesium stearate (Mallinckrodt, Inc., USA), and colloidal silicon dioxide (Aerosil® 200, Degussa, Japan) were used for preparing core tablets. All other reagents were of analytical grade and were used as received.

2.2. Preparation of SC-MAS dispersion

SC (5 g) was dispersed in 80 mL of distilled water. MAS (0, 0.25, 0.5, or 1 g) was dispersed in hot water (10 mL). Next, the MAS dispersion was mixed with the SC dispersion to obtain SC-MAS ratios of 1:0, 1:0.05, 1:0.1, or 1:0.2 by weight, respectively. The pH of the SC and SC-MAS dispersions was adjusted to 6.8 using 0.1 M HCl or 0.1 M NaOH because pH of the dispersion affected ionization of SC [38] and zeta potential of MAS [39]. All dispersions were adjusted to the final volume (100 mL) using distilled water prior to testing. Additionally, MAS dispersion (1% w/v) at pH 6.8 was also prepared and examined for

comparison.

2.3. Characterization of SC-MAS dispersion

2.3.1. Particle size determination

The particle size of the MAS and SC-MAS dispersions was measured by using a laser diffraction particle size analyzer (Mastersizer2000 Model Hydro2000SM, Malvern Instruments, Ltd., UK). The samples were dispersed in 70 mL of distilled water in a sample dispersion unit and stirred at a rate of 50 Hz for 30 s before measurement. The volume weighted mean diameters were determined and reported.

2.3.2. Zeta potential measurement

The zeta potential of the dispersions was measured using a laser Doppler electrophoresis analyzer (Zetasizer Model ZEN 2600, Malvern Instrument Ltd., UK). The temperature of the samples was controlled at 25 °C. The dispersions were diluted to obtain appropriate concentrations (count rates > 20,000 counts s^{-1}) prior to the measurements.

2.3.3. Viscosity determination

The viscosity of the dispersions was determined using a Brookfield digital rheometer (Model DV-III, Brookfield Engineering Laboratories, Inc., Middleboro, MA, USA). The small sample adaptor with spindle no. 31 was used. The temperature of the dispersions was controlled at 35.0 ± 1.0 °C. The single point viscosity of the dispersions at a shear rate of 20.40 s^{-1} was reported.

2.4. Preparation of SC-MAS films

SC and SC-MAS films were prepared by using a casting/solvent evaporation method. SC (5 g) was dispersed in 80 mL of distilled water, and glycerin (30% w/w based on SC content) used as a plasticizer was added into the SC dispersion. MAS (0, 0.25, 0.5, 1, or 2.5 g) was dispersed in hot water (10 mL), and the MAS dispersion was mixed with the SC dispersion to obtain the SC-MAS ratios of 1:0, 1:0.05, 1:0.1, 1:0.2, or 1:0.5 by weight, respectively. The pH of the SC and SC-MAS dispersions was adjusted to 6.8 using 0.1 M HCl or 0.1 M NaOH. All dispersions were adjusted to the final volume (100 mL) using distilled water and stirred for 30 min at room temperature (27 ± 2 °C). Then, 20 mL of the SC and SC-MAS dispersions was cast onto a plastic mold ($6.0 \text{ cm} \times 9.5 \text{ cm}$) and dried at 60 °C for 24 h. The dry films were peeled off and kept in desiccators prior to characterization.

2.5. Characterization of SC-MAS films

2.5.1. Thickness determination

Thickness of the dry and wet films was measured at different places using a microprocessor coating thickness gauge (Minitest600B, ElektroPhysik, Germany). The dry films were cut and placed on a control plate. The probe, which had been connected to the measurement gauge and calibrated using a standard film, gently moved downward to touch the film, and the film thickness was subsequently measured. To determine the film thickness in the wet state, the films were subsequently placed in a small beaker containing 0.1 M HCl or pH 6.8 phosphate buffer, which was shaken occasionally in a water bath at 37.0 ± 0.5 °C for 5 min. The samples were taken and blotted to remove excess water. The thickness of the wet films was immediately determined following the procedure mentioned above.

2.5.2. SEM and DSC studies

Surface and film matrix morphologies of the films were observed by scanning electron microscopy (SEM). The films and cross-sections of films were mounted onto stubs, coated with gold in a vacuum evaporator, and investigated using a scanning electron microscope (Hitachi S-3000N, Tokyo, Japan). The thermal behavior of the films was investigated using differential scanning calorimetry (DSC). The DSC

thermogram of the samples was recorded using a differential scanning calorimeter (DSC822^c, Mettler Toledo, Switzerland). An accurately weighed sample (2.5–3.5 mg) was placed into a 40- μ L aluminum pan without an aluminum cover. The measurements were taken over a temperature range of 30 to 450 °C at a heating rate of 10 °C min⁻¹.

2.5.3. Molecular interaction studies

Molecular interactions between SC and MAS in the SC-MAS films were investigated using Fourier transform infrared (FTIR) spectroscopy (Spectrum One, Perkin Elmer, Norwalk, CT) and the KBr disc method. All films were crashed and triturated with KBr powder and later pressed with 10 tons of a hydrostatic press for 10 min. The samples were placed in a sample holder and scanned from 4000 to 450 cm⁻¹ at the resolution rate of 4 cm⁻¹. Structure arrangement of MAS in the SC-MAS films were studied by powder X-ray diffractometry (PXRD) using Cu K α radiation generated at 40 kV and 40 mA as the X-ray source, an angle of 2–30° 2 θ and a step angle of 0.02° 2 θ s⁻¹ (Bruker D8 Advance diffractometer, Bruker BioSpin AG, Germany). The interlayer distance of the MAS silicate layers was calculated using Bragg's equation:

$$n\lambda = 2d\sin\theta \quad (1)$$

where n is 1 (the first order reflection was used), λ is the X-ray wavelength (1.54 Å), θ is the angle of the basal spacing peak of MAS, and d is the interlayer distance of the MAS silicate layer.

2.5.4. Determination of mechanical properties

Mechanical properties of the films, including puncture strength and elongation, were investigated by using a texture analyzer (TA-XT2, Stable Micro System, Ltd., UK) equipped with a 500 N load cell. Under dry conditions, the films (2 × 2 cm) were cut and kept in a chamber with 55% RH at room temperature (27.0 ± 2.0 °C) for 3 days before testing. Under wet conditions, the films were cut and shaken in 0.1 M HCl or pH 6.8 phosphate buffer for 5 min. Next, the excess water of the wet films was removed by a filter paper. Dry and wet films were fixed using a film holder between two mounting plates. A 5-mm-diameter spherical stainless steel puncturing probe was fixed at the load cell and moved downwards at 0.1 mm s⁻¹. The applied force and displacement were recorded. The puncture strength and % elongation at the break were calculated as follows [27]:

$$\text{Puncture strength} = \frac{F}{A} \quad (2)$$

where F is the maximum force for puncture, and A is the cross-sectional area of the edge of the film located in the path of cylindrical opening of the film holder.

$$\text{Elongation (\%)} = \frac{\sqrt{r^2 + D^2} - r}{r} \times 100 \quad (3)$$

where r is the radius of the film exposed in the cylindrical hole of the film holder, and D is the displacement of the probe from the point of contact to the point of film puncture.

2.5.5. Water vapor permeability studies

Discs were punched from the films, placed on open 5-mL glass vials containing 3.5 g silica gel beads and held in place with a screw lid with a test area of 0.58 cm². The vials were placed in a desiccator containing a saturated aqueous sodium chloride solution (75% RH). The desiccator was kept at room temperature (26.0 ± 2.0 °C) with 50 ± 2% RH. The weight change of the vials was recorded periodically over 72 h. The WVP rate was obtained from the slope of the relationship between the amount of water vapor permeated and time. The WVP coefficient of the films was calculated using the following equation [36]:

$$\text{WVP coefficient} = \frac{Mh}{A\Delta P_0} \quad (4)$$

where M is the WVP rate, h is the mean thickness of the film, A is the

area of the exposed film, and ΔP_0 is the vapor pressure difference.

2.5.6. Water uptake and erosion studies

Water uptake and erosion of the films were investigated using a gravimetric method. Films (1.5 cm × 1.5 cm in size) were weighed (W_0) and later soaked in 0.1 M HCl that had been incubated at 37.0 ± 0.5 °C and shaken occasionally. After a predetermined interval, each film was withdrawn, blotted to remove excess water, immediately weighed (W_t), and then dried in a hot air oven at 50 °C to constant weight (W_d). The water uptake and erosion can be calculated from the following equation [37,40]:

$$\text{Water uptake (\%)} = \frac{W_t - W_d}{W_d} \times 100 \quad (5)$$

$$\text{Erosion (\%)} = \frac{W_0 - W_d}{W_0} \times 100 \quad (6)$$

2.5.7. Drug permeability studies

ACT permeability across the films was investigated by using a side-by-side diffusion cell. The donor and acceptor compartments had a volume of 3 mL each; the film surface area for drug diffusion was 0.66 cm². The permeation fluid was 0.1 M HCl, and the temperature was controlled at 37 °C. The films were cut into circular pieces and gripped between donor and receptor compartments. ACT at the concentration of 4 mg mL⁻¹ (3 mL) was filled into the donor compartment, and 3 mL of medium was placed in the receptor compartment. Both compartments were continuously stirred throughout the tests. At predetermined intervals, 2.7 mL of medium in the receptor compartment was collected and replaced with an equal volume of fresh medium. The amount of ACT in the collected samples was measured by a UV-visible spectrophotometer (Shimadzu UV1201, Japan) at a wavelength of 265 nm.

Drug permeation through the films was determined under steady state conditions by means of Fick's first law [41], which can be expressed as

$$\frac{dQ}{Adt} = P_{app}C_0 \quad (7)$$

where dQ/Adt is the permeation flux (the slope calculated using the linear regression analysis of the relationship between the amount of drug permeated per surface area of the films (A) and time). C_0 is the concentration of the drug in the donor compartment, and P_{app} is the apparent permeability coefficient. The apparent diffusion coefficient (D_{app}) was estimated from the following equation:

$$t_L = \frac{h^2}{6D_{app}} \quad (8)$$

where t_L is the lag time, obtained from the x-intercept of the permeation profiles, and h is the mean thickness of the wet films.

2.6. Preparation of SC-MAS coated tablets

Core tablets containing ACT were prepared using a direct compression method. The core tablets contained acetaminophen powder (16% w/w), spray-dried lactose (54.75% w/w), microcrystalline cellulose (28% w/w), colloidal silicon dioxide (0.25% w/w), and magnesium stearate (1% w/w). The drug powder, microcrystalline cellulose, spray-dried lactose and colloidal silicon dioxide were mixed using a Y-shaped mixer for 30 min. Next, magnesium stearate was added and mixed into the mixture for 5 min before tablet compression. The mixtures were compressed into tablets using a single punch machine (YeoHeng Co., Ltd., Bangkok, Thailand), and a biconvex punch and die measuring 8 mm in diameter was used. Average weight of the core tablets obtained was 253.8 ± 4.0 mg per tablet ($n = 20$) with 112.4 ± 13.3 N ($n = 10$) of hardness. Friability of the core tablets was

$0.25 \pm 0.09\%$ ($n = 3$). The drug content in the core tablets was extracted using 0.1 M HCl and measured by UV–visible spectrophotometer (Shimadzu UV1201, Japan) at a wavelength of 265 nm. The core tablets had 39.6 ± 0.2 mg each of acetaminophen content ($n = 3$).

The 5% w/v SC dispersion and SC-MAS dispersions at the ratios of 1:0.05, 1:0.1, and 1:0.2, which were prepared following the method in Section 2.4, were used as a coating material. The core tablets obtained were coated using a side-vented pan coating machine (Thai Coater Model FC15, Pharmaceuticals and Medical Supply, Thailand). The core tablets (900 g) were warmed in the coating pan at an inlet temperature of 70–75 °C, and the coating pan was rotated at a rate of 10 revolutions min^{-1} . The spray rate of the coating dispersions was 4 mL min^{-1} under spray pressure of 0.38 mPa. After the coating process, the coated tablets were stored in a desiccator prior to further examination.

The effect of SC–MAS ratio on the characteristics of the coated tablets was investigated. The core tablets were coated with SC film and SC–MAS films at the ratios of 1:0.05, 1:0.1, and 1:0.2 at a mean weight gain of 3.3% w/w. To investigate the effect of coating level, the core tablets were coated with the SC-MAS (1:0.1) films at the mean weight gains of 3.3, 6.1, and 8.2% w/w.

2.7. Evaluation of SC-MAS coated tablets

2.7.1. SEM studies

Surface and film matrix morphology of the coated tablet were observed by scanning electron microscopy (SEM). The coated tablets and cross-sections of tablets were mounted onto stubs, coated with gold in a vacuum evaporator, and investigated using a scanning electron microscope (Hitachi S-3000N, Tokyo, Japan).

2.7.2. In vitro drug release studies

In vitro drug release from the coated tablets was studied using the USP dissolution apparatus I (basket) with 900 mL of medium. The dissolution media were 0.1 M HCl and pH 6.8 phosphate buffer, and the temperature of system was controlled at 37.0 ± 1.0 °C. The baskets were rotated at a rate of 50 revolutions min^{-1} . The simulated gastrointestinal conditions used to test drug release were 0.1 M HCl (900 mL) for 2 h, and then the medium was changed to pH 6.8 phosphate buffer (900 mL). At predetermined intervals, samples were collected and replaced with an equal volume of fresh medium. The concentration of ACT released was analyzed by UV–visible spectrophotometer (Shimadzu UV1201, Japan) at wavelength of 265 nm.

2.7.3. Water uptake studies

Water uptake of the coated tablets in both 0.1 M HCl and pH 6.8 phosphate buffer was determined using USP dissolution apparatus I (basket), and the test conditions were the same as in the drug release study. The coated tablets were weighed (W_i), placed into baskets and immersed into the medium. At predetermined intervals, wet coated tablets were collected, carefully blotted with filter paper to remove surface water and weighed (W_c). Water uptake of the coated tablets could be calculated as follows [42]:

$$\text{Water uptake (\%)} = \frac{W_c - W_i}{W_i} \times 100 \quad (9)$$

3. Results and discussion

3.1. Characteristics of SC-MAS dispersions

The SC dispersion was milky with viscosity of 2.34 mPa as shown in Table 1. SC possessed a negative charge with zeta potential value of -18.36 mV because the pH of the dispersion (pH = 6.8) was higher than the SC isoelectric point (4.6 to 4.8), where the carboxyl groups of SC could be ionized. Unfortunately, the particle size of SC could not be

Table 1
Characteristics of SC-MAS dispersions.

Component	Particle size (μm)	Zeta potential (mV)	Viscosity (mPa.s)
5% w/v SC dispersion	ND	-18.36 ± 1.63	2.34 ± 0.06
1% w/v MAS dispersion	4.60 ± 0.01	-19.16 ± 1.80	22.7 ± 0.46
SC-MAS dispersion			
1:0.05	30.24 ± 2.89	-33.23 ± 2.46	3.66 ± 0.06
1:0.1	26.71 ± 5.06	-31.21 ± 2.42	4.17 ± 0.16
1:0.2	23.29 ± 2.78	-33.34 ± 2.13	6.32 ± 0.38

Data are mean \pm S.D., $n = 3$. ND = could not be determined.

determined due to its very small size. The MAS dispersion (1% w/v) showed a negative charge with $4.60\text{-}\mu\text{m}$ particle size, and the viscosity was observed to be 22.7 mPa. Incorporation of MAS into the SC dispersion resulted in greater particle size and a higher zeta potential value of the dispersed phase. Moreover, the viscosity of the SC-MAS dispersions was higher than the viscosity of the SC dispersion and increased with increasing MAS content. However, the SC-MAS (1:0.2) composite dispersion (containing MAS equivalent to 1% w/v) gave remarkably lower viscosity than the 1% w/v MAS dispersion.

The silicate layers of MAS could be separated in water, and the three-dimension structure of the silicate layers could then be created, resulting in a higher viscosity of the MAS dispersion [43]. When MAS was incorporated into SC dispersion, the three-dimensional structure of the MAS could not be formed, leading to lower viscosity of the SC-MAS (1:0.2) dispersion compared to the 1% w/v MAS dispersion. However, adding the MAS into the SC dispersion caused a viscosity synergism that could be observed from the increase in the viscosity of the SC dispersion when adding MAS. In addition, the larger particle size of the dispersed phase with a higher density of negative charge was formed because of the feasibility of the formation of the SC-MAS flocculates [27,33]. These findings indicated that the molecular interaction between SC and MAS in the dispersion could readily occur after simple mixing.

3.2. Appearance and thickness of the SC-MAS films

The SC films were prepared using a casting/solvent evaporation method. Actually, SC could not form a good continuous film; therefore, plasticizers were needed, and glycerin with 30% w/w of SC content was used in this study. Thus, the SC films (with glycerin) obtained were quite transparent and provided a good homogeneous sheet for further investigation. In the case of the SC-MAS films, the SC-MAS dispersions prepared had no sedimentation of the dispersed phase when allowed to settle for 12 h, so the SC-MAS films obtained after the drying process showed an opaque continuous sheet at all SC-MAS ratios used. However, the SC-MAS films at the ratio of 1:0.5 had a high brittleness, and the films were liable to break easily, thus this film was excluded from this study. Using SEM, the SC films had a quite smooth surface (Fig. 1a), whereas a rougher film surface was observed when adding MAS (Fig. 1b). Moreover, the incorporation of MAS resulted in a different matrix structure for the films. The dry thickness of the SC films was $133.0\text{ }\mu\text{m}$, and incorporation of MAS into the films resulted in an increase in the film thickness (Table 2). The wet thickness of the films was also determined after immersing in 0.1 M HCl for 5 min. The results showed that the thickness of the wet films was greater than the films with a dry thickness, indicative of the swelling property of the films under acidic conditions. However, the wet film thickness in pH 6.8 phosphate buffer was not determined because the wet films could not be handled due to very high swelling property in this medium.

3.3. Thermal properties of the films

DSC thermograms of the films are displayed in Fig. 2. MAS showed a

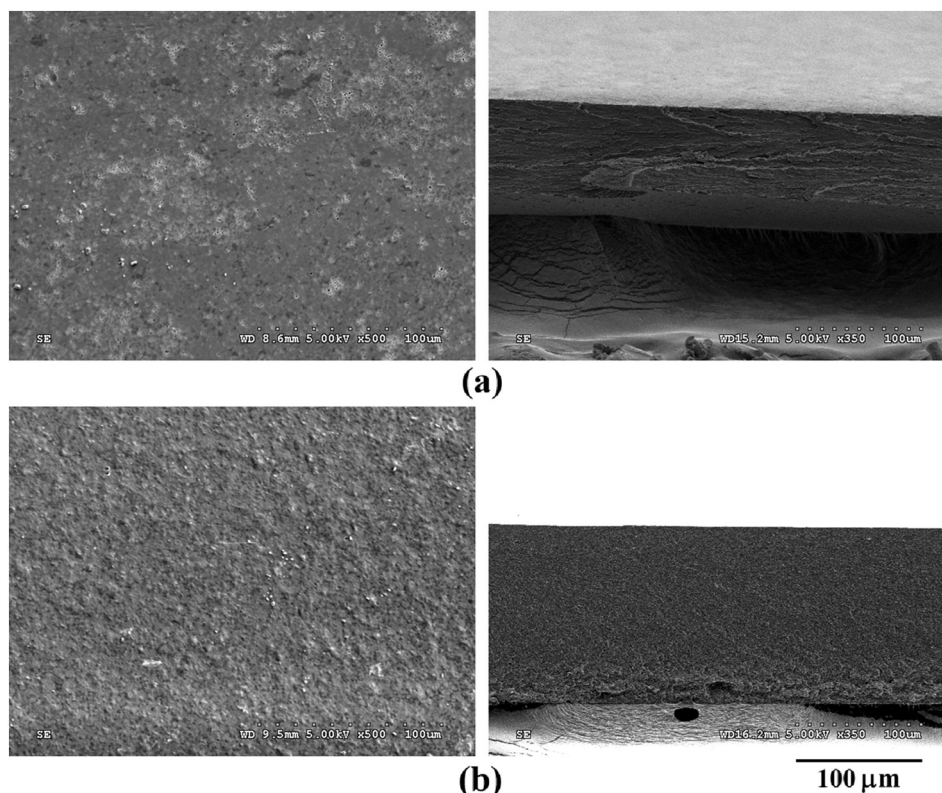


Fig. 1. Surface and cross-section morphologies of SC film (a) and SC-MAS (1:0.2) film (b).

broad endothermic peak at approximately 75 °C due to a dehydration of the water residue, whereas SC powder presented two exothermic degradation peaks at 290 and 357 °C. The formation of the SC films without glycerin caused a shift of the exothermic peaks to 296 and 358 °C. Addition of glycerin, a plasticizer, obviously affected the thermal behavior of the SC films because the small exothermic peak appeared at 308 °C for the SC film with glycerin. Furthermore, the film with MAS incorporated resulted in a shift of the exothermic peak to a higher temperature, and the peak intensity decreased with increasing MAS ratios. The thermal patterns of the SC-MAS films were remarkably different from those of SC-MAS physical mixtures. The results showed that MAS could enhance the thermal stability of the SC films.

3.4. Molecular interaction and nanocomposite formation of the films

Molecular interaction of the components in the films was investigated using FTIR spectroscopy and PXRD. The FTIR spectrum of MAS showed the O–H stretching of SiOH (3610 cm^{-1}), the O–H stretching of H_2O (3434 cm^{-1}), the O–H bending of H_2O (1638 cm^{-1}),

and the Si–O–Si stretching (1016 cm^{-1}) [36], as shown in Fig. 3. SC presented the N–H stretching overlapped with the O–H stretching at 3399 cm^{-1} , the C–H stretching at 2934 and 2963 cm^{-1} , the C=O stretching (amide I) at 1657 cm^{-1} , the N–H bending (amide II) at 1536 cm^{-1} and the C–N stretching at 1237 cm^{-1} [16,44]. The film formation of SC (without glycerin) caused a shift of the N–H stretching (with the O–H stretching) of amide I and amide II because of hydrogen bonding with the water residues. Incorporation of glycerin had an impact on the FTIR pattern of the SC films, and the N–H stretching (with the O–H stretching) showed a sharper peak and moved to a lower wavenumber (3429 cm^{-1}), and the C–H stretching peak of SC was also shifted to a lower wavenumber, suggesting the formation of intermolecular hydrogen bonding and greater flexibility of the main structure of the SC molecules. In addition, the SC film with glycerin also presented a new peak at 1134 cm^{-1} that was the C–O stretching peak of glycerin. The SC-MAS films showed a different FTIR pattern when compared with the SC-MAS physical mixtures. MAS added into the SC films caused a shift of the N–H stretching (with O–H stretching), and the peaks of amide I and amide II. These changes could clearly be

Table 2

Thickness and film permeability of SC and SC-MAS films.

Film	Dry thickness ^a	Wet thickness ^a	WVP rate ^b	WVP coefficient ^b $\times 10^4$	Acetaminophen permeation ^c			
	(μm)	(μm)	($\text{mg cm}^{-2}\text{ h}^{-1}$)	($\text{mg mm}^{-1}\text{ h}^{-1}\text{ mm Hg}^{-1}$)	Flux ($\mu\text{m cm}^{-2}\text{ min}^{-1}$)	Lag time (min)	$P_{\text{app}} \times 10^4$ (cm s^{-1})	$D_{\text{app}} \times 10^7$ ($\text{cm}^2\text{ s}^{-1}$)
SC film	133.0 ± 6.8	220.8 ± 27.7	2.44 ± 0.20	4.12 ± 0.33	71.0 ± 3.6	1.87 ± 0.20	2.96 ± 0.15	7.29 ± 0.72
SC-MAS film								
1:0.05	128.8 ± 2.2	195.3 ± 17.0	2.31 ± 0.19	4.25 ± 0.35	42.2 ± 0.8	1.71 ± 0.44	1.76 ± 0.44	6.50 ± 1.76
1:0.1	141.2 ± 4.8	197.7 ± 4.0	2.05 ± 0.29	4.12 ± 0.58	36.5 ± 1.3	1.94 ± 0.24	1.52 ± 0.05	5.66 ± 0.66
1:0.2	169.4 ± 8.1	250.0 ± 16.4	1.65 ± 0.37	4.74 ± 1.06	16.7 ± 0.6	3.40 ± 0.03	0.69 ± 0.03	5.11 ± 0.04

^a Data are mean \pm S.D., $n = 6$.

^b Data are mean \pm S.D., $n = 5$.

^c Data are mean \pm S.D., $n = 3$.

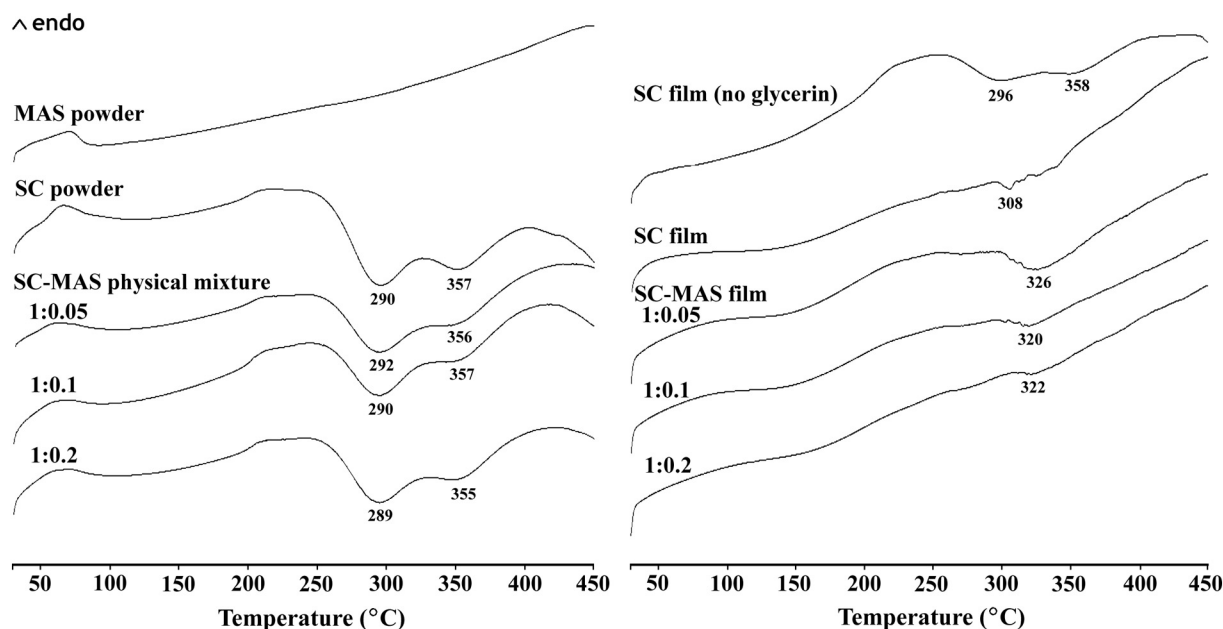


Fig. 2. DSC thermograms of MAS, SC, SC-MAS physical mixture, SC film, and SC-MAS films.

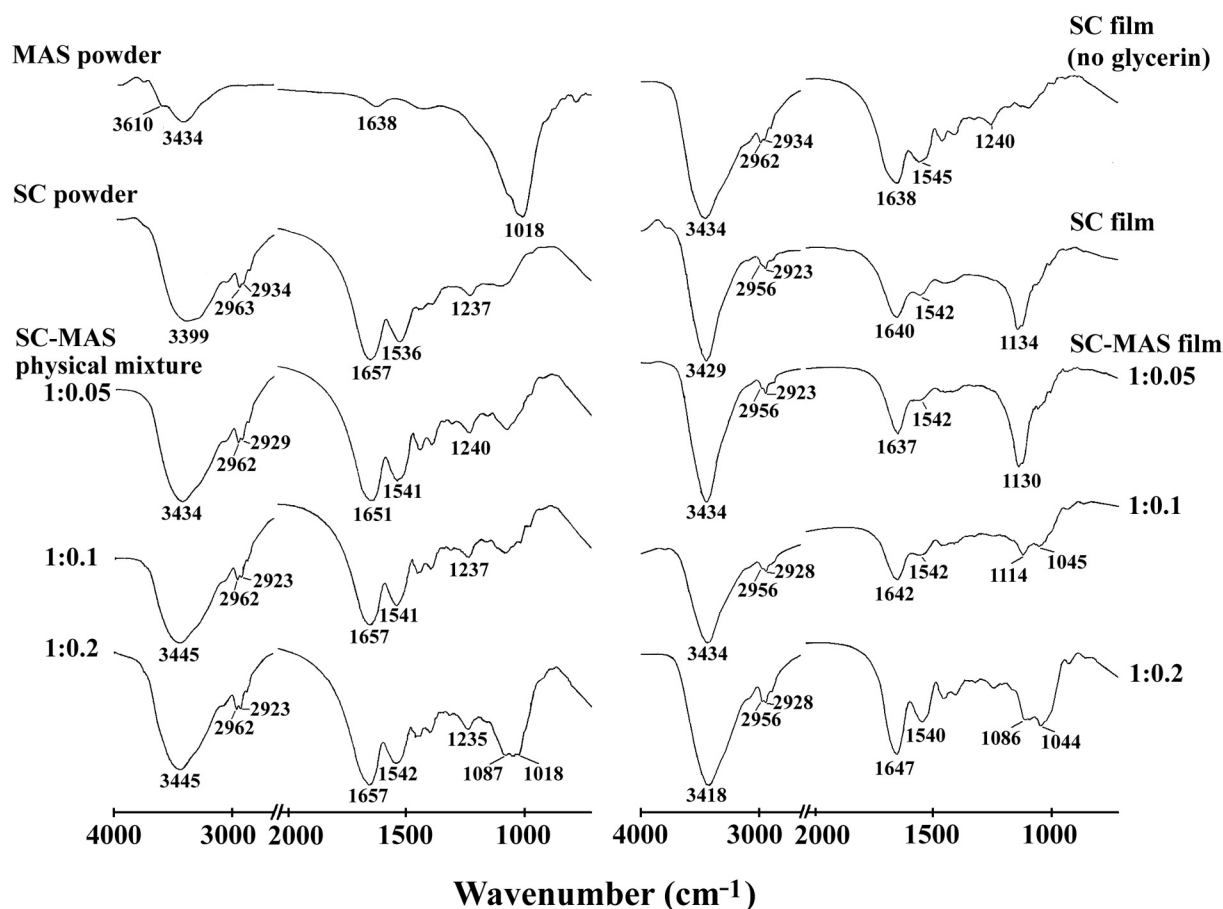


Fig. 3. FTIR spectra of MAS, SC, SC-MAS physical mixture, SC film, and SC-MAS films.

observed in the SC-MAS (1:0.2) films. This result indicated that the silanol groups of MAS could interact mainly with the amide and amino groups of SC via an intermolecular hydrogen bonding mechanism. These interactions could occur when mixing MAS with SC in the dispersion, leading to the viscosity synergism that was mentioned above.

The structure arrangement of MAS in the SC-MAS films was investigated using PXRD. The PXRD pattern of MAS showed the basal spacing peak at $7.0^\circ 2\theta$ (Fig. 4), and the interlayer distance of the silicate layers was 1.26 nm when calculated using Eq. (1) [36]. The crystallinity of the SC powder showed broad peaks at approximately $8^\circ 2\theta$

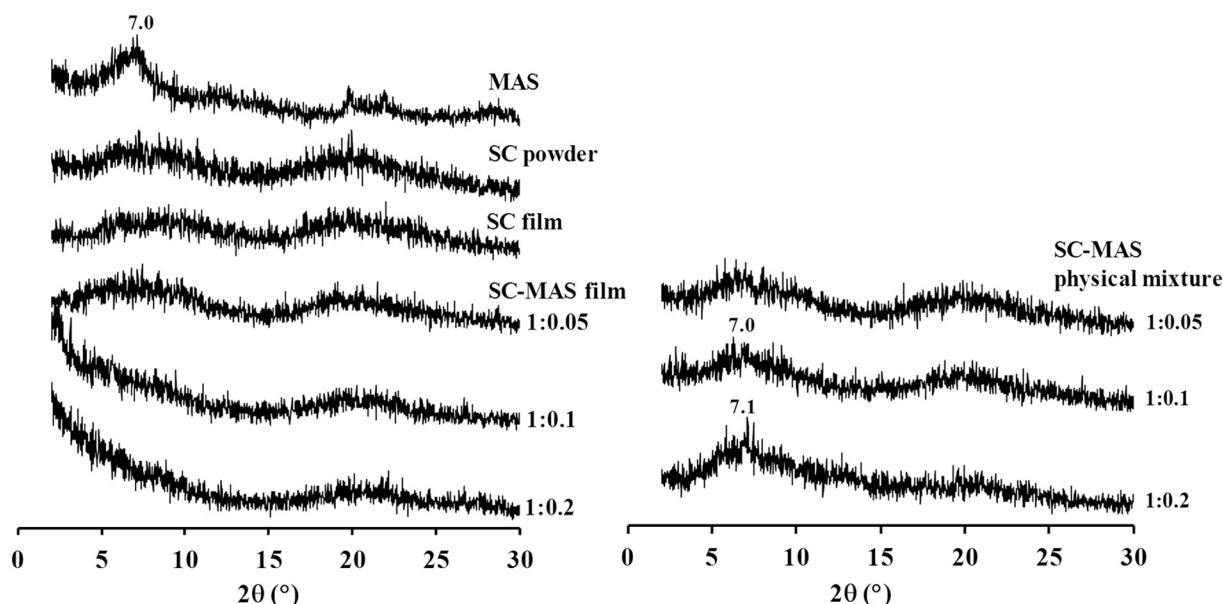


Fig. 4. PXRD patterns of MAS, SC, SC-MAS physical mixture, SC film, and SC-MAS films.

and $20^\circ 2\theta$, similar to the SC film with glycerin, indicative of an amorphous form of the SC powder and film. Addition of MAS at all ratios in the SC films brought about the disappearance of the basal spacing peak of the MAS silicate layers, whereas this peak of MAS was located at approximately $7^\circ 2\theta$ in the SC-MAS physical mixtures at the ratios of 1:0.1 and 1:0.2. Due to the limitation of detection of PXRD (the lowest angle = $2^\circ 2\theta$), the basal spacing peak of the MAS silicate layers at 2θ lower than 2° may be occurred. These results indicated that the interlayer distance of the silicate layers was possibly higher than 4.4 nm, or the complete separation of the MAS silicate layers in the SC matrix may be formed as well, suggesting a formation of intercalated or exfoliated nanocomposites, respectively. The exfoliated nanocomposites could be created because low amounts of clay were added [27,30]. Additionally, glycerin could interact with MAS by hydrogen bonding and could induce a formation of intercalated nanocomposites in alginate-MAS films when used as a plasticizer [45]. Therefore, glycerin may involve the nanocomposite formation of the SC-MAS films. However, the SC-MAS flocculates formed in the dispersion and FTIR data of the films could prove that SC could interact strongly with MAS in the films by hydrogen bonding, which was the main interaction for hindering the structure arrangement of the MAS silicate layers, leading to the film structures of intercalated or exfoliated nanocomposites in this study.

3.5. Water uptake and erosion of the films

The water uptake and erosion of the films were tested in both 0.1 M HCl and pH 6.8 phosphate buffer. When the films were immersed in an acidic medium, they still provided a continuous sheet because sodium caseinate was changed to casein salt that had a water-insoluble property [9]. Therefore, both parameters could be determined under acidic conditions. Unfortunately, the wet films in pH 6.8 phosphate buffer could not be handled properly and blotted to remove excess water due to very high swelling and some matrix dissolutions of the films, leading to a lack of the data for water uptake and matrix erosion in this medium. Fig. 5 presents the water uptake and erosion of the films in 0.1 M HCl. The SC films provided the highest water uptake at 15 min of the test because casein in the acidic form in the hydrated films may have a weak intermolecular bonding, leading to a large aqueous pore in the matrix of the films. However, the wet SC films at 60 and 120 min could not be handled due to very high water imbibition. The water uptake of the SC films decreased with increasing MAS ratios (Fig. 5a).

Apart from film water uptake, the SC films showed 21.3% erosion at 15 min of the test, whereas erosion of the SC-MAS films was found over the range of 21–26% (Fig. 5b). Film erosion could occur by leaching of the added water-soluble plasticizer, such as glycerin [45]. This finding suggested that addition of MAS into the SC films retarded the water absorption process of the films and resulted in a denser matrix structure that could be attributed to SC-MAS nanocomposite formation, reflecting water-filled channels in the film matrix and matrix strength of the wet films under acidic conditions.

3.6. Mechanical properties of the films

Fig. 6 shows the stress-strain (puncture strength-elongation) curves of the films. It was found that addition of MAS resulted in an obvious change of mechanical properties of the dry and wet CS films. The puncture strength and % elongation at break of the films in dry and wet stages are illustrated in Fig. 7. The SC films in the dry state provided the highest puncture strength and % elongation. Both parameters decreased with increasing MAS ratios in the films. These results were in agreement with the previous reports about the effect of solid materials added into polymeric films [27,46]. This finding could probably be attributed to the presence of the MAS particles hindering the formation of a continuous three-dimensional SC network.

The mechanical properties of the wet films tested in 0.1 M HCl are also shown in Fig. 7. The puncture strength of the wet SC films was remarkably lower than that of the dry state, whereas the % elongation of the SC film in both states was comparable. Increasing MAS ratios in the SC films resulted in an increase in the puncture strength due to the decrease in the water uptake of the SC-MAS films with higher MAS ratios (Fig. 5a). However, the % elongation of the SC-MAS films was lower than the % elongation of the SC film, but they still had 11%–15% elongation for all MAS ratios. The results were similar to the effect of clay additive on the mechanical properties of wet polymethacrylate films [27]. These findings suggested that the molecular interaction and nanocomposite formation of SC with MAS could enhance the strength of the films when the films were exposed to an acidic medium, potentially a crucial advantage when used as sustained release film coatings for tablets in an acidic condition. In addition, these films provided good strength for mechanical stress within the gastrointestinal tract.

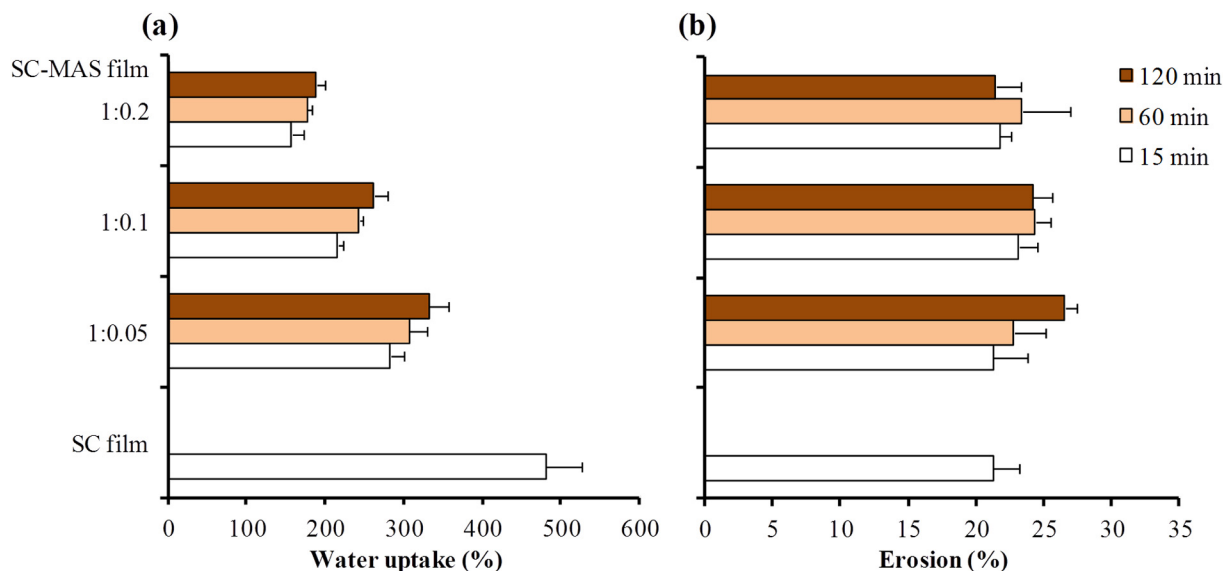


Fig. 5. Water uptake (a) and erosion (b) of the SC film and SC-MAS films at various ratios in 0.1 M HCl. Each value indicates mean \pm SD, $n = 5$.

3.7. Water vapor and drug permeability of the films

Water vapor permeation (WVP) rate and coefficient of the films are listed in Table 2. WVP rate of the SC films obviously decreased with increasing MAS ratios. However, the WVP coefficients were calculated using Eq. (4) that had no effect on dry film thickness. This parameter showed that MAS added did not influence the WVP properties of the SC films. The result suggested that the SC-MAS nanocomposite formation did not clearly increase tortuosity of water vapor pathways in the film matrix.

Drug permeability of the films in 0.1 M HCl was determined using ACT as a model drug. The drug permeation profiles obtained presented good linearity ($R^2 > 0.98$) for the relationship between drug permeated and time, indicating that the drug permeation reached a steady state with a high drug concentration in the donor compartment and could be described using Fick's first law. The drug permeation parameters are listed in Table 2. The drug permeation flux and P_{app} value

were obviously reduced when increasing MAS ratios in the films, whereas the longer lag time for drug permeation was found. Decreasing of the D_{app} values occurred when MAS added in the SC films was increased.

The diffusive transport of drug in a polymeric film can be described using two mechanisms [37,47]. The first mechanism is the partition mechanism of the drug into polymeric films, which is dependent upon drug affinity with film polymer, and the diffusion process in the polymer fraction progressing across the films. The other mechanism is a pore mechanism where the drug diffuses within the structure of the hydrated films via water-filled channels. In this study, both mechanisms could be applied to describe the diffusion of ACT across the SC-MAS films in an acidic medium. The partition mechanism possibly predominated in the initial stage of the permeation process, which could be observed from a longer lag time when the MAS added was increased. However, ACT had a weak affinity with MAS [36] because it was a non-electrolyte molecule [48,49], which caused less partitioning of the drug

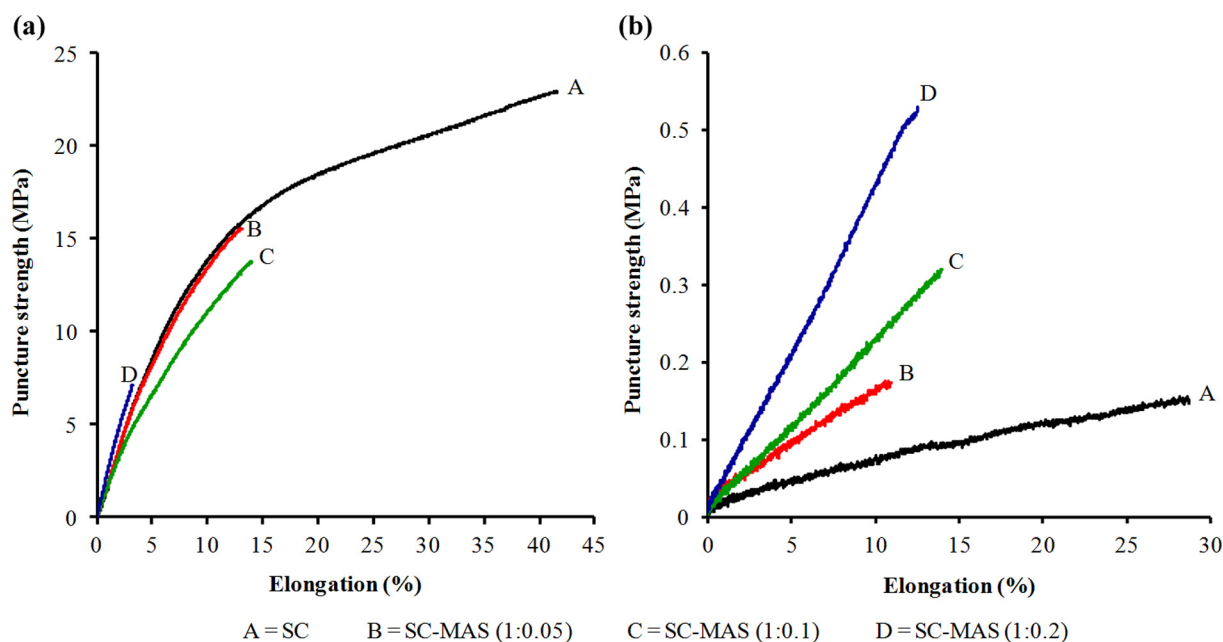


Fig. 6. Stress-strain curves of SC films and SC-MAS films at different ratios in dry (a) and wet (b) states.

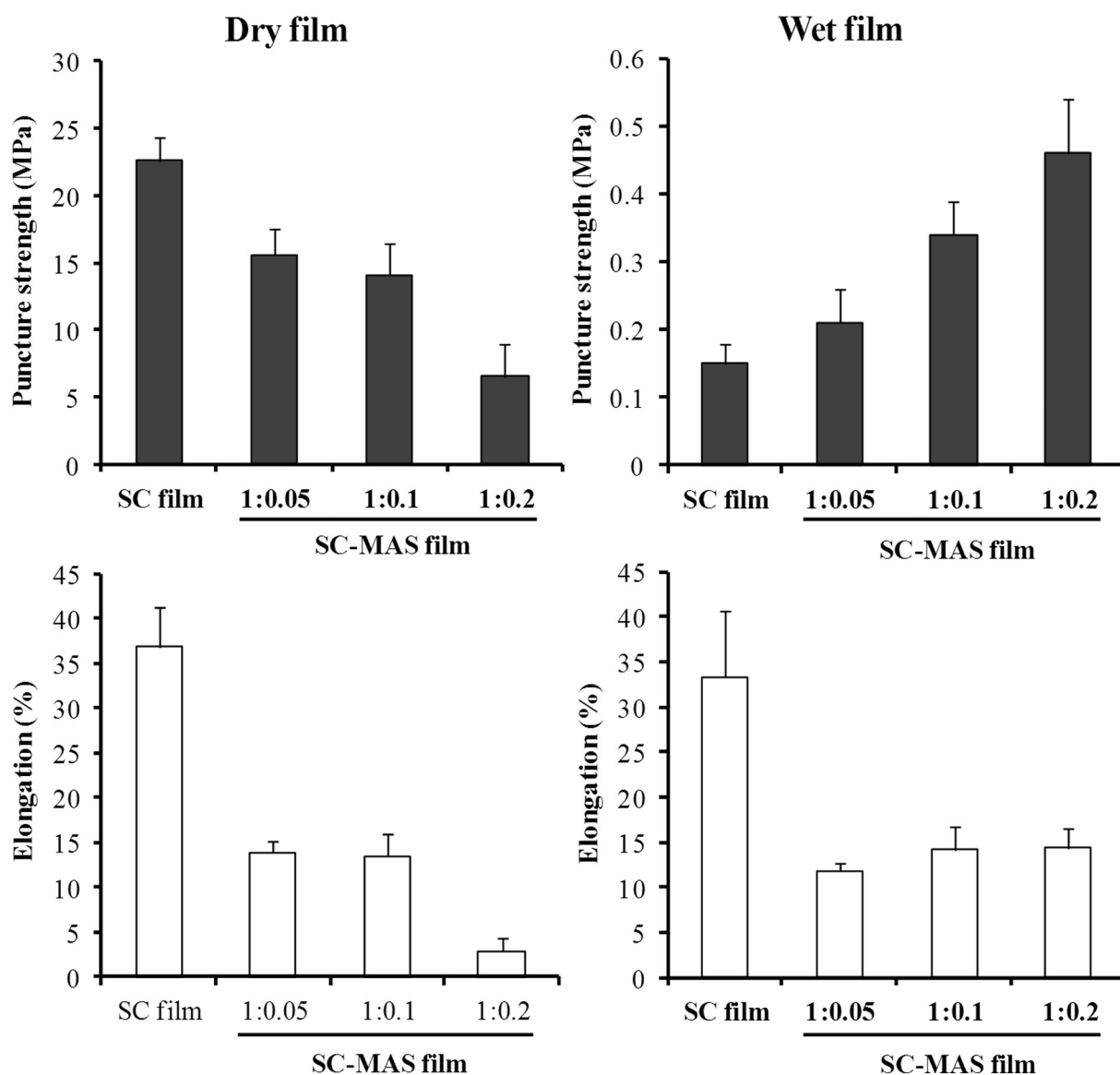


Fig. 7. Puncture strength and elongation of SC films and SC-MAS films at different ratios in dry and wet states. Each value indicates mean \pm SD, $n = 4$.

with the SC-MAS films in the steady state of the permeation process. Thus, the film permeation of ACT was diffused mainly through aqueous-filled channels of the films. Increase of MAS ratios resulted in lower water uptake in the films that meant smaller water-filled channels (or higher tortuosity) in the matrix of the films, leading to the reduction of the drug diffusivity in the matrix network under the same concentration gradient [50,51]. Thus, decrease of D_{app} values of the drug was obtained in this study.

3.8. Use of SC-MAS films for tablet film coatings

The SC and SC-MAS films at different ratios were applied as a coating material for tablets. The appearance of the SC and SC-MAS coated tablets is shown in Fig. 8. A few defects of the coated tablets were found by visible observations. The surface and cross-sectional morphology of the SC-coated films showed features similar to the features of the SC-MAS coated films (Fig. 8). The effect of SC-MAS ratios on drug release and water uptake of the coated tablets was investigated in this study. The ACT core tablets were coated with SC and SC-MAS films at the mean weight gain of 3.3% w/w. The drug release and water uptake using 0.1 M HCl are shown in Fig. 9a and c, respectively. The

core tablets displayed a fast release, and complete release was found within 30 min. The SC-coated tablets showed slower drug release than the core tablets, suggesting that the SC films possessed a stable wet film around the tablets when SC was changed to casein salt, water-insoluble property, under acidic conditions. Then, the wet coated films could retard the diffusion of the dissolved drug. Incorporation of MAS into the coated films could modulate the drug release pattern. The higher the MAS ratios in the coated films, the slower the drug release in the acidic medium was obtained. Moreover, the water uptake of the coated tablets showed that the coated tablets with SC-MAS films at the ratios of 1:0.05 and 1:0.1 had similar %water uptake when compared with the SC coated tablets, while the lowest water uptake was obtained from the SC-MAS (1:0.2) coated tablets (Fig. 9c). The results showed that the SC-MAS coated films could possibly slow down the water penetration process into the coated tablets before drug dissolution and drug release. Additionally, the lower drug diffusivity across the SC-MAS films with higher ratios of MAS (Table 2) also led to slower drug release from the coated tablets.

Effects of film coating level on drug release and water uptake of the coated tablets in 0.1 M HCl are shown in Fig. 9b and d, respectively. The drug release from the SC-MAS (1:0.1) coated tablets decreased with

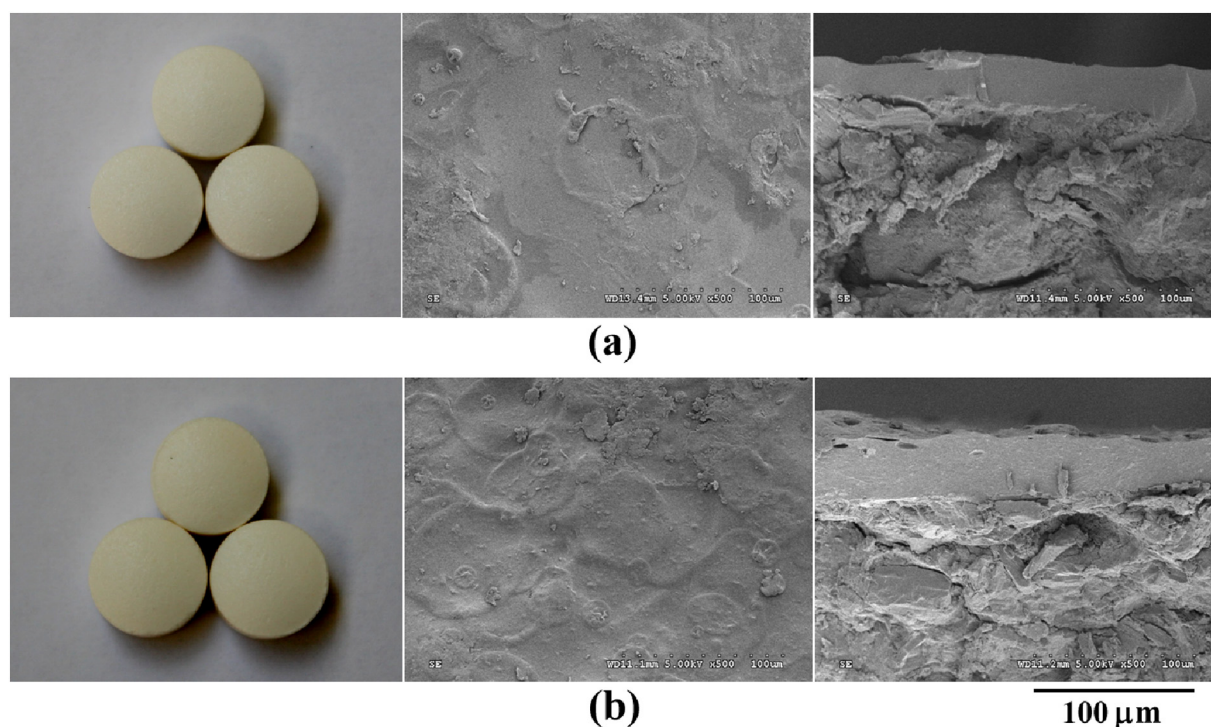


Fig. 8. Appearance and surface and cross-section morphologies of acetaminophen tablets coated with SC film (a) and SC-MAS (1:0.1) film (b) at 3.3% w/w coating level.

increasing film coating levels (Fig. 9b). The 8.2% weight gain coating provided a sustained-release pattern of drug for 10 h. Increasing film coating level could obviously retard the water absorption process of the coated tablets (Fig. 9d). This finding suggested that the higher coating level of the SC-MAS (1:0.1) coated tablets could retard drug release from the coated tablets due to slower water uptake for drug dissolution and longer pathway lengths for drug diffusion.

Apart from acidic conditions, the water uptake and drug release of the coated tablets were also tested in pH 6.8 phosphate buffer as shown in Fig. 10. The drug release and water uptake of the coated tablets in pH 6.8 phosphate buffer were greater than the drug release and water uptake in an acidic medium. The SC and SC-MAS (1:0.05) coated tablets showed fast release comparable to the core tablets (Fig. 10a). Increasing the MAS ratios caused more sustained drug release, while the coated tablets with 6.1 and 8.2% weight gain gave similar drug release profiles but slower than those with 3.3% weight gain. The water uptake study could be only tested within 5 min due to very fast swelling of the coated films. The results showed that the presence of MAS in the coated films provided greater water uptake than the SC coated tablets, and the increase of film coating levels led to higher water uptake of the coated tablets (Fig. 10b). SC could still have swollen in the neutral medium although it interacts and creates nanocomposites with MAS. Swelling of SC loosened the film matrix structure and increased the matrix volume for absorbing water, leading to higher water uptake when increasing the film coating level. Moreover, MAS had water absorption capacity as well. Therefore, the presence of MAS could promote water uptake of the coated tablets. The other factor after swelling of the coated films was dissolution or erosion of SC from the films. This phenomenon may result in faster drug release from the coated tablets, irrespective of the MAS ratios and film coating levels.

The simulated gastrointestinal conditions starting with 0.1 M HCl for 2 h followed by pH 6.8 phosphate buffer were used to test the drug release from the SC-MAS (1:0.1) coated tablets, which is shown in Fig. 11. The drug release from the SC-MAS coated tablet proceeded continuously when the dissolution medium was changed from acidic medium to pH 6.8 phosphate buffer. The drug release patterns obtained

in this test were like those using 0.1 M HCl (Fig. 9b). The results suggested that SC in the coated films, which had been changed to casein salt under acidic conditions, did not readily hydrate and swell when passing to pH 6.8 phosphate buffer. Thus, the drug released from the coated tablets was controlled by the drug diffusion process across the coated films through 8 h of the tests. This finding suggested that the release of the drug could possibly occur continuously when the SC-MAS coated tablets were transferred from the stomach to the small intestine in the gastrointestinal tract.

4. Conclusions

This study demonstrates that SC can interact on a molecular level with MAS in the dispersions after simple mixing, resulting in SC-MAS flocculation and viscosity synergism. The SC-MAS films can be prepared successfully by the casting method. Molecular interaction between the amide and amino groups of SC and the silanol groups of MAS via intermolecular hydrogen bonding results in the formation of exfoliated nanocomposites. Addition of MAS can enhance the thermal stability of the SC films. The puncture strength and elongation of the SC films decreases with an increasing MAS ratio in the dry state. In contrast, increasing the MAS ratio causes an increase of puncture strength of the wet SC-MAS films in an acidic medium. The SC-MAS films do not obviously retard the water vapor permeation, but the drug permeability and diffusivity across the films in an acidic medium remarkably decrease when increasing MAS ratios because the nanocomposite matrix structure possesses smaller water-filled channels with higher tortuosity. The SC-MAS dispersions can be employed as a film coating material of ACT tablets. The SC-MAS coated tablets present several film defects and smooth surface morphology. The ACT release from the coated tablets in an acidic medium can be modified by the varying MAS ratios and film coating levels. The SC-MAS coated tablets also display a sustained-release pattern of the drug in simulated gastrointestinal condition. This finding indicates that the SC-MAS nanocomposite films can be used in modified-release oral tablet coatings.

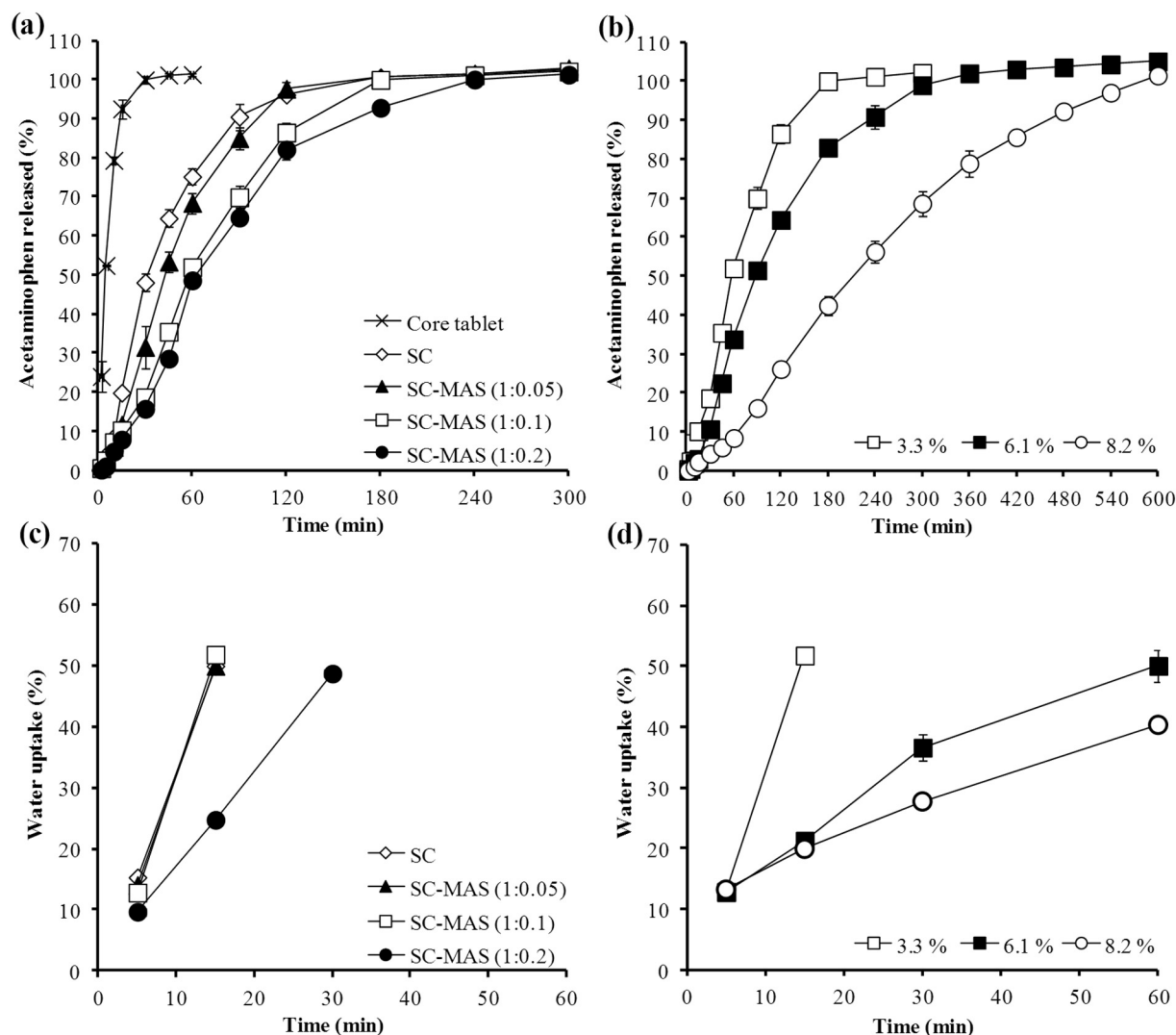


Fig. 9. Effect of SC-MAS ratios (a, c) and film coating levels (b, d) on drug release (a, b) and water uptake (c, d) of coated acetaminophen tablets in 0.1 M HCl. Each point indicates mean \pm SD, $n = 3$.

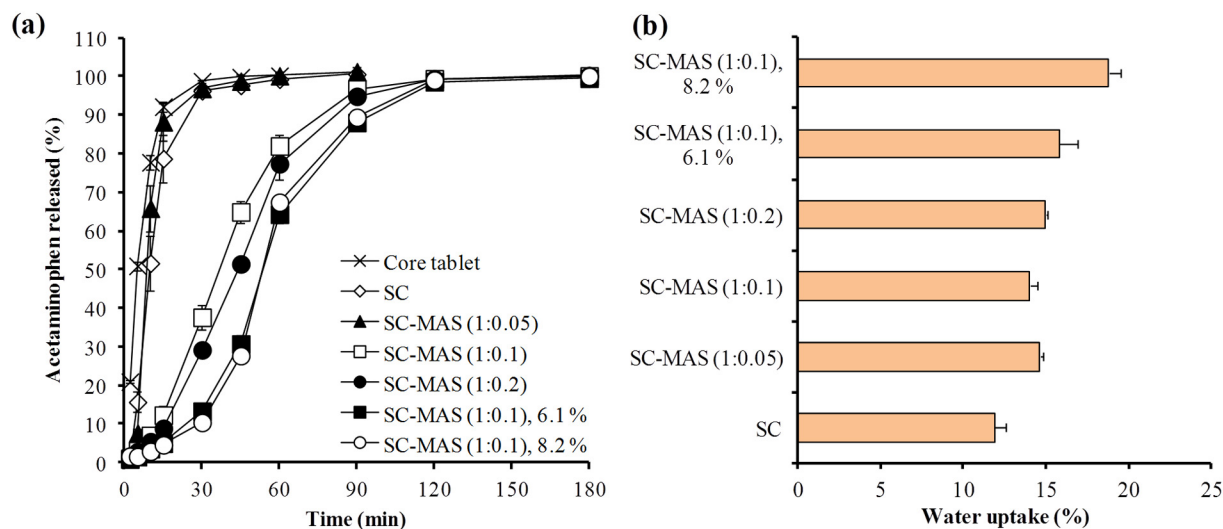


Fig. 10. Effect of SC-MAS ratios and film coating levels on drug release (a) and water uptake at 5 min (b) of coated acetaminophen tablets in pH 6.8 phosphate buffer. Each value indicates mean \pm SD, $n = 3$.

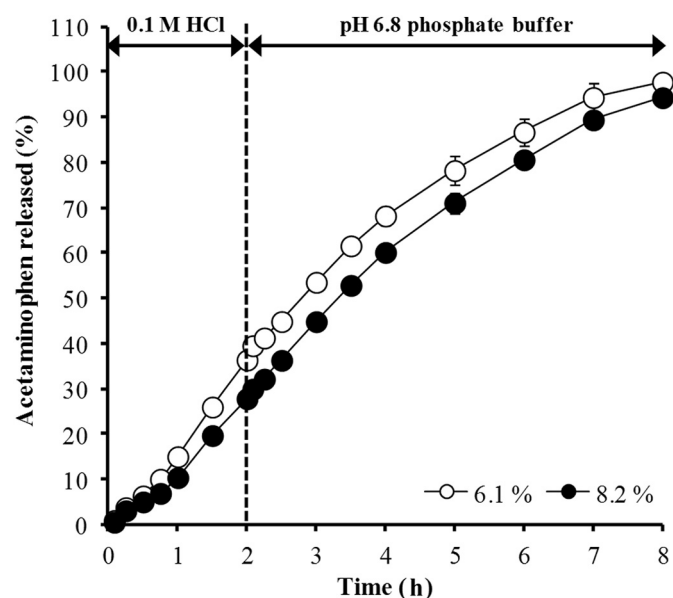


Fig. 11. Drug release profiles of SC-MAS (1:0.1) coated tablets at different coating levels in simulated gastrointestinal condition. Each value indicates mean \pm SD, $n = 6$.

Acknowledgments

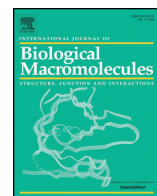
The authors wish to thank the Thailand Research Fund (Bangkok, Thailand) and Khon Kaen University (Khon Kaen, Thailand) for research funding (Grant no. BRG6080016). Financial support from the Thailand Research Fund through the Royal Golden Jubilee Ph.D. Program (Grant No. PHD/0067/2557) for W.K. and T.P. is gratefully acknowledged.

References

- [1] T. Nagai, S. Obara, H. Kokubo, N. Hoshi, Application of HPMC and HPMCAS to aqueous film coating of pharmaceutical dosage forms, in: J.W. McGinity (Ed.), *Aqueous Polymeric Coatings for Pharmaceutical Dosage Forms*, Marcel Dekker Inc., New York, 1997, pp. 177–226.
- [2] S. Karki, H. Kim, S.J. Na, D. Shin, K. Jo, J. Lee, Thin films as an emerging platform for drug delivery, *Asian J. Pharm. Sci.* 11 (2016) 559–574.
- [3] J. Nunthanid, S. Wanchana, P. Sriamornsak, S. Limmatavapirat, M. Luangtanaanan, S. Puttipatkhachorn, Effect of heat on characteristics of chitosan film coated on theophylline tablets, *Drug Dev. Ind. Pharm.* 28 (2002) 919–930.
- [4] L.A.M. Van Den Broek, R.J.I. Knoop, F.H.J. Kappen, C.G. Boeriu, Chitosan films and blends for packaging material, *Carbohydr. Polym.* 116 (2015) 237–242.
- [5] Z.A. Nur Hanani, Y.H. Roos, J.P. Kerry, Use and application of gelatin as potential biodegradable packaging materials for food products, *Int. J. Biol. Macromol.* 71 (2014) 94–102.
- [6] L.M. Bonnaillie, H. Zhang, S. Akkurt, K.L. Yam, P.M. Tomasula, Casein films: the effects of formulation, environmental conditions and the addition of citric pectin on the structure and mechanical properties, *Polymer* 6 (2014) 2018–2036.
- [7] S. Alam, S. Paul, Efficacy of casein coating on storage behavior of kinnow, *J. Food Sci. Technol.* 38 (2001) 235–238.
- [8] P. Walstra, J. Wouters, T. Geurts, *Dairy Science and Technology*, Second ed., Taylor & Francis Group, Boca Raton, 2006.
- [9] A.O. Elzoghby, W.S. El-Fotoh, N.A. Elgindy, Casein-based formulations as promising controlled release drug delivery systems, *J. Control. Release* 153 (2011) 206–216.
- [10] D.S. Horne, S.R. Euston, Simulating the self-association of caseins, *Food Hydrocoll.* 19 (2005) 379–386.
- [11] F.C. Millar, O.I. Corrigan, Influence of sodium caseinate on the dissolution rate of hydrochlorothiazide and chlorothiazide, *Drug Dev. Ind. Pharm.* 17 (1991) 1593–1607.
- [12] F.C. Millar, O.I. Corrigan, Dissolution mechanism of ibuprofen-casein compacts, *Int. J. Pharm.* 92 (1993) 97–104.
- [13] N.N. Li, C.P. Fu, L.M. Zhang, Using casein and oxidized hyaluronic acid to form biocompatible composite hydrogels for controlled drug release, *Mater. Sci. Eng. C* 36 (2014) 287–293.
- [14] A. Bani-Jaber, K. Aideh, I. Hamdan, R. Maraqa, Drug-loaded casein beads: influence of different metal-types as cross-linkers and oleic acid as a plasticizer on some properties of the beads, *J. Drug Deliv. Sci. Technol.* 19 (2009) 125–131.
- [15] W.A. Knepp, A. Jayakrishnan, J.M. Quigg, H.S. Sitren, J.J. Bagnall, E.P. Goldberg, Synthesis, properties, and intratumoral evaluation of mitoxantrone-loaded casein

- microspheres in Lewis lung carcinoma, *J. Pharm. Pharmacol.* 45 (1993) 887–891.
- [16] A.J.P. Santinho, N.L. Pereira, O.D. Freitas, J.H. Collett, Influence of formulation on the physicochemical properties of casein microparticles, *Int. J. Pharm.* 186 (1999) 191–198.
- [17] A.O. Elzoghby, M.W. Helmy, W.M. Samy, N.A. Elgindy, Novel ionically crosslinked casein nanoparticles for flutamide delivery: formulation, characterization, and in vivo pharmacokinetics, *Int. J. Nanomedicine* 8 (2013) 1721–1732.
- [18] K. Pan, Q. Zhong, S.J. Baek, Enhanced dispersibility and bioactivity of curcumin by encapsulation in casein nanoparticles, *J. Agric. Food Chem.* 61 (2013) 6036–6043.
- [19] O. Abu Diak, A. Bani-Jaber, B. Amro, D. Jones, G.P. Andrews, The manufacture and characterization of casein films as novel tablet coating, *Food Bioprod. Process.* 85 (2007) 284–290.
- [20] M. Wihodo, C.I. Moraru, Physical and chemical methods used to enhance the structure and mechanical properties of protein films: a review, *J. Food Eng.* 114 (2013) 292–302.
- [21] K. Khwaldia, S. Banon, C. Perez, S. Desobry, Properties of sodium caseinate film-forming dispersions and films, *J. Dairy Sci.* 87 (2004) 2011–2016.
- [22] J.L. Audic, B. Chaufer, Influence of plasticizers and crosslinking on the properties of biodegradable films made from sodium caseinate, *Eur. Polym. J.* 41 (2005) 1934–1942.
- [23] M. Perada, M.I. Aranguren, N.E. Marcovich, Effect of crosslinking on the properties of sodium caseinate films, *J. Appl. Polym. Sci.* 116 (2010) 18–26.
- [24] M.J. Fabra, P. Talens, A. Chiralt, Tensile properties and water vapor permeability of sodium caseinate films containing oleic acid-beeswax mixtures, *J. Food Eng.* 85 (2008) 393–400.
- [25] M. Pereda, G. Amica, I. Racz, N.E. Marcovich, Preparation and characterization of sodium caseinate films reinforced with cellulose derivatives, *Carbohydr. Polym.* 86 (2011) 1014–1021.
- [26] W. Khunawattanakul, S. Puttipatkhachorn, T. Rades, T. Pongjanyakul, Chitosan-magnesium aluminum silicate nanocomposite films: physicochemical characterization and drug permeability, *Int. J. Pharm.* 393 (2010) 219–229.
- [27] T. Rongthong, S. Sungthongjeen, J. Siepmann, T. Pongjanyakul, Quaternary polymethacrylate-magnesium aluminum silicate films: molecular interactions, mechanical properties and tackiness, *Int. J. Pharm.* 458 (2013) 57–64.
- [28] O. Shakil, F. Masood, T. Yasin, Characterization of physical and biodegradation properties of poly-3-hydroxybutyrate-co-3-hydroxyvalerate/sepiolite nanocomposites, *Mater. Sci. Eng. C* 77 (2017) 173–183.
- [29] R.C. Rowe, P.J. Sheskey, S.C. Owen, *Handbook of Pharmaceutical Excipients*, Fifth ed., Pharmaceutical Press and American Pharmaceutical Association, Washington, 2006.
- [30] M. Alexandre, P. Dubois, Polymer-layered silicate nanocomposites: preparation, properties and uses of a new class of materials, *Mater. Sci. Eng.* 28 (2000) 1–63.
- [31] W. Kanjanakawinkul, T. Rades, S. Puttipatkhachorn, T. Pongjanyakul, Nicotine-magnesium aluminum silicate microparticle surface modified with chitosan for mucosal delivery, *Mater. Sci. Eng. C* 33 (2013) 1727–1736.
- [32] W. Kanjanakawinkul, N.J. Medlicott, T. Rades, S. Puttipatkhachorn, T. Pongjanyakul, Lysozyme-magnesium aluminum silicate microparticles: molecular interaction, bioactivity and release studies, *Int. J. Biol. Macromol.* 80 (2015) 651–658.
- [33] W. Khunawattanakul, S. Puttipatkhachorn, T. Rades, T. Pongjanyakul, Chitosan-magnesium aluminum silicate composite dispersions: characterization of rheology, flocculate size and zeta potential, *Int. J. Pharm.* 351 (2008) 227–235.
- [34] P.A. Cuiello, Rheological properties of magnesium aluminum silicate/xanthan gum dispersions, *J. Soc. Cosmet. Chem.* 32 (1981) 275–285.
- [35] P.A. Cuiello, D.B. Braun, Clay/carbomer mixtures enhance emulsion stability, *Cosmet. Toilet.* 106 (1991) 89–95.
- [36] T. Pongjanyakul, A. Pripem, S. Puttipatkhachorn, Investigation of novel alginate-magnesium aluminum silicate microcomposite films for modified-release tablets, *J. Control. Release* 107 (2005) 343–356.
- [37] T. Pongjanyakul, Alginate-magnesium aluminum silicate films: Importance of alginate block structures, *Int. J. Pharm.* 365 (2009) 100–108.
- [38] M.P. Ennis, D.M. Mulvihill, Milk proteins, in: G.O. Philips, P.A. Williams (Eds.), *Handbook of Hydrocolloids*, Woodhead Publishing, Cambridge, 2000, pp. 189–217.
- [39] H. Sukri, T. Pongjanyakul, Interaction of nicotine with magnesium aluminum silicate at different pHs: characterization of flocculate size, zeta potential and nicotine adsorption behavior, *Colloids Surf. B* 65 (2008) 54–60.
- [40] L. Tuovinen, S. Peltonen, K. Järvinen, Drug release from starch-acetate films, *J. Control. Release* 91 (2003) 345–354.
- [41] G.L. Flynn, S.H. Yalkowsky, T.J. Roseman, Mass transport phenomena and models: theoretical concepts, *J. Pharm. Sci.* 63 (1974) 479–510.
- [42] S. Sungthongjeen, S. Puttipatkhachorn, O. Paeratakul, A. Dashevsky, R. Bodmeier, Development of pulsatile release tablets with swelling and rupturable layers, *J. Control. Release* 95 (2004) 147–159.
- [43] N. Cruz, Y. Peng, Rheology measurements for flotation slurries with high clay contents—a critical review, *Miner. Eng.* 98 (2016) 137–150.
- [44] M. Pereda, M.I. Aranguren, N.E. Marcovich, Caseinate films modified with tung oil, *Food Hydrocoll.* 24 (2010) 800–808.
- [45] T. Pongjanyakul, S. Puttipatkhachorn, Alginate-magnesium aluminum silicate films: effect of plasticizers on film properties, drug permeation and drug release from coated tablets, *Int. J. Pharm.* 333 (2007) 34–44.
- [46] L.A. Felton, J.W. McGinity, Influence of insoluble excipients on film coating systems, *Drug Dev. Ind. Pharm.* 28 (2002) 225–243.
- [47] D. Thacharodi, K. Panduranga Rao, Release of nifedipine through crosslinked chitosan membranes, *Int. J. Pharm.* 96 (1993) 33–39.
- [48] N.I. Nakano, Y. Shimamori, M. Umehashi, M. Nakano, Preparation and drug adsorption characteristics of activated carbon beads suitable for oral administration,

- Chem. Pharm. Bull. 32 (1984) 699–707.
- [49] A.P. Terzyk, G. Rychlicki, S. Biniak, J.P. Łukaszewicz, New correlations between the composition of the surface layer of carbon and its physicochemical properties exposed while paracetamol is adsorbed at different temperature and pH, *J. Colloid Interface Sci.* 257 (2003) 13–30.
- [50] F. Lecomte, J. Siepmann, M. Walther, R.J. MacRae, R. Bodmeier, Blends of enteric and GIT-insoluble polymers used for film coating: physicochemical characterization and drug release patterns, *J. Control. Release* 89 (2003) 457–471.
- [51] T. Rongthong, S. Sungthongjeen, F. Siepmann, J. Siepmann, T. Pongjanyakul, Quaternary polymethacrylate–magnesium aluminum silicate films: water uptake kinetics and film permeability, *Int. J. Pharm.* 490 (2015) 165–172.



Alginate-caseinate composites: Molecular interactions and characterization of cross-linked beads for the delivery of anticandidals

Rapee Khlibsuwan, Watcharee Khunkitti, Thaned Pongjanyakul *

Division of Pharmaceutical Technology, Faculty of Pharmaceutical Sciences, Khon Kaen University, Khon Kaen 40002, Thailand

ARTICLE INFO

Article history:

Received 8 February 2018

Received in revised form 26 March 2018

Accepted 17 April 2018

Available online 19 April 2018

Keywords:

Sodium alginate

Sodium caseinate

Molecular interaction

Beads

Anticandidal

Drug delivery

ABSTRACT

Polysaccharide-protein composites offer potential utility for the delivery of drugs. The objectives of this work were to investigate the molecular interactions between sodium alginate (SA) and sodium caseinate (SC) in dispersions and films and to characterize calcium alginate (CA) beads mixed with SC for the delivery of fluconazole (FZ) and clotrimazole (CZ). The results demonstrated that SA could interact with SC, which caused a viscosity synergism in the dispersions. Hydrogen bonding between the carboxyl or hydroxyl groups of SA and the amide groups of SC led to the formation of soluble complexes that could reinforce the CA beads prepared by calcium cross-linking. The SC-CA beads provided higher drug entrapment efficiency, lower water uptake and erosion, and slower drug release than for the CA beads. The loaded FZ was an amorphous form, but CZ crystals were embedded in the bead matrix due to the low water solubility of this drug. However, SC micellization could enhance the water solubility and efficacy of CZ against *Candida albicans*. This finding indicates that SA can interact with SC via hydrogen bonding to form complexes and that the anticandidal-loaded SC-CA beads can be used as drug delivery systems and drug reservoirs in tablets for oral candidiasis.

© 2018 Elsevier B.V. All rights reserved.

1. Introduction

Polysaccharide-protein blends offer a great potential for use in food and pharmaceutical technologies. Molecular interactions between polysaccharides and proteins lead to the formation of complexes that are dependent on the type of interaction bonding. Basically, these interactions can be classified as covalent and non-covalent interactions [1]. Covalent interactions are highly specific and are characterized by strong binding and irreversible interactions between proteins and polysaccharides. In contrast, non-covalent interactions are non-specific and occur via electrostatic forces, hydrogen bonding, and hydrophobic interactions, resulting in the formation of soluble or insoluble complexes that are dependent upon weak or strong interactions, respectively [2]. Polysaccharide-protein complexes have been characterized and applied as emulsifiers [3], film formers [4], and micro/nanomatrix formers for the delivery of drugs and nutrients [5–7].

Sodium alginate (SA) is a natural anionic polysaccharide found in marine brown algae. SA is composed of (1–4)-linked β -D-mannuronic acid and α -L-guluronic acid [8]. It has regions that are rich in mannuronic acid units, guluronic acid units and regions in which both monomers are equally prevalent. SA can be cross-linked with divalent cations, such as calcium ions, to form microparticles and beads, the structures of which are dependent on the droplet size of the dispersions

added into the divalent ion-rich solution. This method is known as ionotropic gelation [9]. The calcium alginate (CA) in the form of microparticles or beads has been widely used as a delivery system of drugs [10–12] and proteins [13]. Reinforcement of the CA beads can be made before the crosslinking process via the incorporation of water-soluble [14,15] and water-insoluble polymers [16], clays [14,17], and proteins [18] into the drug-loaded SA dispersion. This approach for the CA beads leads to an improvement of the drug entrapment efficiency (DEE) and a retardation of the drug release. Thus, it is important to identify a natural substance to modify the characteristics of the CA beads. One of these natural proteins is casein, which can interact with several polymers, such as pectin [19] and starch [20]. Casein may have the potential to interact with SA and to improve CA bead properties.

Caseins are composed of 94% protein and 6% colloidal calcium phosphate [21], and the molecule weights of caseins are in the range of 19–25 kDa, with an isoelectric point of 4.6–4.8. They are composed of four different peptides: α S₁, α S₂, β , and κ caseins [22]. Caseins in the acidic form demonstrate low aqueous solubility, but sodium caseinate (SC), the sodium salt of casein, is freely soluble in water [23]. Due to the amphiphilic properties of SC molecules, self-assembly into stable micellar structures in aqueous solutions occurs when the SC concentration is higher than 1.0 mg mL^{−1}, a critical micelle concentration [24]. The core of the micelles consists of α S₁, α S₂, and β caseins, whereas κ caseins are located on the surface of the micelles [22]. Due to this characteristic, SC has been pharmaceutically applied as a solubilizing agent for poorly soluble drugs [25,26]. Furthermore, SC has a potential use

* Corresponding author.

E-mail address: thaned@kku.ac.th. (T. Pongjanyakul).

as a drug delivery system, particularly in the form of microparticles [27,28] and nanoparticles [29,30].

Polysaccharide-protein composites between SA and SC have been previously investigated in the form of dispersions and microparticles. A phase separation of SA and SC in the composite dispersion was prepared, and the rheology and viscosity of each phase was characterized by Simeone et al. [31]. The SC-rich phase and SC solution showed Newtonian flow, whereas a shear-thinning system was found in the SA-rich phase and SA solution. The drug-loaded microparticles were prepared by dropping the SA-casein dispersions at a basic pH into calcium chloride solution [32], resulting in a sustained release of the drug from the microparticles. Moreover, CA microgel particles prepared using a spray aerosol method could interact with SC, which was detected by zeta potential studies and the dye-binding method [33]. The viscosity synergism of SA and SC in the composite dispersion after simple mixing has not been well described in literature reviews. Furthermore, the molecular interactions between SA and SC and the characteristics of CA beads incorporated with SC for drug delivery are not yet known.

Therefore, the aims of this study were to examine the molecular interactions between SA and SC in composite dispersions and films and to characterize the SC-CA beads for the delivery of anticandidals. The composite SA-SC dispersions were prepared, and the zeta potential and viscosity of the dispersions were investigated. The solid-state molecular interactions between SA and SC in the films were examined using DSC and FTIR spectroscopy. Then, the SA-SC beads were prepared using ionotropic gelation. The drugs incorporated into the beads were fluconazole (FZ) and clotrimazole (CZ), which were used for candidiasis treatments. The particle size and morphology, DEE, water uptake and erosion, in vitro drug release and anticandidal activity of the released drug were investigated. The anticandidal-loaded SC-CA beads may be utilized as a model delivery system and as drug reservoirs in tablets for oral candidiasis treatment.

2. Materials and methods

2.1. Materials

Alginate sodium salt from brown algae (100–300 cP at 25 °C) was purchased from Sigma-Aldrich, Inc. (MO, USA). The ratios of mannuronic acid to guluronic acid residues were 1.6 [34]. Casein sodium salt from bovine milk (MW = 19–25 kDa) was also obtained from Sigma-Aldrich, Inc. (MO, USA). FZ and CZ were purchased from Hubei Yuancheng Gongchuang Technology Co., Ltd. (Wuhan, China) and Changzhou Yabang Pharmaceutical Co., Ltd. (Jiangsu, China), respectively. Sodium lauryl sulfate (SLS) was obtained from S. Tong Chemicals Co., Ltd. (Bangkok, Thailand). *Candida albicans* ATCC 10231 was a gift from the Biofilm Research Group, Faculty of Dentistry, Khon Kaen University (Khon Kaen, Thailand). All other reagents used were of analytical grade and used as received.

2.2. Preparation of SA-SC dispersions

SC (0, 0.5, 1 and 2 g) was dispersed in purified water (75 mL) at 25 °C. Next, SA (2 g) was gently added and stirred using a magnetic stirrer for 2 h. The SA-SC dispersions were then adjusted to the final volume (100 mL). The zeta potential and viscosity of the dispersions obtained were characterized. Moreover, the SC dispersion in the concentration of 2%w/v was also prepared and characterized for comparison.

2.3. Characterization of SA-SC dispersions

2.3.1. Zeta potential measurement

The zeta potential of the SA-SC dispersions was measured using a laser Doppler electrophoresis analyzer (Zetasizer Model ZEN 2600, Malvern Instrument Ltd., UK). The samples were kept at 25 °C, and the dispersions were diluted using deionized water to obtain the

appropriate concentrations (count rates >20,000 counts per second) prior to measurement.

2.3.2. Viscosity determination

The viscosities of the dispersions were determined using a small sample adapter of a Brookfield Digital Rheometer (Model DV-III, Brookfield Engineering Labs Inc., Stoughton, MA) at 30 ± 2 °C. A spindle #31 was used at the shear rate over the range of 6.8–27.2 s⁻¹. The shear stress and viscosity at different shear rates were recorded.

2.4. Solubility of FZ and CZ

The solubility of FZ and CZ was determined in various media at 37 °C. Excess amounts of drug powder were added to 10 mL of medium in a test tube. Next, the mixture was sonicated for 2 h and shaken in a horizontal water bath shaker at a rate of 80 oscillations min⁻¹ at 37 °C for 5 days to achieve solubility equilibrium for the drug. A clear supernatant (1 mL) was collected, and the concentration of the drug in saturated solution (solubility value) was analyzed using HPLC.

2.5. Molecular interaction studies between SA and SC

2.5.1. Preparation of films

The molecular interactions between SA and SC in the solid state were investigated. SA, SC and SA-SC films were prepared using a casting/solvent evaporation method. The 2%w/v SA, 2%w/v SC, and 2%w/v SA-2%w/v SC dispersions were prepared following the method mentioned above, and the dispersions (20 mL) were then poured into a plastic plate (6 cm × 9.5 cm) and dried using a hot air oven at 50 °C. The dried films were peeled off and kept in a desiccator prior to use.

2.5.2. Fourier transform infrared (FTIR) spectroscopy

The FTIR spectra of the films were determined using the KBr disc method. Each sample was gently triturated with KBr powder at a weight ratio of 1:100 and then pressed with a hydrostatic press at 10 tons for 10 min. The discs were placed in a sample holder and scanned from 4000 to 450 cm⁻¹ at a resolution of 4 cm⁻¹ (Spectrum One, Perkin Elmer, Norwalk, CT).

2.5.3. Differential scanning calorimetry (DSC)

A DSC thermogram of the films was recorded using a differential scanning calorimeter (DSC822, Mettler Toledo, Switzerland). Samples (2.5–3.0 mg) was accurately weighed and placed in a 40-μL aluminum pan without an aluminum cover. The samples were heated from 30 to 450 °C at a heating rate of 10 °C min⁻¹.

2.6. Preparation of drug-loaded beads

SC (0, 0.5, 1 or 2 g) was dispersed in purified water (75 mL) at 25 °C. Next, FZ (0.25 g) or CZ (0.25 g) was gently added into the SC dispersion, and the SC dispersions containing the drugs were stirred and incubated at 25 °C overnight. Next, SA (2 g) was added to the SC dispersions containing the drugs. The composite dispersions were stirred at 25 °C for 2 h and adjusted to a final volume of 100 mL. The composite dispersions obtained were dropped through a nozzle (0.8 mm inner diameter) into a 2%w/v calcium chloride solution (240 mL) with gentle agitation. The gel beads were cured in a calcium chloride solution for 30 min, washed with 240 mL of purified water, blotted to remove excess water, and then dried at 50 °C using a hot air oven for 24 h.

2.7. Characterization of beads

2.7.1. Particle size and morphology

The particle size of the drug-loaded beads was determined using an optical microscope (Olympus CH300RF200, Olympus Optical Co., Ltd., Japan). Three hundred beads were randomized, the Feret's diameters

were measured, and the mean diameters of the beads were calculated. The particle morphology of the beads was also observed using scanning electron microscopy (SEM). The samples were mounted onto dummies, coated with gold in a vacuum evaporator, and then viewed using a scanning electron microscope (Hitachi Se3000 N, Tokyo, Japan).

2.7.2. Drug content and entrapment efficiency

The drug-loaded beads (50 mg) were immersed in pH 6.8 phosphate buffer (10 mL) to completely disintegrate the beads. The mixture was sonicated for 4 h and incubated in a shaking water bath overnight. Next, the mixture was mixed with the mixed solvent (acetonitrile: water (7:3) for FZ and acetonitrile: dipotassium phosphate (3:1) at pH 5.8 for CZ), sonicated for 15 min, and adjusted to a final volume of 50 mL. The mixture was filtered using a 0.2- μ m nylon membrane before HPLC analysis. The amount of drug was determined using HPLC analysis. The ratio of the actual to theoretical drug contents in the beads was termed as the DEE [35].

2.7.3. DSC and FTIR spectroscopy

The FTIR spectra and DSC thermogram of the beads were investigated using the same procedure described in Sections 2.5.2 and 2.5.3, respectively.

2.7.4. In vitro drug release studies

The FZ released from the beads was investigated using pH 5.8 simulated salivary fluid (SSF) as a release medium. The SSF consisted of 2.38 g Na_2HPO_4 , 0.19 g KH_2PO_4 and 8 g NaCl per liter of purified water, and the final pH was adjusted to 5.8 using phosphoric acid. The beads equivalent to 50 mg of FZ were weighed and placed in an Erlenmeyer flask containing 100 mL of release medium. The flasks were incubated in a water bath at 37 °C with shaking at 90 oscillations min^{-1} . At different time intervals, samples (5 mL) were collected and replaced with fresh medium. The amount of FZ released was analyzed using HPLC.

Due to the very low solubility of CZ, testing of the release system was changed to use the USP dissolution apparatus 2 with paddle method, (Hanson Research, Northridge, USA) because it was necessary to increase both the release medium volume and stirring efficiency to maintain a sink condition. Moreover, the release medium used was SSF with 0.1%w/v SLS added for the dissolution enhancement of CZ. The beads were equivalently weighed to 5 mg of CZ and placed in a vessel containing 350 mL of release medium at $37.0 \pm 1^\circ\text{C}$. The paddles were rotated at a rate of 50 revolution min^{-1} . Samples (7 mL) were collected and replaced with fresh media at various time intervals. The amount of CZ released was analyzed using HPLC.

2.7.5. Water uptake and erosion studies

The drug-loaded beads were placed in a small basket, immersed in SSF, and shaken occasionally in a water bath at 37 °C. After a predetermined time interval, each basket was withdrawn, blotted to remove excess water and immediately weighed on an analytical balance. The wet beads after soaking for 60 min were dried at 50 °C using a hot air oven until a constant weight of the beads was obtained. The water uptake and erosion of the beads were determined according to the following equations [36]:

$$\text{Water uptake (\%)} = \frac{(W_w - W_i)}{W_i} \times 100$$

$$\text{Erosion (\%)} = \frac{W_i - W_d - R_c}{W_i} \times 100$$

where W_w is the weight of the wet beads, W_i is the initial weight of the beads, W_d is the weight of the beads after drying process, and R_c is the mean amount of drug released at 60 min obtained from in vitro release studies.

2.7.6. Anticandidal activity study

The FZ and CZ released from the beads were tested for antimicrobial activity against *C. albicans* using by an agar diffusion method that has been used for evaluating antifungal activity of drug formulations [37–39]. *C. albicans* was inoculated into 20 mL of Sabouraud dextrose broth. At the exponential period of growth, the culture broth was diluted. The concentration of *C. albicans* was diluted to 10^6 CFU mL^{-1} . Next, plates with Sabouraud dextrose agar (20 mL) were prepared in which 200 μL of the microbe suspension was added and spread uniformly with sterile cotton swabs. The agar was punched using a Pasteur pipet to make 6-mm diameter holes, and four holes were made in each plate. The 45 μL solutions of the negative control, positive control and release medium from the drug release testing were dropped into the holes. All plates were incubated at $32.0 \pm 1.0^\circ\text{C}$ for 24 h. Next, the diameters of the inhibition zones were measured. The negative controls included SSF with or without 0.1%w/v SLS for CZ or FZ, respectively. The positive controls included 80 and 2.0 $\mu\text{g mL}^{-1}$ of FZ and CZ in SSF with or without 0.1%w/v SLS, respectively. To test the anticandidal activities, the FZ and CZ release media were collected at 60 and 120 min from the start of the release studies, respectively. In addition, this method was validated by investigating relationship between drug concentration and inhibition zone. The inhibition zones of FZ concentrations of 60, 80, and 100 $\mu\text{g mL}^{-1}$ were found to be 8.19 ± 0.85 , 10.27 ± 0.31 , and 11.53 ± 0.24 mm ($n = 3$), respectively, whereas CZ in concentrations of 1, 2, and 5 $\mu\text{g mL}^{-1}$ provided 17.75 ± 0.37 , 19.89 ± 0.08 , and 21.06 ± 0.84 mm ($n = 3$) of inhibition zone, respectively.

2.8. HPLC analysis

The concentration of FZ or CZ in the samples was analyzed using an HPLC system that consisted of Waters 1525 binary pumps, 2489 dual absorbance detector and Waters Breeze Software 2.0 versions (Waters Corporation, MA, USA). A reversed-phase HPLC using a C-18 column (Mightysil RP-18 GP, 4.6 mm \times 150 mm, 5- μ m particle size; Kanto Chemical Co., Inc., Tokyo, Japan) was employed. The mobile phases of FZ and CZ were acetonitrile: water (30:70) and acetonitrile: 0.025 M dipotassium phosphate (K_2HPO_4) (3:1) at pH 5.8, respectively. The flow rate of the mobile phases was 1 mL min^{-1} . The detection wavelength was set at 210 nm. The retention times of FZ and CZ were approximately 3.1 and 4.5 min, respectively. Under these conditions, good linearity and reproducibility were shown over the range of 10–120 $\mu\text{g mL}^{-1}$ for FZ and 0.2–100 $\mu\text{g mL}^{-1}$ for CZ.

3. Results and discussion

3.1. Molecular interaction between SA and SC

The molecular interaction between SA and SC was investigated in the form of dispersions and films. The SA-SC dispersions showed white turbid liquids due to the milky appearance of SC when dispersed in water. The pH of all dispersions in this study was found in the range of 5.9–6.5. The zeta potential of the 2%w/v SC dispersion was -13.3 ± 0.87 mV ($n = 3$), whereas that of the 2%w/v SA dispersion was found to be -96.6 ± 3.75 mV ($n = 3$). The pH of the SA-SC dispersions was higher than the pK_a (3.38–3.65) of SA [8] and the isoelectric point (4.6–4.9) of SC [23]. This led to ionization of carboxyl groups on SA and SC molecules to display a negative charge. The 2%w/v SA dispersions incorporated with 0.5, 1, and 2%w/v SC also presented a negative charge of zeta potential values that were determined to be -56.5 ± 3.12 , -46.7 ± 1.06 , and -41.4 ± 0.15 mV ($n = 3$), respectively. The increase in SC content caused a decrease in zeta potential values of the SA-SC dispersions. Apart from the zeta potential, the viscosity of the dispersions was also reported, and the relationship between the shear rate and viscosity of the dispersions is shown in Fig. 1. The 2%w/v SC dispersion showed very low viscosity, but it still presented a shear-thinning system because the viscosity value decreased with an increasing shear

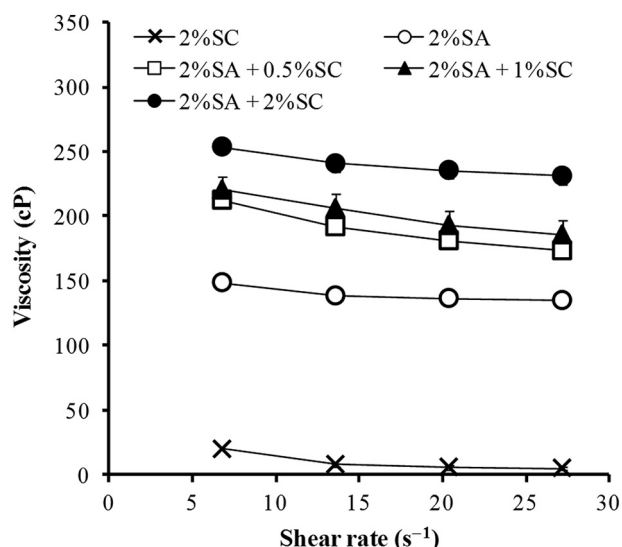


Fig. 1. Relationship between the shear rate and viscosity of the SA, SC, and SA-SC dispersions. Each value indicates the mean \pm SD, $n = 3$.

rate [40]. The 2% SA dispersion presented higher viscosity than the 2% SC dispersion, and demonstrated shear-thinning behavior as well. The addition of SC resulted in an increase in the viscosity of the SA dispersion, such that the higher the amount of SC that was added, the higher the observed viscosity of the SA-SC dispersion (Fig. 1). These results suggested that the viscosity synergism could be explained by a molecular interaction between both components.

DSC and FTIR spectroscopy were used to investigate the solid-state molecular interactions of SA and SC in this study. The SA films showed a small exothermic peak at 224 °C and was followed by an endothermic peak at approximately 230 °C (Fig. 2a). This finding may be due to a recrystallization and phase transition of SA after heat induction [41,42]. The first and second exothermic degradation peaks were found at 251 °C and 367 °C, respectively. The SC films presented two exothermic peaks at 297 °C and 353 °C (Fig. 2a). The SA-SC films showed an exothermic peak at 225 °C and was followed by an endothermic peak at approximately 230 °C. The first degradation peak of SA was slightly shifted to a higher temperature (253 °C). Moreover, both exothermic peaks at 343 °C and 381 °C were found for the composite films. Changes in the

thermal properties of the SA-SC films suggested that molecular interactions occurred after a simple mixing of both components.

The FTIR spectra of the SA, SC, and SA-SC films are illustrated in Fig. 2b. The SA films showed absorption peaks at 3445 cm^{-1} (O—H stretching), 1617 cm^{-1} (COO^- asymmetric stretching), 1412 cm^{-1} (COO^- symmetric stretching) and 1030 cm^{-1} (C—O—C stretching), which were similar to previous studies [41,42]. For the SC films, the peak at 3436 cm^{-1} corresponded to the O—H stretching vibrations, which overlapped with the N—H stretching vibrations. The strong peak at 1638 cm^{-1} was due to the C=O stretching vibrations of the amide I groups, and the peaks at 1535 and 1242 cm^{-1} were from N—H bending (amide II) and C—N stretching vibrations, respectively [28,43]. The spectra of the SA-SC films showed that the O—H stretching peaks coupled with the N—H stretching peaks and moved to lower wavenumbers, while the peaks of amide I and II were shifted to higher wavenumbers. Moreover, the C—O—C stretching peaks of SA also shifted to 1038 cm^{-1} . These results suggested that the carboxyl and hydroxyl groups of SA could strongly interact with the amide I and II groups of SC via intermolecular hydrogen bonding.

Taken together, the present model of the SA-SC composites is illustrated in Fig. 3. SA side chains could possibly interact with SC micelles that are covered with κ -caseins. The outer parts of the surface are known as caseinomacropetide chains [22], and the amino acids in this chain may potentially interact with SA. For example, the last three amino acids in the sequence of κ -caseins are threonine, alanine and valine [44]. The amide I and II groups of these amino acids could interact with the hydroxyl and carboxyl groups of SA via hydrogen bonding, resulting in the formation of SA-SC soluble complexes and an enhanced complexity of the matrix network in the dispersions. This result may not only lead to a suppression of the overall negative charge and a decreasing zeta potential value but also an enhancement of the viscosity of the composite dispersions. In addition, the SA-SC complexes influence the thermal behavior of the composite films.

3.2. Particle characteristics and DEE of the beads

The particle sizes of the beads are listed in Table 1. The CA beads loaded with FZ or CZ showed a comparable particle size of approximately 825–855 μm . The CA beads showed a relatively spherical shape with a few fractures on the particle surface. However, the CZ-loaded CA bead presented a rougher surface than that of the FZ-loaded CA beads (Fig. 4). The particle size of the SC-CA beads tended to increase

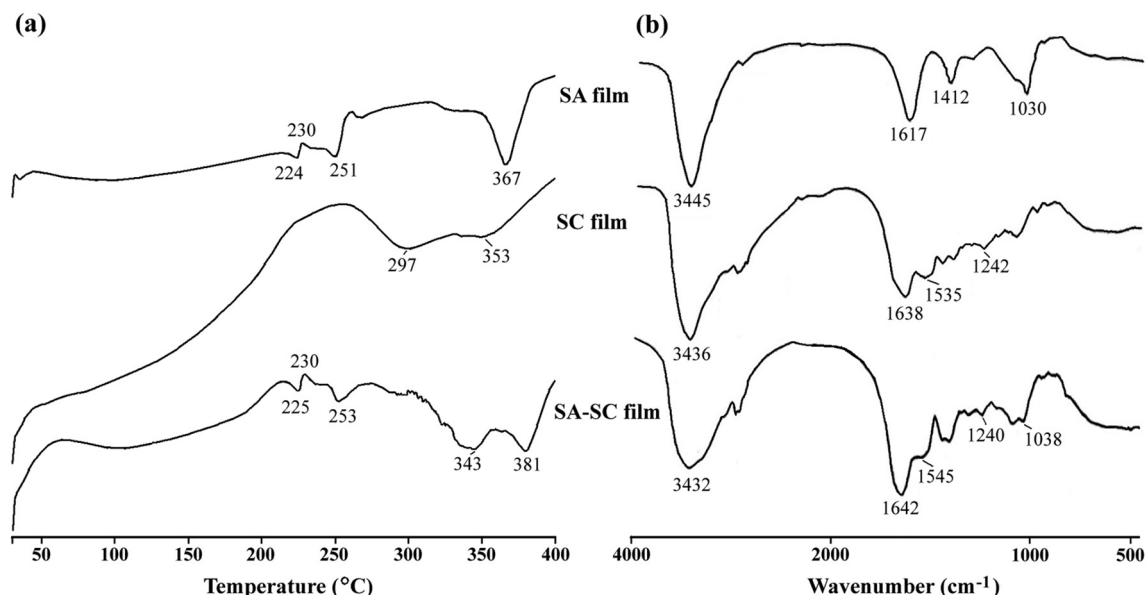


Fig. 2. DSC thermogram (a) and FTIR spectra (b) of SA, SC, and SA-SC films.

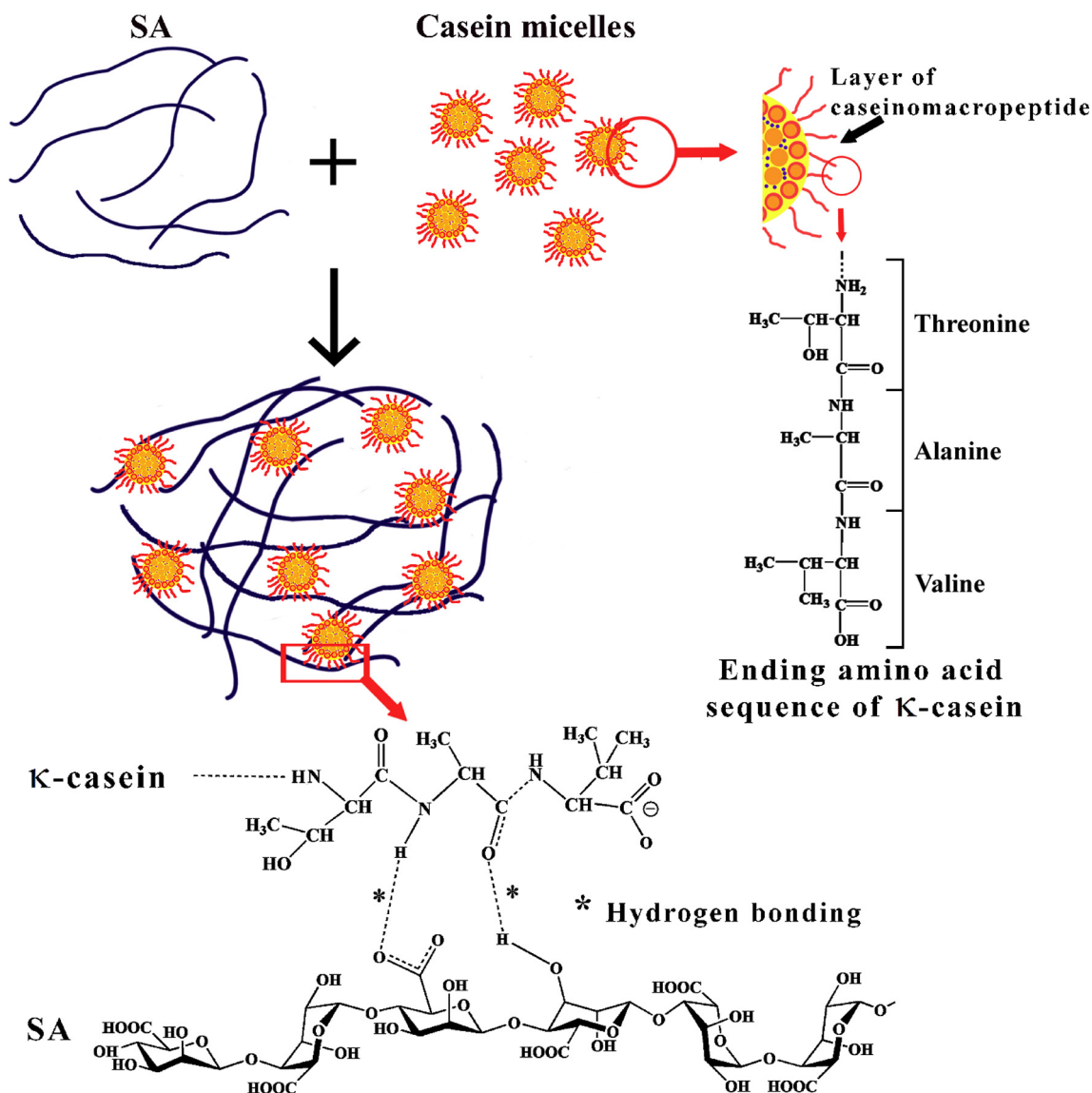


Fig. 3. Schematic presentation of the molecular interactions between SA and SC.

with increasing SC content (Table 1) because the higher density and enhanced viscosity of the SC-SA dispersion in the droplets may cause lower shrinkage during cross-linking with calcium ions. The SEM image also demonstrated that the 2%SC-CA beads containing FZ or CZ were larger than the CA beads containing the drugs, but a different surface morphology was observed (Fig. 4).

The FZ and CZ drug content of the beads decreased with increasing SC amounts (Table 1) due to an increase in the polymer content in the bead preparation [45]. The DEE of the CA and SC-CA beads with FZ was in the range of 19.3–23.3%. An increase from 0.5 to 1% SC appeared to decrease the %DEE, but the addition of 2% SC resulted in an increase in the %DEE (Table 1). The loss of FZ from the beads was due to water

Table 1

Components and characteristics of SC-CA beads loaded with FZ or CZ.

Components	Particle size ^a (μm)	Drug content ^b (%w/w)	DEE ^b (%)	T ₂₅ ^b (min)	T ₅₀ ^b (min)
0.25%w/v FZ					
2%w/v SA	825.2 ± 123.4	2.19 ± 0.03	21.91 ± 0.26	–	<2
+0.5%w/v SC	855.6 ± 101.6	1.75 ± 0.03	19.27 ± 0.36	–	4.23 ± 0.99
+1.0%w/v SC	978.1 ± 125.0	1.53 ± 0.03	19.86 ± 0.36	–	6.29 ± 1.68
+2.0%w/v SC	1117.8 ± 173.6	1.37 ± 0.03	23.27 ± 0.48	–	7.79 ± 0.63
0.25%w/v CZ					
2%w/v SA	849.7 ± 78.4	10.26 ± 0.01	93.25 ± 0.08	163.62 ± 4.57	>240
+0.5%w/v SC	832.8 ± 86.7	7.42 ± 0.07	81.59 ± 0.73	161.96 ± 2.24	>240
+1.0%w/v SC	896.2 ± 78.6	6.56 ± 0.05	85.23 ± 0.64	186.64 ± 6.66	>240
+2.0%w/v SC	1100.3 ± 114.3	5.64 ± 0.03	95.59 ± 0.47	195.76 ± 8.43	>240

–: Could not be calculated.

^a n = 300.

^b n = 3.

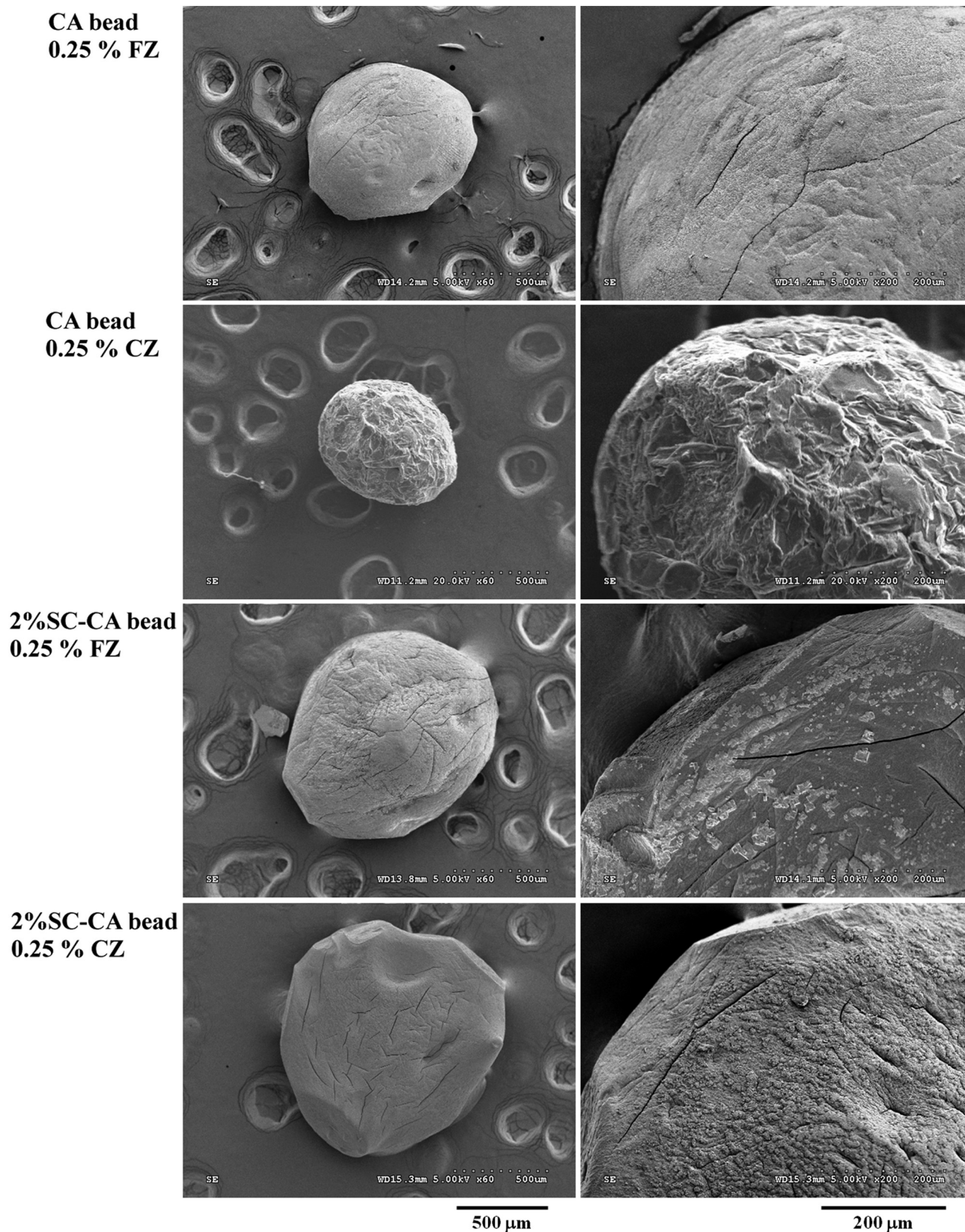


Fig. 4. Particle and surface morphology of CA and 2%SC-CA beads prepared using 0.25% FZ or CZ.

leakage from the beads during the preparation period. Moreover, FZ was slightly soluble in water, such that the water solubility of FZ was found to be $6.69 \pm 0.08 \text{ mg mL}^{-1}$ ($n = 3$) in this study. The complete dissolution of 0.25% FZ in the dispersions before the cross-linking process

elicited a loss of FZ in the water leakage process. Incorporation of 2% SC could increase the %DEE of the CA beads due to the interaction between SA and SC, which created a denser matrix network that functioned as a barrier to prevent water leakage from the beads.

The %DEE of the CA or SC-CA beads for CZ was remarkably greater than that for FZ (Table 1) because water solubility of the drug mainly influenced the DEE values [46]. CZ was practically insoluble in water and the solubility was found to be $3.47 \pm 0.44 \mu\text{g mL}^{-1}$ ($n = 3$). Thus, CZ particles were suspended in the dispersion before cross-linking, resulting in very low CZ loss during the water leakage process of the wet beads. However, the addition of SC in the dispersion could enhance CZ solubility, such that the CZ solubility in the 0.5, 1, and 2%w/v SC dispersions was 4.13 ± 0.23 , 7.75 ± 1.31 , and $19.20 \pm 1.12 \mu\text{g mL}^{-1}$ ($n = 3$). These results revealed the micellization property of SC that has been previously reported with many hydrophobic drugs [25,26,47,48]. Enhancement of CZ solubility may cause a decrease in the %DEE for the CA beads using 0.5 and 1%SC. However, a denser matrix network of the 2%SC-CA beads could prevent drug loss during cross-linking. Thus, a higher %DEE was obtained.

3.3. DSC and FTIR patterns

The molecular interactions of the CA or 2%SC-CA beads loaded with drugs were investigated using FTIR spectroscopy as shown in Fig. 5. The CA beads without drugs presented a change in the FTIR spectra compared to the SA films (Fig. 2). The higher wavenumber shifts of the COO^- (asymmetric) and COO^- (symmetric) stretching peaks to 1626 and 1435 cm^{-1} , respectively, and the lower wavenumber shift of O—H stretching peak to 3436 cm^{-1} was observed. The 2%SC-CA beads without drugs caused shifts of the amide I (1643 cm^{-1}) and amide II (1544 cm^{-1}) peaks of SC, and the FTIR spectrum of these beads was similar to that of a freeze-dried casein-CA microparticle previously reported [32]. The addition of FZ into the CA beads resulted in a shift of the COO^- (symmetric) stretching peak to 1425 cm^{-1} . Moreover, the amide II peak of SC in the SC-CA beads moved to a higher wavenumber with the addition of FZ. The 2%SC-CA beads loaded with CZ showed a shift of COO^- (symmetric) stretching peak of SA. However, the SA-CA beads loaded with FZ or CZ did not present the peak characteristics of FZ or CZ. This result is likely to be due to a very low amount of drug in the beads when compared with SC and CA. These results suggested that the SC-CA beads still demonstrated FTIR features characteristic of the molecular interactions between SC and SA after cross-linking with

calcium ions, and FZ and CZ loaded into the beads could possibly interact with SA or SC via hydrogen bonding.

DSC thermograms of the CA and 2%SC-CA beads with drugs are presented in Fig. 6. The thermal behavior of the CA beads without drug showed an endothermic peak followed by an exothermic peak approximately $190\text{--}210^\circ\text{C}$ and exothermic degradation peak at 297°C . Incorporation of SC did not affect the DSC thermogram of the CA beads. FZ had a sharp melting peak at 142°C . The SC-CA beads loaded with FZ did not show the melting peak of FZ. This result suggested that FZ was completely dissolved and dispersed as an amorphous form in the bead matrix. In contrast, the CA and SC-CA beads presented a small melting peak of CZ at approximately $142\text{--}148^\circ\text{C}$, suggesting that some CZ crystals were embedded in the bead matrix due to the low solubility of CZ.

3.4. Water uptake and erosion

The SSF with or without 0.1%SLS was used to test the water uptake and erosion of CA or SC-CA beads containing FZ or CZ, respectively, such that the medium used was the same as that used during drug release testing. The % water uptake of the beads increased with an increase in the testing time. The water uptake and erosion of the CA and SC-CA beads loaded with FZ and CZ at 1 h of the test are presented in Fig. 7. The % water uptake of the CA beads gradually decreased when adding the SC dispersions of 0.5 and 1%, but the 2%SC-CA beads showed a higher % water uptake than that of the 1%SC-CA beads. The beads with FZ and CZ showed a similar effect as the addition of SC on water uptake results, but the % water uptake of the beads with CZ was greater than with FZ (Fig. 7a and b). The use of 0.1% SLS for CZ raises the question about the effect of this surfactant on water uptake values. To prove the effect of SLS, the water uptake of the CA beads containing CZ in SSF without 0.1% SLS was examined, and the result was $1114.72 \pm 75.08\%$ water uptake at 1 h. This result indicated that the SLS did not affect the water uptake of the CA beads with CZ. For erosion results, incorporation of SC decreased % erosion of the beads. The % erosion of the beads with FZ was higher than that with CZ.

The water uptake of the CA beads occurred because CA could be changed to SA when exposed to a medium containing monovalent cations [49], for example, the SSF used in this study. The water absorption

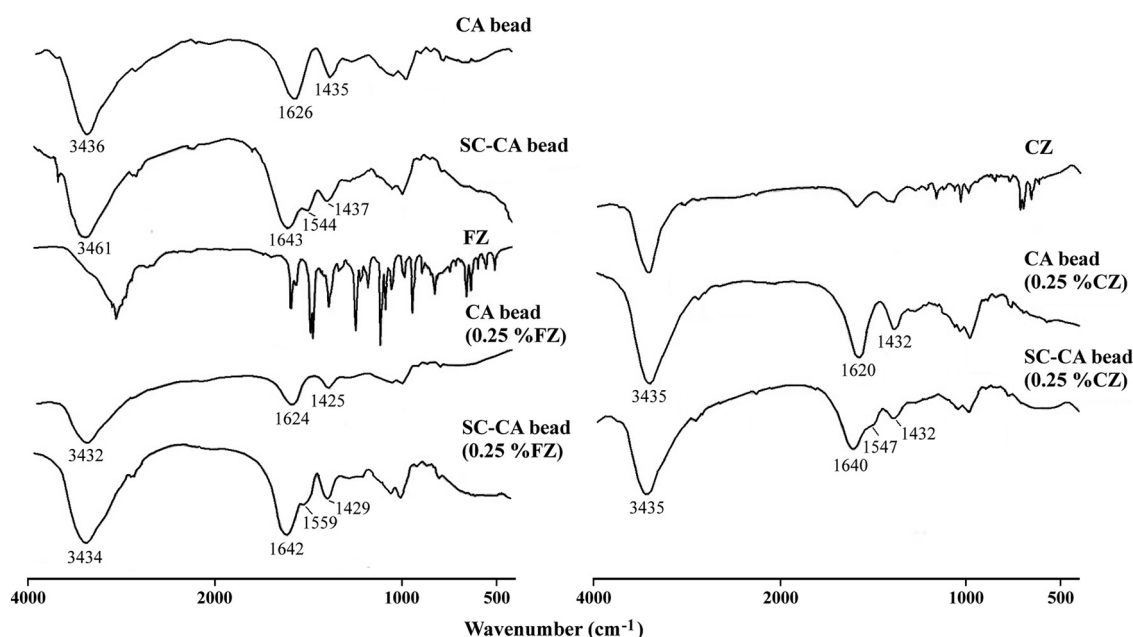


Fig. 5. FTIR spectra of CA and 2%SC-CA beads prepared using 0.25% FZ or CZ.

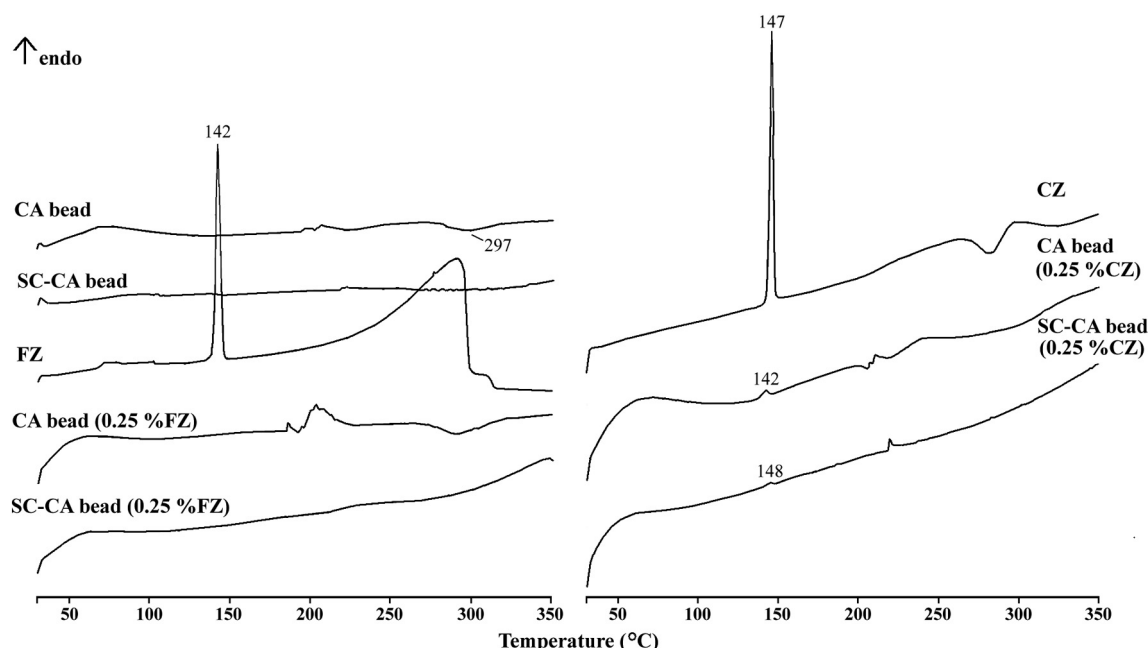


Fig. 6. DSC thermograms of CA and 2%SC-CA beads prepared using 0.25% FZ or CZ.

properties of the CA beads decreased with an increase in SC content, suggesting that the molecular interaction between SA and SC induced a denser matrix structure of the beads. This also led to a decrease in the dissolution of soluble substances in the matrices, such as SA, SC, and SC micelles. Moreover, this study showed that the incorporation of 1%SC in the beads could create the densest matrix structure of the beads, in which the lowest % water uptake was obtained. However, the % water uptake of the beads containing FZ was remarkably lower than for those of the beads containing CZ, whereas opposite results of % erosion were obtained. It is possible that the CZ particles suspended in the SA or SA-SC dispersions may hinder the cross-linking process of SA promoted by calcium ions, in contrast with FZ, which was completely dissolved when a similar concentration of 0.25%w/v was used. This result may lead to higher free SA remaining in the beads containing CZ, which could cause greater water uptake at the time of the investigation. Furthermore, the gel formation of SA and SC embedded in the beads containing CZ possibly acted as a barrier to prevent the soluble

substances from leaching out of the beads. Thus, a lower % erosion of the beads containing CZ was obtained.

3.5. In vitro drug release

The SSF was used as a release medium for the beads containing FZ. For the beads loaded with CZ, 0.1% SLS was added to enhance CZ solubility. The CZ solubility in SSF without and with 0.1% SLS was 3.04 ± 0.52 and $159.81 \pm 2.13 \mu\text{g mL}^{-1}$ ($n = 3$), respectively. The use of 0.1% SLS yielded a 52.3-fold increase in CZ solubility in SSF. For FZ, a $6.16 \pm 0.03 \text{ mg mL}^{-1}$ ($n = 3$) solubility value was observed in SSF. Thus, the expected maximum of drug concentration in the release system was lower than 10% of drug solubility [50], resulting in a perfect sink condition of the release testing system.

The FZ release profiles showed a complete release after testing within 60 min (Fig. 8a). $T_{50\%}$, the time to achieve release of 50% of drug content, was calculated as a drug release rate for comparison.

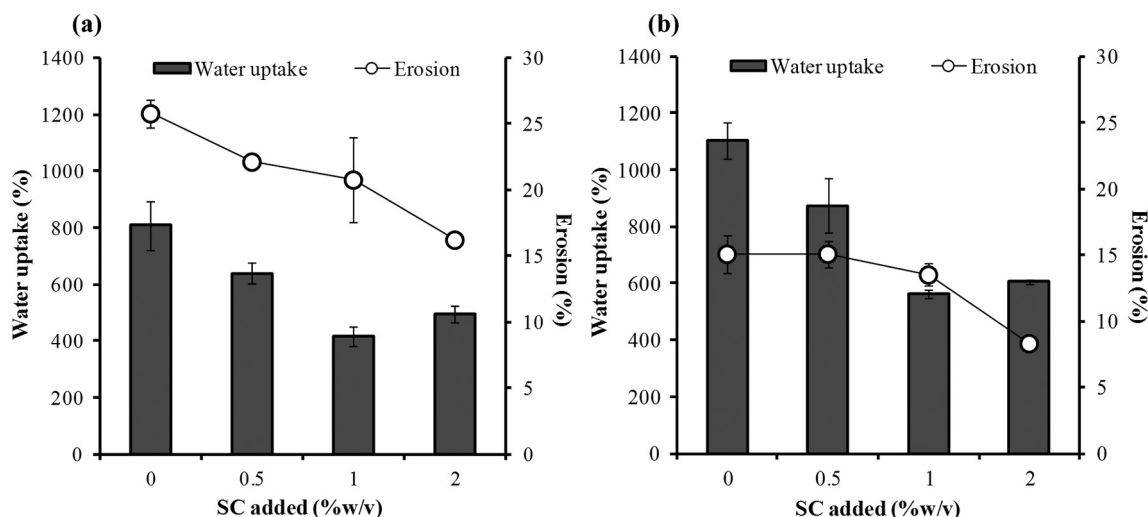


Fig. 7. Water uptake and erosion of CA beads prepared using various contents of SC and 0.25% FZ (a) or CZ (b). Each value indicates the mean \pm SD, $n = 3$.

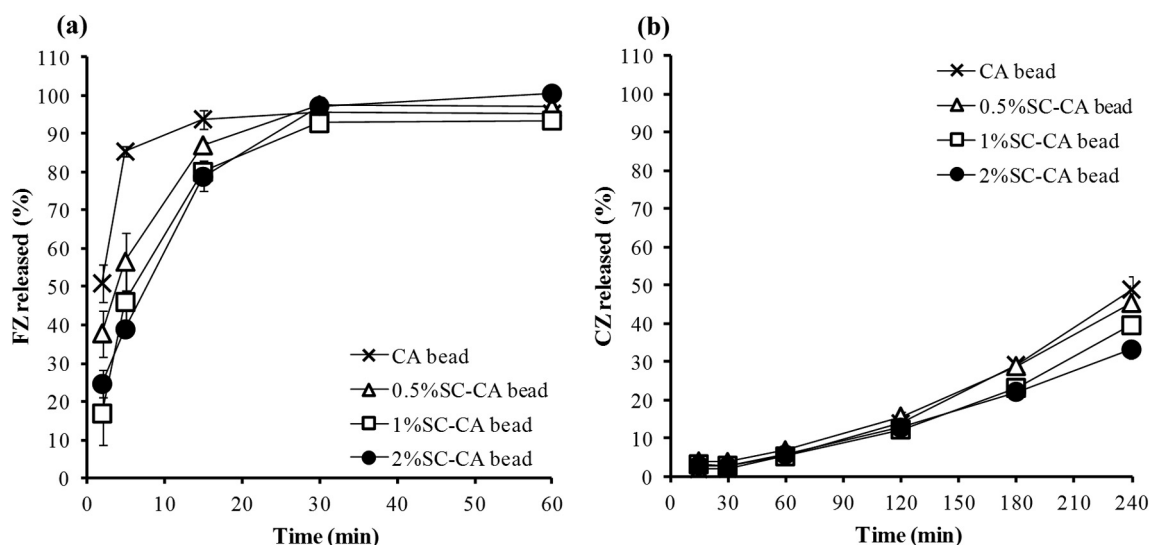


Fig. 8. Drug release profiles of CA and SC-CA beads loaded with 0.25% FZ (a) or CZ (b). Each value indicates the mean \pm SD, $n = 3$.

The higher the $T_{50\%}$ value was, the slower the drug release rate obtained. These results showed that the CA beads presented the most rapid drug release, whereas the drug release seemed to be slower (higher $T_{50\%}$ value) with the addition of SC into the beads (Table 1). The higher the amount of SC added, the greater the $T_{50\%}$ value that was obtained. The FZ release from the beads was faster than the release of CZ as shown in Fig. 8b. Less than 50% of the CZ amount in the beads was released within 240 min of the test. Thus, $T_{25\%}$ was used for comparison (Table 1). An increase in the amount of SC added resulted in higher $T_{25\%}$ values, indicating that the addition of SC to the beads could possibly retard CZ release, although it enhanced the solubility of CZ. These results suggested that the addition of SC into the CA beads could slow down the release of drug due to the denser matrix structure and lower water uptake of the SC-CA beads.

3.6. Anticandidal activity

The anticandidal activity of FZ and CZ after release from the beads was investigated in this study. The concentration of FZ or CZ in the samples and inhibition zone are presented in Fig. 9. The FZ in the concentration of $80 \mu\text{g mL}^{-1}$ (positive control) provided an inhibition zone diameter of $9.57 \pm 0.94 \text{ mm}$ ($n = 3$). The concentrations of FZ released

from the CA and SC-CA beads were over the range of $80.1\text{--}89.8 \mu\text{g mL}^{-1}$, which could inhibit *C. albicans* with an inhibition zone diameter of $9.0\text{--}12.9 \text{ mm}$ (Fig. 9a). The inhibition zone seemed to increase with increasing FZ concentrations during the release testing. The SC loaded in the beads did not obviously affect the antimicrobial activity of FZ.

The $2 \mu\text{g mL}^{-1}$ concentration of CZ, which served as a positive control, showed a $19.89 \pm 0.08 \text{ mm}$ ($n = 3$) inhibition zone (Fig. 9b). The CA beads demonstrated an obvious decrease of inhibition zone, although the CZ concentration ($2.02 \mu\text{g mL}^{-1}$) was similar to the positive control. This result suggested a lower efficiency of CZ released from the CA beads. However, the decrease in CZ concentration with increasing amounts of SC in the CA beads still provided the similar results of inhibition zone when compared to the positive control, suggesting that a higher efficiency of CZ released. One potential explanation is that some of the CZ released may be in the form of CZ-loaded SC micelles, which would likely be nanoparticles. The SC nanoparticles could enhance the antimicrobial activity of lipophilic substances, for example, thymol-loaded SC nanoparticles [51]. Moreover, CZ loaded in lipid nanoparticles showed more activity against *C. albicans* than did a CZ solution [52]. These results differed from that of FZ because FZ is a hydrophilic molecule that shows low affinity with the hydrophobic core of SC micelles. This result led to a low probability to form FZ-loaded SC

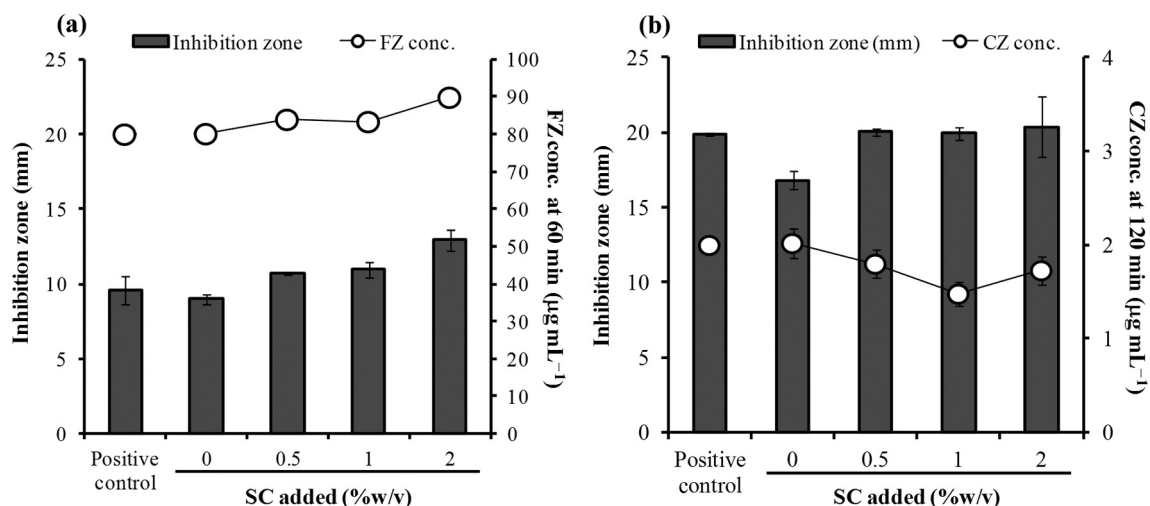


Fig. 9. Anticandidal activity of 0.25% FZ (a) or CZ (b) released from CA beads prepared using varying amounts of SC. Each value indicates the mean \pm SD, $n = 3$.

micelles. However, these anticandidal activity studies suggested that CZ and FZ loaded in the CA or SC-CA beads are still effective against *C. albicans*.

4. Conclusions

SA can interact with SC by simple mixing of the dispersions. Complexation between SA and SC occurs due to intermolecular hydrogen bonding between the carboxyl or hydroxyl groups of SA and amide I or II groups of SC, resulting in viscosity synergism for the composite dispersions. The SC-CA beads with FZ or CZ added can be prepared using calcium ions as a cross-linking agent. FZ is present in an amorphous form, whereas the crystalline form of CZ is found in the beads, and the form is dependent on the water solubility of the drugs. The CA beads can be reinforced by incorporating SC, resulting in an increase in %DEE when using 2%SC, a decrease in water uptake and erosion, and a retardation of drug release. Moreover, the solubility of CZ can be enhanced by micellization of SC, thereby becoming more effective against *C. albicans* for CZ released from the SC-CA beads. This study shows that the molecular interactions between SA and SC can reinforce the CA beads, and the SC-CA beads show good potential for delivery of anticandidals to treat oral candidiasis.

Acknowledgments

The authors wish to thank the Thailand Research Fund (Bangkok, Thailand) and Khon Kaen University (Khon Kaen, Thailand) for research funding (Grant no. BRG6080016). Scholarship under the Post-Doctoral Training Program from Research Affairs and Graduate School, Khon Kaen University, Thailand (Grant no. 59148) for R.K. is gratefully acknowledged. We also thank the Biofilm Research Group, Faculty of Dentistry, Khon Kaen University (Khon Kaen, Thailand) for supporting *C. albicans* ATCC 10231.

References

- [1] E. Dickinson, Interfacial structure and stability of food emulsions as affected by protein-polysaccharide interactions, *Soft Matter* 4 (2008) 932–942.
- [2] W. Wijaya, A.R. Patel, A.D. Setiowati, P. Van der Meer, Functional colloids from proteins and polysaccharides for food applications, *Trends Food Sci. Technol.* 68 (2017) 56–69.
- [3] M. Evans, I. Ratcliffe, P.A. Williams, Emulsion stabilisation using polysaccharide-protein complexes, *Curr. Opin. Colloid Interface Sci.* 18 (2013) 272–282.
- [4] R. Mohammadi, M.A. Mohammadifar, M. Rouhi, M. Kariminejad, A.M. Mortazavian, E. Sadeghi, S. Hasanvand, Physico-mechanical and structural properties of eggshell membrane gelatin-chitosan blend edible films, *Int. J. Biol. Macromol.* 107 (2018) 406–412.
- [5] A. Jain, D. Thakur, G. Ghoshal, O.P. Katore, U.S. Shivhare, Characterization of microcapsulated β -carotene formed by complex coacervation using casein and gum tragacanth, *Int. J. Biol. Macromol.* 87 (2016) 101–113.
- [6] C. Chang, T. Wang, Q. Hu, Y. Luo, Caseinate-zein-polysaccharide complex nanoparticles as potential oral delivery vehicles for curcumin: effect of polysaccharide type and chemical cross-linking, *Food Hydrocoll.* 72 (2017) 254–262.
- [7] R. Shaddel, J. Hesari, S. Azadmard-Damirchi, H. Hamishehkar, B. Fathi-Achachlouei, Q. Huang, Use of gelatin and gum Arabic for encapsulation of black raspberry anthocyanins by complex coacervation, *Int. J. Biol. Macromol.* 107 (2018) 1800–1810.
- [8] K.I. Draget, Alginates, in: G.O. Philips, P.A. Williams (Eds.), *Handbook of Hydrocolloids*, Woodhead Publishing, Cambridge 2000, pp. 379–395.
- [9] V. Pillay, C.M. Dangor, T. Govender, K.R. Moopanan, N. Hurbans, Ionotropic gelation: encapsulation of indomethacin in calcium alginate gel discs, *J. Microencapsul.* 15 (1998) 215–226.
- [10] S. Sugawara, T. Imai, M. Otogiri, The controlled release of prednisolone using alginate gel, *Pharm. Res.* 11 (1994) 272–277.
- [11] M.R. El-Aassar, E.E. Hafez, N.M. El-Deeb, M.M.G. Fouda, Microencapsulation of lectin anti-cancer agent and controlled release by alginate beads, biosafety approach, *Int. J. Biol. Macromol.* 69 (2014) 88–94.
- [12] E.E. Ozseker, A. Akkaya, Development of a new antibacterial biomaterial by tetracycline immobilization on calcium-alginate beads, *Carbohydr. Polym.* 151 (2016) 441–451.
- [13] T. Haider, Q. Husain, Calcium alginate entrapped preparations of *Aspergillus oryzae* β -galactosidase: its stability and applications in the hydrolysis of lactose, *Int. J. Biol. Macromol.* 41 (2007) 72–80.
- [14] S. Puttipipatkachorn, T. Pongjanyakul, A. Pripem, Molecular interaction in alginate beads reinforced with sodium starch glycolate or magnesium aluminum silicate, and their physical characteristics, *Int. J. Pharm.* 293 (2005) 51–62.
- [15] T. Pongjanyakul, S. Puttipipatkachorn, Xanthan-alginate composite gel beads: molecular interaction and in vitro characterization, *Int. J. Pharm.* 331 (2007) 61–71.
- [16] T. Pongjanyakul, Characterization of microcrystalline cellulose loaded diclofenac calcium alginate gel beads in vitro, *Pharmazie* 62 (2007) 493–498.
- [17] T. Pongjanyakul, T. Rongthong, Enhanced entrapment efficiency and modulated drug release of alginate beads loaded with drug-clay intercalated complexes as microreservoirs, *Carbohydr. Polym.* 81 (2010) 409–419.
- [18] P.F. Almeida, A.J. Almeida, Cross-linked alginate-gelatin beads: a new matrix for controlled release of pindolol, *J. Control. Release* 97 (2004) 431–439.
- [19] A. Marozienė, C.G. De Kruijff, Interaction of pectin and casein micelles, *Food Hydrocoll.* 14 (2000) 391–394.
- [20] N.X. Sun, Y. Liang, B. Yu, C.P. Tan, B. Cui, Interaction of starch and casein, *Food Hydrocoll.* 60 (2016) 572–579.
- [21] P. Walstra, J.T.M. Wouters, T.J. Geurts, *Dairy Science and Technology*, second ed. Taylor & Francis, Boca Raton, 2006.
- [22] D.G. Dalgleish, M. Corredig, The structure of the casein micelle of milk and its changes during processing, *Annu. Rev. Food Sci. Technol.* 3 (2012) 449–467.
- [23] A.O. Elzoghby, W.S. El-Fotoh, N.A. Elgindy, Casein-based formulations as promising controlled release drug delivery systems, *J. Control. Release* 153 (2011) 206–216.
- [24] D.S. Horne, S.R. Euston, Simulating the self-association of caseins, *Food Hydrocoll.* 19 (2005) 379–386.
- [25] F.C. Millar, O.I. Corrigan, Influence of sodium caseinate on the dissolution rate of hydrochlorothiazide and chlorothiazide, *Drug Dev. Ind. Pharm.* 17 (1991) 1593–1607.
- [26] F.C. Millar, O.I. Corrigan, Dissolution mechanism of ibuprofen-casein compacts, *Int. J. Pharm.* 92 (1993) 97–104.
- [27] W.A. Knepp, A. Jayakrishnan, J.M. Quigg, H.S. Sitren, J.J. Bagnall, E.P. Goldberg, Synthesis, properties, and intratumoral evaluation of mitoxantrone-loaded casein microspheres in Lewis lung carcinoma, *J. Pharm. Pharmacol.* 45 (1993) 887–891.
- [28] A.J.P. Santinho, N.L. Pereira, O.D. Freitas, J.H. Collett, Influence of formulation on the physicochemical properties of casein microparticles, *Int. J. Pharm.* 186 (1999) 191–198.
- [29] A.O. Elzoghby, M.W. Helmy, W.M. Samy, N.A. Elgindy, Novel ionically crosslinked casein nanoparticles for flutamide delivery: formulation, characterization, and in vivo pharmacokinetics, *Int. J. Nanomedicine* 8 (2013) 1721–1732.
- [30] K. Pan, Q. Zhong, S.J. Baek, Enhanced dispersibility and bioactivity of curcumin by encapsulation in casein nanoparticles, *J. Agric. Food Chem.* 61 (2013) 6036–6043.
- [31] M. Simeone, A. Alfani, S. Guido, Phase diagram, rheology and interfacial tension of aqueous mixtures of Na-caseinate and Na-alginate, *Food Hydrocoll.* 18 (2004) 463–470.
- [32] Z. He, X. Zhang, W. Qi, R. Huang, R. Su, Alginate-casein microspheres as bioactive vehicles for nutrients, *Trans. Tianjin Univ.* 21 (2015) 383–391.
- [33] S.H. Ching, B. Bhandari, R. Webb, N. Bansal, Visualizing the interaction between sodium caseinate and calcium alginate microgel particles, *Food Hydrocoll.* 43 (2015) 165–171.
- [34] D. Lemoine, F. Wauters, S. Bouchend'homme, V. Préat, Preparation and characterization of alginate microspheres containing a model antigen, *Int. J. Pharm.* 176 (1998) 9–19.
- [35] K. Wang, Z. He, Alginate-konjac glucomannan-chitosan beads as controlled release matrix, *Int. J. Pharm.* 244 (2002) 117–126.
- [36] W. Sutananta, D.Q.M. Craig, J.M. Newton, An evaluation of the mechanisms of drug release from glyceride bases, *J. Pharm. Pharmacol.* 47 (1995) 182–187.
- [37] K. Winnicka, M. Wroblewska, P. Wieczorek, P.T. Sacha, E. Trynieszewska, Hydrogel of ketoconazole and PAMAM dendrimers: formulation and antifungal activity, *Molecules* 17 (2012) 4612–4624.
- [38] A.I. Mendes, A.C. Silva, J.A.M. Catita, F. Cerqueira, C. Gabriel, C.M. Lopes, Miconazole-loaded nanostructured lipid carriers (NLC) for local delivery to the oral mucosa: improving antifungal activity, *Colloids Surf. B: Biointerfaces* 111 (2013) 755–763.
- [39] P. Verma, M. Ahuja, Optimization, characterization and evaluation of chitosan-tailored cubic nanoparticles of clotrimazole, *Int. J. Biol. Macromol.* 73 (2015) 138–145.
- [40] C.H. Lee, V. Moturi, Y. Lee, Thixotropic property in pharmaceutical formulations, *J. Control. Release* 136 (2009) 88–98.
- [41] T. Pongjanyakul, A. Pripem, S. Puttipipatkachorn, Investigation of novel alginate-magnesium aluminum silicate microcomposite films for modified release tablets, *J. Control. Release* 107 (2005) 343–356.
- [42] T. Pongjanyakul, Alginate-magnesium aluminum silicate films: importance of alginate block structures, *Int. J. Pharm.* 365 (2009) 100–108.
- [43] M. Perada, M.I. Aranguren, N.E. Marcovich, Effect of crosslinking on the properties of sodium caseinate films, *J. Appl. Polym. Sci.* 116 (2010) 18–26.
- [44] P.F. Fox, P.L.H. McSweeney, *Dairy Chemistry and Biochemistry*, First ed. Blackie Academic & Professional, London, 1998.
- [45] A. Dashevsky, Protein loss by the microencapsulation of an enzyme (lactase) in alginate beads, *Int. J. Pharm.* 161 (1998) 1–5.
- [46] B.J. Lee, G.H. Min, J.H. Cui, Correlation of drug solubility with trapping efficiency and release characteristics of alginate beads, *Pharm. Pharmacol. Commun.* 5 (1999) 85–89.
- [47] M. Esmaili, S.M. Ghaffari, Z. Moosavi-Movahedi, M.S. Atri, A. Sharifzadeh, M. Farhadi, R. Yousefi, J.-M. Chobert, T. Haertle, A.A. Moosavi-Movahedi, Beta casein-micelle as a nano vehicle for solubility enhancement of curcumin; food industry application, *LWT Food Sci. Technol.* 44 (2011) 2166–2172.
- [48] A.O. Elzoghby, M.W. Helmy, W.M. Samy, N.A. Elgindy, Spray-dried casein-based micelles as a vehicle for solubilization and controlled delivery of flutamide: formulation, characterization, and in vivo pharmacokinetics, *Eur. J. Pharm. Biopharm.* 84 (2013) 487–496.
- [49] T. Østberg, E.M. Lund, C. Graffner, Calcium alginate matrices for oral multiple unit administration IV release characteristics in different media, *Int. J. Pharm.* 112 (1994) 241–248.

- [50] M. Rapedius, J. Blanchard, Comparison of the Hanson Microette and the Van Kel Apparatus for in vitro release testing of topical semisolid formulations, *Pharm. Res.* 18 (2001) 1440–1447.
- [51] K. Pan, H. Chen, P.M. Davidson, Q. Zhong, Thymol nanoencapsulated by sodium caseinate: physical and antilisterial properties, *J. Agric. Food Chem.* 62 (2014) 1649–1657.
- [52] E. Esposito, L. Ravani, C. Contado, A. Costenaro, M. Drechsler, D. Rossi, E. Menegatti, A. Grandini, R. Cortesi, Clotrimazole nanoparticle gel for mucosal administration, *Mater. Sci. Eng. C* 33 (2013) 411–418.



Modification of alginate beads using gelatinized and ungelatinized arrowroot (*Tacca leontopetaloides* L. Kuntze) starch for drug delivery

Rapee Khlibsuan, Wirinya Tansena, Thaned Pongjanyakul *

Division of Pharmaceutical Technology, Faculty of Pharmaceutical Sciences, Khon Kaen University, Khon Kaen 40002, Thailand

ARTICLE INFO

Article history:

Received 28 March 2018

Received in revised form 15 June 2018

Accepted 24 June 2018

Available online xxxx

Keywords:

Alginate bead

Arrowroot starch

Molecular interaction

Gelatinized starch

Drug delivery

ABSTRACT

Arrowroot (*Tacca leontopetaloides* L. Kuntze) starch in gelatinized and ungelatinized forms was used to modify the characteristics of calcium alginate (CA) beads containing diclofenac sodium (DS). Sodium alginate (SA) was able to molecularly interact with ungelatinized starch (UGS) granules and gelatinized starch (GS) gel via hydrogen bonding mechanisms in the dispersions, leading to viscosity synergism before cross-linking. The GS-CA beads provided a significantly higher DS entrapment efficiency than the UGS-CA beads. The added UGS retarded the water uptake of the CA beads, resulting in slower DS release profiles in purified water and a longer lag time of DS release in pH 6.8 phosphate buffer. On the other hand, GS enhanced water uptake and accelerated the DS release of the beads in both media. Moreover, the 1%GS-CA beads displayed slower DS release than the CA and 1% UGS-CA beads in pH 6.8 phosphate buffer when simulated gastro-intestinal (GI) condition was used. This study shows that UGS and GS obtained from *Tacca leontopetaloides* L. Kuntze have good potential to improve drug entrapment efficiency of the CA beads, and the DS-loaded GS-CA beads can be used as multiunit dosage forms for sustaining drug release in simulated GI condition.

© 2018 Elsevier B.V. All rights reserved.

1. Introduction

Polysaccharides obtained from natural sources have been widely employed in the food, biomedical and pharmaceutical fields. Polysaccharides can be used as an important ingredients and additives in pharmaceutical products because of their biodegradability and biocompatibility [1, 2]. Among known biopolysaccharides, sodium alginate (SA), which found in marine brown algae, has been popularly used in pharmaceutical applications as a tablet disintegrant, matrix-forming agent, film former and gelling agent [3]. SA consists of α -L-guluronic and β -D-mannuronic acids and is composed of homopolymeric blocks and blocks with an alternating sequence [4]. Gelation occurs by cross-linking uronic acid with divalent cations—for example, calcium ions—in so-called ionotropic gelation [5]. Formation of calcium alginate (CA) beads is achieved by dropping a drug-containing SA dispersion into a calcium chloride solution [6, 7]. CA bead matrix systems have been investigated as controlled release systems for drugs [8, 9] and proteins [10, 11]. Drug release from CA beads depends on the swelling of the beads and diffusion of the drug in the gel matrix [7]. The beads also have potential as a pulsatile release system for macromolecular drugs [12]. Moreover, they can protect acid-sensitive drugs from gastric juices, with the drug consequently released from the beads into the small

intestine. In addition, CA beads are suitable for delivery of nonsteroidal anti-inflammatory drugs (NSAIDs) that cause gastric irritation [13, 14].

Modification of the CA beads characteristics can be achieved by incorporating substances in a drug-loaded SA dispersion before the cross-linking process, resulting in a higher drug entrapment efficiency (DEE) and slower drug release. Water-soluble polymers, such as chondroitin sulfate [15], konjac glucomannan [16], gelatin [17], sodium starch glycolate [18], xanthan gum [19], gum Arabic [20, 21], and agar [22], have been used for this purpose. Furthermore, addition of water-insoluble substances, such as chitin [23] and clays [18, 24–26], can enhance the DEE and retard drug release from the beads. These modifications are achieved through molecular interactions between the carboxyl groups of alginate and functional groups of the additives. Additionally, starch is a potential material for CA bead modification. Not only starch granules [27, 28] but also starch gels [29, 30] can be used to modify CA beads containing drugs and cells. As determined from a literature review, comparative studies of the effect of starch granules and gel on the characteristics of CA beads for drug delivery are not yet available.

Starch consists of amylose, a linear polysaccharide of glucose linked via α -1–4 glycosidic bonds, and amylopectin, a branched polysaccharide of glucose with an additional linkage of α -1–6 glycosidic bonds, at different ratios depending on its source [31]. In nature, starch is insoluble in water because it has numerous crystalline regions in its granules. Hydration of starch can be increased by heat treatment, in which the starch dispersion appears as a viscous transparent liquid. This phenomenon is called gelatinization [32]. *Tacca leontopetaloides*

* Corresponding author.

E-mail address: thaned@kku.ac.th (T. Pongjanyakul).

starch (Polynesian arrowroot starch) has been used for the treatment of stomach ailments such as diarrhea and dysentery [33]. This starch was also used as a main material to develop a thermoplastic film [34], and a filler in tablets [35]. Thus, this study focused on one of the traditional starches in Thailand—arrowroot starch extracted from *Tacca leontopetaloides* L. Kuntze (green stem *Tacca*). This arrowroot starch has been used as a main ingredient or additive in some Thai desserts because it provides a highly viscous and desirably textured paste after gelatinization. These characteristics indicate its good potential for modifying the properties of CA beads, such as DEE and drug release patterns.

Therefore, the objective of this study was to investigate the effects of ungelatinized and gelatinized starch (UGS and GS) from *Tacca leontopetaloides* L. Kuntze on the characteristics of CA beads containing diclofenac sodium (DS). DS is a NSAID that has been used in the treatment of rheumatic disorders. It is a sodium salt of a weak acid with a pK_a of 4, and it also has a short biological half life (1–2 h) [36]. A long-term oral administration of DS often caused gastro-intestinal (GI) disturbances and peptic ulceration due to high local concentration of drug in GI tract when oral DS tablets were administered [36]. Alternatively, multiunit dosage forms of DS, for example small beads, could be widely dispersed in the GI tract to reduce local irritation of the drugs [37]. Moreover, the small beads containing DS may offer a sustained-release pattern for a prolonged action. In this study, the physical properties of the UGS-CA and GS-CA beads containing DS, such as the particle size, particle and surface morphology, DEE, water uptake and drug release behavior, were investigated. Furthermore, molecular interactions between SA and UGS or GS in the form of dispersions and films were examined to describe the property changes in the DS-loaded CA beads with incorporation of UGS or GS.

2. Materials and methods

2.1. Materials

SA (viscosity grade of 300 cP and mannuronic acid-to-guluronic acid ratio = 0.59) was obtained from Onimax Co., Ltd. (Bangkok, Thailand). Commercial arrowroot (*Tacca leontopetaloides* L. Kuntze) starch was purchased from Choothin (Bangkok, Thailand). This starch has 24.53% amylose with a low protein content of 0.11%, and its gelatinization temperature is 72.25 °C [38]. The particle morphology of the starch granules is shown in Fig. 1. DS was obtained from Bang Trading 1992 Co., Ltd. (Bangkok, Thailand). All other reagents were of analytical grade and used as received.

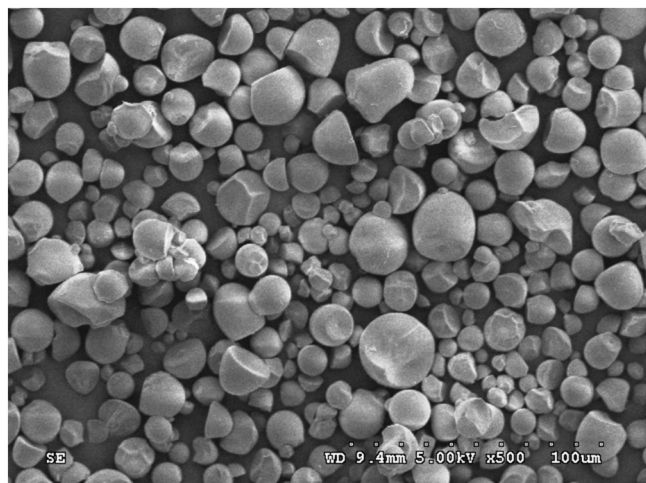


Fig. 1. Particle morphology of arrowroot (*Tacca leontopetaloides* L. Kuntze) starch granules.

2.2. Characterization of UGS-SA and GS-SA dispersions and films

2.2.1. Preparation of UGS-SA and GS-SA dispersions

SA (1.5 g) was dispersed in 75 mL of purified water. Arrowroot starch (0.25, 0.5, or 1 g) was dispersed in purified water (20 mL). Next, the UGS dispersion was added and mixed into the SA dispersion. The final volume of the UGS-SA dispersion was adjusted to 100 mL using purified water. For GS, the UGS dispersions were incubated and stirred in a water bath at 80 °C for 10 min to obtain a viscous dispersion, and the dispersion was cooled to room temperature. Next, the GS dispersion was mixed into the SA dispersions; then, the GS-SA dispersions were adjusted to a final volume of 100 mL. The viscosity of all dispersions was determined, and 1.5% w/v SA, 1% w/v UGS, and 1% w/v GS dispersions were prepared and used as the control in this study.

2.2.2. Viscosity determination

The viscosities of the dispersions were measured using a Brookfield Digital Rheometer (Model DV-III, Brookfield Engineering Labs, Inc., Stoughton, MA) at 30.0 ± 2.0 °C. A small sample adapter with a no. 31 spindle was used. The apparent viscosity of the dispersions at a 13.6 s^{-1} shear rate was reported.

2.2.3. Preparation of UGS-SA and GS-SA films

Dispersions of 1.5% w/v SA containing UGS or GS at concentrations of 0.25, 0.5 and 1% w/v were prepared using the procedure mentioned in Section 2.2.1. Dispersions of 1% w/v UGS and GS were also prepared. Next, 20 mL of each of the dispersions was poured into a plastic mold ($5.9 \text{ cm} \times 9.4 \text{ cm}$) and dried at 50 °C using a hot air oven for 24 h. After drying, the films were kept in desiccators with a relative humidity of $40 \pm 2\%$ before characterization.

2.2.4. Molecular interaction studies

The thermal properties of the films were examined using differential scanning calorimetry (DSC). The sample (2.5–3.0 mg) was weighed and placed in an aluminum pan. The sample was heated over a range of 30–450 °C at a heating rate of 10 °C min^{-1} (DSC822, Mettler Toledo, Switzerland). DSC thermograms were recorded. Fourier transform infrared (FTIR) spectra of the films were also obtained. The sample was gently triturated with KBr powder at a weight ratio of 1:100 and then pressed with a hydrostatic press at 8 tons for 10 min. The discs obtained were placed in a sample holder and scanned from 4000 to 450 cm^{-1} at a resolution of 4 cm^{-1} (Spectrum One, Perkin Elmer, Norwalk, CT).

Particle size analysis of the dispersed phase of the UGS and GS dispersions was performed, and used for describing molecular interaction between SA and arrowroot starch. The 1% UGS and GS dispersions were prepared using the method mentioned in Section 2.2.1. The particle size of the samples was determined using a laser diffraction particle size analyzer (Mastersizer2000, Malvern Instrument Ltd., UK). The samples were dispersed in 70 mL of purified water in a small volume sample dispersion unit and stirred at a rate of 50 Hz for 30 s before the measurement. The size-frequency distributions were plotted and the mean particle sizes were reported.

2.3. Preparation of DS-loaded beads

SA (1.5 g) was dispersed in 75 mL of purified water, and then, DS (1 g) was gently added and dissolved in the SA dispersion. Next, arrowroot starch (0.25, 0.5, or 1 g) was dispersed in purified water (20 mL) and prepared as UGS or GS dispersions using the method described in Section 2.2.1. The UGS or GS dispersions were poured and blended into the DS-loaded SA dispersions. The final volume of the dispersions was adjusted to 100 mL. Then, the resulting dispersion (20 mL) was dropped into 1% w/v CaCl_2 solution (200 mL) through a nozzle (0.5-mm inner diameter) with gentle stirring. The gel beads were cured in a calcium chloride solution for 1 h, rinsed with 50 mL of purified water, blotted to remove excess water, and dried at 50 °C for 8–9 h.

2.4. Characterization of DS-loaded beads

2.4.1. Particle size and morphology

The particle size of the beads was measured using an optical microscope (Olympus CH30, Japan). Two hundred beads were randomly selected, and their Feret's diameters were determined. The particle and surface morphologies of the beads and arrowroot starch granules were observed using scanning electron microscopy. The samples were mounted on dummies, coated with gold in a vacuum evaporator (Model Emitech K500X, Ashford, Kent, England) at a pressure of 9×10^{-2} mbar for 4 min, and then viewed using a scanning electron microscope (Hitachi Se3000 N, Tokyo, Japan).

2.4.2. Determination of the drug content and entrapment efficiency

DS-loaded beads (50 mg) were immersed in pH 6.8 phosphate buffer (75 mL) to completely disintegrate the beads. The mixture was sonicated for 15 min and incubated in a shaking water bath at 37 °C for 12 h. Then, the mixture was adjusted to a final volume of 100 mL and filtered using a 0.45 µm nylon membrane. The concentration of DS in the filtrates was analyzed using a UV–visible spectrophotometer (Shimadzu UV1201, Japan) at 260 nm. The DS content was calculated as the weight percentage of the beads. The DEE was calculated according to the ratio of the actual to theoretical drug contents in the beads [16].

2.4.3. Water uptake studies

DS-loaded beads were placed in a small basket, soaked in purified water, 0.1 M HCl or pH 6.8 phosphate buffer, and shaken occasionally in a water bath at 37 °C. At 15, 30, and 60 min of the test, each basket was withdrawn, blotted to remove excess water and immediately weighed on an analytical balance. The water uptake of the beads was determined according to the following equation:

$$\text{Water uptake (\%)} = \frac{(W_w - W_i)}{W_i} \times 100 \quad (1)$$

where W_w is the weight of the wet beads and W_i is the initial weight of the beads.

2.4.4. In vitro drug release

Due to the water-insoluble property of DS in an acidic medium, the release media used in this study were purified water and pH 6.8 phosphate buffer. Release of DS from the beads was investigated using a USP dissolution apparatus I (Hanson Research, Northridge, USA). A bead amount equivalent to DS 25 mg was weighed and added to 750 mL of the release medium at 37 °C. The baskets were rotated at a rate of 50 revolutions min^{-1} . The simulated GI conditions used to test drug release were performed using 0.1 M HCl (750 mL) for 2 h, followed by pH 6.8 phosphate buffer (750 mL). Samples (7 mL) were collected and replaced with fresh media at various time intervals. The concentration of DS released was analyzed using a UV–visible spectrophotometer at 260 nm. The release data from the DS-loaded beads in purified water or pH 6.8 phosphate buffer were fitted using the Higuchi model (Eq. (2)) or the zero-order model (Eq. (3)), respectively, which are expressed as the following equations [39]:

$$Q = K_H t^{0.5} \quad (2)$$

$$Q = K_0 t + B \quad (3)$$

where Q is the percentage of drug released at a given time (t), K_H is the Higuchi release rate, K_0 is the zero-order release rate, and B is a constant value used for computing the lag time of DS released from the beads when Q equals zero.

3. Results and discussion

3.1. Molecular interaction of SA with GS or UGS in dispersions and films

The viscosity of SA dispersions with various contents of UGS and GS added was determined to preliminarily study the molecular interaction between SA and GS or UGS. The SA dispersion was transparent liquid, while a white opaque liquid was obtained for the GS-SA and UGS-SA dispersions. The viscosity of the 1.5% SA dispersion was $292.7 \pm 2.7 \text{ mPa s}$ ($n = 3$) at a 13.6 s^{-1} shear rate, whereas the 1% GS dispersion had a low viscosity of $3.01 \pm 0.74 \text{ mPa s}$ ($n = 3$). The viscosity of the 1% UGS dispersion could not be determined because of its very low viscosity. The effects of UGS and GS on the viscosity of the SA dispersion are shown in Fig. 2. Incorporation of GS into the SA dispersion gave an obviously higher viscosity than that of the SA dispersion alone, which was related to the amount of GS added. UGS added at 0.25 and 0.5% did not affect the viscosity of the SA dispersion, but the addition of 1% UGS led to a slight increase of the SA dispersion viscosity. These results suggested that blending of higher contents of GS and UGS with the SA dispersions resulted in viscosity synergism in the composite dispersions.

The molecular interactions between SA and GS or UGS in the solid state were investigated in the prepared UGS-SA and GS-SA films. DSC and FTIR spectroscopy were used for this investigation. The GS and SA films were transparent, whereas the UGS films could not be formed into a continuous sheet; a powder from the cracking of this film was obtained. The GS-SA and UGS-SA films were transparent and opaque in nature, respectively. The FTIR spectra of the SA, UGS-SA and GS-SA films are presented in Fig. 3. The FTIR spectra of the SA films presented an O—H stretching peak at 3439 cm^{-1} , COO^- asymmetric stretching peak at 1615 cm^{-1} , COO^- symmetric stretching peak at 1416 cm^{-1} and C—O—C stretching peak at 1028 cm^{-1} [40]. The native arrowroot starch showed absorption peaks at 3432 cm^{-1} (O—H stretching) and 1647 cm^{-1} (O—H bending) due to water residues in the amorphous region of the starch and at $1371\text{--}1459 \text{ cm}^{-1}$ (C—H bending) and $1017\text{--}1160 \text{ cm}^{-1}$ (C—O and C—O—C stretching of the glucose structure) [41]. The UGS films had a similar FTIR pattern to that of the native starch, except that a sharper peak of O—H stretching of the UGS films was observed. This sharper peak was likely due to water residues in the starch granules. Gelatinization caused changes in the FTIR spectra, including a shift of the O—H bending peak to a lower wavenumber, disappearance of the C—H bending peak at $1372\text{--}1451 \text{ cm}^{-1}$, and decrease

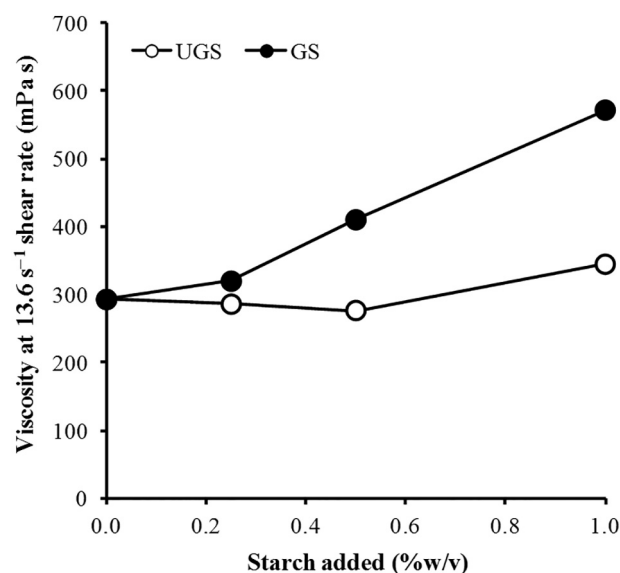


Fig. 2. Viscosity of 1.5% w/v SA dispersion incorporating various concentrations of UGS and GS. Each point is the mean \pm S.D., $n = 3$.

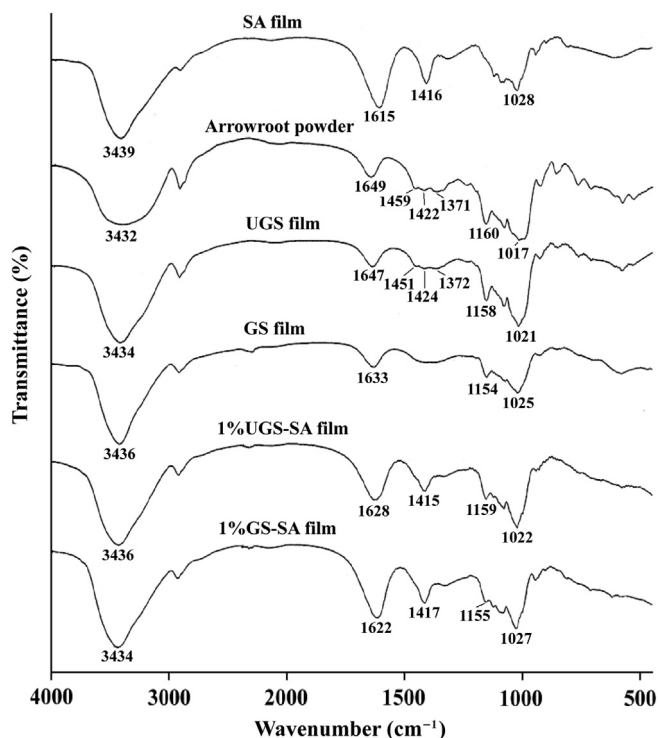


Fig. 3. FTIR spectra of SA film, native arrowroot starch, UGS film, GS film, 1%UGS-SA film, and 1%GS-SA film.

of the peak intensities of the C—O and C—O—C stretching peaks. These results suggested that disentanglement of the starch molecules and decrease of the crystallinity of the starch occurred after gelatinization by heat treatment. The 1%UGS-SA films showed the same FTIR pattern to those of the SA films, but an obvious shift of the COO[−] stretching peak at 1615 cm^{−1} to a higher wavenumber and a small shift of the O—H stretching peak to a lower wavenumber occurred. These changes could also be observed upon addition of 0.25 and 0.5% UGS into the SA films (data not shown). Moreover, it is interesting that the FTIR pattern of the 1%GS-SA films was similar to that of the 1%UGS-SA films, suggesting that UGS interacted with SA in the same manner as GS, indicating

that hydrogen bonding between carboxyl groups of SA molecules and hydroxyl groups of the granule surface of UGS and GS molecules occurred.

DSC thermograms of the native arrowroot starch, SA and composite films are presented in Fig. 4. The native starch showed an exothermic degradation peak at 351 °C. The UGS films produced a new endothermic peak at 291 °C, followed by an exothermic peak at 359 °C. Similarly, an endothermic peak at 282 °C was also observed for the GS films, and a degradation peak appeared at 353 °C. The endothermic peak of the UGS film at 291 °C and of the GS film at 282 °C may have been caused by phase transition after heat induction and before film degradation. The SA films showed exothermic degradation peaks at 258 and 366 °C [40]. The 0.25% UGS-SA and 0.5% UGS-SA films presented the first degradation peak of SA at 259–260 °C and the second exothermic peak at approximately 368 °C. Addition of 1 % UGS into the films led to a strong degradation peak at 285 °C and a second degradation peak at 411 °C. This phenomenon suggested that the first degradation at 260 °C of SA may induce degradation of UGS embedded in the films, leading to a change of the thermal behavior at higher temperatures. On the other hand, incorporation of GS at various contents produced a similar DSC pattern to that of the SA films, but a higher temperature of the second degradation peak was observed with the increasing GS content. These findings showed that phase separation of the UGS granules embedded in the SA film matrix could occur with a higher content of UGS, whereas GS could be completely blended into the SA matrix at the molecular level to obtain homogenous GS-SA films.

From all of these results, the model of the molecular interaction between SA and UGS or GS is illustrated in Fig. 5. The particle size analysis of the UGS and GS dispersions was involved for describing possible molecular interaction between SA and arrowroot starch. The size-frequency of the dispersed phase of the 1% UGS and 1% GS dispersions is shown in Fig. 6. The size of UGS granules was found to be $16.21 \pm 0.04 \mu\text{m}$ ($n = 3$), whereas the 1% GS dispersion showed obviously bigger size of the dispersed phase ($42.69 \pm 0.49 \mu\text{m}$, $n = 3$). This result suggested that the structure transformation of the UGS granules could be induced by thermal treatment. The granules could be hydrated, swollen and rupture during heating [32], resulting in decreasing of crystalline regions of the starch granules, and disentanglement of the starch molecules, amylose and amylopectin, which small aggregates of the starch molecules could be formed (Fig. 5). Numerous hydroxyl groups of the starch molecules could interact with the carboxyl groups of SA via

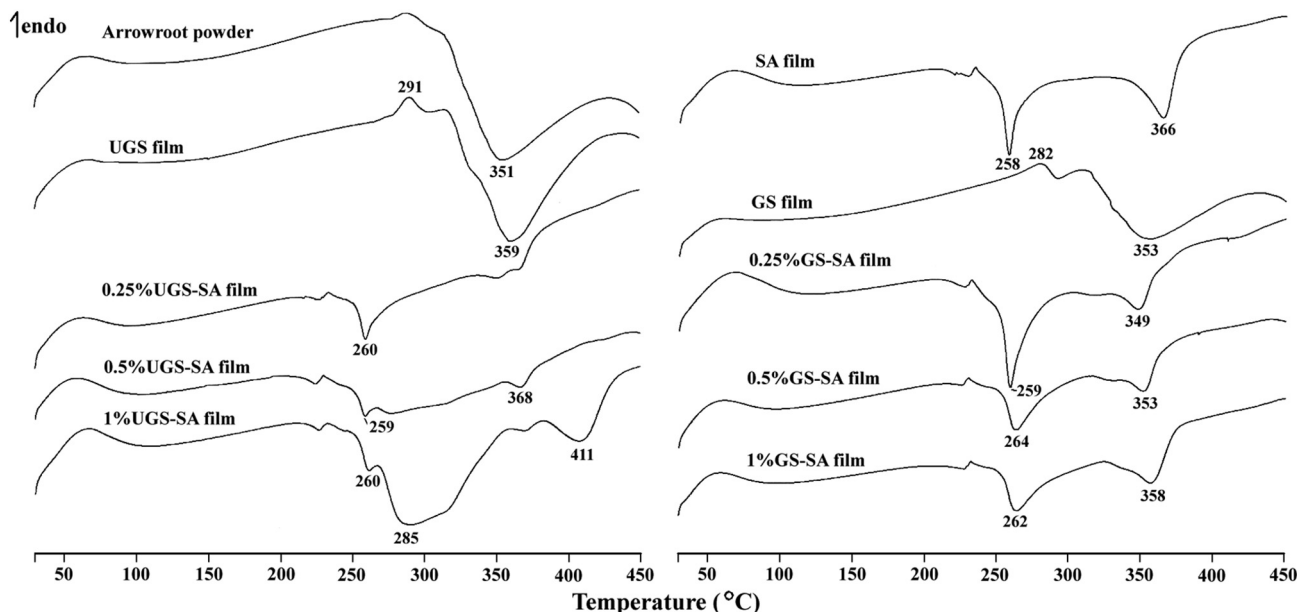


Fig. 4. DSC thermogram of SA film, native arrowroot starch, UGS film, GS film, UGS-SA film, and GS-SA film.

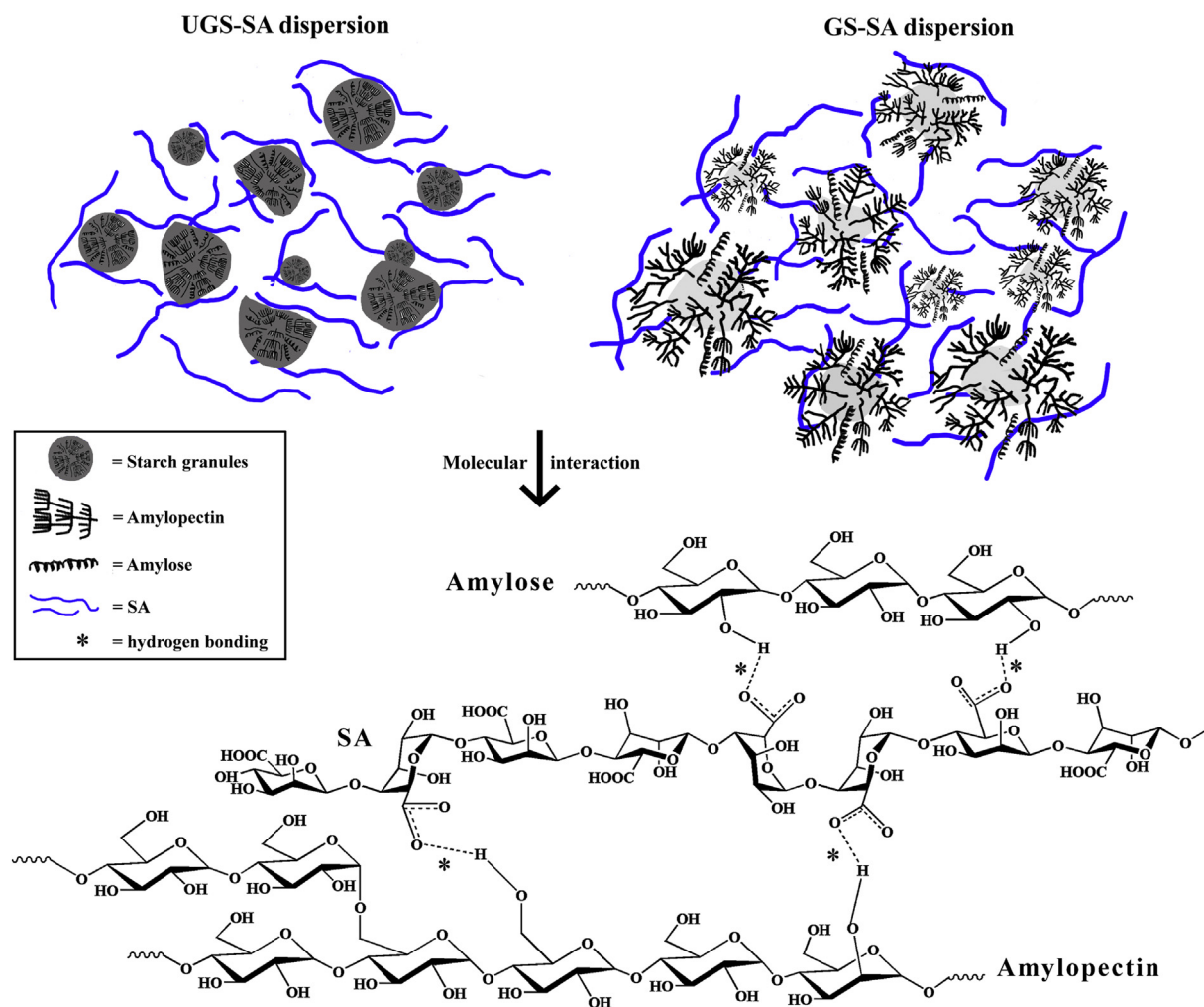


Fig. 5. Schematic presentation of the molecular interactions between SA and UGS or GS.

intermolecular hydrogen bonding [29]. The branched chain of amylopectin created numerous contact points, leading to viscosity synergism and a more complex matrix network in the GS-SA composite dispersions. Moreover, the carboxyl groups of the SA molecules slightly

interacted with the hydroxyl groups on the surface of the UGS granules. Therefore, these findings showed that the molecular interaction between SA and GS or UGS in the dispersions via hydrogen bonding before calcium ion cross-linking could possibly influence the characteristics of the CA beads containing DS.

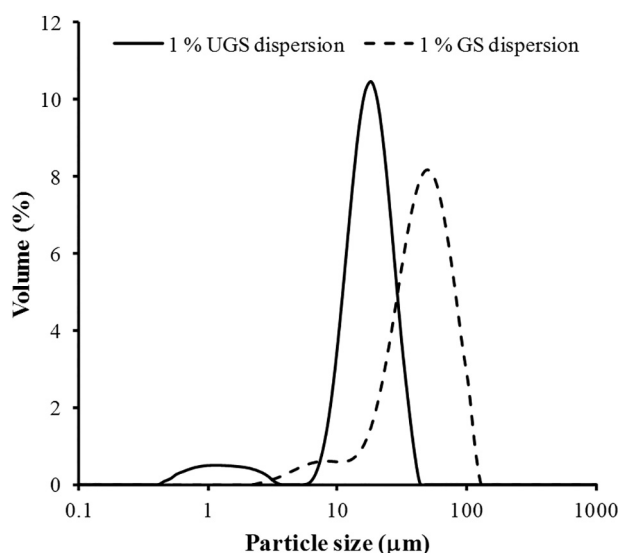


Fig. 6. Size-frequency distribution of 1% UGS and 1 % GS dispersions.

3.2. Particle size and DEE of the beads

The average particle sizes of the beads are listed in Table 1. The particle size of the CA beads was 1.17 mm. Addition of GS seemed to increase the size of the CA beads because the higher viscosity of the dispersion may have led to less shrinkage during cross-linking. The particle and surface morphologies of the beads were observed by SEM, as shown in Fig. 7 (Row 1 and 2). All of the beads had a spherical shape with a collapsed center. The CA beads had a rough surface, and some DS crystals were deposited on the bead surface. The surface of the UGS-CA beads showed numerous starch granules that had a different morphology compared to that of the GS-CA beads.

The DS content of the beads ranged from 19.16–24.36% w/w (Table 1). The DEE value of the CA beads was 54.25%. Incorporation of UGS and GS caused an obviously higher DEE than that of the CA beads. Additionally, the GS-CA beads provided a significantly greater DEE than the UGS-CA beads. These results suggested that addition of UGS and GS led to a denser matrix barrier, retarding water leakage from the wet beads during the preparation process [42] and leading to decrease of drug loss from the beads. However, GS molecules composed of linear amylose and branched amylopectin, interacted with SA before

Table 1
Characteristics of CA, UGS-CA, and GS-CA beads containing DS.

Components	Particle size ^a (mm)	Drug content ^b (% w/w)	DEE ^b (%)	Purified water	pH 6.8 phosphate buffer	
				K _H ^b (% min ^{-0.5})	Lag time ^b (min)	K ₀ ^b (% min ⁻¹)
1.5% SA	1.17 ± 0.18	21.70 ± 0.54	54.25 ± 0.67	1.05 ± 0.03	4.65 ± 1.09	0.77 ± 0.04
1.5% SA						
+0.25% UGS	1.02 ± 0.17	22.83 ± 0.57	62.80 ± 0.79	0.75 ± 0.03	26.79 ± 0.40	0.80 ± 0.02
+0.5% UGS	1.07 ± 0.19	22.27 ± 0.04	66.81 ± 0.21	1.38 ± 0.02	24.73 ± 2.80	0.87 ± 0.03
+1% UGS	1.17 ± 0.15	19.16 ± 0.52	67.05 ± 0.91	1.13 ± 0.06	23.33 ± 0.91	0.79 ± 0.03
+0.25% GS	1.16 ± 0.18	24.31 ± 0.51	66.84 ± 0.70	1.87 ± 0.03	7.46 ± 0.28	0.88 ± 0.01
+0.5% GS	1.22 ± 0.18	24.36 ± 0.60	73.07 ± 0.90	2.64 ± 0.03	2.03 ± 0.45	0.99 ± 0.01
+1% GS	1.24 ± 0.16	22.03 ± 0.22	77.11 ± 0.39	2.49 ± 0.05	3.52 ± 0.53	0.78 ± 0.02

^a n = 500.

^b n = 3.

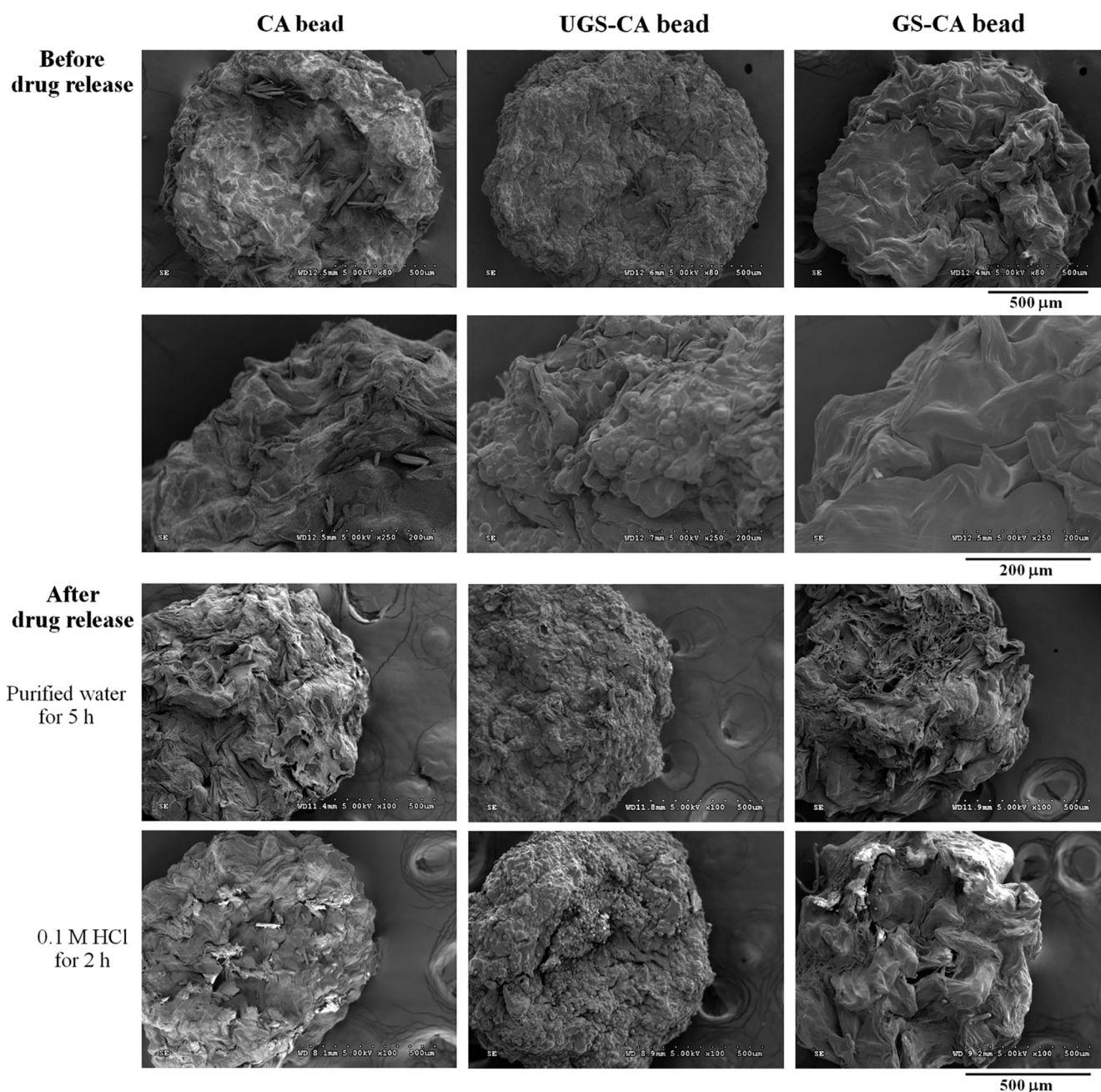


Fig. 7. Particle and surface morphology of CA, 1%UGS-CA, and 1%GS-CA beads containing DS before and after drug release testing in purified water and 0.1 M HCl.

cross-linking to create a stronger matrix network than that produced from granules of UGS, resulting in a higher efficiency at preventing drug molecule leakage from the wet beads. Thus, a higher DEE was found for the GS-CA beads in this study.

3.3. Water uptake of the beads

The water uptake of the beads in purified water, 0.1 M HCl and pH 6.8 phosphate buffer is shown in Fig. 8. In purified water (Fig. 8a), the water uptake of the CA beads seemed to decrease with the addition of 0.25 and 0.5% UGS, whereas 1% UGS increased the water uptake at 1 h of the test. By contrast, the water uptake of the CA beads obviously increased with the increasing GS content, and the longer the testing time, the greater the water uptake. The water uptake of the CA beads in 0.1 M HCl was lower than those in purified water (Fig. 8b), but the similar water uptake effects of UGS or GS on the CA beads were obtained. In contrast, the water uptake of the beads in pH 6.8 phosphate buffer was significantly higher than that in purified water and acidic medium (Fig. 8c). The test in pH 6.8 phosphate buffer was performed for 15 and 30 min, but the wet beads could not be handled at 60 min due to the very high swelling and disintegration of the beads. The water uptake of the CA beads decreased with the increasing UGS content at 15 and 30 min. On the other hand, GS caused an increase of the water uptake of the beads at 15 min, but a decrease of the water uptake was found in 30 min of the test.

Alginate in the form of calcium salt is water-insoluble, and the CA beads existed as a stable polymer matrix in purified water; thus, limitation of water absorption by the CA beads was observed. In acidic medium, the calcium ions in the CA beads were totally exchanged with hydrogen ions, resulting in the matrix formation of water-insoluble alginic acid that was a unionized form of the carboxyl groups of SA [4].

However, the alginic acid matrix still had water absorption properties, but lower than the CA beads in purified water. It may be explained that the CA beads possibly contained small amount of SA that did not react with the calcium ions during the cross-linking process [43], leading to higher water uptake of the CA beads in purified water. The addition of UGS and GS affected water absorption capacity of the CA beads. UGS has lower water absorption properties and retarded the water uptake of the CA beads. On the other hand, addition of GS promoted water absorption by the CA beads in purified water and acidic medium because of the higher water absorption properties of GS, a hydrophilic polymer. This result was in agreement with those of previous reports using sodium starch glycolate [18], xanthan gum [19], and starch [29] when tested using purified water. Moreover, increased water uptake also occurred when GS was dissolved and eroded from the beads in both media.

In contrast with pH 6.8 phosphate buffer, calcium ions cross-linked with alginate were rapidly exchanged in sodium ion-rich medium [6]. The partial formation of SA strongly promoted water uptake into the beads. Insoluble UGS particles embedded in the bead matrix interacted with SA to retard the water uptake of the CA beads. However, the molecules of GS interacted with SA to strengthen and stabilize the wet beads, resulting in a decrease of the water uptake at 30 min when using 1% GS.

3.4. Drug release of the beads

DS release from the UGS- and GS-CA beads in purified water is shown in Fig. 9a and b, respectively. The relationship between the % drug release and square root of time provided good linearity with a determination coefficient (R^2) greater than 0.99, suggesting that the drug release mechanism was matrix diffusion controlled. The drug release

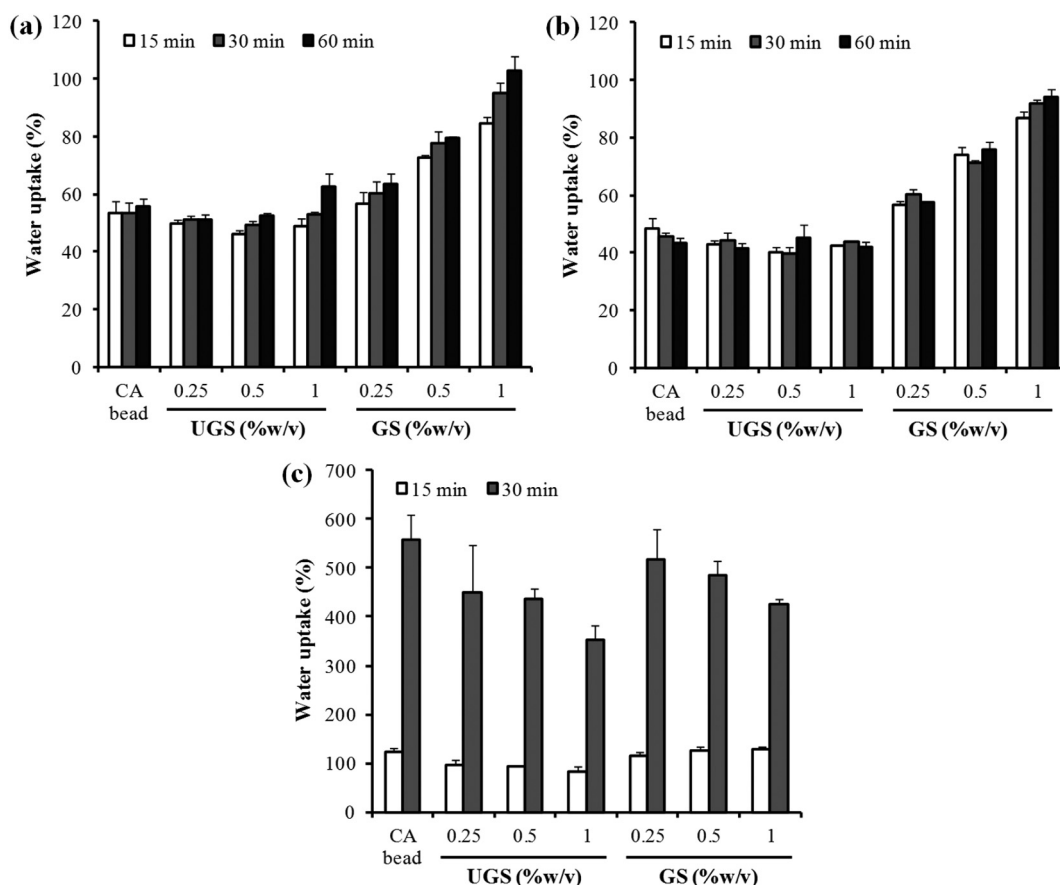


Fig. 8. Water uptake of DS-loaded CA beads adding different amount of UGS and GS in purified water (a), 0.1 M HCl (b) and pH 6.8 phosphate buffer (c). Each value is the mean \pm S.D., $n = 3$.

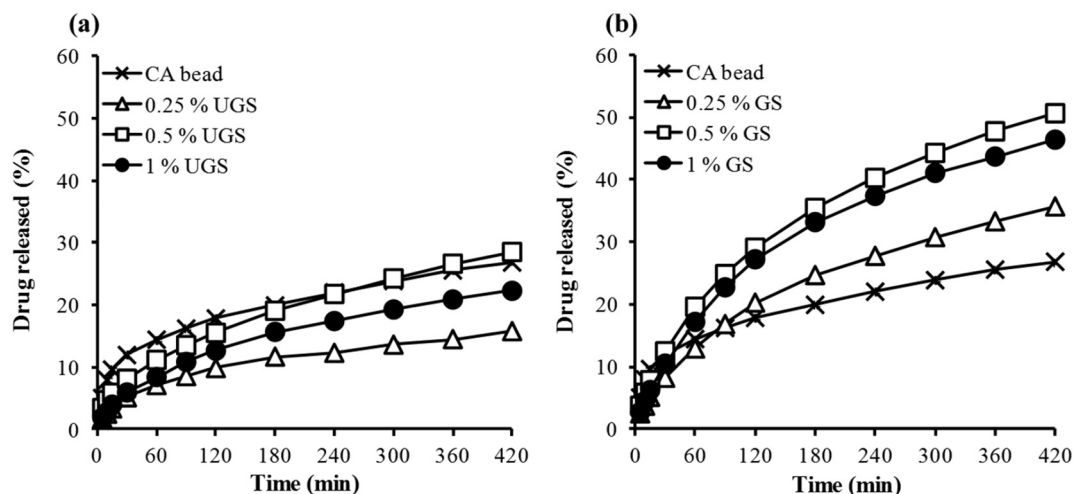


Fig. 9. Drug release profiles of CA beads adding different contents of UGS (a) and GS (b) in purified water. Each value is the mean \pm S.D., $n = 3$.

rate (K_H) of the 0.25%UGS-CA beads was lower than that of the CA beads, whereas the increased UGS content caused a slightly higher K_H value compared to that of the CA beads (Table 1). The K_H result contradicted the drug release profile (Fig. 9a), in that the UGS-CA beads had a lower % drug release than the CA beads. This difference could be due to differences in the % initial drug release of the beads. It was observed that the initial drug release of the CA beads at 15 min was 9.58%, which was obviously higher than that of the UGS-CA beads. The % drug release at 15 min of the 0.25%UGS-, 0.5%UGS-, and 1%UGS-CA beads was found to be 3.35, 5.86, and 3.96%, respectively. Moreover, the total drug release of the UGS-CA beads at 420 min tended to be lower compared to that of the CA beads. By contrast, the GS-CA beads gave obviously higher K_H values than the UGS-CA and CA beads (Table 1). SEM photographs showed erosion of the surface of the CA beads after release testing in purified water (Fig. 7, Row 3). Erosion of the beads could have occurred due to residual alginate release from the beads [43], which was caused by a small amount of calcium ion released into the purified water [6]. The surface morphology of the UGS-CA beads after drug release was similar to that before drug release. Therefore, the lower initial drug release and total drug release could be described by the restriction of water uptake of the beads with the addition of UGS (Fig. 8a). On the other hand, many pores were observed on the surface of the GS-CA beads after drug release testing likely because of the dissolution of GS from the bead surface, suggesting that GS

acted as a pore-forming agent in this case and that the formation of pore channels could accelerate drug release from the beads.

The drug release profile of the UGS- and GS-CA beads in pH 6.8 phosphate buffer produced a sigmoidal curve with complete release (Fig. 10a and b, respectively). The release data showed good fitting with the zero-order model, with an R^2 value higher than 0.99. This result suggested that drug release could be controlled by a swelling mechanism. The lag time and drug release rate (K_0) computed using Eq. (3) are listed in Table 1. The UGS-CA beads presented obviously longer lag times than the CA beads, whereas shorter lag times were observed for the GS-CA beads using 0.5 and 1% GS. Additionally, the UGS- and GS-CA beads seemed to present increased K_0 values compared to those of the CA beads. Drug release from the CA beads in pH 6.8 phosphate buffer was depressed by formation of a gel layer at the initial stage, but was gradually enhanced by increasing the water content and erosion of the swollen gel phase in the later stage [7]. This phenomenon was due to the ion exchange process between calcium ions in the beads and sodium ions in the medium. In the initial stage, incorporation of UGS retarded water uptake of the CA beads (Fig. 8c) and led to a longer lag time of drug release. On the other hand, GS led to shorter lag times of drug release, which was attributed to the increased water absorption capacity of GS. However, addition of UGS and GS to the beads did not clearly influence the drug release rate because of the very high swelling and disintegration of the CA beads in this medium.

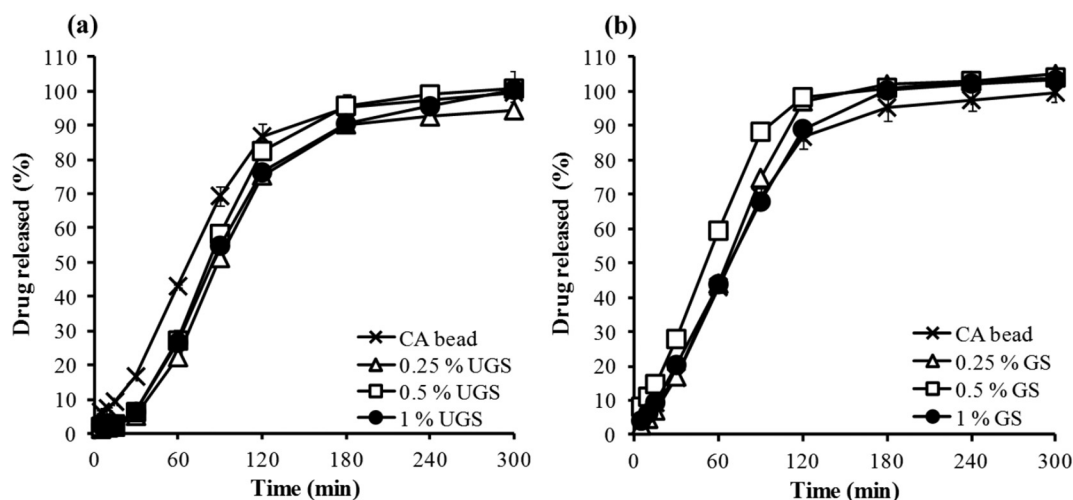


Fig. 10. Drug release profiles of CA beads adding different contents of UGS (a) and GS (b) in pH 6.8 phosphate buffer. Each value is the mean \pm S.D., $n = 3$.

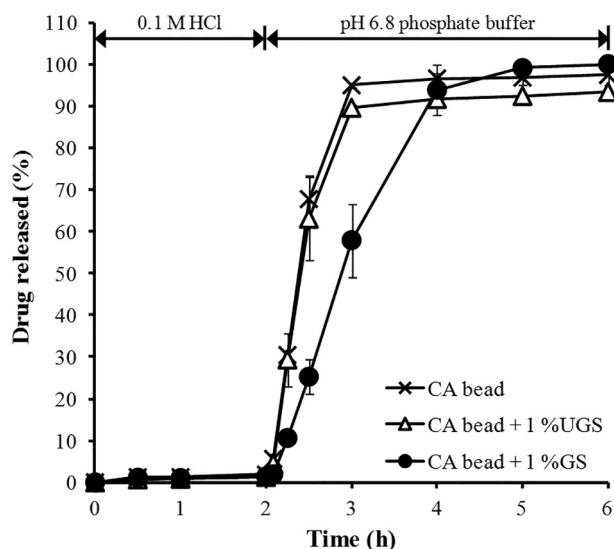


Fig. 11. DS release profiles of CA, 1%UGS-CA, and 1%GS-CA beads in simulated GI condition. Each point is the mean \pm S.D., $n = 6$.

In simulated GI condition, the DS release profile of the CA, 1%UGS-CA, and 1%GS-CA beads is shown in Fig. 11. The drug release in 0.1 M HCl for 2 h gave very low amount of DS that was found to be 1.84 ± 0.21 , 1.29 ± 0.10 , and $1.43 \pm 0.06\%$ ($n = 6$) for the CA, 1%UGS-CA, and 1%GS-CA beads, respectively. This was due to a very low water solubility of DS in acidic medium, and the CA beads could be changed to water-insoluble alginic acid matrices [24]. However, the CA beads showed the fastest DS release, and the 1%UGS-CA beads gave lower amount of DS released than the 1%GS-CA beads. This result suggested that incorporation of GS and UGS could retard DS release in acidic medium. Additionally, the dissolution of GS from the surface of the 1%GS-CA beads brought about faster drug release when compared to the 1%UGS-CA beads, which could be confirmed by SEM pictures of the beads after release in 0.1 M HCl for 2 h (Fig. 7, Row 4). After drug release in acidic medium, the CA and 1%UGS-CA beads provided a fast DS release in pH 6.8 phosphate buffer, whereas the 1%GS-CA beads displayed more sustained-release of DS (Fig. 11). The swollen CA beads could be visualized when the medium was changed to pH 6.8 phosphate buffer, suggesting the alginic matrix beads formed in the acidic medium could be converted to SA. In addition, DS could be ionized and dissolved in the neutral medium, leading to fast release of DS from the CA beads. However, UGS incorporated did not strengthen the swollen beads, whereas the swollen beads could be reinforced via molecular interaction between GS and SA. Thus, slower release of DS from the 1%GS-CA beads was obtained.

4. Conclusions

This study shows that SA interacted with arrowroot (*Tacca leontopetaloides* L. Kuntze) starch in the form of granules and gels via hydrogen bonding, leading to viscosity synergism in the composite dispersions before cross-linking using calcium ions. The UGS-CA and GS-CA beads loaded with DS presented different surface morphologies, and the GS-CA beads had significantly a higher DEE than the UGS-CA beads. Incorporation of UGS tended to retard water absorption by the CA beads, resulting in lower initial drug release and total drug release from the beads in purified water and a longer lag time of drug release from the beads in pH 6.8 phosphate buffer. On the other hand, GS enhanced water uptake and accelerated drug release from the beads in purified water. The GS-CA beads gave shorter lag time and higher drug release than the CA beads in the neutral medium. In simulated GI condition, the beads showed very low amount of DS release in acidic medium. However, the 1%GS-CA beads displayed more sustained-release of DS

than the CA and 1%UGS-CA beads in pH 6.8 phosphate buffer. These findings indicate that arrowroot starch in the forms of UGS and GS can improve DEE of DS, and the GS-CA beads has strong potential as drug delivery systems for sustaining DS release in simulated GI condition.

Acknowledgments

The authors would like to thank the Thailand Research Fund (Bangkok, Thailand) and Khon Kaen University (Khon Kaen, Thailand) for research funding (Grant no. BRG6080016). Scholarship under the Post-Doctoral Training Program from Research Affairs and Graduate School, Khon Kaen University, Thailand (grant no. 59148) for R.K. is gratefully acknowledged.

References

- [1] P.B. Malafaya, G.A. Silva, R.L. Reis, Natural-origin polymers as carriers and scaffolds for biomolecules and cell delivery in tissue engineering applications, *Adv. Drug Deliv. Rev.* 59 (2007) 207–233.
- [2] N.B. Shelke, R. James, C.T. Laurencin, S.G. Kumbar, Polysaccharide biomaterials for drug delivery and regenerative engineering, *Polym. Adv. Technol.* 25 (2014) 448–460.
- [3] H.H. Tønnesen, J. Karlsen, Alginate in drug delivery systems, *Drug Dev. Ind. Pharm.* 28 (2002) 621–630.
- [4] K.I. Draet, Alginates, in: G.O. Philips, P.A. Williams (Eds.), *Handbook of Hydrocolloids*, Woodhead Publishing, Cambridge 2000, pp. 379–395.
- [5] V. Pillay, C.M. Dangor, T. Govender, K.R. Moopanar, N. Hurbans, Ionotropic gelation: encapsulation of indomethacin in calcium alginate gel discs, *J. Microencapsul.* 15 (1998) 215–226.
- [6] T. Østberg, E.M. Lund, C. Graffner, Calcium–alginate matrices for oral multiple unit administration: IV release characteristics in different media, *Int. J. Pharm.* 112 (1994) 241–248.
- [7] S. Sugawara, T. Imai, M. Otagiri, The controlled release of prednisolone using alginate gel, *Pharm. Res.* 11 (1994) 272–277.
- [8] R.S. Al-Kassas, O.M.N. Al-Gohary, M.M. Al-Faadhel, Controlling of systemic absorption of glimepiride through incorporation into alginate beads, *Int. J. Pharm.* 341 (2007) 230–237.
- [9] L. Segale, P. Mannina, L. Giovannelli, F. Pattarino, Calcium alginate multi-unit oral dosage form for delayed release of celecoxib, *J. Drug Delivery Sci. Technol.* 26 (2015) 35–43.
- [10] D.M. Hariyadi, Y. Ma, Y. Wang, T. Bostrom, J. Malouf, M.S. Turner, B. Bhandari, A.G.A. Coombes, The potential for production of freeze-dried oral vaccines using alginate hydrogel microspheres as protein carriers, *J. Drug Delivery Sci. Technol.* 24 (2014) 178–184.
- [11] S.B. Jadhav, R.S. Singhal, Pullulan-complexed α -amylase and glucosidase in alginate beads: enhanced entrapment and stability, *Carbohydr. Polym.* 105 (2014) 49–56.
- [12] A. Kikuchi, M. Kawabuchi, M. Sugihara, Y. Sakurai, T. Okano, Pulsed dextran release from calcium–alginate gel beads, *J. Control. Release* 47 (1997) 21–29.
- [13] S.J. Hwang, G.J. Rhee, K.M. Lee, K.H. Oh, C.K. Kim, Release characteristics of ibuprofen from excipient-loaded alginate gel beads, *Int. J. Pharm.* 116 (1995) 125–128.
- [14] M.J. Fernandez-Hervás, M.A. Holgado, A. Fini, J.T. Fell, In vitro evaluation of alginate beads of a diclofenac salt, *Int. J. Pharm.* 163 (1998) 23–34.
- [15] Y. Murata, E. Miyamoto, S. Kawashima, Additive effect of chondroitin sulfate and chitosan on drug release from calcium-induced alginate gel beads, *J. Control. Release* 38 (1996) 108–110.
- [16] K. Wang, Z. He, Alginate–konjac glucomannan–chitosan beads as controlled release matrix, *Int. J. Pharm.* 244 (2002) 117–126.
- [17] P.F. Almeida, A.J. Almeida, Cross-linked alginate–gelatin beads: a new matrix for controlled release of pindolol, *J. Control. Release* 97 (2004) 431–439.
- [18] S. Puttipipatkachorn, T. Pongjanyakul, A. Priprom, Molecular interaction in alginate beads reinforced with sodium starch glycolate or magnesium aluminum silicate, and their physical characteristics, *Int. J. Pharm.* 293 (2005) 51–62.
- [19] T. Pongjanyakul, S. Puttipipatkachorn, Xanthan–alginate composite gel beads: molecular interaction and in vitro characterization, *Int. J. Pharm.* 331 (2007) 61–71.
- [20] A.K. Nayak, B. Das, R. Maji, Calcium alginate/gum Arabic beads containing glibenclamide: development and in vitro characterization, *Int. J. Biol. Macromol.* 51 (2012) 1070–1078.
- [21] F.H. Tsai, Y. Kitamura, M. Kokawa, Effect of gum arabic-modified alginate on physicochemical properties, release kinetics, and storage stability of liquid-core hydrogel beads, *Carbohydr. Polym.* 174 (2017) 1069–1077.
- [22] Z.C. Yin, Y.L. Wang, K. Wang, A pH-responsive composite hydrogel beads based on agar and alginate for oral drug delivery, *J. Drug Delivery Sci. Technol.* 43 (2018) 12–18.
- [23] Y. Murata, K. Tsumoto, K. Kofuji, S. Kawashima, Effect of natural polysaccharide addition on drug release from calcium induced alginate gel beads, *Chem. Pharm. Bull.* 51 (2002) 218–220.
- [24] T. Pongjanyakul, T. Rongthong, Enhanced entrapment efficiency and modulated drug release of alginate beads loaded with drug–clay intercalated complexes as microreservoirs, *Carbohydr. Polym.* 81 (2010) 409–419.
- [25] N. Djebri, M. Boutahala, N.E. Chelali, N. Boukhalfa, L. Zeroual, Enhanced removal of cationic dye by calcium alginate/organobentonite beads: modeling, kinetics,

- equilibriums, thermodynamic and reusability studies, *Int. J. Biol. Macromol.* 92 (2016) 1277–1287.
- [26] S. Jain, M. Datta, Montmorillonite-alginate microspheres as a delivery vehicle for oral extended release of Venlafaxine hydrochloride, *J. Drug Delivery Sci. Technol.* 33 (2016) 149–156.
- [27] E.S. Chan, S.L. Wang, P.P. Lee, J.S. Lee, T.B. Ti, Z. Zhang, D. Poncelet, P. Ravindra, S.H. Phan, Z.H. Yim, Effects of starch filler on the physical properties of lyophilized calcium-alginate beads and the viability of encapsulated cells, *Carbohydr. Polym.* 83 (2011) 225–232.
- [28] G. Lozano-Vazquez, C. Lobato-Calleros, H. Escalona-Buendia, G. Chavez, J. Alvarez-Ramirez, E.J. Vernon-Carter, Effect of the weight ratio of alginate-modified tapioca starch on the physicochemical properties and release kinetics of chlorogenic acid containing beads, *Food Hydrocoll.* 48 (2015) 301–311.
- [29] B. Singh, D.K. Sharma, A. Gupta, A study towards release dynamics of thiram fungicide from starch-alginate beads to control environmental and health hazards, *J. Hazard. Mater.* 161 (2009) 208–216.
- [30] N. Biswas, R.K. Sahoo, Tapioca starch blended alginate mucoadhesive-floating beads for intragastric delivery of Metoprolol Tartrate, *Int. J. Biol. Macromol.* 83 (2016) 61–70.
- [31] N. Masina, Y.E. Choonara, P. Kumar, L.C. du Toit, M. Govender, S. Indermun, V. Pillay, A review of the chemical modification techniques of starch, *Carbohydr. Polym.* 157 (2017) 1226–1236.
- [32] P. Murphy, Starch, in: G.O. Philips, P.A. Williams (Eds.), *Handbook of Hydrocolloids*, Woodhead Publishing, Cambridge 2000, pp. 41–65.
- [33] U.J. Ukpabi, E. Ukenye, A.O. Olojede, Raw-material potentials of Nigerian wild polynesian arrowroot (*Tacca leontopetaloides*) tubers and starch, *J. Food Technol.* 7 (2009) 135–138.
- [34] N.S.M. Makhtar, M.F.M. Rais, M.N.M. Rodhi, M. Musa, K.H.K. Hamid, *Tacca leontopetaloides* starch: new sources starch for biodegradable plastic, *Procedia Eng.* 68 (2013) 385–391.
- [35] T.W. Underwood, D.E. Cadwallader, Influence of various starches on dissolution rate of salicylic acid from tablets, *J. Pharm. Sci.* 61 (1972) 239–243.
- [36] S.C. Dollery, *Therapeutic Drugs*, Churchill Livingstone, Edinburgh, 1991 D96–D100.
- [37] H. Bechgaard, G.H. Nielson, Controlled release multiunit and single unit dosage, *Drug Dev. Ind. Pharm.* 4 (1978) 53–67.
- [38] T. Auttapornpitak, *Physicochemical Properties of Arrowroot Tacca leontopetaloides Ktze. Starch*, Chulalongkorn University, Bangkok, 2003 (Master's thesis).
- [39] P. Costa, J.M.S. Lobo, Modeling and comparison of dissolution profiles, *Eur. J. Pharm. Sci.* 13 (2001) 123–133.
- [40] T. Pongjanyakul, Alginate–magnesium aluminum silicate films: importance of alginate block structures, *Int. J. Pharm.* 365 (2009) 100–108.
- [41] R. Kizil, J. Irudayaraj, K. Seetharaman, Characterization of irradiated starches by using FT-Raman and FTIR spectroscopy, *J. Agric. Food Chem.* 50 (2002) 3912–3918.
- [42] A. Dashevsky, Protein loss by the microencapsulation of an enzyme (lactase) in alginate beads, *Int. J. Pharm.* 161 (1998) 1–5.
- [43] Y. Murata, K. Nakada, E. Miyamoto, S. Kawashima, S.H. Seo, Influence of erosion of calcium-induced alginate gel matrix on the release of brilliant blue, *J. Control. Release* 23 (1993) 21–26.



การประชุมวิชาการ

“นักวิจัยรุ่นใหม่...พบ...เมธีวิจัยอาวุโส สกว.” ครั้งที่ 18

วันที่ 9-11 มกราคม 2562 โรงแรมเดอะรีเจนท์ เซอร์วิส รีสอร์ท จังหวัดเพชรบุรี

Check your presentation schedule by entering the following information:

TRF Grant Code BRG6080016

Presenter Name Thaned (in English, only partial name may be used)

Presentation Details

Presenter full name: Thaned Pongjanyakul

Abstract ID: OS-BIO-C5-088

Abstract Title: Investigation of sodium caseinate-clay nanocomposite films for tablet coatings

Discipline: BIO - Biomedical Science and Health Science⁽¹⁾

Sub-discipline: Pharmaceutical Science

Requested presentation: oral

Allocated presentation: oral⁽²⁾

Presentation date: 10/1/2019⁽³⁾

Presentation time: 1445-1505

⁽¹⁾ The TOAC2019 committee reserves the right to assign the discipline/sub-discipline as appropriate.

⁽²⁾ Due to the limited time slot available, all requested oral presentations may not be granted. The decision is based on recommendation by the committee.

⁽³⁾ All poster sessions for MRG/TRG grants are on 09 Jan 2019; all oral poster sessions for RSA/BRG/DBG grants are on 10 Jan 2019. These cannot be changed.

The purpose of this is to quickly inform the presenter about the presentation details. A formal letter will be issued in early December.

In case of problems or questions, please contact TOAC2019 secretariat office at: tel. 0 2714 2590; 08 0995 8284; e-mail: toacsecretariat@gmail.com

More details about the oral and poster preparation will be available shortly at <https://toac2019.com>

Please kindly note that request for changing type of presentation from poster to oral, or changing of oral or poster schedules are not normally considered.

Search Abstract by Discipline: (no selection will show abstracts from all disciplines)

Biological Science (BIO)

- ☐ A1: Biochemistry ☐ A2: MicroBiology ☐ A3: Biology ☐ A4: Biotechnology
☐ B1: Animal Science ☐ B2: Aquatic Science ☐ B3: Agricultural Science ☐ B4: Food Science ☐ B5: Veterinary Science
☐ C1: Biomedical Science ☐ C2: Health Science ☐ C3: Communicable Diseases ☐ C4: Non-Communicable Diseases ☒
C5: Pharmaceutical Science

Physical Science (PHY)

- ☐ A1: Org Chem ☐ A2: Inorg Chem ☐ A3: Anal Chem/Sensors ☐ A4: Med Chem/Natural Products ☐ A5: Phys/Theo Chem
☐ B1: Materials Science ☐ B2: Polymers ☐ C1: Mathematics ☐ C2: Physics ☐ D: Other Areas

Engineering Science (ENG)

- ☐ A1: Chemical Eng ☐ A2: Civil Eng ☐ A3: Comp Sci/Eng and IT ☐ A4: Electrical&Electronic Eng ☐ A5: Industrial&Production Eng
☐ A6: Mechanical Eng ☐ A7: Other Areas

Humanities and Social Science (SOC)

- ☐ A: Economics, Management&Business Admin ☐ B: Language&Culture ☐ C: Education, Psychology&Behavioral Sciences ☐ D: Architecture
☐ E: Public Administration ☐ F: Communication Arts ☐ G: History&Archaeology ☐ H: Other Areas

Search by ID/Author/Title/Keywords: (optional, discipline selection will be ignored in keywords search mode)

Keyword(s)

[View Abstract](#)

List of abstracts that matched your search criteria:

Entry	ID	PI	Title	Date/Time	Room	Abstract
1	OS-BIO-C5-025	Supachoke Mangmool	Stimulation of adenosine A2B receptor inhibits endothelin-1-induced cardiac fibroblast proliferation and alpha-smooth muscle actin synthesis	10-Jan-19 1350-1410	Petchburi 2	view PDF
2	PJ-BIO-C5-036	Thirapit Subongkot	Development of a novel microemulsion for oral absorption enhancement of all-trans retinoic acid	09-Jan-19 1630-1800	Grand Sema Hall	view PDF
3	PJ-BIO-C5-050	Wantida Chaiyana	Development of dermal nanodelivery system containing anti-ageing compounds from Ocimum sanctum Linn. extracts	09-Jan-19 1630-1800	Grand Sema Hall	view PDF
4	PJ-BIO-C5-061	Atchariya Yosboonruang	Development of biocellulose/aloe gel film for wound dressing application	09-Jan-19 1630-1800	Grand Sema Hall	view PDF
5	PS-BIO-C5-066	Phatsawee Jansook	Development of celecoxib eye drop solution and microsuspension for targeted delivery to the posterior segment of the eye	10-Jan-19 1630-1800	Grand Sema Hall	view PDF
6	OS-BIO-C5-088	Thaned Pongjanyakul	Investigation of sodium caseinate-clay nanocomposite films for tablet coatings	10-Jan-19 1445-1505	Petchburi 2	view PDF
7	PJ-BIO-C5-101	Jutamas Jiaranaikulwanitch	Multiple actions of ascorbic derivatives on amyloid cascade hypothesis for Alzheimer's disease	09-Jan-19 1630-1800	Grand Sema Hall	view PDF
8	PS-BIO-C5-117	Damrongsak Faroongsarng	Differential scanning calorimetric analysis of thermally induced	10-Jan-19 1630-1800	Grand Sema Hall	view PDF

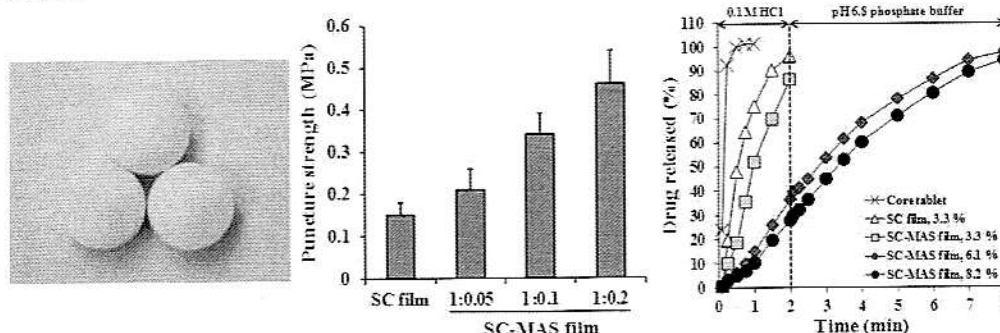
Investigation of sodium caseinate-clay nanocomposite films for tablet coatings

Thaned Pongjanyakul,* Wanassnant Kajthunyakarn, Duangkamon Sakloetsakun

*Division of Pharmaceutical Technology, Faculty of Pharmaceutical Sciences,
Khon Kaen University, Khon Kaen 40002*

Abstract

The objective of this study was to investigate the effect of montmorillonite clay, magnesium aluminum silicate (MAS), on the properties of sodium caseinate (SC) films. Moreover, the SC-MAS dispersions were evaluated for film coating of sustained-release tablets. The results showed that exfoliated or intercalated nanocomposites of the SC-MAS films could be formed due to the molecular interaction of both components via hydrogen bonding. The puncture strength and elongation of the dry SC films reduced when increasing MAS ratios. However, MAS could strengthen the wet films and reduce drug permeability and diffusivity across the films in an acidic medium. The SC-MAS dispersions could be used as a coating material with few defects in the coated tablets. The drug release of the coated tablets in acidic media could be modulated by varying not only MAS ratios added but also coating levels of the films. Furthermore, the SC-MAS coated tablets possessed sustained-release behavior for the drug under simulated gastro-intestinal conditions. This finding indicates that the SC-MAS nanocomposite films can be employed as a tablet coating material to sustain drug release.



Keywords: sodium caseinate; magnesium aluminum silicate; nanocomposites; films; tablet coatings

Outputs

1. Kajthunyakarn W, Sakloetsakun D, Pongjanyakul T. Sodium caseinate-magnesium aluminum silicate nanocomposite films for modified-release tablets. *Mater Sci Eng C*. 2018;92:827-839.
2. Khlibsuwan R, Khunkitti W, Pongjanyakul T. Alginate-caseinate composites: Molecular interactions and characterization of cross-linked beads for the delivery of anticandidals. *Int J Biol Macromol*. 2018;115:483-493.

*Corresponding author

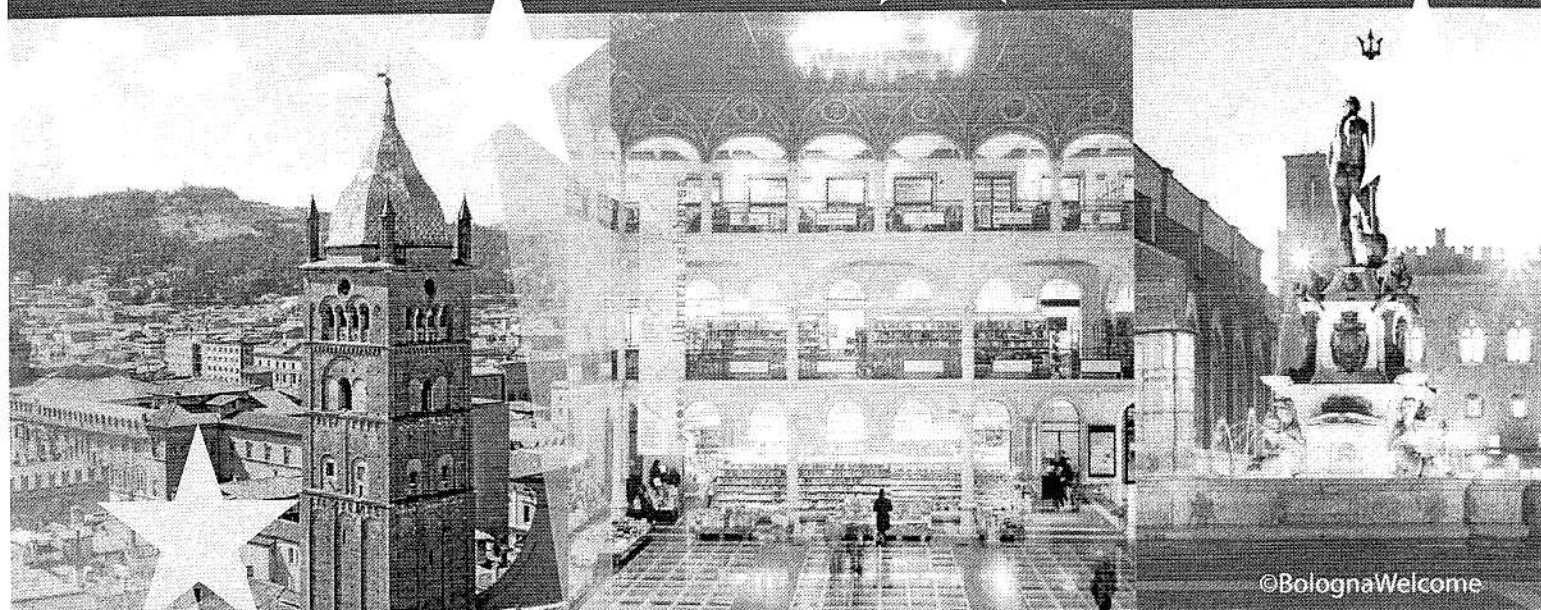
Tel: 08 5011 3176; Fax: 0 4336 2092

E-mail: thaned@kku.ac.th

3rd
European
Conference on
Pharmaceutics

ABSTRACTBOOK

25 to 26 March 2019
Bologna, Italy



©BolognaWelcome



127. Withdrawn
128. Transformation of a manufacturing process, from wet granulation to direct compression, of dextetopfen trometamol tablets
D. Biagi, M. Valleri and P. Mura
129. Cellulose nanocrystals: a candidate excipient for oral drug delivery
A. Omita, S. Barker, M. Orlu, S. Eichhorn, M. Lynch, D. Lafargue and D. Craig
130. Effect of poloxamer407 on calcium alginate beads for anticandidal delivery
R. Khlibsuan, W. Khunkitti and T. Pongjanyakul
131. Investigation of fluconazole-loaded sodium caseinate-clay films for oral candidiasis
W. Kajthanyakarn and T. Pongjanyakul
132. Modification of sodium caseinate films using halloysite and montmorillonite for tablet coating
T. Pongjanyakul, W. Kajthanyakarn and D. Sakloetsakun
133. Wet granulation for the preparation of phospholipid based solid oral dosage forms
D. R. Perinelli, M. Cespi, G. Bonacucina and G. F. Palmieri
134. Formulation study of nanonized itraconazole powder by compression simulator
A. Rossi, A. Montepietra, L. Palugan, F. Pattarino, M. Cerea, R. Bettini, P. Colombo, I. Colombo and C. Vecchio
135. Influence of copovidone and crospovidone of different particle sizes on tablet characteristics
N. Rottmann, T. Cech, C. Hubert and V. Geiselhart
136. Simvastatin /Omega 3-acid ethyl esters fixed dose combination
M. Santaniello, G. Giannini, M. Marzi and F. Giorgi
137. Impact of surface properties of core material on the stability of hot melt coated multiparticulate systems
S. Schertel, A. Zimmer and S. Salar-Behzadi
138. Impact of antacids on gastric fluid in in vitro experiments
D. Segregur, T. Flanagan, J. Mann and J. Dressman
139. An engineered platform for high-loaded dosage forms of amorphous solid dispersions
D. Mudie, K. Shepard, M. Morgen and J. Baumann
140. Formulation of proniosomes for the nanoincorporation of resveratrol
M. Schlich, R. Pireddu, F. Lai, E. Pini, D. Valentí, A. M. Fadda and C. Sinico
141. Investigation of hyperbranched polyglycerol as affinity-based stabilizer and release modifier in polymeric free films
T. Sovány, B. Bánfi, Z. Aigner, G. Kasza, A. Domján and G. Regdon jr.
142. Tablets made from paper – an industrially feasible approach?
F. Stumpf, L. Yutong and C. M. Keck
143. A comparative study of granules and tablets manufactured by dry granulation methods
A. Szepes, E. Gavi, J. Lamerz and S. Ziffels
144. Utilization of aqueous ethylcellulose dispersions for obtaining taste-masked microparticles with rupatadine fumarate as model bitter drug by the spray drying technique
K. Wasilewska, A. Basa and K. Winnicka
145. Formulation of mini-tablets with diclofenac sodium and dibasic calcium phosphate by direct compression
D. Zakowiecki, M. Freitag and K. Cal
146. Nanostructured lipid carriers for oral delivery of silymarin: in vitro and in vivo evaluation in a diabetes and metabolic syndrome model
V. Piazzini, L. Micheli, M. D'Ambrosio, L. Cinci, G. Vanti, C. Ghelardini, L. Di Cesare Mannelli, C. Luceri, A. R. Bilia and M. C. Bergonzi

Modification of sodium caseinate films using halloysite and montmorillonite for tablet coating

Thaned Pongjanyakul, Wanassnant Kajthunyakarn, Duangkamon Sakloetsakun

Khon Kaen University, Faculty of Pharmaceutical Sciences, Khon Kaen 40002, Thailand
e-mail: thaned@kku.ac.th

INTRODUCTION

Caseins are biomacromolecules from milk with molecular weights in the range of 19 and 25 kDa. The isoelectric point of caseins is approximately 4.6 to 4.8. Caseins in an acidic form (casein salt) have a low aqueous solubility, but sodium caseinate (SC), the sodium salt of casein, is freely soluble in water, except when the pH is close to the isoelectric point [1]. SC possesses water-holding and film-forming properties. A continuous film of SC can be formed by adding plasticizer, such as glycerin [2]. Some physical properties of the SC films can be modulated by incorporating oil and wax [3]. Moreover, the SC films have been applied in tablet coating for modifying drug release [4].

Montmorillonite (MMT), a silicate layer structure of clay, has been widely used as a pharmaceutical excipient. It is used to modify physical properties of the SC films and the SC-MMT films are employed in a film coating of modified-release tablets [5]. Unfortunately, effect of clay with a tubular structure, such as halloysite (HS), on the SC film properties is unknown yet. Therefore, the objectives of this study were to investigate and compare the effect of HS and MMT on mechanical properties and drug permeability of the SC films. Additionally, the comparison of drug release from tablets coated with SC-HS and SC-MMT films was examined.

EXPERIMENTAL METHODS

Preparation of films

SC and SC-clay films were prepared by using a casting/solvent evaporation method. SC (5 g) was dispersed in 80 mL of distilled water, and glycerin (30 % w/w based on SC content) used as a plasticizer was added into the SC dispersion. HS or MMT (0, 0.5, or 1 g) was dispersed in hot water (10 mL), and the clay dispersion was mixed with the SC dispersion to obtain the clay amounts of 0, 10%, or 20 % by weight of SC, respectively. All dispersions were adjusted to the final volume (100 mL) using distilled water. The dispersions were cast onto a plastic mold and dried at 60 °C for 24 h.

Determination of mechanical properties

Mechanical properties of the films were investigated using a texture analyzer equipped with a 500 N load cell. The films in

dry and wet (exposed to 0.1 M HCl for 5 min) states were fixed using a film holder between two mounting plates. A 5-mm-diameter spherical stainless steel puncturing probe was fixed at the load cell and moved downwards at 0.1 mm s⁻¹. The applied force and displacement were recorded. The puncture strength and % elongation at the break were calculated.

Drug permeability studies

Acetaminophen (ACT) permeability across the films was investigated by using a side-by-side diffusion cell. Donor and receptor compartments were 4 mg mL⁻¹ of drug solution and 0.1 M HCl in the volume of 3 mL at 37 °C, respectively. Samples were collected, and concentration of ACT was analyzed by a UV-visible spectrophotometer at a wavelength of 265 nm. The relationship between drug permeated and time was plotted, and permeability value was calculated using the equation of Fick's first law.

Preparation and drug release testing of coated tablets

Core tablets containing ACT were prepared using a direct compression method. The SC, SC-10%HS, or SC-10%MMT dispersions were used as a coating material. The core tablets obtained were coated using a side-vented pan coating machine. The core tablets were coated with the films at the mean weight gains of 3.3 % w/w. Drug release from the coated tablets was studied using the USP dissolution apparatus I (basket) with 900 mL of 0.1 M HCl at 37.0°C. The baskets were rotated at a rate of 50 revolutions min⁻¹. The concentration of ACT released was analyzed by UV-visible spectrophotometer at wavelength of 265 nm.

RESULTS AND DISCUSSION

The thickness of the films obtained was over the range of 133.0-169.4 µm. The puncture strength and %elongation of the dry films decreased with increasing HS or MMT. Furthermore, the SC-MMT films displayed greater puncture strength than the SC-HS films. For the wet films exposed to 0.1 M HCl, incorporation of HS or MMT into the SC films resulted in an increase of puncture strength, but %elongation decreased when increasing amount of HS or MMT (Figure 1).

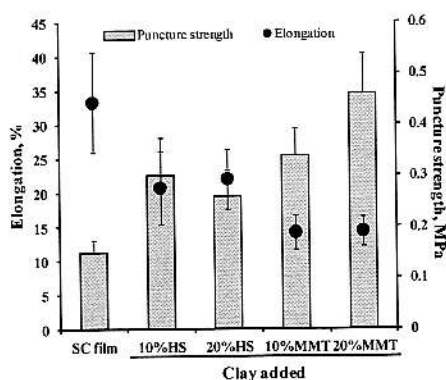


Figure 1. Mechanical properties of the films in wet state.

Drug permeation profiles of the films are presented in Figure 2. Incorporation of HS or MMT into the SC films showed lower amount of drug diffused across the films in acidic condition, leading to lower drug permeability of the films added HS and MMT. However, the permeability coefficient values of the SC-MMT films were lower than those of the SC-HS films.

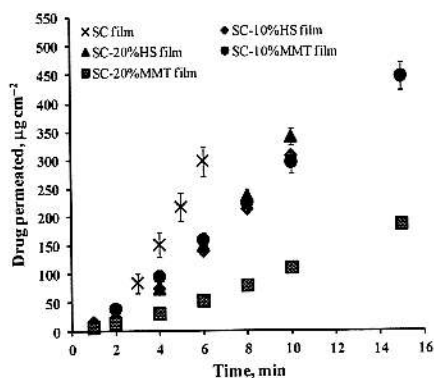


Figure 2. Drug permeation profiles of the films in 0.1 M HCl.

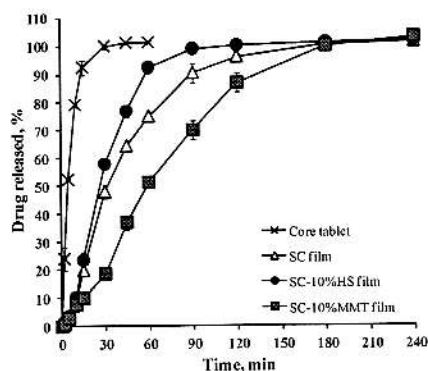


Figure 3. Drug release profiles of film coated tablets.

The SC, SC-10%HS and SC-10%MMT dispersions could be used as a tablet coating materials. The SC films could retard the drug release from the tablets when compared to the core tablets (Figure 3) because SC could be changed to an insoluble casein salt in acidic condition, resulting in an insoluble films formed for sustaining drug release. The SC-HS coated tablets showed faster drug release than the SC-MMT coated tablets, and the lowest drug release was found in the SC-MMT coated tablets.

CONCLUSION

The characteristics of the SC film can be modified by incorporating HS and MMT. The SC-MMT films present higher puncture strength and lower drug permeability than the SC-HS films in wet state using acidic condition. This results in slower drug release from the SC-MMT coated tablets when compared to the SC-HS coated tablets. The finding suggests that the SC-HS and SC-MMT films can be used as a tablet film coating for modifying drug release.

ACKNOWLEDGEMENT

This study was supported by the Thailand Research Fund (TRF) through the Royal Golden Jubilee Ph.D. Program (Grant No. PHD/0067/2557), and TRF Advanced Research Scholar from TRF and Khon Kaen University (Grant No. BRG6080016).

REFERENCES

1. Elzoghby, A.O.; El-Fotoh, W.S. and Elgindy, N.A. Casein-based formulations as promising controlled release drug delivery systems, *J. Control. Release*, 153, 206–216. (2011).
2. Audic, J.L. and Chaufer, B. Influence of plasticizers and crosslinking on the properties of biodegradable films made from sodium caseinate, *Eur. Polym. J.* 41, 1934–1942 (2005).
3. Fabra, M.J.; Talens, P. and Chiralt, A. Tensile properties and water vapor permeability of sodium caseinate films containing oleic acid-beeswax mixtures, *J. Food Eng.* 85, 393–400 (2008).
4. Abu Diak, O.; Bani-Jaber, A.; Amro, B.; Jones, D. and Andrews, G.P. The manufacture and characterization of casein films as novel tablet coating, *Food Bioprod. Process.* 85, 284–290 (2007).
5. Kajthunyakarn, W.; Sakloetsakun, D. and Pongjanyakul, T. Sodium caseinate-magnesium aluminum silicate nanocomposite films for modified-release tablets, *Mater. Sci. Eng. C* 92, 827–839 (2018).

Thaned Pongjanyakul, Wanassnant Kajthunyakarn, Duangkamon Sakloetsakun

Faculty of Pharmaceutical Sciences, Khon Kaen University, Khon Kaen 40002, Thailand

INTRODUCTION

Caseins are biomacromolecules from milk with molecular weights in the range of 19 and 25 kDa. The isoelectric point of caseins is approximately 4.6 to 4.8. Caseins in an acidic form (casein salt) have a low aqueous solubility, but sodium caseinate (SC), the sodium salt of casein, is freely soluble in water, except when the pH is close to the isoelectric point [1]. SC possesses film-forming properties that a continuous film of SC can be formed by adding plasticizer, such as glycerin [2]. Some physical properties of the SC films can be modulated by incorporating oil and wax [3]. Moreover, the SC films have been applied in tablet coating for modifying drug release [4].

Montmorillonite (MMT), a silicate layer structure of clay, has been widely used as a pharmaceutical excipient. It is used to modify physical properties of the SC films and the SC-MMT films are employed in a film coating of modified-release tablets [5]. Unfortunately, effect of clay with a tubular structure, such as halloysite (HS), on the SC film properties is unknown yet. Therefore, the objectives of this study were to investigate and compare the effect of HS and MMT on mechanical properties and drug permeability of the SC films. Additionally, the comparison of drug release from tablets coated with SC-HS and SC-MMT films was examined.

RESULTS

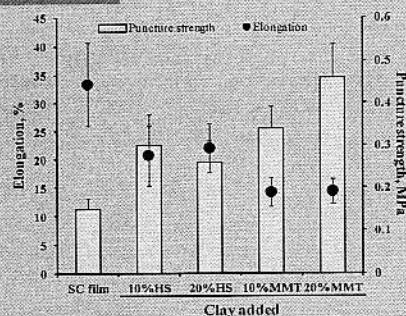


Figure 1. Mechanical properties of the films in wet state.

The puncture strength and %elongation of the dry films decreased with increasing HS or MMT. For the wet films exposed to 0.1 M HCl, incorporation of HS or MMT into the SC films resulted in an increase of puncture strength, but %elongation decreased when increasing amount of HS or MMT (Figure 1).

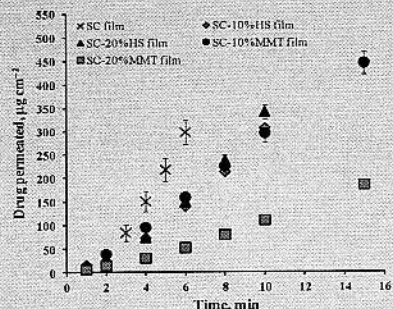


Figure 2. Drug permeation profiles of the films in 0.1 M HCl.

Incorporation of HS or MMT into the SC films showed lower amount of drug diffused across the films in acidic condition, leading to lower drug permeability of the films added HS and MMT. However, the permeability coefficient values of the SC-MMT films were lower than those of the SC-HS films.

ACKNOWLEDGEMENTS

This study was supported by the Thailand Research Fund (TRF) through the Royal Golden Jubilee Ph.D. Program (Grant No. PHD/0067/2557), and TRF Advanced Research Scholar from TRF and Khon Kaen University (Grant No. BRG6080016).

METHODOLOGY

SC and SC-clay films were prepared by using a casting/solvent evaporation method. The SC-clay films in the ratios of 1:0.1 and 1:0.2 were used in this study. Mechanical properties, puncture strength and %elongation, of the films (dry and wet states in 0.1 M HCl) were investigated using a texture analyzer. Acetaminophen (ACT) permeability across the films was investigated by using a side-by-side diffusion cell. Donor and receptor compartments were 4 mg mL⁻¹ of drug solution and 0.1 M HCl in the volume of 3 mL at 37 °C, respectively.

Core tablets containing ACT were prepared using a direct compression method. The SC, SC-10%HS, or SC-10%MMT dispersions were used as a coating material. The core tablets obtained were coated using a side-vented pan coating machine at the mean weight gains of 3.3 % w/w. Drug release from the coated tablets was studied using the USP dissolution apparatus I (basket) with 900 mL of 0.1 M HCl at 37.0°C. The baskets were rotated at a rate of 50 revolutions/min. The concentration of ACT released was analyzed by UV-visible spectrophotometer at wavelength of 265 nm.

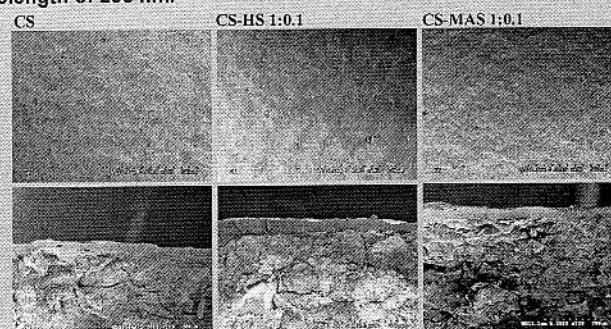


Figure 3. Surface and cross-section morphology of coated tablets.

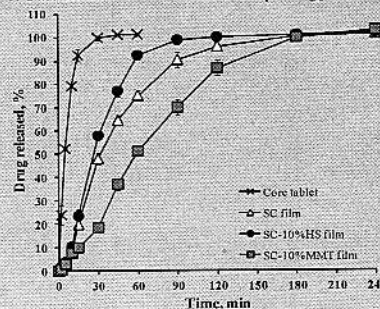


Figure 4. Drug release profiles of film coated tablets.

The SC films could retard the drug release from the tablets when compared to the core tablets (Figure 4) because SC could be changed to an insoluble casein salt in acidic condition, resulting in an insoluble films formed for sustaining drug release. The SC-HS coated tablets showed faster drug release than the SC-MMT coated tablets, and the lowest drug release was found in the SC-MMT coated tablets.

CONCLUSION

The SC-MMT films present higher puncture strength and lower drug permeability than the SC-HS films in wet state using acidic condition. This results in slower drug release from the SC-MMT coated tablets when compared to the SC-HS coated tablets. The finding suggests that the SC-HS and SC-MMT films can be used as a tablet film coating for modifying drug release.

REFERENCES

- [1] Elzoghby, A.O.; El-Fotoh, W.S. and Elgindy, N.A., J. Control. Release, 153, 206–216. (2011).
- [2] Audic, J.L. and Chaufer, B., Eur. Polym. J. 41, 1934–1942 (2005).
- [3] Fabra, M.J.; Talens, P. and Chiralt, A., J. Food Eng. 85, 393–400 (2008).
- [4] Abu Diak, O.; Bani-Jaber, A.; Amro, B.; Jones, D. and Andrews, G.P., Food Bioprod. Process. 85, 284–290 (2007).
- [5] Kajthunyakarn, W.; Sakloetsakun, D. and Pongjanyakul, T., Mater. Sci. Eng. C 92, 827–839 (2018).

Investigation of fluconazole-loaded sodium caseinate-clay films for oral candidiasis

Wanassnant Kajthunyakarn, Thaned Pongjanyakul

Khon Kaen University, Faculty of Pharmaceutical Sciences, Khon Kaen 40002, Thailand
email: wanassnant@gmail.com

INTRODUCTION

Sodium caseinate (SC) is a sodium salt of casein protein from milk. It presents film-forming properties when adding a plasticizer and the SC films are used as a film packaging for food [1] and film coating for tablets [2]. Recently, addition of magnesium aluminum silicate (MAS), a pharmaceutical clay, can modify physical properties and drug permeability of the SC films. Moreover, SC-MAS films are used for film coating of modified-release tablets [3]. Thus, it is interesting to use the SC-MAS film for drug delivery system. The aim of this study was to prepare the SC-MAS films loaded with fluconazole (FCZ) by a spray method. FCZ is a slightly soluble drug and used for treatment of oral candidiasis [4]. The films were characterized including film thickness, crystallinity, drug content, drug release, and mucoadhesive properties. Furthermore, anticandidal activity of the drug released from the films was examined.

METHODOLOGY

Preparation of FCZ-loaded SC-MAS film

SC (5% w/v) was dispersed in distilled water at room temperature. Various amounts of MAS (0%, 5%, 10%, or 20% based on SC content) were dispersed in hot water, and then MAS dispersions were mixed with SC dispersion. After that, FCZ powder (20% w/v based on SC content) was dispersed into the SC-MAS dispersions and the dispersions were stirred at room temperature for overnight. Then, the mixture dispersions were sprayed on a plastic sheet that had been attached on the wall of tablet coating pan to get drug-loaded SC-MAS films. The films were kept in the refrigerator prior to measurement.

Determination of film thickness and crystallinity

The film thicknesses were measured by a microprocessor coating thickness gauge. The crystallinity of the films was determined by using a powder x-ray diffractometry (PXRD).

Drug content and drug release tests

The films were cut into a disc and weighted accurately, and then the films were added into 50 mL of acetonitrile:water

(3:7) mixed solvents in a volumetric flask. Next, the flasks were sonicated until the films dissolved. The FCZ content was measured by HPLC at the wavelength of 210 nm. The FCZ content in the films was calculated. The FCZ release was investigated by using a side-by-side diffusion cell. The films were cut into a disc, weighted accurately, and gripped with the cell. The release medium was pH 5.8 stimulated saliva fluid (SSF). The FCZ released was analyzed HPLC at the wavelength of 210 nm.

Mucoadhesive property test

Mucoadhesive properties of the films were studied by using a texture analyzer, and porcine esophageal mucosa was used as a membrane. Before testing, the porcine esophageal mucosa was soaked into the pH 7.4 phosphate buffer, and then the mucosa was fixed on a platform. The films were cut into a disc and attached to the cylinder probe. The maximum force that used to remove the films from mucosa was recorded.

Anticandidal activity test

The antifungal activity of the FCZ released from the films was studied by an agar diffusion assay. The sabouraud dextrose agar was dispersed in sterile petri dish. The 200 μ L of *Candida albican* ATCC 10231 was spread on surface sabouraud dextrose agar, and then the petri dishes were bored 4 cavities. The drug release samples at 15 min were added into the cavity. After that, the petri dishes were incubated at 37°C for 24 hr. The diameter of inhibition zone was measured.

RESULTS AND DISCUSSION

The films obtained were yellow thin films. The thickness and FCZ content of the films were in the range of 90-130 μ m, and 11.06-13.43 %w/w, respectively.

The PXRD patterns of the FCZ-loaded SC-MAS film did not show the basal spacing peak of MAS at $7.0^\circ 2\theta$ (Figure 1), indicating a formation of nanocomposite material [3]. The PXRD peaks of FCZ in the films showed a different pattern with pure FCZ. These results suggested that the recrystallization of FCZ caused a different polymorphism during film formation [5].

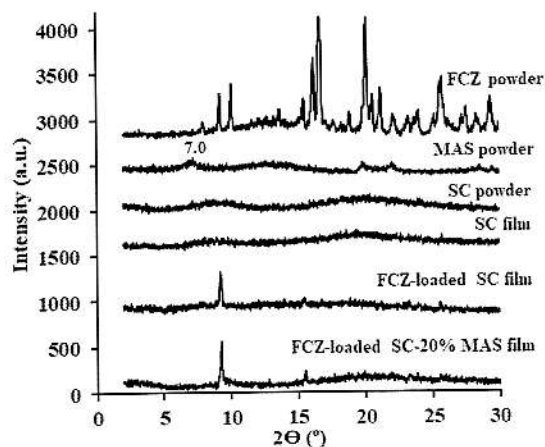


Figure 1. PXRD patterns of FCZ-loaded SC-MAS films.

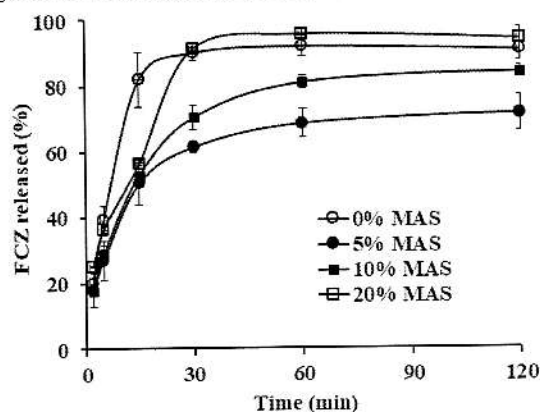


Figure 2. FCZ release profiles of FCZ-loaded SC-MAS films.

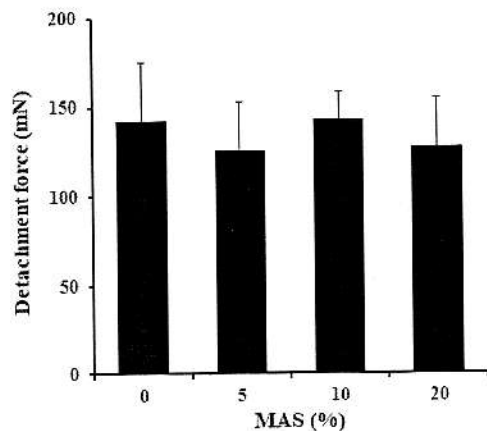


Figure 3. Mucoadhesive property of FCZ-loaded SC-MAS films.

Incorporation of MAS into the films resulted in slower drug release (Figure 2). This may be due to the denser structure of SC-MAS film [3] and adsorption of FCZ onto the MAS silicate layer.

The FCZ-loaded SC film presented a mucoadhesive property that is shown in Figure 3. Addition of MAS into the films did not affect the detachment force in this study. Moreover, the FCZ released from the films still had anticandidal activities that the inhibition zones were in the range of 14.35 to 15.45 mm.

CONCLUSION

The FCZ-loaded SC-MAS films present a sustained-release pattern of FCZ and a mucoadhesive property. The polymorphism of FCZ in the films can be changed after recrystallization during film preparation. However, FCZ released from the films still possess anticandidal activity. So, the FCZ-loaded SC-MAS films display a potential use as a local drug delivery system in oral candidiasis.

ACKNOWLEDGEMENT

This study was supported by the Thailand Research Fund (TRF) through the Royal Golden Jubilee Ph.D. Program (Grant No. PHD/0067/2557), and TRF Advanced Research Scholar from TRF and Khon Kaen University (Grant No. BRG6080016).

REFERENCES

1. Pereda M., Amica G., Racz I. and Marcovich N.E. Preparation and characterization of sodium caseinate films reinforced with cellulose derivatives. *Carbohydr. Polym.*, 86, 1014-1021 (2011).
2. Diak O.A.; Jaber A.B.; Amro B., Jones D. and Andrews G.P. The manufacture and characterization of casein films as novel tablet coatings. *Food. Bioprod. Process.*, 85, 284-290 (2007).
3. Kajthunyakarn W.; Sakloetsakun D. and Pongjanyakul T. Sodium caseinate-magnesium aluminum silicate nanocomposite films for modified-release tablets. *Mater. Sci. Eng. C*, 92, 827-839 (2018).
4. Yehia S.A.; El-Gazayerly O.N. and Basalious E.B. Fluconazole mucoadhesive buccal films: *In vitro*/*In vivo* performance. *Curr. Drug. Deliv.*, 6, 17-27 (2009).
5. Alkhamis K.A.; Obaidat A.A. and Nuseirat A.F. Solid-state characterization of fluconazole. *Pharm. Dev. Technol.*, 7, 491-503 (2002).

CHARACTERIZATION OF FLUCONAZOLE-LOADED SODIUM CASEINATE-CLAY FILMS FOR ORAL CANDIDIASIS

Wanassnant Kajthunyakarn, Thaned Pongjanyakul

Faculty of Pharmaceutical Sciences, Khon Kaen University, Khon Kaen 40002, Thailand

Email: wanassnant@gmail.com and thaned@kku.ac.th



INTRODUCTION

Sodium caseinate (SC) is a sodium salt of casein protein from milk. It presented film-forming properties when adding a plasticizer and the SC films were used as a film packaging for food [1] and film coating for tablets [2]. Recently, addition of magnesium aluminum silicate (MAS), a pharmaceutical clay, could modify physical properties and drug permeability of the SC films. Moreover, SC-MAS film was used for film coating of modified-release tablets [3]. Thus, it is interesting to use the SC-MAS film for drug delivery system.

The aim of this study was to prepare the SC-MAS films loaded with fluconazole (FCZ) by a spray method. FCZ is a slightly soluble drug and used for treatment of oral candidiasis [4]. The films were characterized including film thickness, crystallinity, drug content, drug release, mucoadhesive properties, and antifungal activity. So, the FCZ-loaded SC-MAS films may be used as a local delivery system in oral candidiasis.

METHODOLOGY

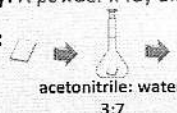
❖ Preparation of FCZ-loaded SC-MAS film

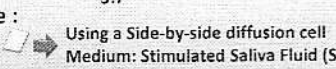
SC (5% w/v) was dispersed in distilled water. Various amounts of MAS (0%, 5%, 10%, or 20% based on SC content) were dispersed in hot water, and then MAS dispersions were mixed with SC dispersion. After that, FCZ powder (20% w/v based on SC content) was dispersed into the SC-MAS dispersions and the dispersions were stirred at room temperature for overnight. Then, the mixture dispersions were sprayed on a plastic sheet that had been attached on the wall of tablet coating pan to get drug-loaded SC-MAS films.

❖ Characterization of the films

➤ Thickness: A microprocessor coating thickness gauge

➤ Crystallinity: A powder x-ray diffractometer (PXRD)

Drug content:  Sonicated ➤ Analyzed by HPLC

In vitro release:  Using a Side-by-side diffusion cell ➤ Analyzed by HPLC
Medium: Stimulated Saliva Fluid (SSF) pH 5.8

Mucoadhesive properties of the films were studied by using a texture analyzer, and porcine esophageal mucosa was used as a membrane.

The antifungal activity of the FCZ released from the films was studied by an agar diffusion assay. *Candida albican* ATCC 10231 was spread on surface sabouraud dextrose agar, and then the petri dishes were bored 4 cavities. The drug release samples at 15 min were added into the cavity. After that, the petri dishes were incubated at 37°C for 24 hr. The diameter of inhibition zone was measured.

CONCLUSIONS

The FCZ-loaded SC-MAS films present a sustained-release pattern of FCZ and a mucoadhesive property. The polymorphism of FCZ can be changed after recrystallization during film preparation. However, FCZ released from the films still possess antifungal activity. So, the FCZ-loaded SC-MAS films display a potential use as a local drug delivery system in oral candidiasis.

RESULTS AND DISCUSSION

The films obtained were yellow thin films. The thickness and FCZ content of the films were 90-130 µm, and 11.06-13.43 %w/w, respectively.

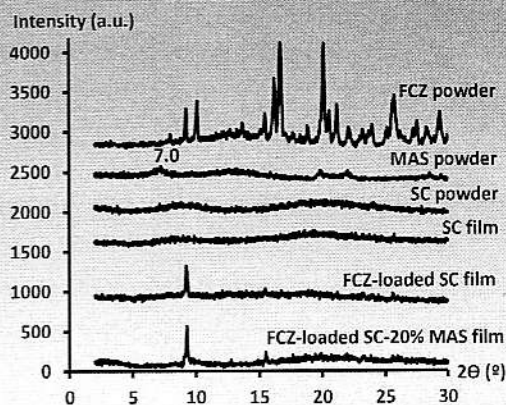


Figure 1. PXRD of FCZ-loaded SC-MAS films

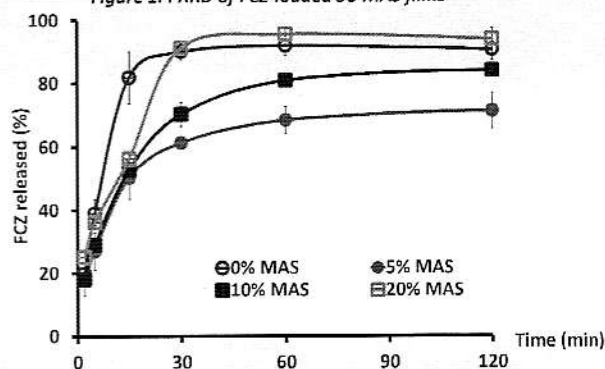


Figure 2. FCZ release profiles of FCZ-loaded SC-MAS films

The PXRD patterns of the FCZ-loaded SC-MAS film did not show the basal spacing peak of MAS, indicating a formation of nanocomposite (Figure 1). The films with FCZ showed a different pattern. These results suggest that the recrystallization of FCZ caused a different polymorphism during film formation [5]. Incorporation of MAS into the films resulted in slower drug release (Figure 2). This may be due to the denser structure of SC-MAS film [3] and adsorption of FCZ onto the MAS silicate layer.

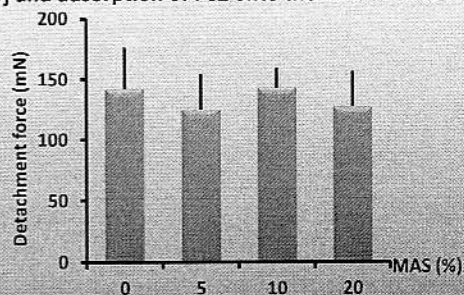


Figure 3. Mucoadhesive properties of FCZ-loaded SC-MAS films

Addition of MAS into the films did not affect the detachment force in this study (Figure 3). Moreover, the FCZ released from the films still had antifungal activities that the inhibition zones were in the range of 14.35 to 15.45 mm.

ACKNOWLEDGEMENTS

The authors would like to thank the Thailand Research Fund (TRF) through the Royal Golden Jubilee Ph.D. Program (Grant No. PHD/0067/2557) and TRF Advanced Research Scholar from TRF and Khon Kaen University (Grant No. BRG6080016).

1. Pereda M., Amica G., Racz I. and Marcovich N.E., Carbohydr. Polym., 86, 1014-1021 (2011).
2. Diak O.A.; Jaber A.B.; Amro B., Jones D. and Andrews G.P., Food. Bioprod. Process., 85, 284-290 (2007).
3. Kajthunyakarn W.; Sakloetsakun D. and Pongjanyakul T., Mater. Sci. Eng. C, 92, 827-839 (2018).
4. Yehia S.A.; El-Gazayerly O.N. and Basalious E.B., Curr. Drug. Deliv., 6, 17-27 (2009).
5. Alkhamis K.A.; Obaidat A.A. and Nusairat A.F., Pharm. Dev. Technol., 7, 491-503 (2002).